

JSCSEN 87(2)169–291(2022)

ISSN 1820-7421(Online)

Journal of the Serbian Chemical Society

ersion
lectronic

VOLUME 87

No 2

BELGRADE 2022



Available on line at



www.shd.org.rs/JSCS/

The full search of JSCS
is available through

DOAJ DIRECTORY OF
OPEN ACCESS
JOURNALS

www.doaj.org

The **Journal of the Serbian Chemical Society** (formerly Glasnik Hemijskog društva Beograd), one volume (12 issues) per year, publishes articles from the fields of chemistry. The **Journal** is financially supported by the **Ministry of Education, Science and Technological Development of the Republic of Serbia**.

Articles published in the **Journal** are indexed in **Clarivate Analytics products: Science Citation Index-ExpandedTM** – accessed via **Web of Science[®]** and **Journal Citation Reports[®]**.

Impact Factor announced 2021: **1.240**; **5-year Impact Factor**: **1.144**.

Articles appearing in the **Journal** are also abstracted by: **Scopus**, **Chemical Abstracts Plus (CAplusSM)**, **Directory of Open Access Journals**, **Referativnii Zhurnal (VINITI)**, **RSC Analytical Abstracts**, **EuroPub**, **Pro Quest** and **Asian Digital Library**.

Publisher:

Serbian Chemical Society, Karnegijeva 4/III, P. O. Box 36, 1120 Belgrade 35, Serbia
tel./fax: +381–11–3370–467, E-mails: **Society** – shd@shd.org.rs; **Journal** – jscs@shd.org.rs
Home Pages: **Society** – <http://www.shd.org.rs/>; **Journal** – <http://www.shd.org.rs/JSCS/>
Contents, Abstracts and full papers (from Vol 64, No. 1, 1999) are available in the electronic form at the Web Site of the **Journal** (<http://www.shd.org.rs/JSCS/>).

Internet Service:

Former Editors:

Nikola A. Pušin (1930–1947), **Aleksandar M. Leko** (1948–1954),
Panta S. Tutundžić (1955–1961), **Miloš K. Mladenović** (1962–1964),
Đorđe M. Dimitrijević (1965–1969), **Aleksandar R. Despić** (1969–1975),
Slobodan V. Ribnikar (1975–1985), **Dragutin M. Dražić** (1986–2006).

Editor-in-Chief:

BRANISLAV Ž. NIKOLIĆ, Serbian Chemical Society (E-mail: jscs-ed@shd.org.rs)

Deputy Editor:

DUŠAN SLADIĆ, Faculty of Chemistry, University of Belgrade

Sub editors:

Organic Chemistry

DEJAN OPSENIKA, Institute of Chemistry, Technology and Metallurgy, University of Belgrade

Biochemistry and

Biotechnology

JÁNOS CSANÁDI, Faculty of Science, University of Novi Sad

Inorganic Chemistry

OLGICA NEDIĆ, INEP – Institute for the Application of Nuclear Energy, University of Belgrade

Theoretical Chemistry

MILOŠ ĐURAN, Serbian Chemical Society

Physical Chemistry

IVAN JURANIĆ, Serbian Chemical Society

Electrochemistry

LJILJANA DAMJANOVIĆ-VASILJIĆ, Faculty of Physical Chemistry, University of Belgrade

Analytical Chemistry

SNEŽANA GOJKOVIĆ, Faculty of Technology and Metallurgy, University of Belgrade

Polymers

SLAVICA RAŽIĆ, Faculty of Pharmacy, University of Belgrade

Thermodynamics

BRANKO DUNJIĆ, Faculty of Technology and Metallurgy, University of Belgrade

Chemical Engineering

MIRJANA KIJEVCANIN, Faculty of Technology and Metallurgy, University of Belgrade

Materials

TATJANA KALUĐEROVIĆ RADOIČIĆ, Faculty of Technology and Metallurgy, University of Belgrade

Metallic Materials and

Metallurgy

RADA PETROVIĆ, Faculty of Technology and Metallurgy, University of Belgrade

Environmental and

Geochemistry

ANA KOSTOV, Mining and Metallurgy Institute Bor, University of Belgrade

History of and

Education in Chemistry

VESNA ANTIĆ, Faculty of Agriculture, University of Belgrade

English Language

DRAGICA TRIVIĆ, Faculty of Chemistry, University of Belgrade

Editors:

LYNNE KATSIKAS, Serbian Chemical Society

VLATKA VAJS, Serbian Chemical Society

JASMINA NIKOLIĆ, Faculty of Technology and Metallurgy, University of Belgrade

Technical Editors:

VLADIMIR PANIĆ, ALEKSANDAR DEKANSKI, VUK FILIPOVIĆ, Institute of

Chemistry, Technology and Metallurgy, University of Belgrade

Journal Manager &

Web Master:

ALEKSANDAR DEKANSKI, Institute of Chemistry, Technology and Metallurgy,

University of Belgrade

Office:

VERA ČUŠIĆ, Serbian Chemical Society

Editorial Board

From abroad: R. Adžić, Brookhaven National Laboratory (USA); A. Casini, University of Groningen (The Netherlands); G. Cobb, Baylor University (USA); D. Douglas, University of British Columbia (Canada); G. Inzelt, Etvos Lorand University (Hungary); N. Katsaros, NCSR “Demokritos”, Institute of Physical Chemistry (Greece); J. Kenny, University of Perugia (Italy); Ya. I. Korenman, Voronezh Academy of Technology (Russian Federation); M. D. Lechner, University of Osnabrueck (Germany); S. Macura, Mayo Clinic (USA); M. Spiteller, INFU, Technical University Dortmund (Germany); M. Stratakis, University of Crete (Greece); M. Swart, University de Girona (Cataluna, Spain); G. Vunjak-Novaković, Columbia University (USA); P. Worsfold, University of Plymouth (UK); J. Zagal, Universidad de Santiago de Chile (Chile).

From Serbia: B. Abramović, V. Antić, V. Bešković, J. Csanadi, Lj. Damjanović-Vasiljić, A. Dekanski, V. Dondur, B. Dunjić, M. Đuran, S. Gojković, I. Gutman, B. Jovančević, I. Juranić, T. Kaluđerović Radičić, L. Katsikas, M. Kijevcanin, A. Kostov, V. Leovac, S. Milonjić, V.B. Mišković-Stanković, O. Nedić, B. Nikolić, J. Nikolić, D. Opsenica, V. Panić, M. Petkovska, R. Petrović, I. Popović, B. Radak, S. Ražić, D. Sladić, S. Sovilj, S. Šerbanović, B. Šolaja, Ž. Tešić, D. Trivić, V. Vajs.

Subscription: The annual subscription rate is **150.00 €** including postage (surface mail) and handling. For Society members from abroad rate is **50.00 €**. For the proforma invoice with the instruction for bank payment contact the Society Office (E-mail: shd@shd.org.rs) or see JSCS Web Site: <http://www.shd.org.rs/JSCS/>, option Subscription.

Godišnja pretplata: Za članove SHD: **2.500,00 RSD**, za penzionere i studente: **1000,00 RSD**, a za ostale: **3.500,00 RSD**; za organizacije i ustanove: **16.000,00 RSD**. Uplate se vrše na tekući račun Društva: **205-13815-62**, poziv na broj **320**, sa naznakom “pretplata za JSCS”.

Nota: Radovi čiji su svi autori članovi SHD prioritarno se publikuju.

Odlukom Odbora za hemiju Republičkog fonda za nauku Srbije, br. 66788/1 od 22.11.1990. godine, koja je kasnije potvrđena odlukom Saveta Fonda, časopis je uvršten u kategoriju međunarodnih časopisa (M-23). Takođe, aktom Ministarstva za nauku i tehnologiju Republike Srbije, 413-00-247/2000-01 od 15.06.2000. godine, ovaj časopis je proglašen za publikaciju od posebnog interesa za nauku. **Impact Factor** časopisa objavljen 2021. godine iznosi **1,240**, a petogodišnji **Impact Factor 1,144**.

INSTRUCTIONS FOR AUTHORS (2021)

GENERAL

The *Journal of the Serbian Chemical Society* (the *Journal* in further text) is an international journal publishing papers from all fields of chemistry and related disciplines. Twelve issues are published annually. The Editorial Board expects the editors, reviewers, and authors to respect the well-known standard of professional ethics.

Types of Contributions

Original scientific papers	(up to 15 typewritten pages, including Figures, Tables and References) report original research which must not have been previously published.
Short communications	(up to 8 pages) report unpublished preliminary results of sufficient importance to merit rapid publication.
Notes	(up to 5 pages) report unpublished results of short, but complete, original research
Authors' reviews	(up to 40 pages) present an overview of the author's current research with comparison to data of other scientists working in the field
Reviews ^a	(up to 40 pages) present a concise and critical survey of a specific research area. Generally, these are prepared at the invitation of the Editor
Surveys	(about 25 pages) communicate a short review of a specific research area.
Book and Web site reviews	(1 - 2 pages)
Extended abstracts	(about 4 pages) of Lectures given at meetings of the Serbian Chemical Society Divisions
Letters to the Editor	report miscellaneous topics directed directly to the Editor

^aGenerally, Authors' reviews, Reviews and Surveys are prepared at the invitation of the Editor.

Submission of manuscripts

Manuscripts should be submitted using the **OnLine Submission Form**, available on the JSCS Web Site (<http://www.shd-pub.org.rs/index.php/JSCS>). The manuscript must be uploaded as a Word.doc or .rtf file, with tables and figures (including the corresponding captions – above Tables and below Figures), placed within the text to follow the paragraph in which they were mentioned for the first time.

Please note that **Full Names** (First Name, Last Name), **Full Affiliation** and **Country** (from drop down menu) of **ALL OF AUTHORS** (written in accordance with English spelling rules - the first letter capitalized) must be entered in the manuscript Submission Form (Step 3). Manuscript Title, authors' names and affiliations, as well as the Abstract, **WILL APPEAR** in the article listing, as well as in **BIBLIOGRAPHIC DATABASES (WoS, SCOPUS...)**, in the form and in the order entered in the author details

Graphical abstract

Graphical abstract is a one-image file containing the main depiction of the authors work and/or conclusion and must be supplied along with the manuscript. It must enable readers to quickly gain the main message of the paper and to encourage browsing, help readers identify which papers are most relevant to their research interests. Authors must provide an image that clearly represents the research described in the paper. The most relevant figure from the work, which summarizes the content, can also be submitted. The image should be submitted as a separate file in **Online Submission Form - Step 2**.

Specifications: The graphical abstract should have a clear start and end, reading from top to bottom or left to right. Please omit unnecessary distractions as much as possible.

- **Image size:** minimum of 500×800 pixels (W×H) and a minimum resolution of 300 dpi. If a larger image is sent, then please use the same ratio: 16 wide × 9 high. Please note that your image will be scaled proportionally to fit in the available window in TOC; a 150×240 pixel rectangle. Please be sure that the quality of an image cannot be increased by changing the resolution from lower to higher, but only by rescanning or exporting the image with a higher resolution, which can be set in usual "settings" option.
- **Font:** Please use Calibri and Symbol font with a large enough font size, so it is readable even from the image of a smaller size (150 × 240 px) in TOC.
- **File type:** JPG and PNG only.

No additional text, outline or synopsis should be included. Please do not use white space or any heading within the image.

Cover Letter

Manuscripts must be accompanied by a cover letter (strictly uploaded in **Online Submission Step 2**) in which the type of the submitted manuscript and a warranty as given below are given. The Author(s) has(have) to warranty that the manuscript submitted to the *Journal* for review is original, has been written by the stated author(s) and has not been published elsewhere; is currently not being considered for publication by any other journal and will not be submitted for such a review while under review by the *Journal*; the manuscript contains no libellous or other unlawful statements and does not contain any materials that violate any personal or proprietary rights of any other person or entity. All manuscripts will be acknowledged on receipt (by e-mail).

Illustrations

Illustrations (Figs, schemes, photos...) in TIF or EPS format (JPG format is acceptable for colour and greyscale photos, only), must be additionally uploaded (Online Submission Step 2) as a separate file or one archived (.zip, .rar or .arj) file. Figures and/or Schemes should be prepared according to the **Artwork Instructions** - http://www.shd.org.rs/JSCS/jscs-pdf/Artwork_Instructions.pdf!

For any difficulties and questions related to **OnLine Submission Form** - <https://www.shd-pub.org.rs/index.php/JSCS/submission/wizard>, please refer to **User Guide** - <https://openjournal-systems.com/ojs-3-user-guide/>, Chapter **Submitting an Article** - <https://openjournal-systems.com/ojs-3-user-guide/submitting-an-article/>. If difficulties still persist, please contact JSCS Editorial Office at JSCS@shd.org.rs

A manuscript not prepared according to these instructions will be returned for resubmission without being assigned a reference number.

Conflict-of-Interest Statement*: Public trust in the peer review process and the credibility of published articles depend in part on how well a conflict of interest is handled during writing, peer review, and editorial decision making. A conflict of interest exists when an author (or the author's institution), reviewer, or editor has financial or personal relationships that inappropriately influence (bias) his or her actions (such relationships are also known as dual commitments, competing interests, or competing loyalties). These relationships vary from those with negligible potential to those with great potential to influence judgment, and not all relationships represent true conflict of interest. The potential for a conflict of interest can exist whether or not an individual believes that the relationship affects his or her scientific judgment. Financial relationships (such as employment, consultancies, stock ownership, honoraria, paid expert testimony) are the most easily identifiable conflicts of interest and the most likely to undermine the credibility of the journal, the authors, and of science itself. However, conflicts can occur for other reasons, such as personal relationships, academic competition, and intellectual passion.

Informed Consent Statement*: Patients have a right to privacy that should not be infringed without informed consent. Identifying information, including patients' names, initials, or hospital numbers, should not be published in written descriptions, photographs, and pedigrees unless the information is essential for scientific purposes and the patient (or parent or guardian) gives written informed consent for publication. Informed consent for this purpose requires that a patient who is identifiable be shown the manuscript to be published. Authors should identify Individuals who provide writing assistance and disclose the funding source for this assistance. Identifying details should be omitted if they are not essential. Complete anonymity is difficult to achieve, however, and informed consent should be obtained if there is any doubt. For example, masking the eye region in photographs of patients is inadequate protection of anonymity. If identifying characteristics are altered to protect anonymity, such as in genetic pedigrees, authors should provide assurance that alterations do not distort scientific meaning and editors should so note. The requirement for informed consent should be included in the journal's instructions for authors. When informed consent has been obtained it should be indicated in the published article.

Human and Animal Rights Statement* When reporting experiments on human subjects, authors should indicate whether the procedures followed were in accordance with the ethical standards of the responsible committee on human experimentation (institutional and national) and with the Helsinki Declaration of 1975, as revised in 2000 (5). If doubt exists whether the research was conducted in accordance with the Helsinki Declaration, the authors must explain the rationale for their approach, and demonstrate that the institutional review body explicitly approved the doubtful aspects of the study. When reporting experiments on animals, authors should be asked to indicate whether the institutional and national guide for the care and use of laboratory animals was followed.

*International Committee of Medical Journal Editors ("Uniform Requirements for Manuscripts Submitted to Biomedical Journals"), February 2006

PROCEDURE

All contributions will be peer reviewed and only those deemed worthy and suitable will be accepted for publication. The Editor has the final decision. To facilitate the reviewing process, authors are encouraged to suggest up to three persons competent to review their manuscript. Such suggestions will be taken into consideration but not always accepted. If authors would prefer a specific person not be a reviewer, this should be announced. The Cover Letter must be accompanied by these suggestions. Manuscripts requiring revision should be returned according to the requirement of the Editor, within 60 days upon reception of the reviewing comments by e-mail.

The *Journal* maintains its policy and takes the liberty of correcting the English as well as false content of manuscripts **provisionally accepted** for publication in the first stage of reviewing process. In this second stage of manuscript preparation by JSCS Editorial Office, the author(s) may be required to supply some **additional clarifications and corrections**. This procedure will be executed during copyediting actions, with a demand to author(s) to perform corrections of unclear parts before the manuscript would be published OnLine as **finally accepted manuscript (OLF Section of the JSCS website)**. Please note that the manuscript can receive the status of **final rejection** if the author's corrections would not be satisfactory.

When finally accepted manuscript is ready for printing, the corresponding author will receive a request for proof reading, which should be performed within 2 days. Failure to do so will be taken as the authors agree with any alteration which may have occurred during the preparation of the manuscript for printing.

Accepted manuscripts of active members of the Serbian Chemical Society (all authors) have publishing priority.

MANUSCRIPT PRESENTATION

Manuscripts should be typed in English (either standard British or American English, but consistent throughout) with 1.5 spacing (12 points Times New Roman; Greek letters in the character font Symbol) in A4 format leaving 2.5 cm for margins. For Regional specific, non-standard characters that may appear in the text, save documents with Embed fonts Word option: *Save as -> (Tools) -> Save Options... -> Embed fonts in the text.*

The authors are requested to seek the assistance of competent English language expert, if necessary, to ensure their English is of a reasonable standard. The Serbian Chemical Society can provide this service in advance of submission of the manuscript. If this service is required, please contact the office of the Society by e-mail (jscs-info@shd.org.rs).

Tables, figures and/or schemes must be embedded in the main text of the manuscript and should follow the paragraph in which they are mentioned for the first time. **Tables** must be prepared with the aid of the **WORD table function**, without vertical lines. The minimum size of the font in the tables should be **10 pt**. Table columns must not be formatted using multiple spaces. Table rows must not be formatted using any returns (enter key; ↵ key) and are **limited to 12 cm width**. Tables should not be incorporated as graphical objects. **Footnotes to Tables** should follow them and are to be indicated consequently (in a single line) in superscript letters and separated by semi-column.

Table caption must be placed above corresponding Table, while **Captions of the Illustrations** (Figs. Schemes...) must follow the corresponding item. **The captions, either for Tables or Illustrations**, should make the items comprehensible without reading of the main text (but clearly referenced in), must follow numerical order (Roman for Tables, Arabic for Illustrations), and should not be provided on separate sheets or as separate files.

High resolution Illustrations (named as Fig. 1, Fig. 2... and/or Scheme 1, Scheme 2...) in **TIF or EPS format** (JPG format is acceptable for photos, only) **must be additionally uploaded as a separate files or one archived (.zip, .rar) file.**

Illustrations should be prepared according to the [ARTWORK INSTRUCTIONS](http://www.shd.org.rs/JSCS/jscs-pdf/Artwork_Instructions.pdf) - http://www.shd.org.rs/JSCS/jscs-pdf/Artwork_Instructions.pdf. !

All pages of the manuscript must be numbered continuously.

DESIGNATION OF PHYSICAL QUANTITIES AND UNITS

IUPAC recommendations for the naming of compounds should be followed. SI units, or other permissible units, should be employed. The designation of physical quantities must be in italic throughout the text (including figures, tables and equations), whereas the units and indexes (except for indexes having the meaning of physical quantities) are in upright letters. They should be in Times New Roman font. In graphs and tables, a slash should be used to separate the designation of a physical quantity from the unit

(example: p / kPa, j / mA cm², t / °C, T_0 / K, τ / h, $\ln(j$ / mA cm²)...). Designations such as: p (kPa), t [min]..., are not acceptable. However, if the full name of a physical quantity is unavoidable, it should be given in upright letters and separated from the unit by a comma (example: Pressure, kPa; Temperature, K; Current density, mA cm²...). Please do not use the axes of graphs for additional explanations; these should be mentioned in the figure captions and/or the manuscript (example: “pressure at the inlet of the system, kPa” should be avoided). The axis name should follow the direction of the axis (the name of y-axis should be rotated by 90°). Top and right axes should be avoided in diagrams, unless they are absolutely necessary.

Latin words, as well as the names of species, should be in *italic*, as for example: *i.e.*, *e.g.*, *in vivo*, *ibid*, *Calendula officinalis* L., *etc.* The branching of organic compound should also be indicated in *italic*, for example, *n*-butanol, *tert*-butanol, *etc.*

Decimal numbers must have decimal points and not commas in the text (except in the Serbian abstract), tables and axis labels in graphical presentations of results. Thousands are separated, if at all, by a comma and not a point.

Mathematical and chemical equations should be given in separate lines and must be numbered, Arabic numbers, consecutively in parenthesis at the end of the line. All equations should be embedded in the text. Complex equations (fractions, integrals, matrix...) should be prepared with the aid of the **Microsoft Equation 3.0** (or higher) or **MathType** (Do not use them to create simple equations and labels). **Using the Insert -> Equation option, integrated in MS Office 2010 and MS Office 2013, as well as insertion of equation objects within paragraph text IS NOT ALLOWED.**

ARTICLE STRUCTURE

- TITLE PAGE;
- MAIN TEXT – including Tables and Illustrations with corresponding captions;
- SUPPLEMENTARY MATERIAL (optional)

Title page

- **Title** in bold letters, should be clear and concise, preferably 12 words or less. The use of non-standard abbreviations, symbols and formulae is discouraged.
- **AUTHORS' NAMES** in capital letters with the full first name, initials of further names separated by a space and surname. Commas should separate the author's names except for the last two names when 'and' is to be used. In multi-affiliation manuscripts, the author's affiliation should be indicated by an Arabic number placed in superscript after the name and before the affiliation. Use * to denote the corresponding author(s).
- *Affiliations* should be written in *italic*. The e-mail address of the corresponding author should be given after the affiliation(s).
- *Abstract*: A one-paragraph abstract written of 150 – 200 words in an impersonal form indicating the aims of the work, the main results and conclusions should be given and clearly set off from the text. Domestic authors should also submit, on a separate page, an Abstract - Izvod, the author's name(s) and affiliation(s) in Serbian (Cyrillic letters). (Домаћи аутори морају доставити Извод (укључујући имена аутора и афилијацију) на српском језику, исписане ћирилицом, иза Захвалнице, а пре списка референци.) For authors outside Serbia, the Editorial Board will provide a Serbian translation of their English abstract.
- *Keywords*: Up to 6 keywords should be given. Do not use words appearing in the manuscript title
- **RUNNING TITLE**: A one line (maximum five words) short title in capital letters should be provided.

Main text – should have the form:

- **INTRODUCTION**,
- **EXPERIMENTAL (RESULTS AND DISCUSSION)**,
- **RESULTS AND DISCUSSION (EXPERIMENTAL)**,
- **CONCLUSIONS**,
- **NOMENCLATURE (optional) and**
- **Acknowledgements: If any.**
- **REFERENCES** (Citation of recent papers published in chemistry journals that highlight the significance of work to the general readership is encouraged.)

The sections should be arranged in a sequence generally accepted for publication in the respective fields. They subtitles should be in capital letters, centred and NOT numbered.

- The INTRODUCTION should include the aim of the research and a concise description of background information and related studies directly connected to the paper.
- The EXPERIMENTAL section should give the purity and source of all employed materials, as well as details of the instruments used. The employed methods should be described in sufficient detail to enable experienced persons to repeat them. Standard procedures should be referenced and only modifications described in detail. On no account should results be included in the experimental section.

Chemistry

Detailed information about instruments and general experimental techniques should be given in all necessary details. If special treatment for solvents or chemical purification were applied that must be emphasized.

Example: Melting points were determined on a Boetius PMHK or a Mel-Temp apparatus and were not corrected. Optical rotations were measured on a Rudolph Research Analytical automatic polarimeter, Autopol IV in dichloromethane (DCM) or methanol (MeOH) as solvent. IR spectra were recorded on a Perkin-Elmer spectrophotometer FT-IR 1725X. ¹H and ¹³C NMR spectra were recorded on a Varian Gemini-200 spectrometer (at 200 and 50 MHz, respectively), and on a Bruker Ultrashield Advance III spectrometer (at 500 and 125 MHz, respectively) employing indicated solvents (*vide infra*) using TMS as the internal standard. Chemical shifts are expressed in ppm (δ / ppm) values and coupling constants in Hz (J / Hz). ESI-MS spectra were recorded on Agilent Technologies 6210 Time-Of-Flight LC-MS instrument in positive ion mode with CH₃CN/H₂O 1/1 with 0.2 % HCOOH as the carrying solvent solution. Samples were dissolved in CH₃CN or MeOH (HPLC grade purity). The selected values were as follows: capillary voltage = 4 kV, gas temperature = 350 °C, drying gas flow 12 L min⁻¹, nebulizer pressure = 310 kPa, fragmentator voltage = 70 V. The elemental analysis was performed on the Vario EL III- C,H,N,S/O Elemental Analyzer (Elementar Analysensysteme GmbH, Hanau-Germany). Thin-layer chromatography (TLC) was performed on precoated Merck silica gel 60 F254 and RP-18 F254 plates. Column chromatography was performed on Lobar LichroPrep Si 60 (40-63 μ m), RP-18 (40-63 μ m) columns coupled to a Waters RI 401 detector, and on Biotage SP1 system with UV detector and FLASH 12+, FLASH 25+ or FLASH 40+ columns pre packed with KP-SIL [40-63 μ m, pore diameter 6 nm (60 Å)], KP-C18-HS (40-63 μ m, pore diameter 9 nm (90 Å) or KP-NH [40-63 μ m, pore diameter 10 nm (100 Å)] as adsorbent. Compounds were analyzed for purity (HPLC) using a Waters 1525 HPLC dual pump system equipped with an Alltech, Select degasser system, and dual λ 2487 UV-VIS detector. For data processing, Empower software was used (methods A and B). Methods C and D: Agilent Technologies 1260 Liquid Chromatograph equipped with Quat Pump (G1311B), Injector (G1329B) 1260 ALS, TCC 1260 (G1316A) and Detector 1260 DAD VL+ (G1315C). For data processing, LC OpenLab CDS ChemStation software was used. For details, see Supporting Information.

1. Synthesis experiments

Each paragraph describing a synthesis experiment should begin with the name of the product and any structure number assigned to the compound in the Results and Discussions section. Thereafter, the compound should be identified by its structure number. Use of standard abbreviations or unambiguous molecular formulas for reagents and solvents, and of structure numbers rather than chemical names to identify starting materials and intermediates, is encouraged.

When a new or improved synthetic method is described, the yields reported in key experimental examples, and yields used for comparison with existing methods, should represent amounts of isolated and purified products, rather than chromatographically or spectroscopically determined yields. Reactant quantities should be reported in weight and molar units and for product yields should be reported in weight units; percentage yields should only be reported for materials of demonstrated purity. When chromatography is used for product purification, both the support and solvent should be identified.

2. Microwave experiments

Reports of syntheses conducted in microwave reactors must clearly indicate whether sealed or open reaction vessels were used and must document the manufacturer and model of the reactor, the method of monitoring the reaction mixture temperature, and the temperature-time profile. Reporting a wattage rating or power setting is not an acceptable alternative to providing temperature data. Manuscripts describing work done with domestic (kitchen) microwave ovens will not be accepted except for studies where the unit is used for heating reaction mixtures at atmospheric pressure.

3. Compound characterization

The Journal upholds a high standard for compound characterization to ensure that substances being added to the chemical literature have been correctly identified and can be synthesized in known yield and purity by the reported preparation and isolation methods. For **all new** compounds, evidence adequate to establish both **identity** and **degree of purity** (homogeneity) must be provided.

Identity - Melting point. All homogeneous solid products (*e.g.* not mixtures of isomers) should be characterized by melting or decomposition points. The colors and morphologies of the products should also be noted.

Specific rotations. Specific rotations based on the equation $[\alpha]_D = (100 \alpha) / (l c)$ should be reported as unitless numbers as in the following example: $[\alpha]^{20}_D = -25.4$ (c 1.93, CHCl_3), where $c / \text{g mL}^{-1}$ is concentration and l / dm is path length. The units of the specific rotation, $(\text{deg mL}) / (\text{g dm})$, are implicit and are not included with the reported value.

Spectra/Spectral Data. Important IR adsorptions should be given.

For all new diamagnetic substances, NMR data should be reported (^1H , ^{13}C , and relevant heteronuclei).

^1H NMR chemical shifts should be given with two digits after the decimal point. Include the number of protons represented by the signal, signal multiplicity, and coupling constants as needed (J italicized, reported with up to one digit after the decimal). The number of bonds through which the coupling is operative, nJ , may be specified by the author if known with a high degree of certainty. ^{13}C NMR signal shifts should be rounded to the nearest 0.01 ppm unless greater precision is needed to distinguish closely spaced signals. Field strength should be noted for each spectrum, not as a comment in the general experimental section. Hydrogen multiplicity (C, CH, CH_2 , CH_3) information obtained from routine DEPT spectra should be included. If detailed signal assignments are made, the type of NOESY or COSY methods used to establish atom connectivity and spatial relationships should be identified in the Supporting Information. Copies of spectra should also be included where structure assignments of complex molecules depend heavily on NMR interpretation. Numbering system used for assignments of signals should be given in the Supporting Information with corresponding general structural formula of named derivative.

HPLC/LCMS can be substituted for biochemistry papers where the main focus is not on compound synthesis.

HRMS/elemental analysis. To support the molecular formula assignment, HRMS data accurate within 5 ppm, or combustion elemental analysis [carbon and hydrogen (and nitrogen, if present)] data accurate within 0.5 %, should be reported for new compounds. HRMS data should be given in format as is usually given for combustion analysis: calculated mass for given formula following with observed mass: (+)ESI-HRMS m/z : [molecular formula + H]⁺ calculated mass, observed mass. Example: (+)ESI-HRMS m/z : calculated for $[\text{C}_{13}\text{H}_8\text{BrCl}_2\text{N} + \text{H}^+]$ 327.92899, observed 327.92792.

NOTE: in certain cases, a crystal structure may be an acceptable substitute for HRMS/elemental analysis.

Biomacromolecules. The structures of biomacromolecules may be established by providing evidence about sequence and mass. Sequences may be inferred from the experimental order of amino acid, saccharide, or nucleotide coupling, from known sequences of templates in enzyme-mediated syntheses, or through standard sequencing techniques. Typically, a sequence will be accompanied by MS data that establish the molecular weight.

Example: Product was isolated upon column chromatography [dry flash (SiO_2 , eluent EA, EA/MeOH gradient 95/5 \rightarrow 9/1, EA/MeOH/ NH_3 gradient 18/0.5/0.5 \rightarrow 9/1/1, and flash chromatography (Biotage SP1, RP column, eluent MeOH/ H_2O gradient 75/25 \rightarrow 95/5, N-H column, eluent EA/Hex gradient 6/3 \rightarrow EA). was obtained after flash column chromatography (Biotage SP NH column, eluent hexane/EA 4:6 \rightarrow 2:6). Yield 968.4 mg (95 %). Colorless foam softens at 96-101 °C. $[\alpha]^{20}_D = +0.163$ ($c = 2.0 \times 10^{-3}$ g/mL, CH_2Cl_2). IR (ATR): 3376w, 2949m, 2868w, 2802w, 1731s, 1611w, 1581s, 1528m, 1452m, 1374s, 1331w, 1246s, 1171m, 1063w, 1023m, 965w, 940w, 881w, 850w, 807w, cm^{-1} . ^1H NMR (500 MHz, CDCl_3 , δ): 8.46 (*d*, 1H, $J = 5.4$, H-2'), 7.89 (*s*, 1H, $J = 2.0$, H-8'), 7.71 (*d*, 1H, $J = 8.9$, H-5'), 7.30 (*dd*, 1H, $J_1 = 8.8$, $J_2 = 2.1$, H-6'), 6.33 (*d*, 1H, $J = 5.4$, H-3'), 6.07 (*s*, HN-Boc, exchangeable with D_2O), 5.06 (*s*, 1H, H-12), 4.92-4.88 (*m*, 1H, H-7), 4.42 (*bs*, H-3), 3.45 (*s*, CH_3 -N), 3.33 (*bs*, H-9'), 3.05-2.95 (*m*, 2H, H-11'), 2.70-2.43 (*m*, 2H, H-24) and HN, exchangeable with D_2O), 2.07 (*s*, CH_3COO), 2.04 (*s*, CH_3COO), 1.42 (*s*, 9H, $(\text{CH}_3)_3\text{C-N}(\text{Boc})$), 0.88 (*s*, 3H, CH_3 -10), 0.79 (*d*, 3H, $J = 6.6$, CH_3 -20), 0.68 (*s*, 3H, CH_3 -13). ^{13}C NMR (125 MHz, CDCl_3 , δ): 170.34, 170.27, 151.80, 149.92, 148.87, 134.77, 128.36, 125.11, 121.43, 117.29, 99.98, 75.41, 70.82, 50.43, 49.66, 47.60, 47.33, 44.97, 43.30, 41.83, 41.48, 37.65, 36.35, 35.44, 34.89,

34.19, 33.23, 31.24, 28.79, 28.35, 27.25, 26.45, 25.45, 22.74, 22.63, 21.57, 21.31, 17.85, 12.15. (+)ESI-HRMS (*m/z*): calculated for [C₄₅H₆₇CIN₄O₆ + H]⁺ 795.48219, observed 795.48185. Combustion analysis for C₄₅H₆₇CIN₄O₆: Calculated. C 67.94, H 8.49, N 7.04; found C 67.72, H 8.63, N 6.75. HPLC purity: method A: RT 1.994, area 99.12 %; method C: RT 9.936, area 98.20 %.

Purity - Evidence for documenting compound purity should include one or more of the following:

- Well-resolved high field 1D ¹H NMR spectrum showing at most only trace peaks not attributable to the assigned structure and a standard 1D proton-decoupled ¹³C NMR spectrum. Copies of the spectra should be included as figures in the Supporting Information.
- Quantitative gas chromatographic analytical data for distilled or vacuum-transferred samples, or quantitative HPLC analytical data for materials isolated by column chromatography or separation from a solid support. HPLC analyses should be performed in two diverse systems. The stationary phase, solvents (HPLC), detector type, and percentage of total chromatogram integration should be reported; a copy of the chromatograms may be included as a figure in the Supporting Information.
- Electrophoretic analytical data obtained under conditions that permit observing impurities present at the 5 % level.

HRMS data may be used to support a molecular formula assignment **but cannot be used as a criterion of purity.**

4. Biological Data

Quantitative biological data are required for all tested compounds. Biological test methods must be referenced or described in sufficient detail to permit the experiments to be repeated by others. Detailed descriptions of biological methods should be placed in the experimental section. Standard compounds or established drugs should be tested in the same system for comparison. Data may be presented as numerical expressions or in graphical form; biological data for extensive series of compounds should be presented in tabular form. Tables consisting primarily of negative data will not usually be accepted; however, for purposes of documentation they may be submitted as supporting information. Active compounds obtained from combinatorial syntheses should be resynthesized and retested to verify that the biology conforms to the initial observation.

Statistical limits (statistical significance) for the biological data are usually required. If statistical limits cannot be provided, the number of determinations and some indication of the variability and reliability of the results should be given. References to statistical methods of calculation should be included. Doses and concentrations should be expressed as molar quantities (*e.g.*, mol/kg, μmol/kg, M, mM). The routes of administration of test compounds and vehicles used should be indicated, and any salt forms used (hydrochlorides, sulfates, *etc.*) should be noted. The physical state of the compound dosed (crystalline, amorphous; solution, suspension) and the formulation for dosing (micronized, jet-milled, nanoparticles) should be indicated. For those compounds found to be inactive, the highest concentration (*in vitro*) or dose level (*in vivo*) tested should be indicated.

- The RESULTS AND DISCUSSION should include concisely presented results and their significance discussed and compared to relevant literature data. The results and discussion may be combined or kept separate.
- The inclusion of a CONCLUSION section, which briefly summarizes the principal conclusions, is recommended.
- NOMENCLATURE is optional but, if the authors wish, a list of employed symbols may be included.
- REFERENCES should be numbered sequentially as they appear in the text. Please note that any reference numbers appearing in the Illustrations and/or Tables and corresponding captions must follow the numbering sequence of the paragraph in which they appear for the first time. When cited, the reference number should be superscripted in Font 12, following any punctuation mark. In the reference list, they should be in normal position followed by a full stop. Reference entry must not be formatted using Carriage returns (enter key; ↵ key) or multiple space key. The formatting of references to published work should follow the *Journal's* style as follows:

- Journals^a: A. B. Surname1, C. D. Surname2, *J. Serb. Chem. Soc.* **Vol** (Year) first page Number
(<https://doi.org/doi>)^b
- Books: A. B. Surname1, C. D. Surname2, *Name of Book*, Publisher, City, Year, pp. 100-101
(<https://doi.org/doi>)^b
- Compilations: A. B. Surname1, C. D. Surname2, in *Name of Compilation*, A. Editor1, C. Editor2, Ed(s)., Publisher, City, Year, p. 100 (<https://doi.org/doi>)^b
- Proceedings: A. B. Surname1, C. D. Surname2, in *Proceedings of Name of the Conference or Symposium*, (Year), Place of the Conference, Country, *Title of the Proceeding*, Publisher, City, Year, p. or Abstract No. 100
- Patents: A. B. Inventor1, C. D. Inventor2, (Holder), Country Code and patent number (registration year)
- Chemical Abstracts: A. B. Surname1, C. D. Surname2, *Chem. Abstr.* CA 234 567a; For non-readily available literature, the Chemical Abstracts reference should be given in square brackets: [C.A. 139/2003 357348t] after the reference
- Standards: EN ISO 250: *Name of the Standard* (Year)
- Websites: Title of the website, URL in full (date accessed)
- ^a When citing Journals, the International Library Journal abbreviation is required. Please consult, e.g., https://images.wobofknowledge.com/WOK46/help/WOS/A_abrvjt.html
- ^b doi should be replaced by doi number of the Article, for example: <http://dx.doi.org/10.2298/JSC161212085B> (as active link). If doi do not exist, provide the link to the online version of the publication.

Only the last entry in the reference list should end with a full stop.

The names of all authors should be given in the list of references; the abbreviation *et al.* may only be used in the text. The original journal title is to be retained in the case of publications published in any language other than English (please denote the language in parenthesis after the reference). Titles of publications in non-Latin alphabets should be transliterated. Russian references are to be transliterated using the following transcriptions:

ж→zh, х→kh, ц→ts, ч→ch, ш→sh, щ→shch, ы→y, ю→yu, я→ya, э→e, й→i, ь→'.

Supplementary material

Authors are encouraged to present the information and results non-essential to the understanding of their paper as SUPPLEMENTARY MATERIAL (can be uploaded in Step 4 of Online Submission). This material may include as a rule, but is not limited to, the presentation of analytical and spectral data demonstrating the identity and purity of synthesized compounds, tables containing raw data on which calculations were based, series of figures where one example would remain in the main text, etc. The Editorial Board retain the right to assign such information and results to the Supplementary material when deemed fit. Supplementary material does not appear in printed form but can be downloaded from the web site of the JSCS.

Mathematical and chemical equations should be given in separate lines and must be numbered, Arabic numbers, consecutively in parenthesis at the end of the line. All equations should be embedded in the text. Complex equations (fractions, integrals, matrix...) should be prepared with the aid of the Microsoft Equation 3.0 (or higher) or MathType (Do not use them to create simple equations and labels). Using the Insert -> Equation option, integrated in MS Office 2010 and MS Office 2013, as well as insertion of equation objects within paragraph text IS NOT ALLOWED.

Deposition of crystallographic data

Prior to submission, the crystallographic data included in a manuscript presenting such data should be deposited at the appropriate database. Crystallographic data associated with organic and metal-organic structures should be deposited at the Cambridge Crystallographic Data Centre (CCDC) by e-mail to deposit@ccdc.cam.ac.uk

Crystallographic data associated with inorganic structures should be deposited with the Fachinformationszentrum Karlsruhe (FIZ) by e-mail to crysdata@fiz-karlsruhe.de. A deposition number will then be provided, which should be added to the reference section of the manuscript.

For detailed instructions please visit the JSCS website:
<https://www.shd-pub.org.rs/index.php/JSCS/Instructions>

ARTWORK INSTRUCTIONS

JSCS accepts only **TIFF** or **EPS** formats, as well as **JPEG** format (only for colour and greyscale photographs) for electronic artwork and graphic files. **MS files** (Word, PowerPoint, Excel, Visio) **NOT acceptable**. Generally, scanned instrument data sheets should be avoided. Authors are responsible for the quality of their submitted artwork. Every single Figure or Scheme, as well as any part of the Figure (A, B, C...) should be prepared according to following instructions (every part of the figure, A, B, C..., must be submitted as an independent single graphic file):

TIFF

Virtually all common artwork and graphic creation software is capable of saving files in TIFF format. This 'option' can normally be found under 'the 'Save As...' or 'Export...' commands in the 'File' menu.

TIFF (Tagged Image File Format) is the recommended file format for bitmap, greyscale and colour images.

- Colour images should be in the RGB mode
- When supplying TIFF files, please ensure that the files are supplied at the correct resolution:
 1. Line artwork: minimum of 1000 dpi
 2. RGB image: minimum of 300 dpi
 3. Greyscale image: minimum of 300 dpi
 4. Combination artwork (line/greyscale/RGB): minimum of 500 dpi
- Images should be tightly cropped, without frame and any caption.
- If applicable please re-label artwork with a font supported by JSCS (Arial, Helvetica, Times, Symbol) and ensure it is of an appropriate font size.
- Save an image in TIFF format with LZW compression applied.
- It is recommended to remove Alpha channels before submitting TIFF files.
- It is recommended to flatten layers before submitting TIFF files.

Please be sure that quality of an image cannot be increased by changing the resolution from lower to higher, but only by rescanning or exporting the image with higher resolution, which can be set in usual "settings" facilities.

EPS

Virtually all common artwork creation software, such as Canvas, ChemDraw, CorelDraw, SigmaPlot, Origin Lab..., are capable of saving files in EPS format. This 'option' can normally be found under the 'Save As...' or 'Export...' commands in the 'File' menu.

For vector graphics, EPS (Encapsulated PostScript) files are the preferred format as long as they are provided in accordance with the following conditions:

- when they contain bitmap images, the bitmaps should be of good resolution (see instructions for TIFF files)
- when colour is involved, it should be encoded as RGB
- an 8-bit preview/header at a resolution of 72 dpi should always be included
- embed fonts should always included and only the following fonts should be used in artwork: Arial, Helvetica, Times, Symbol
- the vertical space between the parts of an illustration should be limited to the bare necessity for visual clarity
- no data should be present outside the actual illustration area
- line weights should range from 0.35 pt to 1.5 pt
- when using layers, they should be reduced to one layer before saving the image (Flatten Artwork)

JPEG

Virtually all common artwork and graphic creation software is capable of saving files in JPEG format. This 'option' can normally be found under 'the 'Save As...' or 'Export...' commands in the 'File' menu.

JPEG (Joint Photographic Experts Group) is the acceptable file format **only for colour and greyscale photographs**. JPEG can be created with respect to photo quality (low, medium, high; from 1 to 10), ensuring file sizes are kept to a minimum to aid easy file transfer. Images should have a minimum resolution of 300 dpi. Image width: minimum 3.0 cm; maximum 12.0 cm.

Please be sure that quality of an image cannot be increased by changing the resolution from lower to higher, but only by rescanning or exporting the image with higher resolution, which can be set in usual "settings" facilities.

SIZING OF ARTWORK

- JSCS aspires to have a uniform look for all artwork contained in a single article. Hence, it is important to be aware of the style of the journal.
- Figures should be submitted in black and white or, if required, colour (charged). If coloured figures or photographs are required, this must be stated in the cover letter and arrangements made for payment through the office of the Serbian Chemical Society.
- As a general rule, the lettering on an artwork should have a finished, printed size of 11 pt for normal text and no smaller than 7 pt for subscript and superscript characters. Smaller lettering will yield a text that is barely legible. This is a rule-of-thumb rather than a strict rule. There are instances where other factors in the artwork, (for example, tints and shadings) dictate a finished size of perhaps 10 pt. Lines should be of at least 1 pt thickness.
- When deciding on the size of a line art graphic, in addition to the lettering, there are several other factors to address. These all have a bearing on the reproducibility/readability of the final artwork. Tints and shadings have to be printable at the finished size. All relevant detail in the illustration, the graph symbols (squares, triangles, circles, *etc.*) and a key to the diagram (to explain the explanation of the graph symbols used) must be discernible.
- The sizing of halftones (photographs, micrographs,...) normally causes more problems than line art. It is sometimes difficult to know what an author is trying to emphasize on a photograph, so you can help us by identifying the important parts of the image, perhaps by highlighting the relevant areas on a photocopy. The best advice that can be given to graphics suppliers is not to over-reduce halftones. Attention should also be paid to magnification factors or scale bars on the artwork and they should be compared with the details inside. If a set of artwork contains more than one halftone, again please ensure that there is consistency in size between similar diagrams.

General sizing of illustrations which can be used for the Journal of the Serbian Chemical Society:

- Minimum fig. size: 30 mm width
- Small fig. size - 60 mm width
- Large fig. size - 90 mm width
- Maximum fig. size - 120 mm width

Pixel requirements (width) per print size and resolution for bitmap images:

	Image width	A	B	C
Minimal size	30 mm	354	591	1181
Small size	60 mm	709	1181	2362
Large size	90 mm	1063	1772	3543
Maximal size	120 mm	1417	2362	4724

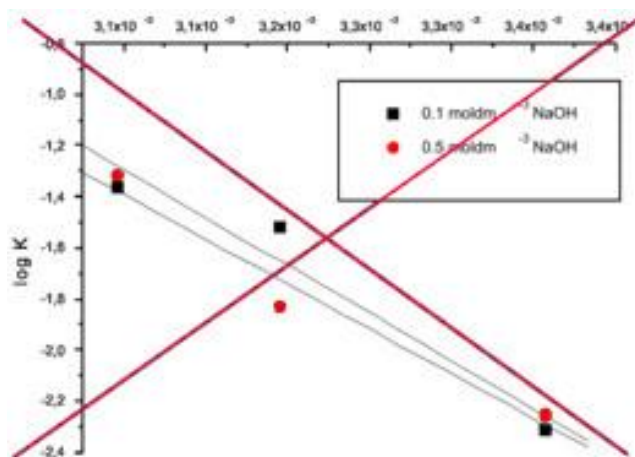
A: 300 dpi > RGB or Greyscale image

B: 500 dpi > Combination artwork (line/greyscale/RGB)

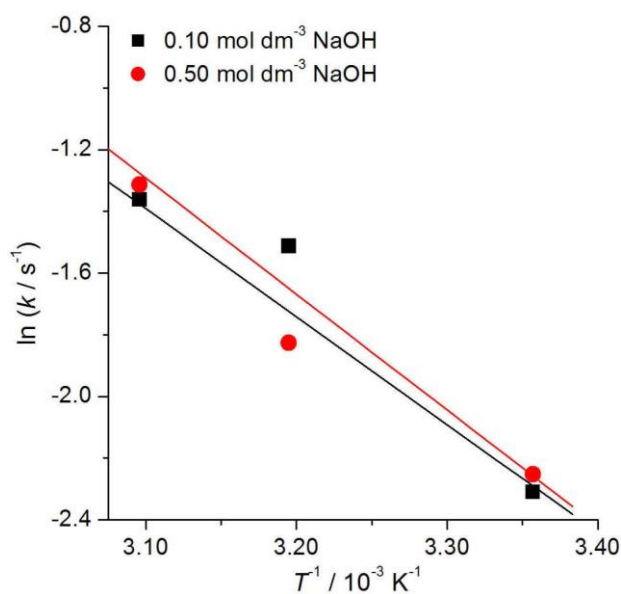
C: 1000 dpi > Line artwork

The designation of physical quantities and graphs formatting

The designation of physical quantities on figures must be in italic, whereas the units are in upright letters. They should be in Times New Roman font. In graphs a slash should be used to separate the designation of a physical quantity from the unit (example: p / kPa , $t / ^\circ\text{C}$, T_0 / K , τ / h , $\ln(j / \text{mA cm}^{-2})$...). Designations such as: p (kPa), t [min]..., are not acceptable. However, if the full name of a physical quantity is unavoidable, it should be given in upright letters and separated from the unit by a comma (example: Pressure, kPa, Temperature, K...). Please do not use the axes of graphs for additional explanations; these should be mentioned in the figure captions and/or the manuscript (example: “pressure at the inlet of the system, kPa” should be avoided). The axis name should follow the direction of the axis (the name of y-axis should be rotated by 90°). Top and right axes should be avoided in diagrams, unless they are absolutely necessary. Decimal numbers must have decimal points and not commas in the axis labels in graphical presentations of results. Thousands are separated, if at all, by a comma and not a point.



INCORRECT



CORRECT



CONTENTS*

Organic Chemistry

- M. J. Krunić, I. I. Jevtić, J. Z. Penjišević and S. V. Kostić-Rajačić*: Synthetic route towards 1,2,3,4-tetrahydroquinoxaline/piperidine combined tricyclic ring system 169

Inorganic Chemistry

- N. Stevanović, M. Jevtović, D. Mitić, I. Z. Matić, M. Đorđić Crnogorac, M. Vujčić, D. Sladić, B. Čobeljić and K. Anđelković*: Evaluation of antitumor potential of Cu(II) complex with hydrazone of 2-acetylthiazole and Girard's T reagent..... 181

Theoretical Chemistry

- N. M. Mahani, S. Z. Mohammadi and K. Anjomshoa*: Density functional theory calculations and molecular docking of 2-phenylbenzimidazoles with estrogen receptor for quantitative structure–activity relationship studies..... 193

Physical Chemistry

- M. M. Vukčević, M. M. Maletić, T. M. Đurkić, B. M. Babić and A. M. Kalijadis*: Beech sawdust based adsorbents for solid-phase extraction of pesticides and pharmaceuticals 205

Electrochemistry

- A. Shukla, N. V. Selvam and M. Ramachandran*: Urea as a complexing agent for selective removal of Ta and Cu in sodium carbonate based alumina chemical–mechanical planarization slurry 219

Analytical Chemistry

- T. Rozsypal*: Development of a method for the derivatization of ethanolamines and its application to sand samples..... 233

Polymers

- I. Landolsi, N. Rjiba, M. Hamdaoui, O. A. Harzallah and C. Boudokhane*: Homogeneous microwave-assisted carboxymethylation from totally chlorine free bleached olive tree pruning residues pulp 247

Thermodynamics

- S. Demirci, V. Adiguzel and O. Sahin*: Solid–liquid phase equilibria in the ternary systems $H_2O+ZnCl_2+NaCl$ at temperatures of 298, 313 and 333 K 263

History of and Education in Chemistry

- K. S. Wissiak Grm and I. Devetak*: The influence of active learning and submicro-representations on 14-year-old students' understanding of the alkaline earth metal concepts 275

- Erratum* 291

Published by the Serbian Chemical Society
Karnegijeva 4/III, P.O. Box 36, 11120 Belgrade, Serbia
Printed by the Faculty of Technology and Metallurgy
Karnegijeva 4, P.O. Box 35-03, 11120 Belgrade, Serbia

* For colored figures in this issue please see electronic version at the Journal Home Page:
<http://www.shd.org.rs/JSCS/>



J. Serb. Chem. Soc. 87 (2) 169–179 (2021)
JSCS–5513

Synthetic route towards 1,2,3,4-tetrahydroquinoxaline/ piperidine combined tricyclic ring system

MIHAJLO J. KRUNIC[#], IVANA I. JEVTIĆ^{*#}, JELENA Z. PENJIŠEVIĆ[#]
and SLADANA V. KOSTIĆ-RAJAČIĆ[#]

*University of Belgrade-Institute of Chemistry, Technology and Metallurgy, Department of
Chemistry, Njegoševa 12, 11000 Belgrade, Serbia*

(Received 16 April, revised 2 August, accepted 20 August 2021)

Abstract: The synthetic route toward novel tricyclic, nitrogen-containing system is disclosed. Three novel compounds possessing structural features of 1,2,3,4-tetrahydroquinoxaline and decahydropyrido[3,4-*b*]pyrazine are synthesized starting from readily available precursors in six or seven steps, of which the last three or four steps respectively are diastereoselective. Key reaction steps include *N*-acylation, Hofmann rearrangement and ring-closing Buchwald–Hartwig reaction. Compounds *trans*-**8**, *cis*-**12** and *trans*-**12** are synthesized in order to prove that this novel, tricyclic system can be functionalized with various groups. Synthetic significance of this heterocyclic system lies in the possibility for the orthogonal functionalization of three different amino groups, allowing fine structural tuning.

Keywords: heterocycles; 1,2,3,4-tetrahydroquinoxaline; piperazine; anilidopiperidine; Buchwald–Hartwig reaction.

INTRODUCTION

Nitrogen-containing heterocycles represent very important structural moieties occurring in many pharmacologically active compounds.^{1,2} Almost 75 % of all Food and Drug Administration (FDA) approved drugs possess nitrogen heterocycles as pharmacophores.³

The possibilities for the derivatization of nitrogen functional groups make these heterocycles significant as intermediates in the organic synthesis. Moreover, nitrogen heterocycles can form versatile noncovalent interactions with the protein target including electrostatic interactions, hydrogen bonding, dipole–dipole interactions, etc., which makes them desirable as pharmacophores in medicinal chemistry.⁴ Due to their significance for organic chemistry in general,

* Corresponding author. E-mail: ivana.jevtic@ihtm.bg.ac.rs

[#] Serbian Chemical Society member.

<https://doi.org/10.2298/JSC210416068K>

the design of new nitrogen heterocycles and the development of new, more efficient ways for their synthesis has been a subject of many research projects, for several decades now.⁵

Both quinoxalines and their derivatives 1,2,3,4-tetrahydroquinoxalines represent an important class of nitrogen-containing heterocycles that can be found in many pharmacologically active natural and synthetic compounds (Fig. 1).^{6,7} 1,2,3,4-tetrahydroquinoxalines are structural motifs present in compounds that act as anticancer agents,⁸ prostaglandin D2 receptor antagonists,⁹ cholesteryl ester transfer protein inhibitors,¹⁰ and others.^{11–13}

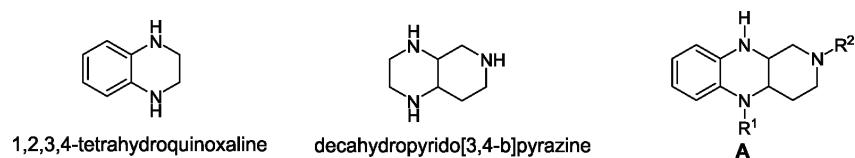


Fig. 1. Structures of the novel tricyclic system of general structure **A** and similar known heterocycles.

Many synthetic procedures for the synthesis of functionalized 1,2,3,4-tetrahydroquinoxalines have been reported so far. Among the most common approaches are the catalytic hydrogenation of quinoxaline,^{14–16} and reactions including aniline derivatives such as cyclization/reduction or oxidation/cyclization reactions, including reactions of *o*-phenylenediamines or *o*-nitroanilines,¹⁷ with various ketones,^{18,19} dihydroxy compounds²⁰ or butanedione.¹⁷ Majumdar *et al.* proposed iodocyclization as a method for constructing 1,2,3,4-tetrahydroquinoxalines among the other heterocycles, starting from *o*-substituted aniline derivatives possessing an isolated, unsaturated C–C bond.²¹ Tandem reduction/reductive aminations,²² and reduction/Michael addition,²³ have been reported by Bunce *et al.* to produce functionalized 1,2,3,4-tetrahydroquinoxalines, starting from *o*-nitroaniline. Organometallic catalyzed intramolecular couplings have also been reported. Yang *et al.* reported the synthesis of 1,2,3,4-tetrahydro-2-vinylquinoxalines *via* palladium (II)-catalyzed tandem allylation of *o*-phenylenediamines with *cis*-1,4-diacetoxy-2-butene.²⁴ Palladium-catalyzed regio- and stereoselective tandem arylation/heteroannulation reaction afforded 2-alkyl(aryl)idenequinoxalines,²⁵ while intramolecular Buchwald–Hartwig reaction of 2-haloanilines with sulfonamido group has also been reported.²⁶ Krchnak *et al.* reported tin (II)-catalyzed solid-phase cyclization of functionalized *o*-nitroanilines, *via* intramolecular nucleophilic substitution.²⁷ Microwave assisted reductive cyclization of substituted *o*-nitroaniline afforded 1,2,3,4-tetrahydroquinoxalines, as reported by Merisor *et al.*²⁸ However, limitations in most cases include low yields, complicated reaction procedures and expensive catalysts. Cyclization/acylation of *o*-phenylenediamines with α -chloroketones²⁹ and diboronic acid

mediated cyclization/cascade transfer hydrogenation of *o*-phenylenediamines and *o*-nitroanilines with 1,2-dicarbonyl compounds,³⁰ are some recent examples towards more efficient synthesis of 1,2,3,4-tetrahydroquinoxalines.

On the contrary to the well-known 1,2,3,4-tetrahydroquinoxalines, there are only a few reports on decahydropyrido[3,4-*b*]pyrazines (Fig. 1). Those include several indole derivatives investigated for their antihypertensive^{31,32} and analgesic³³ activity more than three decades ago, among which the most notable example was the antihypertensive agent atrioposin, albeit it was never marketed.

The value of polycyclic nitrogen-containing heterocycles for synthetic and medicinal chemistry has already been disclosed. As a part of our ongoing research on functionalized nitrogen heterocycles, we envisaged the synthesis of general structure **A** possessing 1,2,3,4-tetrahydroquinoxaline and decahydropyrido[3,4-*b*]pyrazine moieties fused in a novel tricyclic system (Fig. 1). The presence of three secondary amino groups that can be selectively functionalized in different reaction steps, thus allowing the formation of orthogonally protected or highly functionalized derivatives, is a valuable asset in synthetic chemistry. That can be especially important for the synthesis of bifunctional or bidentate ligands in multi-target drug design. The tricyclic system presented in this paper is practically unknown, except for the single lactam structure.³⁴

EXPERIMENTAL

General information

Unless stated otherwise all solvents were freshly distilled under argon prior to being used. All reagents that were purchased from a commercial vendor were used as supplied.

¹H- and ¹³C-NMR spectra were recorded on Bruker Avance III spectrometer, at 500 MHz for the proton (¹H) and at 126 MHz for the carbon (¹³C), and Varian/Agilent, at 400 MHz for the proton (¹H) and at 101 MHz for the carbon (¹³C). Chemical shifts are given in ppm from tetramethylsilane (TMS) as internal standard in deuterated chloroform (CDCl₃). 2D NMR spectra (HSQC) were recorded at 400 and 500 MHz. Coupling constants (*J*) are reported in Hz. Unless stated otherwise, all spectra were recorded at 25 °C. High resolution mass spectra (HRMS) were obtained with a heated ESI (HESI)-LTQ Orbitrap XL spectrometer.

All reactions were monitored by thin layer chromatography (TLC). Dry-column flash chromatography was carried out using silica gel (10–18 or 18–32 μm, ICN-Woelm). Melting points were obtained at a heating rate of 4 °C/min, and are uncorrected.

IR spectra were recorded by using a Thermo Scientific Nicolet 6700 Fourier-transform spectrometer operated in the ATR mode.

Structures of all new compounds were determined by methods of 1D, 2D NMR and IR spectroscopy. Structures of the final two compounds were additionally confirmed by high resolution mass spectrometry (HRMS).

Analytical and spectral data of the compounds are given in Supplementary material to this paper.

Syntheses

*General procedure for the synthesis of enamines 3a and 3b.*³⁵ To a magnetically stirred solution of methyl 1-benzyl-4-oxopiperidine-3-carboxylate **1** (20.0 mmol) in acetic acid

(AcOH, 20 ml), 2-bromoaniline **2a** or 2-iodoaniline **2b** (28.0 mmol) was added, and the mixture was stirred at room temperature. The reaction was monitored by TLC (SiO₂ plates; petroleum ether/ethyl acetate (EtOAc), 8:2). After 24 h, the mixture was concentrated by rotary evaporator, and then neutralized with 1.5 M solution of Na₂CO₃ (pH ~11). The mixture was extracted with EtOAc (2×50 ml), and collected organic layers were concentrated by rotary evaporator. The product was purified by recrystallization from isopropyl alcohol (*i*-PrOH).

*General procedure for the synthesis of anilinoesters 4a and 4b.*³⁵ To a magnetically stirred solution of enamine **3a** or **3b** (9.4 mmol) in methanol (MeOH, 65 ml), NaBH₃CN (13.2 mmol) and AcOH (28.2 mmol) were added and the mixture was stirred at room temperature. The reaction was monitored by TLC (SiO₂ plates; petroleum ether/EtOAc, 8:2). After 24 h, conc. HCl was added to pH ~1, and the mixture was concentrated by rotary evaporator. The mixture was neutralized with 1.5 M solution of Na₂CO₃ (pH ~11) and extracted with EtOAc (3×50 ml). The combined organic layers were concentrated by rotary evaporator providing the crude product (mixture of *cis*- and *trans*-diastereomers). Diastereomers were separated by dry-column flash chromatography (SiO₂; petroleum ether/EtOAc, 10:0 to 7:3) for the spectroscopic analysis; however, the mixture of *cis/trans* diastereomers was used in the next step, without separation.

*General procedure for the synthesis of anilinoester 4a and 4b.*³⁵ To a magnetically stirred solution of anilinoester *cis/trans*-**4a** or *cis/trans*-**4b** (4.4 mmol) in *N,N*-dimethylformamide (DMF, 8 ml), LiH (8.8 mmol) and formamide (HCONH₂, 17.6 mmol) were added. The mixture was stirred at room temperature. The reaction was monitored by TLC (SiO₂ plates; CH₂Cl₂/MeOH, 95:5). After 24 h, the mixture was concentrated by rotary evaporator and partitioned between water (100 ml) and CH₂Cl₂ (3×30 ml). The combined organic layers were concentrated by rotary evaporator, affording the crude product as a mixture of *cis*- and *trans*-diastereomers. Diastereomers were separated by dry-column flash chromatography (SiO₂; CH₂Cl₂/MeOH, 100:0 to 95:5) and used in the next step as separate diastereomers.

General procedure for the synthesis of anilidocarboxamides 9a and 9b. To a magnetically stirred solution of anilidocarboxamide **5a** and **5b** (1.1 mmol) in DMF (8 ml), pyridine (3.3 mmol), 4-(dimethylamino)pyridine (DMAP, 0.33 mmol) and propionyl bromide (EtCOBr, 11.0 mmol) were added and the mixture was stirred at room temperature. The reaction was monitored by TLC (SiO₂ plates; CH₂Cl₂/MeOH, 95:5). The mixture was concentrated by rotary evaporator, and a 1.5 M solution of Na₂CO₃ was added (pH ~11). The mixture was extracted with CH₂Cl₂ (3×30 ml), and the combined organic layers were concentrated by rotary evaporator. The product was dissolved in methanolic ammonia (7–9 M, 30 ml) and the mixture was stirred at room temperature. The reaction was monitored by TLC (SiO₂ plates; CH₂Cl₂/MeOH, 95:5). After 24 h, the mixture was concentrated by rotary evaporator and the crude product was purified by dry-column flash chromatography (SiO₂; CH₂Cl₂/MeOH, 100:0 to 95:5).

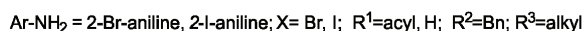
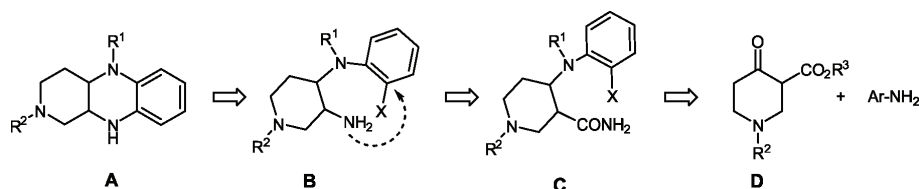
*General procedure for the synthesis of carbamates 6a, 10a and 10b.*³⁶ To a magnetically stirred solution of carboxamide *trans*-**5a**, *trans*-**9a**, *cis*-**9b** or *trans*-**9b** (1.0 mmol) in MeOH (8 ml), LiOH·H₂O (8.0 mmol) was added at room temperature. *N*-Bromoacetamide (NBA, 3.0 mmol) was added in three 1 mmol aliquots while the mixture was stirred at 60 °C in the dark. The reaction was monitored by TLC (SiO₂ plates; Petroleum ether/EtOAc, 6:4). After 5 min, the mixture was concentrated by rotary evaporator, and mixed with a 1 M solution of NaOH. The mixture was extracted with CH₂Cl₂ (3×30 ml), and the collected organic layers were concentrated by rotary evaporator. The crude product was purified by dry-column flash chromatography (SiO₂; petroleum ether/EtOAc, 10:0 to 6:4).

*General procedure for the synthesis of compounds 7a, 11a and 11b.*³⁵ To a magnetically stirred solution of carbamate *trans*-6a, *trans*-10a, *cis*-10b or *trans*-10b (0.22 mmol) in dichloroethane (2 ml), Me₃SiI (0.77 mmol) was added, and the mixture was stirred at room temperature in the dark. The reaction was monitored by TLC (SiO₂ plates; CH₂Cl₂/MeOH, 95:5). After 24 h, excess of MeOH was added and the mixture was allowed to stir for 15 min. The mixture was then concentrated by rotary evaporator and a 1 M HCl was added in excess, followed by the neutralization with 1.5 M Na₂CO₃. The mixture was extracted with CH₂Cl₂ (3×15 ml) and the combined organic layers were concentrated by rotary evaporator affording the crude product. Crude products were used in the next step without further purification.

General procedure for the synthesis of compounds trans-8, cis-12 and trans-12. To a magnetically stirred solution of compound *trans*-7a, *cis*-11b or *trans*-11a (0.17 mmol) in 1,4-dioxane (2 ml), *tert*-butyl alkoxide (*t*-BuONa, 0.26 mmol) or Cs₂CO₃ (0.34 mmol) was added. After 5 min, Pd(OAc)₂ (0.0034 mmol) and 2,2'-bis(diphenylphosphino)-1,1'-binaphthalene (BINAP, 0.01 mmol) were added, and the mixture was stirred at reflux under argon atmosphere. The reaction was monitored by TLC (SiO₂ plates; CH₂Cl₂/MeOH, 95:5). After 8 h, the mixture was concentrated by rotary evaporator. The mixture was partitioned between brine (30 ml) and CH₂Cl₂ (3×10 ml). The combined organic layers were concentrated, and the product was further purified by dry-column flash chromatography (SiO₂; CH₂Cl₂/MeOH, 100:0 to 95:5).

RESULTS AND DISCUSSION

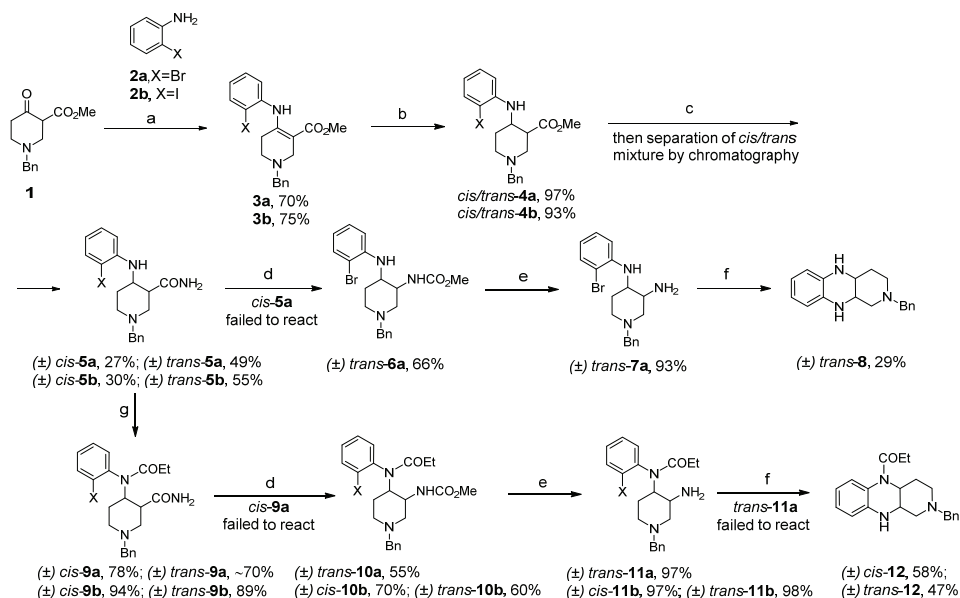
Previously, we disclosed the synthesis of 3-amino-anilidopiperidines, also known as 3-aminofentanyls.^{35,36} These compounds are represented by the general structure **B**, where X is hydrogen (Scheme 1). However, we envisaged that the analogues, where X represents bromine or iodine, may provide access to the novel tricyclic system of general structure **A**. The retrosynthetic approach was based on our previously optimized synthesis of 3-aminofentanyls, starting from β -ketoester **D** (Scheme 1).^{35,36} Therefore, the synthetic protocol was expected to mirror the previous one, except for the use of 2-bromoaniline or 2-iodoaniline that that could possibly influence the reaction conditions and outcomes. The key step, intramolecular Buchwald–Hartwig amination, if successful, would secure the novel heterocyclic system **A**, possessing the combined 1,2,3,4-tetrahydroquinoxaline and decahydropyrido[3,4-*b*]pyrazine moiety.



Scheme 1. The proposed retrosynthetic route to the novel tricyclic system **A**.

The synthetic approach is presented in Scheme 2. The starting β -ketoester **1**, while available commercially, was readily prepared on a multi-gram scale, acc. to

our previously published procedure.³⁷ The *N*-benzyl moiety was chosen since it can be selectively cleaved by various reagents, thus allowing nitrogen functionalization.³⁸ Condensation of **1** with 2-haloaniline **2a** or **2b** afforded stable enamines **3a** and **b**, respectively, followed by the quantitative reduction to *cis/trans* anilinoesters **4a** and **b**. While separable by chromatography, the *cis/trans* mixtures were used directly in the next step. In parallel to the earlier results, formamide-mediated aminolysis of the methoxycarbonyl group provided quantitative conversion to carboxamides **5a** and **b**. The procedure typically results in an extensive, base-catalyzed epimerization at C-3,³⁵ although *cis/trans* ratio may vary, depending on the particular diastereomer. The obtained *cis/trans* mixtures were quantitatively separated by chromatography or crystallization, furnishing pure *cis*-**5a**, *trans*-**5a**, *cis*-**5b** and *trans*-**5b**. The relative stereochemistry was tentatively assigned *via* 2D NMR spectroscopy only, since no X-ray crystal structures are currently available.



Scheme 2. Reagents and conditions: a) **2a**, **2b**, AcOH, r.t., 24 h; b) NaBH₃CN, AcOH, MeOH, r.t., 24 h; c) HCONH₂, LiH, DMF, r.t., 16 h; d) NBA, LiOH·H₂O, MeOH, reflux, 5 min; e) Me₃SiI, (CH₂)₂Cl₂, r.t., 24 h; f) Pd(OAc)₂, BINAP, *t*-BuONa or Cs₂CO₃, dioxane, reflux, 8 h; g) 1. EtCOBr, pyridine, DMAP, DMF, r.t., 24 h, 2. NH₃/MeOH.

The Hofmann rearrangement was then examined on carboxamides **5a** (Scheme 2). We chose our recently published protocol due to good chemoselectivity and generally high yields, compared to the related methods.³⁹ As found in the earlier research, the formation of cyclic ureas was expected, via intramolecular addition of aromatic nitrogen to the intermediate isocyanate.

Surprisingly, *trans*-**5a** furnished carbamate *trans*-**6a**. Apparently, the presence of *ortho* bromine precluded cyclization, and the normal carbamate formed instead. However, *cis*-**5a** failed to react analogously, yielding a complex mixture only.

After the removal of the carbamate group and subsequent intramolecular Buchwald–Hartwig reaction of amine *trans*-**7a**, the cyclization product *trans*-**8** was obtained, although in low yields. Compound *trans*-**8** represents essentially a novel class of heterocycles on its own, not readily accessible by alternative approaches. However, since both piperazine nitrogens are unprotected and the selective functionalization is practically not possible, this particular cyclization appears to be of a limited significance. Nonetheless, a potential improvement of the Hofmann rearrangement and the use of aryl iodides instead of bromides could substantially improve the usefulness of the transformation.

To increase the synthetic significance of this cyclization, and the novel heterocyclic system, the protection of one piperazine nitrogen had to be achieved earlier in the synthetic pathway. In our previous research,³⁵ we found that aromatic amines analogous to **5** (having phenylamino group), were unusually difficult to acylate, likely due to the interference of carboxamido group, rather than the typical steric hindrance. In the case of all four carboxamides **5**, the acylation completely failed with propionyl chloride, under any attempted conditions. Apparently, the presence of *ortho* halogens drastically reduced the nucleophilicity of the aromatic nitrogen. After numerous experiments, it was found that the use of propionyl bromide, in the presence of pyridine and DMAP in DMF, was the only effective reagent for the acylation. Comparable to the previous findings,³⁵ acyl-amido group formed concomitantly (not shown in the Scheme 2), and then was selectively cleaved by methanolic ammonia. The four obtained carboxamides **9** were used as substrates for the Hofmann rearrangement.³⁵ Surprisingly, only *trans*-**9a** and *trans*-**9b** reacted as anticipated, providing carbamates *trans*-**10a** and *trans*-**10b** respectively, albeit in modest yields, with high amount of recovered carboxamides. Carboxamides *cis*-**9a** and *cis*-**9b** yielded complex mixtures with no expected carbamates. Upon further examination of the reaction conditions, we discovered that gradual addition of the small amounts of NBA, not only increase the yields of *trans* carbamates, but also it allowed the formation of *cis*-**10b** carbamate from the carboxamide *cis*-**9b**. Presumably, decomposition of NBA under these conditions occurred more rapidly than the reaction with carboxamides. Carboxamide *cis*-**9a** however, yielded complex mixtures with no expected carbamates, under any attempted conditions, similarly as in the case of *cis*-**5a**. We did not further investigate this phenomena, since we had both diastereomers of **10b** to proceed with the next reaction steps. Subsequent removal of the carbamate group using Me₃SiI, furnished amines *trans*-**11a**, *cis*-**11b** and *trans*-**11b**, in nearly quantitative yields. With the required amines at hand, we

were able to examine the intramolecular Buchwald–Hartwig amination, a key transformation of this synthesis. The reaction conditions were mainly chosen from the numerous literature reports, while the phosphine ligand was limited to BINAP, as the only one available.⁴⁰ Also, having fairly sensitive substrates, strong bases were to be avoided, with the preference to alkaline earth carbonates. Despite numerous attempts, *trans*-**11a** did not produce the expected product. The use of Cs₂CO₃ in dioxane mainly resulted in the recovered reactant, while in diglyme, at 120–140 °C, it decomposed. The reaction also resulted in the decomposition with *t*-BuONa, probably because it is a much stronger base than alkali metal carbonates. Changing molar ratios of Pd(OAc)₂ and BINAP had no significant effect. Fortunately, both diastereomers of **11b**, gave the piperazines *cis*-**12** and *trans*-**12** diastereoselectively, and in moderate yields. The higher yield in the case of *cis*-**12** can be due to the more favorable orientation of the primary amino group and aryl iodide in *cis*-**11b**.

Compounds *cis*-**12** and *trans*-**12** represent another two examples of the novel class of tricyclic, nitrogen-containing system. Obtaining both diastereomers is of significance, since it demonstrates the adaptability of the synthetic route, especially the cyclization process. Also, these heterocycles are suitably functionalized for further elaboration, and as such are potential precursors of pharmacologically active compounds. The piperidine nitrogen, protected by benzyl group, can be readily deprotected and used as a reactive, secondary amino function. One of the piperazine nitrogens is free and can be acylated or alkylated independently, while the other nitrogen is protected as carboxamide.

Thus, we were able to prove that the initial synthetic plan was viable, although, at present, with some limitations. Aryl bromides are apparently insufficiently reactive substrates in these particular aminations, limiting the choice to the iodides. There is a plethora of phosphine ligands, some of which known to be more active than BINAP, permitting additional variations.^{26,40} On the other hand, Cs₂CO₃ as a base is effective, with the potential alternatives including K₂CO₃, K₃PO₄, and other reagents less basic than alkoxides. As already mentioned, the formation of 1,2,3,4-tetrahydroquinoxaline core by Buchwald–Hartwig cyclization is known from literature.²⁶ However, this cyclization is significantly different from ours. The former presents *N*-arylation of a sulfonamido group, whereas in our case, the nucleophile is the primary amino group. From our experience and findings in the literature, the reactivity of amides and amines in Buchwald–Hartwig reaction is different, often requiring very different reaction conditions.

CONCLUSION

The synthetic route toward novel, tricyclic nitrogen containing system is presented herein. Three novel compounds, possessing 1,2,3,4-tetrahydroquinoxaline

and decahydropyrido[3,4-*b*]pyrazine moieties, are synthesized starting from readily available precursors in six or seven steps, of which the last three or four steps respectively, are diastereoselective. Synthetically challenging *N*-acylation of the secondary arylamino group in the presence of adjacent, primary carboxamide function, is optimized. Optimized, NBA-mediated Hofmann rearrangement, gave the desired carbamates in the case of *trans*-**5a** and *trans*-**9a**, *cis*-**9b** and *trans*-**9b**. Carbamate cleavage, followed by the intramolecular Buchwald–Hartwig reaction as the cyclization step, afforded novel tricyclic compounds *trans*-**8**, *cis*-**12** and *trans*-**12** in moderate yields. Such nitrogen containing heterocyclic systems can be of interest for organic synthesis and as building blocks in medicinal chemistry, since the orthogonal functionalization of three different amino groups allows the fine structural tuning. However, an extensive further investigation would be necessary to confirm the potential scope and usefulness of the present results.

SUPPLEMENTARY MATERIAL

Additional data and information are available electronically at the pages of journal website: <https://www.shd-pub.org.rs/index.php/JSCS/article/view/10671>, or from the corresponding author on request.

Acknowledgement. The authors would like to thank the Ministry of Education, Science and Technological Development of the Republic of Serbia (Grant No: 451-03-9/2021-14/200026) for financial support.

ИЗВОД

СИНТЕТСКИ ПУТ ЗА ДОБИЈАЊЕ 1,2,3,4-ТЕТРАХИДРОКИНОКСАЛИНСКО/ПИПЕРИДИНСКОГ ТРИЦИКЛИЧНОГ СИСТЕМА

МИХАЛЛО Ј. КРУНИЋ, ИВАНА И. ЈЕВТИЋ, ЈЕЛЕНА З. ПЕЊИШЕВИЋ И СЛАЂАНА В. КОСТИЋ-РАЈАЧИЋ

Универзитет у Београду-Институт за хемију, технологију и металургију, Центар за хемију,
Ђеђићева 12, 11000 Београд

У овом раду представљена је синтеза новог трицикличног система који садржи азот. Три нова једињења код којих су комбиноване структурне карактеристике 1,2,3,4-тетрахиidroкинoксалина и декахидропиридо[3,4-*b*]пиразина, добијена су полазећи од лако доступних прекурсора, у шест или седам фаза од којих су последње три или четири, редом, диастереоселективне. Кључне синтетичке трансформације укључују *N*-ациловање, Hofmann премештање и интрамолекулску Buchwald–Hartwig реакцију, као фазу у којој долази до циклизације. Једињења *trans*-**8**, *cis*-**12** и *trans*-**12** су синтетисана како би се представила могућност функционализације новог трицикличног система. Синтетички значај новог хетероцикличног система представљен је у могућности ортогоналне функционализације три различите аминок групе, чиме се може постићи фино подешавање структуре.

(Примљено 16. априла, ревидирано 2. августа, прихваћено 20. августа 2021)

REFERENCES

1. B. Zhang, A. Studer, *Chem. Soc. Rev.* **44** (2015) 3505
(<https://doi.org/10.1039/C5CS00083A>)

2. T. Eicher, S. Hauptmann, A. Speicher, *The Chemistry of Heterocycles: Structure, Reactions, Syntheses, and Applications*, Wiley-VCH Verlag GmbH & Co., Weinheim, 2003 (<https://doi.org/10.1002/352760183X>)
3. E. Vitaku, D. T. Smith, J. T. Njardarson, *J. Med. Chem.* **57** (2014) 10257 (<https://doi.org/10.1021/jm501100b>)
4. N. Kerru, L. Gummidi, S. Maddila, K. K. Gangu, S. B. Jonnalagadda, *Molecules* **25** (2020) 1909 (<https://doi.org/10.3390/molecules25081909>)
5. S. Sabir, M. I. Alhazza, A. A. Ibrahim, *Catal. Sustain. Energy* **2** (2015) 99 (<https://doi.org/10.1515/cse-2015-0009>)
6. S. Tariq, K. Somakala, M. Amir, *Eur. J. Med. Chem.* **143** (2018) 542 (<https://doi.org/10.1016/j.ejmech.2017.11.064>)
7. V. A. Mamedov, N. A. Zhukova, *Prog. Heterocyc. Chem.* **24** (2012) 55 (<https://doi.org/10.1016/B978-0-08-096807-0.00002-6>)
8. R. Veligetil, R. B. Madhu, J. Anireddy, V. R. Pasupuleti, V. K. R. Avula, K. S. Ethiraj, S. Uppalanchi, S. Kasturi, Y. Perumal, H. S. Anantaraju, N. Polkam, M. R. Guda, S. Vallela, G. Vasilievich Zyryanov, *Sci. Rep.* **10** (2020) 20720 (<https://doi.org/10.1038/s41598-020-77590-1>)
9. K. Torisu, K. Kobayashi, M. Iwahashi, Y. Nakai, T. Onoda, T. Nagase, I. Sugimoto, Y. Okada, R. Matsumoto, F. Nanbu, S. Ohuchida, H. Nakao, M. Toda, *Bioorg. Med. Chem.* **12** (2004) 5361 (<https://doi.org/10.1016/j.bmc.2004.07.048>)
10. C. T. Eary, Z. S. Jones, R. D. Groneberg, L. E. Burgess, D. A. Mareska, M. D. Drew, J. F. Blake, E. R. Laird, D. Balachari, M. O'Sullivan, A. Allen, V. Marsh, *Bioorg. Med. Chem. Lett.* **17** (2007) 2608 (<https://doi.org/10.1016/j.bmcl.2007.01.112>)
11. J. J. Chen, W. Qian, K. Biswas, V. N. Viswanadhan, B. C. Askew, S. Hitchcock, R. W. Hungate, L. Arik, E. Johnson, *Bioorg. Med. Chem. Lett.* **18** (2008) 4477 (<https://doi.org/10.1016/j.bmcl.2008.07.055>)
12. G. Morissette, J. P. Fortin, S. Otis, J. Bouthillier, F. Marceau, *J. Pharmacol. Exp. Ther.* **311** (2004) 1121 (<https://doi.org/10.1124/jpet.104.071266>)
13. Y. Ohtake, A. Naito, H. Hasegawa, K. Kawano, D. Morizono, M. Taniguchi, Y. Tanaka, H. Matsukawa, K. Naito, T. Oguma, Y. Ezure, Y. Tsuruya, *Bioorg. Med. Chem.* **7** (1999) 1247 ([https://doi.org/10.1016/S0968-0896\(99\)00049-8](https://doi.org/10.1016/S0968-0896(99)00049-8))
14. A. Patti, S. Pedotti, *Tetrahedron* **66** (2010) 5607 (<https://doi.org/10.1016/j.tet.2010.05.090>)
15. R. Rahi, M. Fang, A. Ahmed, R. A. Sánchez-Delgado, *Dalton. Trans.* **41** (2012) 14490 (<https://doi.org/10.1039/C2DT31533E>)
16. W. Tang, L. Xu, Q. H. Fan, J. Wang, B. Fan, Z. Zhou, K. H. Lam, A.S.C. Chan, *Angew. Chem. Int. Ed.* **48** (2009) 9135 (<https://doi.org/10.1002/anie.200904518>)
17. B. B. F. Mirjalili, A. Akbari, *Chin. Chem. Lett.* **22** (2011) 753 (<https://doi.org/10.1016/j.cclet.2010.12.016>)
18. C. S. Cho, W. X. Ren, S. C. Shim, *Tetrahedron Lett.* **48** (2007) 4665 (<https://doi.org/10.1016/j.tetlet.2007.05.044>)
19. F. Pan, T. M. Chen, J. J. Cao, J. P. Zou, W. Zhang, *Tetrahedron Lett.* **53** (2012) 2508 (<https://doi.org/10.1016/j.tetlet.2012.02.113>)
20. M. J. Climent, A. Corma, J. C. Hernández, A. B. Hungría, S. Iborra, S. Martínez-Silvestre, *J. Catal.* **292** (2012) 118 (<https://doi.org/10.1016/j.jcat.2012.05.002>)
21. K. C. Majumdar, K. Ray, S. Ponra, *Tetrahedron Lett.* **51** (2010) 5437 (<https://doi.org/10.1016/j.tetlet.2010.08.016>)

22. R. A. Bunce, D. M. Herron, L. Y. Hale, *J. Heterocycl. Chem.* **40** (2003) 1031 (<https://doi.org/10.1002/jhet.5570400611>)
23. R. A. Bunce, D. M. Herron, M. L. Ackerman, *J. Org. Chem.* **65** (2000) 2847 (<https://doi.org/10.1021/jo991899+>)
24. S.-C. Yang, P.-C. Liu, W.-H. Feng, *Tetrahedron Lett.* **45** (2004) 4951 (<https://doi.org/10.1016/j.tetlet.2004.04.140>)
25. R. Mukhopadhyay, N. G. Kundu, *Synlett* (2001) 1143 (<https://doi.org/10.1055/s-2001-15135>)
26. M. K. Ghorai, A. K. Sahoo, S. Kumar, *Org. Lett.* **13** (2011) 5972 (<https://doi.org/10.1021/ol2023906>)
27. V. Krchnak, J. Smith, J. Vagner, *Tetrahedron Lett.* **42** (2001) 2443 ([https://doi.org/10.1016/S0040-4039\(01\)00197-6](https://doi.org/10.1016/S0040-4039(01)00197-6))
28. E. Merişor, J. Conrad, I. Klaiber, S. Mika, U. Beifuss, *Angew. Chem. Int. Ed.* **46** (2007) 3353 (<https://doi.org/10.1002/anie.200605260>)
29. Y. Fu, J. Y. Wang, W. G. Chen, Y. Li, L. X. Zhao, S. Gao, F. Ye, *Heterocycl. Chem.* **54** (2017) 3023 (<https://doi.org/10.1002/jhet.2911>)
30. S. Liu, Y. Zhou, Y. Sui, H. Liu, H. Zhou, *Org. Chem. Front.* **4** (2017) 2175 (<https://doi.org/10.1039/C7QO00604G>)
31. G. Oshiro, A. Wojdan, M. Klein, G. Metcalf, *J. Cardiovasc. Pharmacol.* **10** (1987) 341 (<https://doi.org/10.1097/00005344-198709000-00014>)
32. I. Jirkovsky, G. Santroch, R. Baudy, G. Oshiro, *J. Med. Chem.* **30** (1987) 388 (<https://doi.org/10.1021/jm00385a022>)
33. A. Nurgiiin, C. François, (Sanofi Aventis France) EP0287468A2 (1988)
34. M. Królikiewicz, K. Błaziak, W. Danikiewicz, Z. Wróbel, *Synlett* **24** (2013) 1945 (<https://doi.org/10.1055/s-0033-1339467>)
35. I. I. Jevtić, Lj. Došen-Mićović, E. R. Ivanović, N. M. Todorović, M. D. Ivanović, *Synthesis* **49** (2017) 3126 (<https://doi.org/10.1055/s-0036-1588985>)
36. I. I. Jevtić, K. Savić Vujović, D. Srebro, S. Vučković, M. D. Ivanović, S. V. Kostić-Rajačić, *Pharmacol. Rep.* **72** (2020) 1069 (<https://doi.org/10.1007/s43440-020-00121-2>)
37. J. Popović-Djordjević, S. Stepanović, Lj. Došen-Mićović, E. Ivanović, M. D. Ivanović, *Green Chem. Lett. Rev.* **9** (2016) 61 (<https://doi.org/10.1080/17518253.2016.1145744>)
38. P. G. M. Wuts, *Greene's Protective Groups in Organic Synthesis*, 5th ed., John Wiley & Sons, Inc., Hoboken, NJ, 2014, pp. 895–4045 (<https://doi.org/10.1002/9781118905074>)
39. I. I. Jevtić, Lj. Došen-Mićović, E. R. Ivanović, M. D. Ivanović. *Synthesis* **48** (2016) 1550 (<https://doi.org/10.1055/s-0035-1561405>)
40. R. Dorel, C. P. Grugel, A. M. Haydl, *Angew. Chem. Int. Ed.* **58** (2019) 17118 (<https://doi.org/10.1002/anie.201904795>).



SUPPLEMENTARY MATERIAL TO
**Synthetic route towards 1,2,3,4-tetrahydroquinoxaline/
piperidine combined tricyclic ring system**

MIHAJLO J. KRUNIĆ, IVANA I. JEVTIĆ*, JELENA Z. PENJIŠEVIĆ
and SLAĐANA V. KOSTIĆ-RAJAČIĆ

University of Belgrade-Institute of Chemistry, Technology and Metallurgy, Department of
Chemistry, Njegoševa 12, 11000 Belgrade, Serbia

J. Serb. Chem. Soc. 87 (2) (2022) 169–179

SPECTROSCOPIC DATA AND YIELDS OF SYNTHESIZED COMPOUNDS 3–12

Methyl 1-benzyl-4-((2-bromophenyl)amino)-1,2,5,6-tetrahydropyridine-3-carboxylate [3a]

Yield: 5.60 g (70 %); off-white solid; mp: 87–88°C; $R_f=0.37$. (SiO₂; petroleum ether/EtOAc, 9:1). IR (ATR): 3239, 3027, 2947, 2807, 2763, 1664, 1615, 1490, 1440, 1367, 1250, 1117, 1059, 738 cm⁻¹. ¹H NMR (500 MHz, CDCl₃) δ = 10.53 (s, 1H), 7.58 (dd, J = 7.9, 1.5 Hz, 1H), 7.39 – 7.29 (m, 4H), 7.29 – 7.24 (m, 1H), 7.25 – 7.20 (m, 1H), 7.20 – 7.14 (m, 1H), 6.98 (td, J = 7.6, 7.5, 1.7 Hz, 1H), 3.72 (s, 3H), 3.64 (s, 2H), 3.35 (br. s, 2H), 2.50 (t, J = 5.7, 5.7 Hz, 2H), 2.39 (t, J = 5.6, 5.6 Hz, 2H) ppm. ¹³C NMR (126 MHz, CDCl₃) δ = 169.3, 153.7, 138.2, 138.0, 133.1, 129.0, 128.3, 127.6, 127.1, 126.6, 125.9, 120.1, 93.2, 62.4, 51.9, 50.8, 48.5, 28.5 ppm.

Methyl 1-benzyl-4-((2-iodophenyl)amino)-1,2,5,6-tetrahydropyridine-3-carboxylate [3b]

Yield: 6.70 g (75 %); off-white solid; mp: 106–108°C; $R_f=0.37$. (SiO₂; petroleum ether/EtOAc, 9:1). IR (ATR): 3130, 3027, 2950, 2791, 2742, 1652, 1606, 1494, 1446, 1364, 1243, 1149, 1060, 776 cm⁻¹. ¹H NMR (400 MHz, CDCl₃) δ = 10.34 (s, 1H), 7.83 (dd, J = 7.9, 1.5 Hz, 1H), 7.37 – 7.28 (m, 4H), 7.28 – 7.21 (m, 2H), 7.18 – 7.11 (m, 1H), 6.85 (td, J = 7.6, 7.6, 1.6 Hz, 1H), 3.71 (s, 3H), 3.62 (s, 2H), 3.33 (br. s, 2H), 2.48 (t, J = 5.7, 5.7 Hz, 2H), 2.27 (t, J = 5.6, 5.6 Hz, 2H) ppm. ¹³C NMR (101 MHz, CDCl₃) δ = 169.3, 153.9, 141.2, 139.3, 138.2, 129.0, 128.6, 128.3, 127.1, 126.9, 126.9, 98.0, 92.9, 62.4, 51.8, 50.8, 48.5, 28.4 ppm.

Methyl (±)-cis-1-benzyl-4-((2-bromophenyl)amino)piperidine-3-carboxylate [(±) cis-4a]

Obtained from **2a**. Yield: 2.31 g (61 %); colorless viscous oil; $R_f=0.39$. (SiO₂; petroleum ether/EtOAc, 9:1). IR (ATR): 3392, 3027, 2949, 2804, 1730,

*Corresponding author. E-mail: ivana.jevtic@ihm.bg.ac.rs

1594, 1510, 1435, 1321, 1215, 1020, 741 cm^{-1} . ^1H NMR (500 MHz, CDCl_3) δ = 7.47 – 7.41 (m, 1H), 7.38 – 7.29 (m, 4H), 7.32 – 7.25 (m, 1H), 7.21 – 7.12 (m, 1H), 6.71 – 6.65 (m, 1H), 6.61 – 6.53 (m, 1H), 5.24 (s, 1H), 3.87 – 3.74 (m, 1H), 3.67 (s, 3H, partially overlapped), 3.64 (d, J = 13.4 Hz, 1H, partially overlapped), 3.50 (d, J = 13.3 Hz, 1H), 3.02 (br. s, 1H, partially overlapped), 2.96 (br. s, 1H, partially overlapped), 2.78 – 2.63 (m, 1H), 2.60 – 2.46 (m, 1H), 2.46 – 2.35 (m, 1H), 2.14 – 2.03 (m, 1H), 1.93 – 1.83 (m, 1H) ppm. ^{13}C NMR (126 MHz, CDCl_3) δ = 172.7, 143.8, 138.2, 132.7, 128.8, 128.3, 128.1, 127.0, 117.8, 111.8, 110.6, 62.6, 53.1, 51.5, 49.9, 44.5, 28.7 ppm.

Methyl (\pm)-trans-1-benzyl-4-((2-bromophenyl)amino)piperidine-3-carboxylate [(\pm) trans-4a]

Obtained from **2a**. Yield: 1.36 g (36 %); colorless viscous oil; R_f =0.53. (SiO_2 ; petroleum ether/EtOAc, 9:1). IR (ATR): 3398, 3027, 2924, 2807, 1735, 1596, 1511, 1437, 1320, 1197, 1020, 743 cm^{-1} . ^1H NMR (500 MHz, CDCl_3) δ = 7.41 (dd, J = 7.9, 1.5 Hz, 1H), 7.37 – 7.32 (m, 4H), 7.33 – 7.26 (m, 1H), 7.20 – 7.11 (m, 1H), 6.75 – 6.69 (m, 1H), 6.60 – 6.53 (m, 1H), 4.31 (d, J = 8.9 Hz, 1H), 3.74 – 3.68 (m, 1H), 3.61 (s, 2H, partially overlapped), 3.59 (s, 3H, partially overlapped), 3.01 (d, J = 10.2 Hz, 1H), 2.90 (d, J = 11.4 Hz, 1H), 2.80 – 2.71 (m, 1H), 2.47 (t, J = 10.8, 10.8 Hz, 1H), 2.30 (t, J = 11.3, 11.3 Hz, 1H), 2.22 – 2.13 (m, 1H), 1.60 (d, J = 11.8 Hz, 1H) ppm. ^{13}C NMR (126 MHz, CDCl_3) δ = 173.1, 143.6, 137.1, 132.5, 129.1, 128.4, 128.3, 127.3, 118.1, 112.3, 110.3, 62.4, 54.0, 52.3, 51.8, 51.6, 48.3, 31.3 ppm.

Methyl (\pm)-cis-1-benzyl-4-((2-iodophenyl)amino)piperidine-3-carboxylate [(\pm) cis-4b]

Obtained from **3b**. Yield: 2.41 g (57 %); colorless viscous oil; R_f =0.39. (SiO_2 ; petroleum ether/EtOAc, 9:1). IR (ATR): 3381, 3026, 2804, 1733, 1588, 1508, 1454, 1319, 1215, 1005, 742, 700 cm^{-1} . ^1H NMR (500 MHz, CDCl_3) δ = 7.64 (dd, J = 7.8, 1.5 Hz, 1H), 7.32 – 7.25 (m, 4H), 7.26 – 7.21 (m, 1H), 7.18 – 7.12 (m, 1H), 6.59 – 6.54 (m, 1H), 6.40 (td, J = 7.6, 7.5, 1.5 Hz, 1H), 5.01 (s, 1H), 3.87 – 3.73 (m, 1H), 3.64 (s, 3H), 3.61 (d, J = 3.9 Hz, 1H), 3.58 (d, J = 4.7 Hz, 1H), 2.97 (br. s, 1H, partially overlapped), 2.95 – 2.87 (m, 1H, partially overlapped), 2.71 – 2.60 (m, 1H), 2.59 – 2.47 (m, 1H), 2.44 – 2.32 (m, 1H), 2.09 – 1.98 (m, 1H), 1.87 – 1.78 (m, 1H) ppm. ^{13}C NMR (126 MHz, CDCl_3) δ = 172.7, 146.1, 139.3, 138.2, 129.2, 128.8, 128.1, 127.1, 118.7, 111.2, 86.4, 62.7, 53.0, 51.6, 50.4, 44.6, 28.7 ppm.

Methyl (\pm)-trans-1-benzyl-4-((2-iodophenyl)amino)piperidine-3-carboxylate [(\pm) trans-4b]

Obtained from **3b**. Yield: 1.52 g (36 %); colorless oil; R_f =0.53. (SiO_2 ; petroleum ether/EtOAc, 9:1). IR (ATR): 3385, 2950, 2807, 1735, 1589, 1510, 1454, 1318, 1197, 1005, 743, 700 cm^{-1} . ^1H NMR (400 MHz, CDCl_3) δ = 7.66 – 7.58 (m, 1H), 7.37 – 7.27 (m, 4H), 7.30 – 7.21 (m, 1H), 7.21 – 7.12 (m, 1H), 6.68 – 6.61 (m, 1H), 6.46 – 6.37 (m, 1H), 4.14 (d, J = 8.7 Hz, 1H), 3.75 – 3.66 (m, 1H), 3.59 (s, 3H), 3.55 (d, J = 5.4 Hz, 2H), 2.94 (d, J = 6.4 Hz, 1H), 2.89 – 2.79

(m, 1H), 2.70 (td, $J = 9.5, 9.5, 3.6$ Hz, 1H), 2.43 (t, $J = 10.6, 10.6$ Hz, 1H), 2.27 (d, $J = 11.1$ Hz, 1H), 2.19 – 2.12 (m, 1H), 1.60 – 1.49 (m, 1H) ppm. ^{13}C NMR (101 MHz, CDCl_3) $\delta = 173.3, 146.0, 139.1, 138.0, 129.4, 128.9, 128.2, 127.1, 119.0, 111.7, 86.3, 62.5, 54.0, 52.7, 51.8, 48.4, 31.4$ ppm.

(±)-*cis*-1-benzyl-4-((2-bromophenyl)amino)piperidine-3-carboxamide [(±) *cis*-5a]

Obtained from *cis/trans*-4a mixture. Yield: 0.45 g (27 %); off-white solid; mp: 185-187°C; $R_f=0.45$. (SiO_2 ; $\text{CH}_2\text{Cl}_2/\text{MeOH}$, 95:5). IR (ATR): 3377, 3331, 3186, 2954, 2820, 1664, 1597, 1507, 1427, 1316, 745 cm^{-1} . ^1H NMR (400 MHz, CDCl_3) $\delta = 8.50$ (s, 1H), 7.40 (dd, $J = 7.8, 1.5$ Hz, 1H), 7.39 – 7.27 (m, 3H), 7.25 (dd, $J = 6.4, 2.0$ Hz, 2H), 7.16 – 7.07 (m, 1H), 6.57 – 6.46 (m, 2H), 6.09 (s, 1H), 5.61 (d, $J = 7.0$ Hz, 1H), 3.59 (d, $J = 12.7$ Hz, 1H), 3.56 – 3.48 (m, 1H, partially overlapped), 3.47 (d, $J = 12.8$ Hz, 1H, partially overlapped), 3.17 (d, $J = 12.1$ Hz, 1H), 3.01 (d, $J = 8.6$ Hz, 1H), 2.79 – 2.72 (m, 1H), 2.30 (dd, $J = 12.2, 2.9$ Hz, 1H), 2.21 (td, $J = 12.0, 11.9, 2.8$ Hz, 1H), 2.09 (d, $J = 10.5$ Hz, 1H), 1.66 (qd, $J = 12.3, 12.3, 12.3, 4.0$ Hz, 1H) ppm. ^{13}C NMR (101 MHz, CDCl_3) $\delta = 175.0, 143.7, 136.9, 132.8, 129.1, 128.6, 128.1, 127.7, 117.2, 110.7, 109.9, 62.8, 54.1, 52.3, 51.3, 44.6, 28.0$ ppm.

(±)-*trans*-1-benzyl-4-((2-bromophenyl)amino)piperidine-3-carboxamide [(±) *trans*-5a]

Obtained from *cis/trans*-4a mixture. Yield: 0.84 g (49 %); off-white solid; mp: 124-126°C; $R_f=0.40$. (SiO_2 ; $\text{CH}_2\text{Cl}_2/\text{MeOH}$, 95:5). IR (ATR): 3327, 3175, 2954, 2811, 1667, 1593, 1516, 1410, 1326, 736 cm^{-1} . ^1H NMR (400 MHz, DMSO) $\delta = 7.39$ (s, 1H), 7.38 – 7.31 (m, 1H), 7.35 – 7.20 (m, 5H), 7.15 – 7.06 (m, 1H), 6.85 (s, 1H), 6.79 – 6.72 (m, 1H), 6.52 – 6.43 (m, 1H), 4.46 (d, $J = 8.5$ Hz, 1H), 3.52 – 3.43 (m, 3H, overlapped CH-H with $\text{PhCH}_2\text{-H}$), 2.83 (d, $J = 10.0$ Hz, 1H), 2.76 (d, $J = 12.3$ Hz, 1H), 2.58 (td, $J = 10.6, 10.6, 3.8$ Hz, 1H), 2.14 (t, $J = 11.1, 11.1$ Hz, 1H, partially overlapped), 2.11 – 2.03 (m, 1H, partially overlapped), 1.96 (d, $J = 12.9$ Hz, 1H), 1.30 (qd, $J = 12.2, 12.2, 12.2, 3.9$ Hz, 1H) ppm. ^{13}C NMR (101 MHz, DMSO) $\delta = 174.3, 144.4, 138.7, 132.8, 129.4, 129.1, 128.7, 127.5, 117.8, 112.7, 109.2, 62.2, 55.8, 52.4, 52.2, 49.0, 31.5$ ppm.

(±)-*cis*-1-benzyl-4-((2-iodophenyl)amino)piperidine-3-carboxamide [(±) *cis*-5b]

Obtained from *cis/trans*-4b mixture. Yield: 0.58 g (30 %); off-white solid; mp: 197-199°C; $R_f=0.45$. (SiO_2 ; $\text{CH}_2\text{Cl}_2/\text{MeOH}$, 95:5). IR (ATR): 3410, 3334, 3273, 2951, 2804, 1637, 1582, 1510, 1313, 746, 649 cm^{-1} . ^1H NMR (400 MHz, CDCl_3) $\delta = 8.48$ (s, 1H), 7.68 – 7.60 (m, 1H), 7.38 – 7.21 (m, 5H), 7.19 – 7.09 (m, 1H), 6.49 – 6.42 (m, 1H), 6.42 – 6.33 (m, 1H), 5.85 (s, 1H), 5.44 (d, $J = 7.0$ Hz, 1H), 3.59 (d, $J = 12.7$ Hz, 1H), 3.57 – 3.48 (m, 1H, partially overlapped), 3.47 (d, $J = 12.8$ Hz, 1H, partially overlapped), 3.17 (d, $J = 12.2$ Hz, 1H), 3.00 (d, $J = 11.5$ Hz, 1H), 2.80 – 2.73 (m, 1H), 2.30 (dd, $J = 12.2, 2.9$ Hz, 1H), 2.20 (td, $J = 11.9, 11.9, 2.8$ Hz, 1H), 2.09 (dd, $J = 13.7, 3.4$ Hz, 1H), 1.65 (qd, $J = 12.2, 12.2, 12.1, 4.0$ Hz, 1H) ppm. ^{13}C NMR (101 MHz, CDCl_3) $\delta = 174.8, 146.1,$

139.6, 137.0, 129.2, 129.0, 128.6, 127.7, 118.1, 110.1, 85.3, 62.9, 54.2, 52.3, 51.9, 44.6, 28.0 ppm.

(±)-trans-1-benzyl-4-((2-iodophenyl)amino)piperidine-3-carboxamide [(±) trans-5b]

Obtained from *cis/trans-4b* mixture. Yield: 1.05 g (55 %); off-white solid; mp: 118-120°C; $R_f=0.40$. (SiO₂; CH₂Cl₂/MeOH, 95:5). IR (ATR): 3383, 3324, 3206, 2943, 2801, 1682, 1671, 1589, 1508, 1452, 1321, 735, 702 cm⁻¹. ¹H NMR (400 MHz, DMSO) δ = 7.56 (dd, J = 7.8, 1.5 Hz, 1H), 7.43 (s, 1H), 7.33 – 7.18 (m, 5H), 7.16 – 7.07 (m, 1H), 6.86 (s, 1H), 6.69 – 6.62 (m, 1H), 6.38 – 6.29 (m, 1H), 4.15 (d, J = 8.3 Hz, 1H), 3.53 – 3.42 (m, 3H, overlapped CH₂-H with PhCH₂-H), 2.82 (d, J = 9.3 Hz, 1H), 2.74 (d, J = 11.7 Hz, 1H), 2.55 (td, J = 10.4, 10.4, 3.7 Hz, 1H), 2.14 (t, J = 11.2, 11.2 Hz, 1H, partially overlapped), 2.13 – 2.01 (m, 1H, partially overlapped), 2.03 – 1.92 (m, 1H), 1.33 – 1.22 (m, 1H) ppm. ¹³C NMR (101 MHz, DMSO) δ = 174.1, 146.7, 139.3, 138.7, 129.8, 129.3, 128.7, 127.4, 118.8, 112.0, 86.0, 62.2, 55.7, 52.7, 52.1, 49.2, 31.5 ppm.

(±)-cis-1-benzyl-4-(N-(2-bromophenyl)propionamido)piperidine-3-carboxamide [(±) cis-9a]

Obtained from *cis-5a*. Yield: 0.38 g (78 %); off-white solid; mp: 189-191°C; $R_f=0.54$. (SiO₂; CH₂Cl₂/MeOH, 95:5). IR (ATR): 3378, 3176, 2939, 2761, 1681, 1646, 1472, 1384, 1267, 729, 699 cm⁻¹. ¹H NMR (400 MHz, CDCl₃) δ = 8.65 (s, 1H), 7.60 – 7.53 (m, 1H), 7.55 – 7.48 (m, 1H), 7.34 – 7.12 (m, 7H), 5.65 (s, 1H), 4.50 (dt, J = 13.3, 4.9, 4.9 Hz, 1H), 3.58 – 3.53 (m, 1H), 3.43 (q, J = 12.8, 12.8, 12.8 Hz, 2H), 3.07 (d, J = 12.2 Hz, 1H), 2.86 (d, J = 9.6 Hz, 1H), 2.37 (dd, J = 12.3, 3.1 Hz, 1H), 2.09 (td, J = 11.8, 11.8, 2.9 Hz, 1H), 1.93 – 1.77 (m, J = 7.7, 7.7, 7.1, 7.1, 7.1, 7.1, 7.1 Hz, 2H), 1.47 – 1.37 (m, 1H), 1.30 (qd, J = 12.9, 12.9, 12.8, 4.2 Hz, 1H), 1.02 (t, J = 7.4, 7.4 Hz, 3H) ppm. ¹³C NMR (101 MHz, CDCl₃) δ = 175.4, 174.1, 139.2, 137.0, 133.1, 132.9, 129.7, 129.0, 128.6, 128.5, 127.5, 126.7, 62.6, 55.4, 54.1, 52.4, 42.9, 28.6, 25.4, 9.1 ppm.

(±)-trans-1-benzyl-4-(N-(2-bromophenyl)propionamido)piperidine-3-carboxamide [(±) trans-9a]

Due to impurities that could not be successfully separated by recrystallization or chromatography, the structure of compound *trans-9a* was determined by comparing the spectroscopic data of crude product with those for *cis-9a*, *cis-9b* and *trans-9b*, and by performing the Hofmann rearrangement that yielded corresponding carbamate *trans-10a*. For this reasons the spectroscopic data of *trans-9a* are omitted from supplemental material, while approximate yield was determined by TLC.

(±)-cis-1-benzyl-4-(N-(2-iodophenyl)propionamido)piperidine-3-carboxamide [(±) cis-9b]

Obtained from *cis-5b*. Yield: 0.51 g (94 %); off-white solid; mp: 173-175°C; $R_f=0.54$. (SiO₂; CH₂Cl₂/MeOH, 95:5). IR (ATR): 3379, 3059, 2934, 2817, 1661, 1638, 1465, 1379, 1283, 745, 676 cm⁻¹. ¹H NMR (400 MHz, CDCl₃) δ = 8.61 (s, 1H), 7.79 (dd, J = 7.9, 1.4 Hz, 1H), 7.49 (dd, J = 7.9, 1.6 Hz, 1H), 7.30 (td, J = 7.6, 7.6, 1.5 Hz, 1H), 7.29 – 7.16 (m, 3H), 7.17 – 7.10 (m, 2H), 6.98 (td, J = 7.6,

7.6, 1.6 Hz, 1H), 5.73 (s, 1H), 4.44 (dt, $J = 13.3, 4.8, 4.8$ Hz, 1H), 3.63 – 3.55 (m, 1H), 3.43 (q, 2H), 3.06 (d, $J = 12.3$ Hz, 1H), 2.88 – 2.80 (m, 1H), 2.35 (dd, $J = 12.3, 3.2$ Hz, 1H), 2.07 (td, $J = 11.9, 11.8, 2.9$ Hz, 1H), 1.92 – 1.73 (m, 2H), 1.42 – 1.35 (m, 1H), 1.26 (qd, $J = 12.9, 12.9, 12.9, 4.2$ Hz, 1H), 1.02 (t, $J = 7.4, 7.4$ Hz, 3H) ppm. ^{13}C NMR (101 MHz, CDCl_3) $\delta = 175.4, 173.8, 142.7, 139.1, 137.0, 132.4, 129.6, 129.4, 129.0, 128.4, 127.5, 104.9, 62.6, 55.3, 54.1, 52.4, 42.5, 29.1, 25.9, 9.1$ ppm.

(±)-*trans*-1-benzyl-4-(*N*-(2-iodophenyl)propionamido)piperidine-3-carboxamide [(±) *trans*-9b]

Obtained from *trans*-5b. Yield: 0.48 g (89 %); off-white solid; mp: 205–208°C; $R_f=0.32$. (SiO_2 ; $\text{CH}_2\text{Cl}_2/\text{MeOH}$, 95:5). IR (ATR): 3385, 3183, 3064, 2939, 2811, 1651, 1465, 1368, 1259, 733, 697 cm^{-1} . ^1H NMR (400 MHz, CDCl_3) $\delta = 7.93$ (dd, $J = 8.0, 1.4$ Hz, 1H), 7.47 – 7.40 (m, 1H), 7.41 – 7.33 (m, 1H), 7.28 – 7.18 (m, 3H), 7.22 – 7.13 (m, 3H), 7.09 – 7.01 (m, 1H), 6.78 (s, 1H), 5.67 (s, 1H), 5.10 (td, $J = 11.9, 11.9, 4.1$ Hz, 1H), 3.48 – 3.37 (m, 2H), 3.23 – 3.14 (m, 1H), 2.67 (td, $J = 11.5, 11.4, 3.7$ Hz, 1H), 2.31 – 2.24 (m, 1H), 2.16 (t, $J = 11.1, 11.1$ Hz, 1H), 2.12 – 2.00 (m, 2H), 1.87 – 1.74 (m, 1H), 1.27 – 1.12 (m, 1H), 0.98 (t, $J = 7.4, 7.4$ Hz, 3H) ppm. ^{13}C NMR (101 MHz, CDCl_3) $\delta = 175.3, 174.7, 140.7, 140.5, 137.4, 131.2, 130.0, 129.9, 129.0, 128.2, 127.1, 103.6, 62.4, 57.1, 53.9, 52.5, 50.6, 29.0, 28.3, 9.6$ ppm.

Methyl (±)-*trans*-[1-benzyl-4-(2-bromophenyl)amino]piperidin-3-yl]carbamate [(±) *trans*-6a]

Obtained from *trans*-5a. Yield: 0.28 g (66 %); pale-yellow viscous oil; $R_f=0.86$. (SiO_2 ; petroleum ether/EtOAc, 6:4). IR (ATR): 3388, 2947, 2809, 1718, 1595, 1506, 1457, 1322, 1239, 1066, 739 cm^{-1} . ^1H NMR (500 MHz, CDCl_3) $\delta = 7.48$ – 7.43 (m, 1H), 7.34 (ddd, $J = 25.4, 13.1, 7.1$ Hz, 5H), 7.26 (t, $J = 7.8, 7.8$ Hz, 1H), 7.04 (s, 1H), 6.61 (t, $J = 7.4, 7.4$ Hz, 1H), 5.40 (br. s, 1H), 4.58 (d, $J = 7.1$ Hz, 1H), 3.93 – 3.86 (m, 1H), 3.74 (s, 3H), 3.62 – 3.51 (m, 3H, overlapped $\text{CH}_2\text{-H}$ with $\text{PhCH}_2\text{-H}$), 2.88 – 2.71 (m, 1H), 2.69 – 2.55 (m, 1H), 2.53 – 2.41 (m, 2H), 2.33 – 2.18 (m, 1H), 1.72 – 1.62 (m, 1H) ppm. ^{13}C NMR (126 MHz, CDCl_3) $\delta = 156.6, 143.5, 137.9, 132.4, 128.9, 128.3, 127.3, 117.8, 111.9, 109.8, 62.7, 54.3, 52.1, 49.4, 27.9$ ppm.

Methyl (±)-*trans*-[1-benzyl-4-(*N*-(2-bromophenyl)propionamido)piperidin-3-yl]carbamate [(±) *trans*-10a]

Obtained from *trans*-9a. Yield: 0.26 g (55 %); off-white solid; mp 129–134°C; $R_f=0.58$. (SiO_2 ; petroleum ether/EtOAc, 6:4). IR (ATR): 3367, 2937, 2871, 1719, 1657, 1513, 1455, 1377, 1253, 1035, 743, 700 cm^{-1} . ^1H NMR (400 MHz, CDCl_3) $\delta = 7.64$ (d, $J = 8.1$ Hz, 1H), 7.45 – 7.39 (m, 2H), 7.28 – 7.16 (m, 6H), 5.44 (d, $J = 8.9$ Hz, 1H), 4.68 (td, $J = 12.0, 11.7, 4.0$ Hz, 1H), 3.89 – 3.76 (m, 1H), 3.63 (s, 3H), 3.52 (d, $J = 13.3$ Hz, 1H), 3.37 (d, $J = 13.0$ Hz, 1H), 3.16 (d, $J = 10.8$ Hz, 1H), 2.72 (d, $J = 11.1$ Hz, 1H), 2.11 – 1.98 (m, 2H, partially overlapped), 1.94 (t, $J = 10.6, 10.6$ Hz, 3H, partially overlapped), 1.89 – 1.80 (m,

1H, partially overlapped), 0.99 (t, $J = 7.4$, 7.4 Hz, 3H) ppm. ^{13}C NMR (101 MHz, CDCl_3) $\delta = 176.1, 157.0, 138.0, 137.6, 133.7, 131.5, 129.9, 129.3, 128.9, 128.1, 127.1, 125.9, 62.2, 58.8, 55.9, 52.8, 52.0, 51.7, 28.2, 27.0, 9.6$ ppm.

Methyl (±)-cis-[1-benzyl-4-(N-(2-iodophenyl)propionamido)piperidin-3-yl]carbamate [(±) cis-10b]

Obtained from *cis-9b*. Yield: 0.39 g (73 %); yellow amorphous solid; $R_f=0.60$. (SiO_2 ; petroleum ether/EtOAc, 6:4). IR (ATR): 3422, 3027, 2938, 1729, 1667, 1501, 1465, 1375, 1259, 1088, 734, 701 cm^{-1} . ^1H NMR (400 MHz, DMSO) $\delta = 7.92$ (dd, $J = 7.9, 1.4$ Hz, 1H), 7.49 (td, $J = 7.6, 7.6, 1.5$ Hz, 1H), 7.38 – 7.31 (m, 2H), 7.27 (t, $J = 7.4, 7.4$ Hz, 2H), 7.25 – 7.16 (m, 3H), 7.14 (td, $J = 7.7, 7.6, 1.5$ Hz, 1H), 6.84 (d, $J = 10.0$ Hz, 1H), 4.54 (d, $J = 9.9$ Hz, 1H), 4.11 (d, $J = 13.1$ Hz, 1H), 3.61 (s, 3H), 3.48 – 3.35 (m, 2H), 2.69 (d, $J = 11.3$ Hz, 2H, overlapped $\text{CH}_2\text{-H}$ with $\text{CH}_2\text{-H}$), 2.24 (d, $J = 11.5$ Hz, 1H), 1.94 (t, $J = 11.5, 11.5$ Hz, 1H), 1.73 – 1.58 (m, 2H), 1.33 – 1.24 (m, 1H), 1.12 – 0.99 (m, 0H), 0.88 (t, $J = 7.4, 7.4$ Hz, 3H) ppm. ^{13}C NMR (101 MHz, DMSO) $\delta = 172.3, 156.7, 142.6, 139.1, 138.3, 131.4, 129.9, 129.4, 128.5, 128.0, 126.8, 105.4, 61.3, 56.7, 55.7, 52.1, 51.5, 46.7, 28.5, 24.5, 9.2$ ppm.

Methyl (±)-trans-[1-benzyl-4-(N-(2-iodophenyl)propionamido)piperidin-3-yl]carbamate [(±) trans-10b]

Obtained from *trans-9b*. Yield: 0.32 g (60 %); yellow amorphous solid; $R_f=0.58$. (SiO_2 ; petroleum ether/EtOAc, 6:4). IR (ATR): 3310, 3054, 2937, 1722, 1650, 1543, 1495, 1464, 1391, 1274, 1046, 742, 698 cm^{-1} . ^1H NMR (400 MHz, CDCl_3) $\delta = 7.93 - 7.86$ (m, 1H), 7.50 – 7.38 (m, 2H), 7.27 – 7.20 (m, 2H), 7.22 – 7.15 (m, 3H), 7.10 – 7.01 (m, 1H), 5.47 (d, $J = 8.9$ Hz, 1H), 4.67 (td, $J = 11.9, 11.8, 4.0$ Hz, 1H), 3.85 (qd, $J = 10.5, 10.5, 10.5, 4.2$ Hz, 1H), 3.62 (s, 3H), 3.52 (d, $J = 13.1$ Hz, 1H), 3.38 (d, $J = 13.1$ Hz, 1H), 3.19 – 3.10 (m, 1H), 2.72 (d, $J = 8.5$ Hz, 1H), 2.11 – 2.03 (m, 1H, partially overlapped), 2.03 – 1.99 (m, 2H, partially overlapped), 1.99 – 1.92 (m, 2H, partially overlapped), 1.90 – 1.78 (m, 1H), 0.99 (t, $J = 7.5, 7.5$ Hz, 3H) ppm. ^{13}C NMR (101 MHz, CDCl_3) $\delta = 176.2, 157.0, 141.4, 140.2, 137.4, 130.7, 130.2, 129.9, 129.0, 128.2, 127.1, 103.8, 62.1, 58.7, 55.9, 53.0, 52.0, 51.7, 28.9, 27.4, 9.7$ ppm.

(±)-trans-1-benzyl- N^4 -(2-bromophenyl)piperidine-3,4-diamine [(±) trans-7a]

Obtained from *trans-6a*. Yield: 0.074 g (93 %); dark-brown viscous oil; $R_f=0.25$. (SiO_2 ; $\text{CH}_2\text{Cl}_2/\text{MeOH}$, 95:5). IR (ATR): 3357, 3027, 2924, 2805, 1595, 1508, 1458, 1320, 1124, 1016, 743 cm^{-1} . ^1H NMR (500 MHz, CDCl_3) $\delta = 7.41$ (dd, $J = 7.9, 1.5$ Hz, 1H), 7.36 – 7.28 (m, 4H), 7.30 – 7.23 (m, 1H), 7.18 – 7.11 (m, 1H), 6.77 – 6.71 (m, 1H), 6.55 (td, $J = 7.7, 7.6, 1.5$ Hz, 1H), 4.20 (d, $J = 8.9$ Hz, 1H), 3.54 (q, $J = 13.1, 13.1, 13.1$ Hz, 2H), 3.14 – 3.05 (m, 1H), 2.98 (d, $J = 11.5$ Hz, 1H), 2.90 (td, $J = 8.9, 8.9, 4.0$ Hz, 1H), 2.85 – 2.79 (m, 1H), 2.21 – 2.13 (m, 1H), 2.13 – 2.04 (m, 1H), 2.00 (t, $J = 10.1, 10.1$ Hz, 1H), 1.74 (br. s, 2H),

1.56 – 1.44 (m, 1H) ppm. ^{13}C NMR (126 MHz, CDCl_3) δ = 144.6, 138.1, 132.6, 129.0, 128.4, 128.2, 127.1, 118.0, 112.2, 110.5, 62.7, 60.0, 57.8, 53.3, 52.2, 30.8 ppm.

(±)-trans-N-(3-amino-1-benzylpiperidin-4-yl)-N-(2-bromophenyl)propionamide [(±) trans-11a]

Obtained from *trans-10a*. Yield: 0.089 g (97 %); pale-yellow viscous oil; $R_f=0.2$. (SiO_2 ; $\text{CH}_2\text{Cl}_2/\text{MeOH}$, 95:5). IR (ATR): 2934, 2807, 1655, 1581, 1471, 1374, 1259, 1028, 734, 699 cm^{-1} . ^1H NMR (400 MHz, CDCl_3) δ = 7.69 – 7.61 (m, 2H), 7.45 – 7.36 (m, 1H), 7.30 – 7.18 (m, 6H), 4.80 – 4.69 (m, 1H), 3.68 (br. s, 2H), 3.57 – 3.48 (m, 2H), 3.16 (d, J = 10.9 Hz, 1H), 3.08 (td, J = 10.4, 10.4, 4.2 Hz, 1H), 2.84 – 2.76 (m, 1H), 2.25 – 2.11 (m, 2H), 2.09 – 1.96 (m, 3H), 1.21 – 1.11 (m, 1H), 1.04 (t, J = 7.3, 7.3 Hz, 3H) ppm. ^{13}C NMR (101 MHz, CDCl_3) δ = 176.0, 137.7, 136.7, 133.8, 132.2, 130.0, 129.3, 129.1, 128.3, 127.4, 125.9, 62.1, 60.1, 57.9, 52.0, 51.7, 28.5, 27.1, 9.5 ppm.

(±)-cis-N-(3-amino-1-benzylpiperidin-4-yl)-N-(2-iodophenyl)propionamide [(±) cis-11b]

Obtained from *cis-10b*. Yield: 0.09 g (97 %); pale-yellow viscous oil; $R_f=0.2$. (SiO_2 ; $\text{CH}_2\text{Cl}_2/\text{MeOH}$, 95:5). IR (ATR): 3375, 3059, 3027, 2931, 2808, 1659, 1577, 1466, 1377, 1274, 733, 700 cm^{-1} . ^1H NMR (400 MHz, CDCl_3) δ = 7.88 (dd, J = 7.9, 1.6 Hz, 1H), 7.82 (dd, J = 7.9, 1.4 Hz, 1H), 7.38 (td, J = 7.7, 7.6, 1.4 Hz, 1H), 7.30 – 7.21 (m, 4H), 7.22 – 7.17 (m, 1H), 7.06 – 6.98 (m, 1H), 4.10 (dt, J = 13.3, 3.9, 3.9 Hz, 1H), 3.91 (s, 1H), 3.52 – 3.33 (m, 4H, overlapped $\text{PhCH}_2\text{-H}$ with $\text{NH}_2\text{-H}$), 2.86 (dt, J = 11.7, 2.9, 2.9 Hz, 1H), 2.79 – 2.71 (m, 1H), 2.35 (dd, J = 11.8, 1.9 Hz, 1H), 2.03 – 1.95 (m, 1H), 1.87 (q, J = 7.4, 7.4, 7.4 Hz, 2H), 1.50 – 1.36 (m, 1H), 1.31 – 1.22 (m, 1H), 1.00 (t, J = 7.4, 7.4 Hz, 3H) ppm. ^{13}C NMR (101 MHz, CDCl_3) δ = 174.5, 143.9, 139.3, 138.0, 132.4, 129.6, 129.2, 128.9, 128.2, 127.1, 104.1, 62.3, 59.3, 58.8, 52.6, 47.4, 29.4, 24.5, 9.2 ppm.

(±)-trans-N-(3-amino-1-benzylpiperidin-4-yl)-N-(2-iodophenyl)propionamide [(±) trans-11b]

Obtained from *trans-10b*. Yield: 0.10 g (98 %); pale-yellow viscous oil; $R_f=0.2$. (SiO_2 ; $\text{CH}_2\text{Cl}_2/\text{MeOH}$, 95:5). IR (ATR): 3366, 3059, 3027, 2935, 2805, 1658, 1577, 1467, 1376, 1260, 749, 700 cm^{-1} . ^1H NMR (400 MHz, CDCl_3) δ = 7.95 – 7.88 (m, 1H), 7.59 – 7.52 (m, 1H), 7.45 – 7.37 (m, 1H), 7.29 – 7.15 (m, 5H), 7.09 – 7.00 (m, 1H), 4.75 – 4.64 (m, 1H), 3.46 (s, 2H), 3.03 (d, J = 12.4 Hz, 1H), 2.87 (td, J = 10.4, 10.4, 4.3 Hz, 1H), 2.79 (d, J = 11.8 Hz, 1H), 2.61 (br. s, 2H), 2.18 – 2.10 (m, 1H, partially overlapped), 2.10 – 1.98 (m, 3H, partially overlapped), 1.99 – 1.86 (m, 1H, partially overlapped), 1.17 – 1.08 (m, 1H, partially overlapped), 1.05 (t, J = 7.5, 7.5 Hz, 3H, partially overlapped) ppm. ^{13}C NMR (101 MHz, CDCl_3) δ = 175.5, 141.4, 140.3, 137.5, 131.3, 129.8, 129.7, 129.1, 128.2, 127.2, 104.0, 77.3, 77.0, 76.7, 62.4, 61.5, 58.6, 52.5, 52.0, 29.0, 27.8, 9.6 ppm.

(±)-trans-2-benzyl-1,2,3,4,4a,5,10,10a-octahydropyrido[3,4-b]quinoxaline [(±) trans-8]

Obtained from *trans-7a*. Yield: 0.014 g (29 %); dark-brown viscous oil; $R_f=0.47$. (SiO₂; CH₂Cl₂/MeOH, 95:5) IR (ATR): 3353, 2926, 2853, 2806, 1599, 1505, 1462, 1368, 1303, 742 cm⁻¹. ¹H NMR (500 MHz, CDCl₃) δ = 7.39 – 7.33 (m, 4H), 7.33 – 7.26 (m, 1H), 6.64 – 6.58 (m, 2H), 6.56 – 6.52 (m, 1H), 6.52 – 6.48 (m, 1H), 3.69 (d, J = 13.0 Hz, 1H), 3.58 (d, J = 13.1 Hz, 1H, partially overlapped), 3.51 (br. s, 2H, partially overlapped), 3.23 – 3.15 (m, 1H), 3.05 – 2.96 (m, 2H, partially overlapped), 2.99 – 2.92 (m, 1H, partially overlapped), 2.25 (td, J = 12.1, 12.0, 2.7 Hz, 1H), 1.93 (t, J = 10.5, 10.5 Hz, 1H, partially overlapped), 1.91 – 1.83 (m, 1H, partially overlapped), 1.69 (td, J = 12.1, 11.9, 4.0 Hz, 1H) ppm. ¹³C NMR (126 MHz, CDCl₃) δ = 137.6, 133.8, 133.6, 129.2, 128.3, 127.3, 119.1, 119.1, 115.0, 114.9, 62.5, 56.7, 54.1, 53.0, 52.0, 30.5 ppm. HRMS (HESI-OT): m/z [M + H]⁺ calcd for C₁₈H₂₁N₃: 280.18082; found: 280.18112.

(±)-cis-1-(2-benzyl-2,3,4,4a,10,10a-hexahydropyrido[3,4-b]quinoxalin-5(1H)-yl)propan-1-one [(±) cis-12]

Obtained from *cis-11b*. Yield: 0.032 g (58 %); pale-yellow viscous oil; $R_f=0.5$. (SiO₂; CH₂Cl₂/MeOH, 95:5) IR (ATR): 3357, 2934, 2808, 1649, 1502, 1379, 1318, 745 cm⁻¹. ¹H NMR (400 MHz, CDCl₃) δ = 7.37 – 7.14 (m, 6H), 7.04 – 6.93 (m, 1H), 6.76 – 6.61 (m, 2H), 4.85 (s, 1H), 3.85 (s, 1H), 3.55 (d, J = 13.2 Hz, 1H), 3.45 (d, J = 13.2 Hz, 1H, partially overlapped), 3.38 (s, 1H, partially overlapped), 2.88 (d, J = 12.5 Hz, 1H, partially overlapped), 2.85 – 2.77 (m, 1H, partially overlapped), 2.70 – 2.56 (m, 1H, partially overlapped), 2.58 – 2.44 (m, 1H, partially overlapped), 2.35 (dd, J = 12.5, 2.2 Hz, 1H), 2.14 (td, J = 11.6, 11.5, 3.6 Hz, 1H), 1.51 – 1.35 (m, 2H), 1.13 (t, J = 7.4, 7.4 Hz, 3H) ppm. ¹³C NMR (101 MHz, CDCl₃) δ = 173.3, 138.0, 134.7, 128.9, 128.4, 127.3, 126.0, 125.3, 121.8, 116.7, 115.2, 62.3, 56.5, 52.2, 50.3, 44.5, 27.9, 24.7, 10.1 ppm. HRMS (HESI-OT): m/z [M + H]⁺ calcd for C₂₁H₂₅N₃O: 336.20704; found: 336.20618.

(±)-trans-1-(2-benzyl-2,3,4,4a,10,10a-hexahydropyrido[3,4-b]quinoxalin-5(1H)-yl)propan-1-one [(±) trans-12]

Obtained from *trans-11b*. Yield: 0.026 g (47 %); pale-yellow viscous oil; $R_f=0.5$. (SiO₂; CH₂Cl₂/MeOH, 95:5) IR (ATR): 3310, 2928, 2803, 1654, 1501, 1368, 1281, 746 cm⁻¹. ¹H NMR (400 MHz, CDCl₃) δ = 7.32 – 7.26 (m, 4H), 7.27 – 7.20 (m, 1H), 7.10 – 7.03 (m, 1H), 7.00 – 6.91 (m, 1H), 6.79 – 6.71 (m, 1H), 6.66 – 6.59 (m, 1H), 3.70 – 3.58 (m, 2H, overlapped PhCH₂-H with CH-H), 3.45 (d, J = 13.1 Hz, 2H, overlapped PhCH₂-H with NH-H), 3.07 (td, J = 10.4, 10.4, 3.6 Hz, 1H), 3.04 – 2.92 (m, 2H), 2.61 – 2.50 (m, 1H), 2.53 – 2.40 (m, 1H), 2.41 – 2.30 (m, 1H), 2.26 (td, J = 11.9, 11.7, 2.7 Hz, 1H), 2.09 (t, J = 10.1, 10.1 Hz, 1H), 1.94 (qd, J = 12.1, 12.1, 12.1, 3.9 Hz, 1H), 1.04 (t, J = 7.3, 7.3 Hz, 3H) ppm. ¹³C NMR (101 MHz, CDCl₃) δ = 175.4, 142.7, 138.3, 129.0, 128.9, 128.3,

127.1, 125.4, 125.3, 118.8, 115.6, 65.5, 62.2, 58.6, 57.5, 53.0, 30.1, 28.8, 9.7 ppm. HRMS (HESI-OT): m/z $[M + H]^+$ calcd for $C_{21}H_{25}N_3O$: 336.20704; found: 336.20703.

SPECTRA OF THE FINAL COMPOUNDS

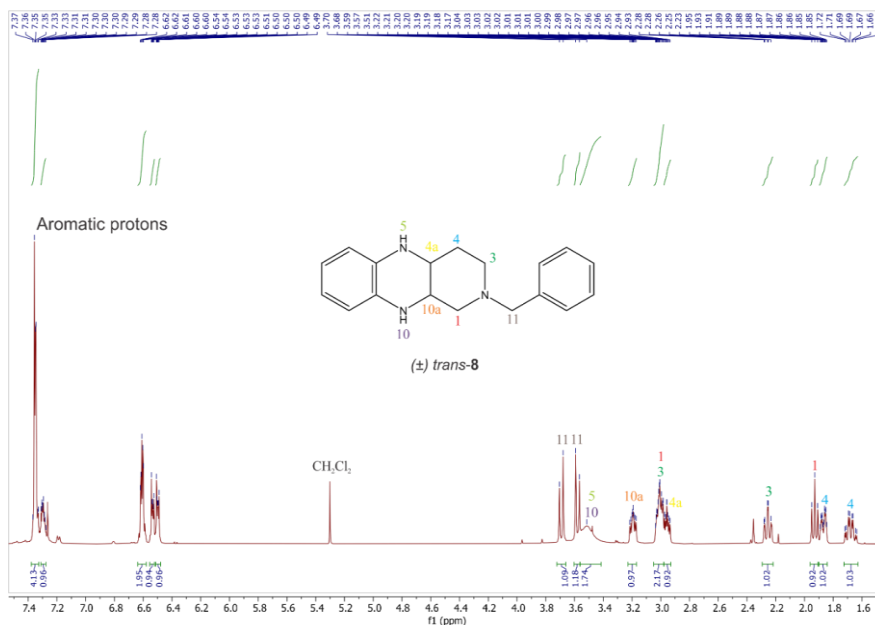
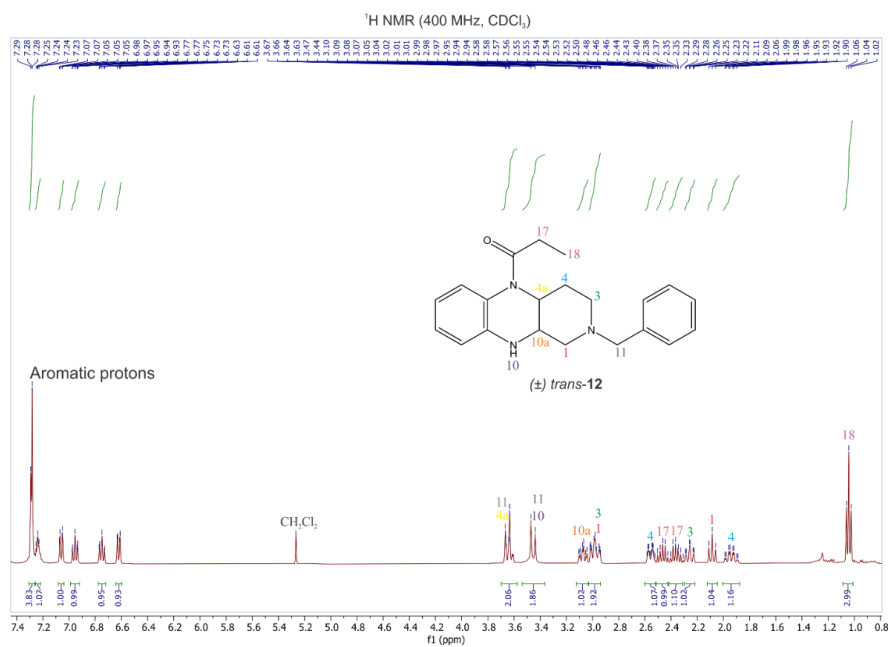
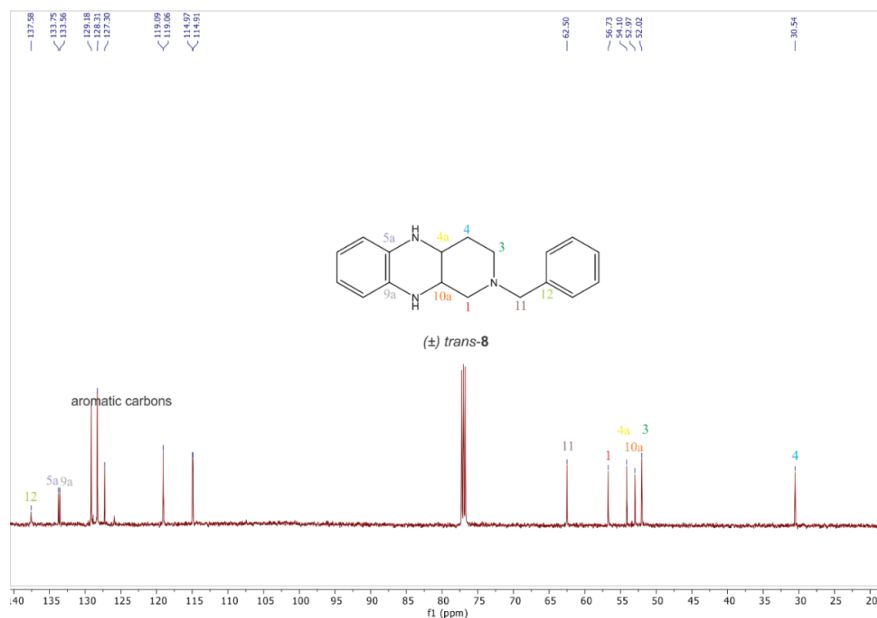


Figure S-1. ^1H NMR of (\pm) -*trans*-2-benzyl-1,2,3,4,4a,5,10,10a-octahydro-pyrido[3,4-b]quinoxaline [(\pm) *trans*-8].



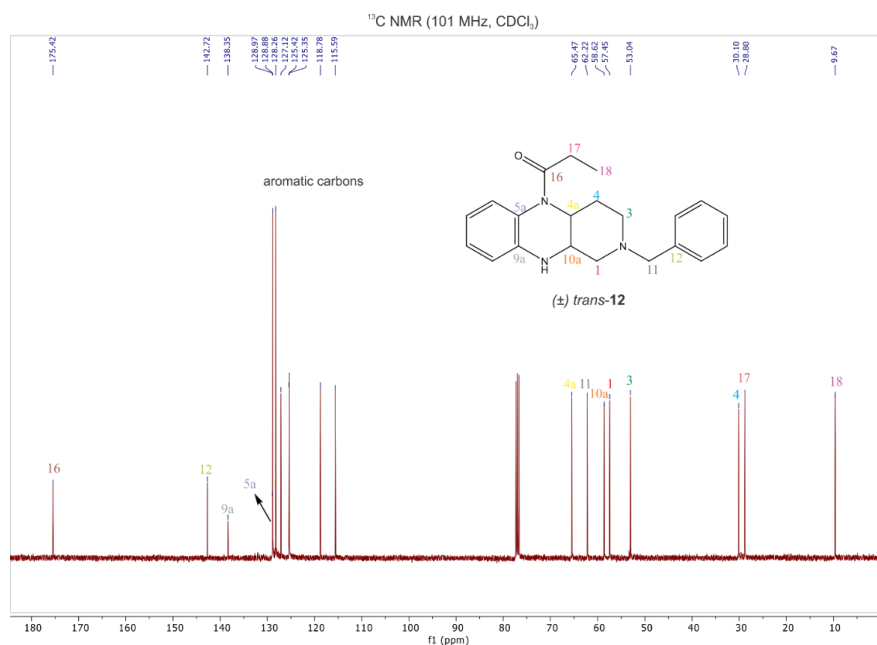


Figure S-4. ¹³C NMR of (±)-*trans*-1-(2-benzyl-2,3,4,4a,10,10a-hexahydro-pyrido[3,4-*b*]quinoxalin-5(1H)-yl)propan-1-one [(±) *trans*-12]

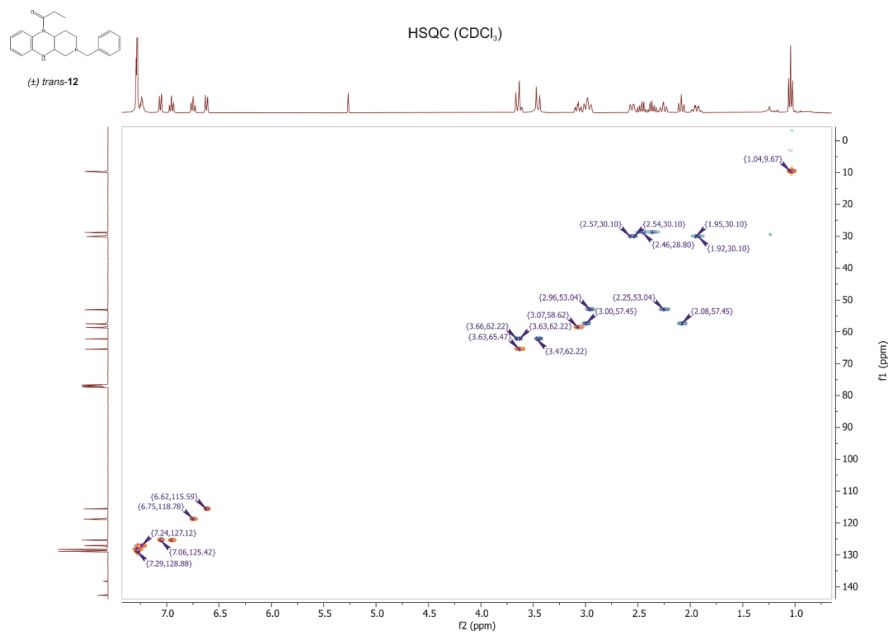


Figure S-5. HSQC of (±)-*trans*-1-(2-benzyl-2,3,4,4a,10,10a-hexahydro-pyrido[3,4-*b*]quinoxalin-5(1H)-yl)propan-1-one [(±) *trans*-12]

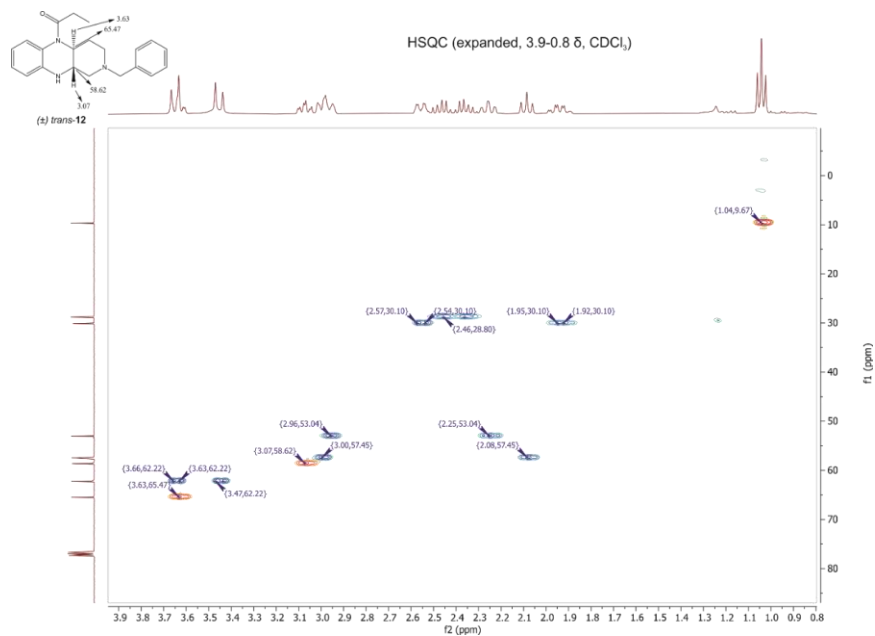


Figure S-6. Expanded HSQC of (\pm)-*trans*-1-(2-benzyl-2,3,4,4a,10,10a-hexahydro-pyrido[3,4-b]quinoxalin-5(1H)-yl)propan-1-one [(\pm) *trans*-**12**]

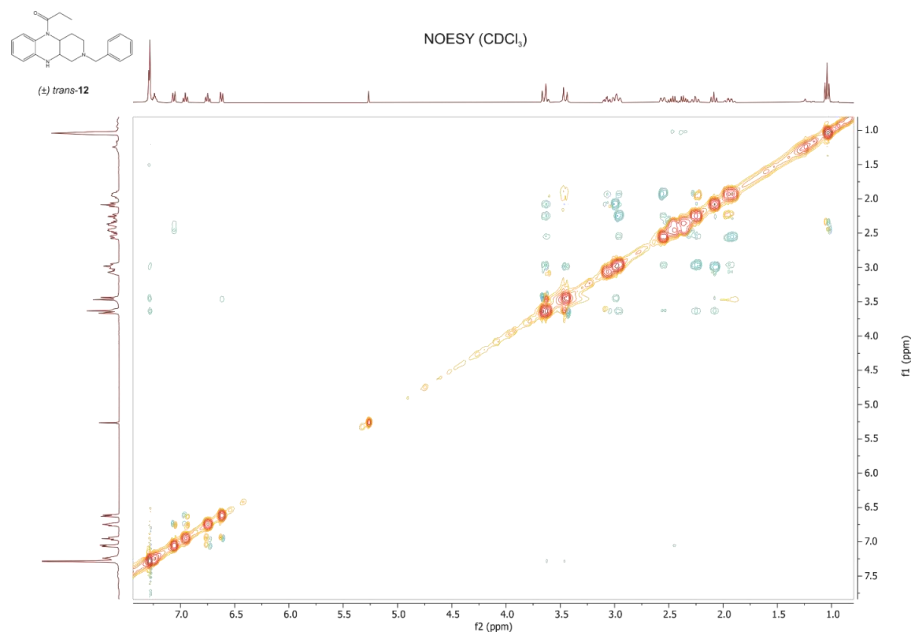


Figure S-7. NOESY of (\pm)-*trans*-1-(2-benzyl-2,3,4,4a,10,10a-hexahydro-pyrido[3,4-b]quinoxalin-5(1H)-yl)propan-1-one [(\pm) *trans*-**12**]

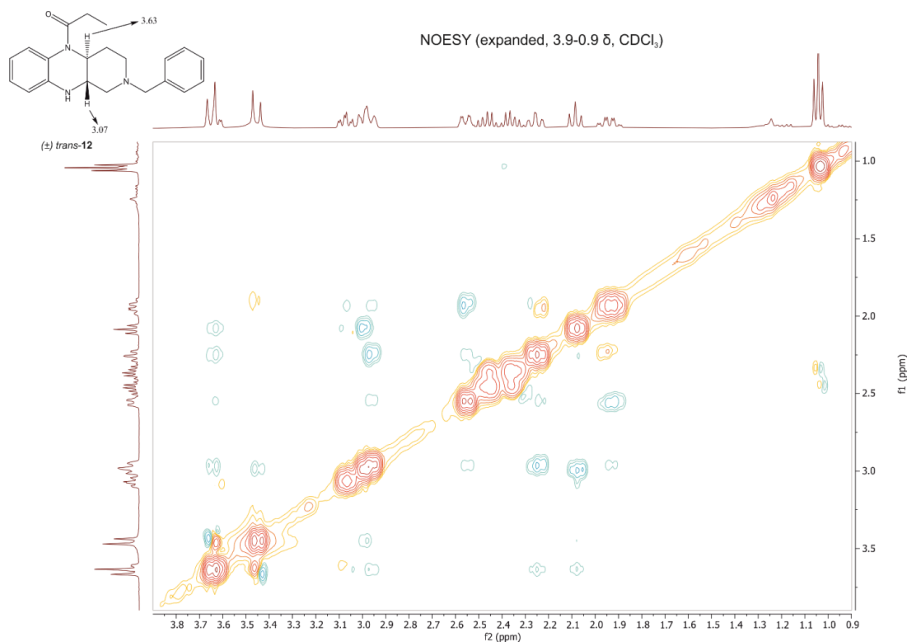


Figure S-8. Expanded NOESY of (\pm) -*trans*-1-(2-benzyl-2,3,4,4a,10,10a-hexahydro-pyrido[3,4-b]quinoxalin-5(1H)-yl)propan-1-one [(\pm) *trans*-12]

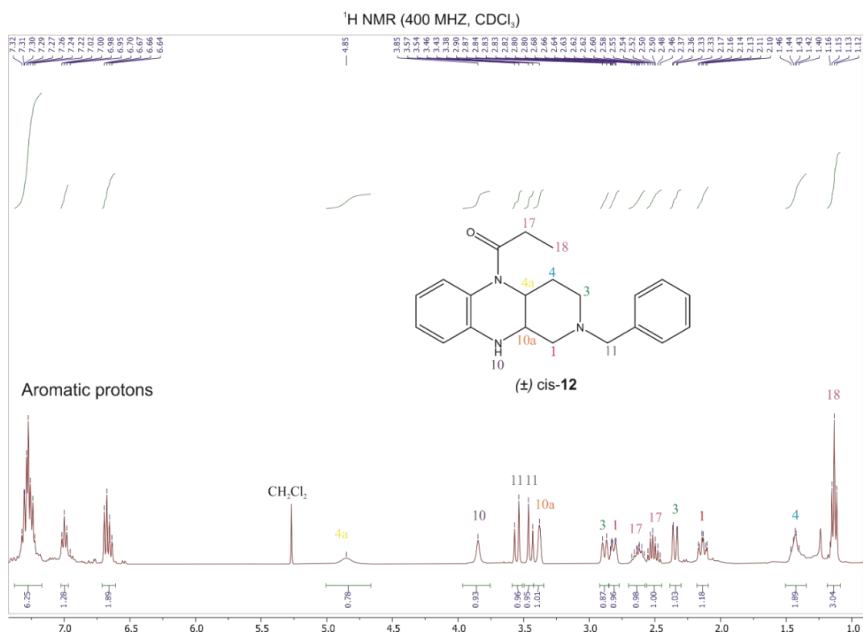


Figure S-9. ^1H NMR of (\pm) -*cis*-1-(2-benzyl-2,3,4,4a,10,10a-hexahydro-pyrido[3,4-b]quinoxalin-5(1H)-yl)propan-1-one [(\pm) *cis*-12]

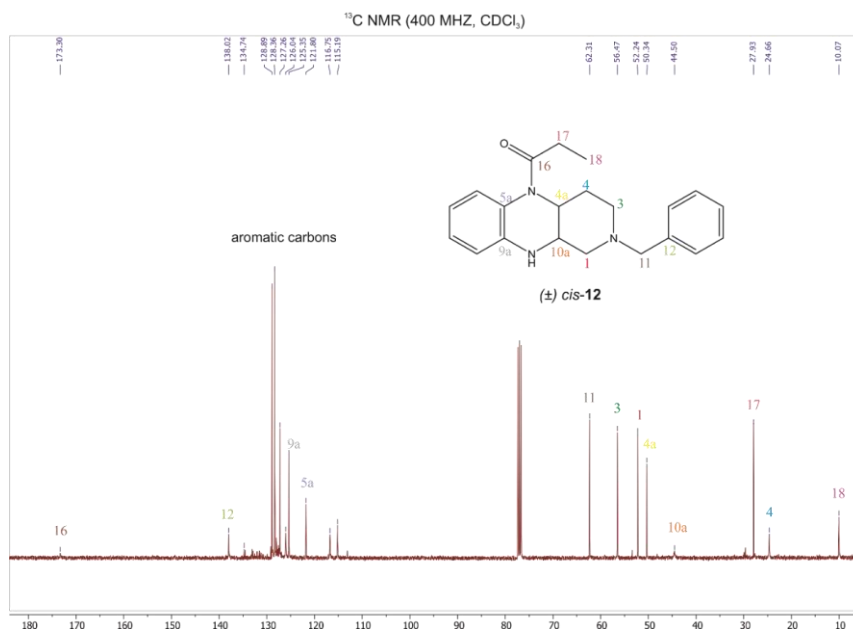


Figure S-10. ¹³C NMR of (±)-*cis*-1-(2-benzyl-2,3,4,4a,10,10a-hexahydro-pyrido[3,4-*b*]quinoxalin-5(1H)-yl)propan-1-one [(±) *cis*-12]

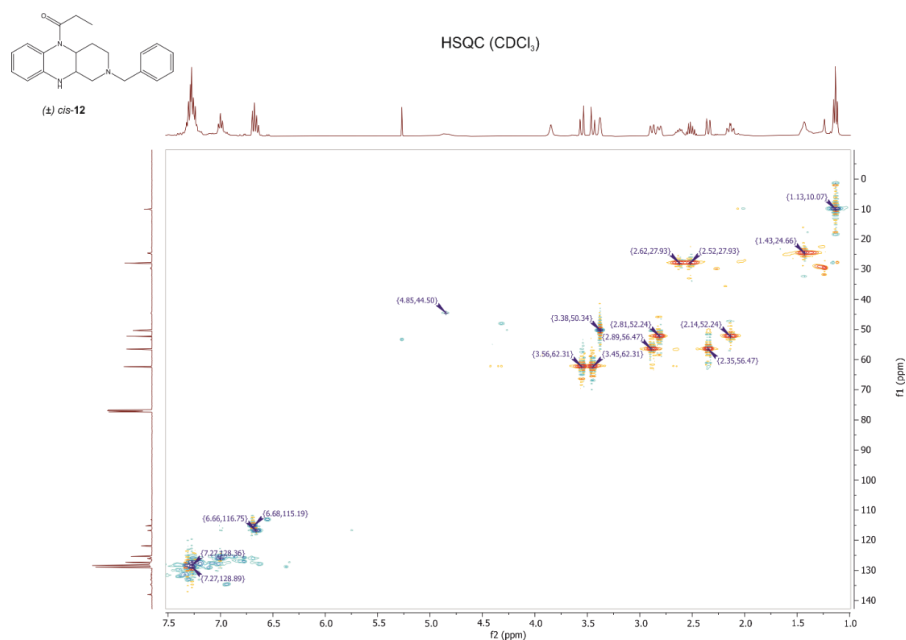


Figure S-11. HSQC of (±)-*cis*-1-(2-benzyl-2,3,4,4a,10,10a-hexahydro-pyrido[3,4-*b*]quinoxalin-5(1H)-yl)propan-1-one [(±) *cis*-12]

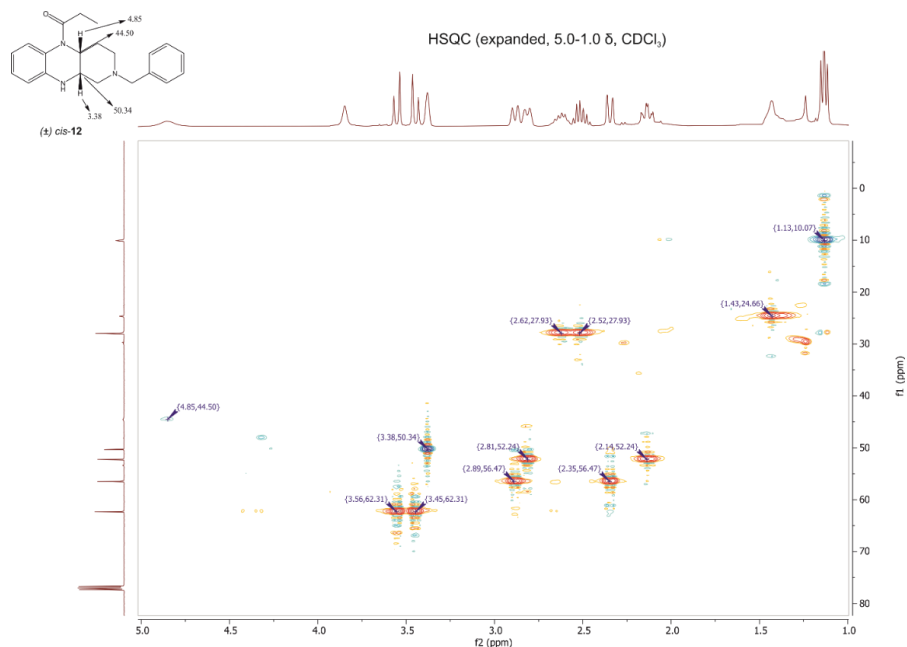


Figure S-12. Expanded HSQC of of (\pm)-*cis*-1-(2-benzyl-2,3,4,4a,10,10a-hexahydro-pyrido[3,4-*b*]quinoxalin-5(1H)-yl)propan-1-one [(\pm) *cis*-12]

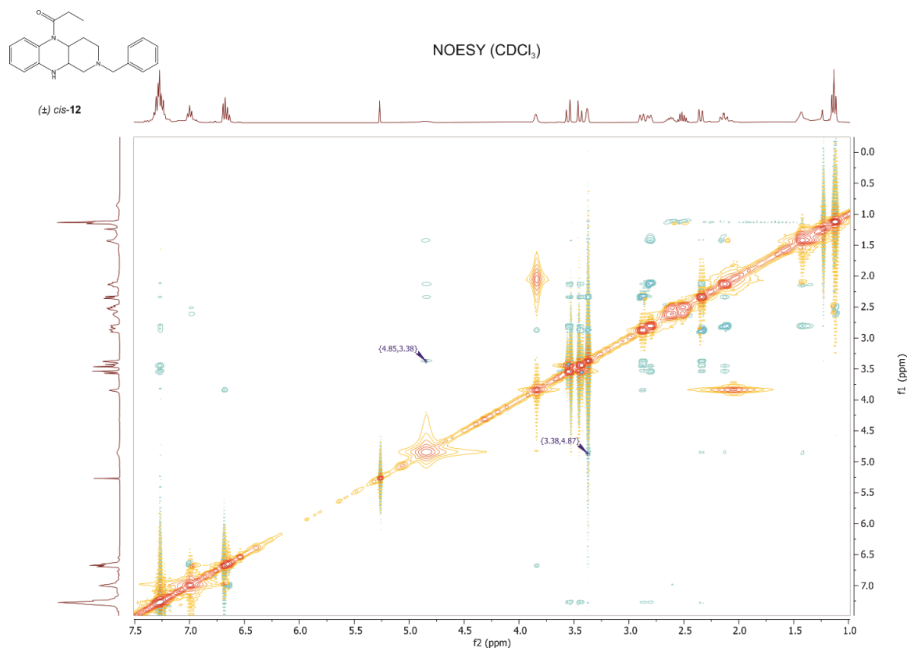


Figure S-13. NOESY of (\pm)-*cis*-1-(2-benzyl-2,3,4,4a,10,10a-hexahydro-pyrido[3,4-*b*]quinoxalin-5(1H)-yl)propan-1-one [(\pm) *cis*-12]

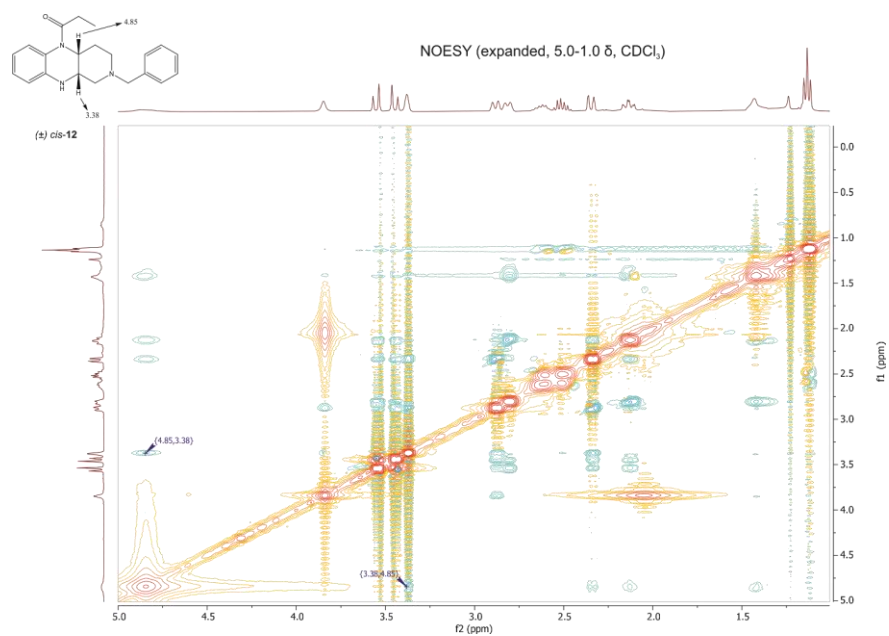


Figure S-14. Expanded NOESY of (±)-*cis*-1-(2-benzyl-2,3,4,4a,10,10a-hexahydro-pyrido[3,4-*b*]quinoxalin-5(1H)-yl)propan-1-one [(±) *cis*-12].



J. Serb. Chem. Soc. 87 (2) 181–192 (2022)
JSCS–5514

Evaluation of antitumor potential of Cu(II) complex with hydrazone of 2-acetylthiazole and Girard's T reagent

NEVENA STEVANOVIĆ^{1#}, MIMA JEVTIČIĆ^{2#}, DRAGANA MITIĆ^{2#}, IVANA Z. MATIĆ³, MARIJA ĐORĐIĆ CRNOGORAC³, MIROSLAVA VUJČIĆ^{4#}, DUŠAN SLADIĆ^{1#}, BOŽIDAR ČOBELJIĆ^{1#} and KATARINA ANĐELKOVIĆ^{1#*}

¹University of Belgrade-Faculty of Chemistry, Studentski trg 12–16, 11000 Belgrade, Serbia, ²Innovative centre of the Faculty of Chemistry, Studentski trg 12–16, 11000 Belgrade, Serbia, ³Institute of Oncology and Radiology of Serbia, 11000 Belgrade, Serbia and

⁴University of Belgrade-Institute of Chemistry, Technology and Metallurgy, Department of Chemistry, Njegoševa 12, 11000 Belgrade, Serbia

(Received 3 December, revised 17 December, accepted 20 December 2021)

Abstract: In this paper, the previously synthesized Cu(II) complex ($[\text{CuL}^1(\text{N}_3)(\text{CH}_3\text{OH})]\text{BF}_4$) with *N,N,N*-trimethyl-2-oxo-2-(2-(1-(thiazol-2-yl)ethylidene)hydrazinyl)ethan-1-aminium chloride, has been characterized and its biological activity has been studied in detail. The Cu(II) complex consists of ligand coordinated in a deprotonated, formally neutral zwitter-ionic form, *via* NNO atoms, one azido ligand and one methanol molecule. The Cu(II) complex was selected due to results of the cytotoxic activity, the brine shrimp test and DPPH radical scavenging activity, which were previously performed. The effects of Cu(II) complex on cell cycle phase distribution of cervical adenocarcinoma HeLa cells were investigated in order to examine the mechanisms of its anticancer activity. The measurement of intracellular ROS levels in HeLa and HaCaT cell lines were evaluated in order to explore their possible generation and the role in cytotoxic activity. The possible anti-invasive and anti-angiogenic properties of Cu(II) complex were evaluated. DNA binding experiments, including fluorescence displacement study and DNA cleavage experiments, were performed in order to obtain information on the type of DNA–metal complex interactions.

Keywords: *N*-acylhydrazone; cell cycle analysis; gene expression analyses; UV–Vis measurements.

INTRODUCTION

In recent years, Schiff base complexes, especially hydrazone based ones, represent an interesting group of complexes, due to its easy preparation and

* Corresponding author. E-mail: kka@chem.bg.ac.rs

Serbian Chemical Society member.

<https://doi.org/10.2298/JSC211203114S>

structural diversity of ligands and wide spectrum of biological activities. *N*-Acylhydrazones contain a carbonyl group that enables the electron delocalization and can act as an additional coordination site. Many hydrazones show different biological activities, but in many cases their metal complexes show higher activity than the free ligand.^{1,2}

Copper (II) complexes have d^9 geometries (Jahn–Teller effect) and therefore show distorted octahedral and tetrahedral symmetries. The distortion is observed as axial elongation so that Cu(II) complexes can have square planar or square pyramidal geometries, but some can also possess trigonal bipyramidal geometry.³

Most biologically active *N*-acylhydrazone copper complexes synthesized so far possess tridentate ligands, with ONO^{4–8} and NNO^{9–12} sets of donor atoms. Considering the structure of the complex, there are no recorded structures of copper complexes with *N*-acylhydrazones containing a five-membered ring in the part of the molecule that originate from aldehyde/ketone, however the analogous structures of thiosemicarbazone Cu(II) complexes have been reported.^{13,14} In all reported complexes, the geometry around copper(II) ion is square pyramidal. Biological studies of these complexes showed moderate antibacterial¹³ and cytotoxic activities.¹⁴

By biological investigation of complexes of copper with *N*-acylhydrazone ligands it was observed that they can show wide spectra of biological activity, such as cytotoxic,^{4,6,7,12} antibacterial^{5,8–11} and antifungal,^{5,8} with higher activity than referent compounds.³

In continuation of our previous investigations of synthesis and characterization of Cu(II) complexes with Girard's reagent T-based hydrazones,^{15–17} biological properties of a previously synthesized Cu(II) complex were investigated in this paper. In previous biological studies Cu(II) complex with *N,N,N*-trimethyl-2-oxo-2-(2-(1-(thiazol-2-yl)ethylidene)hydrazinyl)ethan-1-aminium chloride showed moderate antibacterial activity against all tested bacterial strains (best activity towards *Escherichia coli* strain and very weak selectivity towards Gram-negative bacteria) and moderate antifungal activity.¹⁹ Also, this complex exhibited high radical-scavenging activity which is not surprising given the existence of a redox-active Cu^{2+} in structure. Another significant feature is the pronounced cytotoxic activity against tested human cancer cell lines.

Bearing that in mind, in this paper the previously synthesized Cu(II) complex has been subjected to further biological examination that includes: investigation of mechanisms of anticancer activity, ROS generation in mediating cytotoxic effects, *in vitro* anti-angiogenic activity, effects on gene expression levels and DNA interaction studies.

EXPERIMENTAL

Chemistry

2-Acetylthiazole (99 %) was obtained from Acros, and Girard's T reagent (99 %) from Aldrich. IR spectra were recorded on a Nicolet 6700 FT-IR spectrometer using the ATR technique in the region 4000–400 cm^{-1} (*vs* – very strong, *s* – strong, *m* – medium, *w* – weak). Elemental analyses (C, H and N) were performed by standard micro-methods using the Elementar Vario ELIII C.H.N.S.O analyzer.

General procedure for the synthesis of the ligand and Cu(II) complex (1). The ligand **HLCl** was synthesized by the reaction of Girard's T reagent and 2-acetylthiazole according to the previously described method.¹⁸

The Cu(II) complex **1** was synthesized according to the previously described method,¹⁹ equimolar amounts of ligand **HLCl** and $\text{Cu}(\text{BF}_4)_2 \cdot 6\text{H}_2\text{O}$ were briefly dissolved in methanol. After complete dissolution of $\text{Cu}(\text{BF}_4)_2 \cdot 6\text{H}_2\text{O}$ in the reaction mixture, 4 eq. of NaN_3 were added and mixture was refluxed.

Biology

Cell cycle analysis. The changes in cell cycle distribution of HeLa cells treated with Cu(II) complex were analyzed by flow cytometry. HeLa cells were exposed to IC_{50} and $2IC_{50}$ concentrations of Cu(II) complex for 24 h. Afterwards, the cells were collected by trypsinization, washed with phosphate buffered saline (PBS) and fixed in 70 % ethanol on ice, according to standard protocol.²⁰ The cell samples were stored at -20°C for at least one week before analysis. At the day of analysis, the cell samples were washed, resuspended in PBS containing RNase A and incubated for 30 min at 37°C . Subsequently, the propidium iodide solution was added to cell samples. Percentages of cells within subG1, G1, S, and G2/M phases of the cell cycle were assessed using a BD FACS Calibur flow cytometer. The analyses of acquired data (10000 events collected for each gated cell sample) were performed by BD CellQuest software. Cell cycle data are presented as mean \pm S.D. of three independent experiments.

Endothelial cell tube formation assay. The possible *in vitro* anti-angiogenic activity of tested Cu(II) complex was investigated on human umbilical vein EA.hy926 cells using endothelial cell tube formation assay.^{21,22} The EA.hy926 cells were seeded on the surface of Corning® Matrigel® basement membrane matrix and incubated with subtoxic IC_{20} concentration of the complex for 24 h (the applied concentration was 20 μM , as determined by MTT test for 24 h treatment). After the incubation of 20 h, the photomicrographs of control and treated EA.hy926 cells were captured under the inverted phase-contrast microscope.

Gene expression analyses. HeLa cells were seeded into 25 cm^2 cell culture flasks (1.5×10^6 cells per flask). After 24 h, the cells were treated with subtoxic IC_{20} concentration of Cu(II) complex (the applied concentration was 15 μM , as determined by MTT test for 24 h treatment). Control cell sample was incubated in nutrient medium only. After 24 h treatment, HeLa cells were collected by trypsinization, washed with PBS, and stored at -80°C . Total RNA was isolated from HeLa cells using TRI Reagent® (Sigma Aldrich) according to the manufacturer's protocol. The concentration and quality of isolated RNA for each sample was determined spectrophotometrically (BioSpec-nano, Shimadzu). High-capacity cDNA reverse transcription kit (Thermo Fisher Scientific) was used for reverse transcription of 1 μg of total RNA into single-stranded cDNA. Measurement of mRNA expression levels of selected genes was done by real-time quantitative PCR (RT-qPCR) and TaqMan® gene expression assays (MMP2-Hs01548727_m1, MMP9-Hs00957562_m1 and VEGFA-Hs00900055_m1) using LightCycler® 480 II system (Roche Diagnostics GmbH, Mannheim, Germany). Gene expres-

sion values were normalized to *GAPDH* (Hs02758991_g1) and were obtained by comparative $\Delta\Delta C_t$ method, analyzed with LightCycler[®] 480 software.

UV-Vis measurements experiments

For DNA binding experiments, calf thymus DNA (CT-DNA, lyophilized, highly polymerized, obtained from Serva, Heidelberg, Germany) was dissolved in 40 mM bicarbonate buffer, pH 8.4) and left overnight at 4 °C. This stock solution was stored at 4 °C and was stable for several days. A solution of CT-DNA in water gave a ratio of UV absorbance at 260 and 280 nm, A_{260}/A_{280} of 1.89–2.01, indicating that DNA was sufficiently free of protein. The concentration of DNA (3 mg/mL, 9.98 mM) was determined from the UV absorbance at 260 nm using the extinction coefficient $\varepsilon_{260} = 6600 \text{ M}^{-1} \text{ cm}^{-1}$.²³ The stock solution of complex $[\text{CuL}^1(\text{N}_3)(\text{CH}_3\text{OH})]\text{BF}_4$ (**1**) was freshly prepared by dissolving the compound in dimethyl sulfoxide at concentrations of 10 mM (5.28 mg/mL).

Reaction mixtures (1 mL in 40 mM bicarbonate buffer, pH 8.4) consisting of different concentrations of the complex **1** (1, 5 and 10 μM) and 49.9 μM of CT-DNA (calculated per phosphate) were incubated at 37 °C for 60 min with occasional vortexing. The absorbance titration was performed at a fixed concentration of the compound (10 μM) with gradual increase of the concentration of double stranded CT-DNA (4.99, 5.98, 6.98, 7.98, 8.98, 9.98, 10.98, 11.97, 12.97, 13.97 and 14.97×10^{-5} M). The absorbance at 258 nm was monitored for each concentration of DNA. The binding constant K_b was determined using:²⁴

$$c_{\text{DNA}}(\varepsilon_a - \varepsilon_f)^{-1} = c_{\text{DNA}}(\varepsilon_b - \varepsilon_f)^{-1} + K_b^{-1}(\varepsilon_b - \varepsilon_f)^{-1} \quad (1)$$

where ε_a , ε_f , ε_b are absorbance/[compound], extinction coefficient of the free compound and extinction coefficient of the bound compound, respectively.

Fluorescence measurements

The competitive interactions of **1** and the fluorescence probe, either ethidium bromide (EB) or Hoechst 33258 (H), with CT-DNA were studied by measuring the change of fluorescence intensity of the probe-DNA solution after addition of the complex. Reaction mixtures containing 50 μM of CT-DNA (calculated per phosphate) in 1 mL of 40 mM bicarbonate solution (pH 8.4) were pretreated with 1.5 μL of 1 % H probe solution (28 μM final concentration) or 1 μL of 1 % EB solution (25 μM final concentration, in separate experiments) for 20 min and the mixture was analyzed by fluorescence measurement. Then the increasing concentrations of the complexes (0.5, 1, 2, 3, 5, 7, 9, 11, 13 and 15×10^{-5} M for displacement of EB and 0.5, 1, 1.5, 2, 2.5, 3, 3.5 and 4×10^{-5} M for displacement of H) were successively added and the changes in the fluorescence intensity were measured using a Thermo Scientific Lumina Fluorescence spectrometer (Finland) equipped with a 150 W Xenon lamp. The slits on the excitation and emission beams were fixed at 10 nm. All measurements were performed by the excitation at 350 nm for Hoechst 33258, and by the excitation at 500 nm for EB in the range of 390–600 nm. The control was probe-CT-DNA solution. The obtained fluorescence quenching data were analyzed according to the Stern–Volmer Equation:

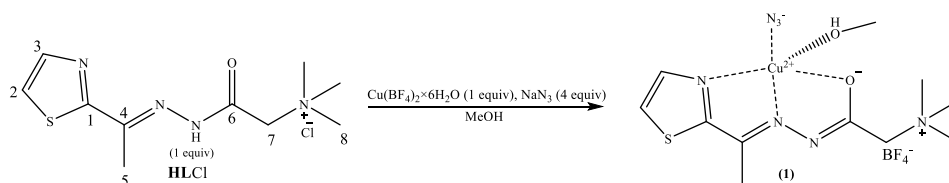
$$I_0/I = 1 + Kc_1/c_{\text{CT-DNA}} \quad (2)$$

where I_0 and I represent the fluorescence intensities of probe-CT-DNA in absence and presence of **1**, respectively, where K is the quenching constant. The K value was calculated from the ratio of the slope to the intercept from the plot of I_0/I versus $c_1/c_{\text{CT-DNA}}$.

The primary spectra of all spectrometric measurements were imported into Origin 2018.

RESULTS AND DISCUSSION

The reaction of 2-acetylthiazole and Girard's T reagent was performed according to the previously reported method¹⁸ and yielded the ligand *N,N,N*-trimethyl-2-oxo-2-(2-(1-(thiazol-2-yl)ethylidene)hydrazinyl)ethan-1-aminium chloride (**HLCl**), which was used for the synthesis of Cu(II) complex (**1**). The reaction of the ligand **HLCl** with metal salt $\text{Cu}(\text{BF}_4) \cdot 6\text{H}_2\text{O}$ and NaN_3 in mole ratio 1:1:4 in methanol resulted in formation of mononuclear Cu(II) complex (**1**) with the composition $[\text{CuL}^1(\text{N}_3)(\text{CH}_3\text{OH})]\text{BF}_4$ (Scheme 1). The ligand is coordinated in a deprotonated formally neutral zwitter-ionic form *via* thiazole nitrogen, azomethine nitrogen and carbonyl oxygen atoms. Ligand and complex **1** were characterized by IR spectroscopy (Figs. S-3 and S-4 of the Supplementary material to this paper) and elemental analysis.



Scheme 1. Synthesis of Cu(II) complex (**1**).

Effects of Cu(II) complex on cell cycle phase distribution

Since the Cu(II) complex **1** exerted a strong cytotoxic activity against cancer cell lines further examination of mechanisms of its anticancer activity was undertaken. The effects of **1** on cell cycle phase distribution of cervical adenocarcinoma HeLa cells were investigated after incubation with IC_{50} and $2IC_{50}$ concentrations of the compound for 24 h. These results are presented in Fig. 1. Cu(II) complex **1** applied at IC_{50} concentration caused a small increase in the percentages of HeLa cells in subG1 and S phases of the cell cycle in comparison with untreated HeLa cell sample as a control. In addition, the pronounced increase in the percentage of cells in G2/M cell cycle phase was observed after the treatment of HeLa cells with IC_{50} concentration of Cu(II) complex **1**, when compared with control cells. These changes were accompanied with a decrease of percentage of HeLa cells in G1 phase. Similar changes in the cell cycle phase distribution were found in HeLa cells exposed to higher ($2IC_{50}$) concentration of complex – a small increase of the percentage of cells in subG1 phase and a prominent increase of the percentage of cells in G2/M phase. The only exception was the absence of changes in the percentage of cells in S phase of the cell cycle. These results suggest that the antiproliferative activity of Cu(II) complex **1** might be attributed to a pronounced arrest of cells in G2/M cell cycle phase. The G2/M cell cycle arrest induced by the complex in HeLa cells might be explained by the

effects on cell cycle progression from G2 phase to mitosis at G2/M checkpoint, or by the effects on cell progression through mitosis – M phase arrest. The observed G2/M phase arrest might be associated with possible DNA damage effects of the copper complex.

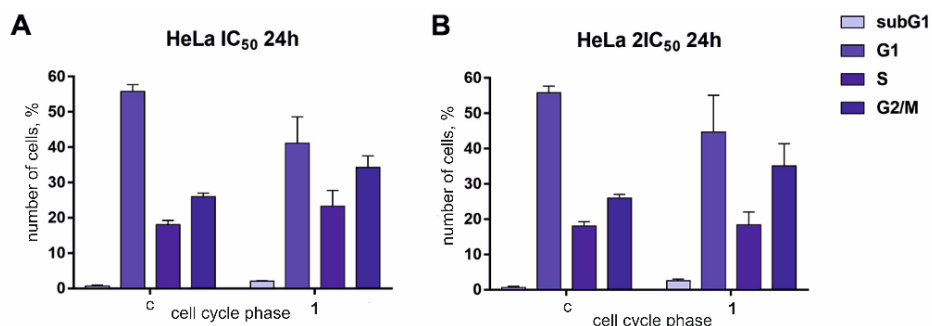


Fig. 1. Changes in the cell cycle phase distribution of HeLa cells treated with IC_{50} (A) and $2IC_{50}$ concentrations (B) of Cu(II) complex for 24 h.

Effect of Cu(II) complex on in vitro angiogenesis

The possible *in vitro* anti-angiogenic activity of the novel Cu(II) complex **1** on human umbilical vein endothelial EA.hy926 cells was investigated using tube formation assay. As it could be seen in Fig. 2 the incubation of EA.hy926 cells with subtoxic IC_{20} concentration of Cu(II) complex **1** for 24 h notably decreased angiogenesis *in vitro*. The complex suppressed the extensive sprouting of elongated EA.hy926 cells and the formation of capillary-like tubes, in comparison with the untreated EA.hy926 cells as control. The *in vitro* anti-angiogenic activity of investigated **1** is in agreement with the findings about inhibitory effects of other Cu(II) complexes on angiogenesis *in vitro*.^{25,26}

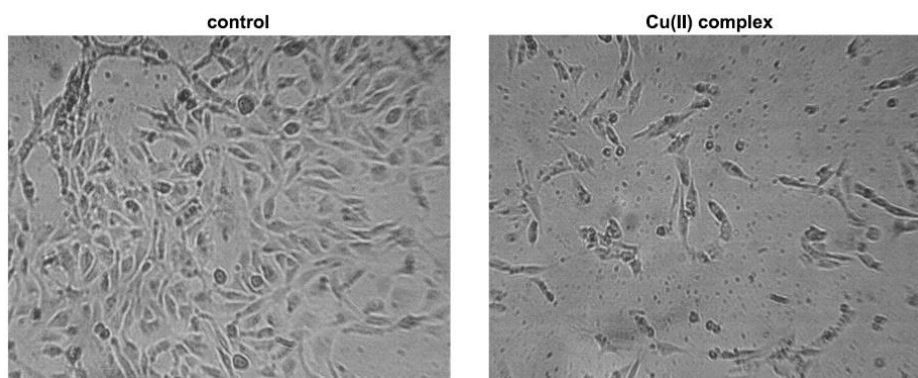


Fig. 2. Photomicrographs of control EA.hy926 cells and EA.hy926 cells treated with subtoxic IC_{20} concentration of Cu(II) complex for 20 h.

Effects of Cu(II) complex on gene expression levels

In order to further explore the possible anti-invasive and anti-angiogenic properties of Cu(II) complex (**1**), its effects in HeLa cells on the expression levels of genes whose protein products are implicated in cancer cell invasion and angiogenesis: matrix metalloproteinase-2 (MMP2), matrix metalloproteinase-9 (MMP9) and vascular endothelial growth factor A (VEGFA) were evaluated.

A slight decrease in MMP9 gene expression level was detected in HeLa cells exposed for 24 h to subtoxic IC_{20} concentration of the complex in comparison with this level in control HeLa cells (Fig. 3). However, the increase in the MMP2 gene expression level was observed in HeLa cells exposed to the tested complex. The Cu(II) complex **1** notably downregulated expression level of VEGFA in HeLa cells, when compared with this level in control cell sample. Since VEGFA gene encodes growth factor, which is involved in activating angiogenesis, lowering its level in cancer cells confirms the anti-angiogenic effect of this complex *in vitro*. The ability of copper complex to suppress angiogenesis *in vitro* represents an important anticancer property of this novel compound because targeting angiogenesis, which is essential for the expansion of malignant tumor growth, can inhibit further cancer progression.²⁷

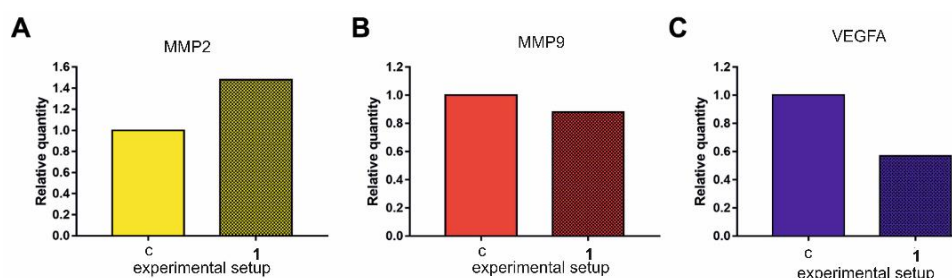


Fig. 3. Changes in gene expression levels of MMP2 (A), MMP9 (B), and VEGFA (C), in HeLa cells treated with subtoxic IC_{20} concentration of Cu(II) complex for 24 h.

DNA interaction studies

DNA is one of the medicinal therapeutic targets of anticancer agents. Transition metal complexes interact with DNA non-covalently or by covalent binding. Non-covalent binding usually occurs either in the minor groove by combination of hydrogen bonding, van der Waals contacts and electrostatic interactions, or by intercalation of a planar aromatic moiety between two base pairs of DNA *via* π -stacking take place.^{28,29} Covalent modifications of DNA usually occur at N7-positions on easily accessible purines in the major groove of the helix.³⁰ A combination of these interactions is possible and the consequences of such interactions might be reversible or irreversible.³¹ In this work, spectroscopic methods were employed to investigate the interaction modes of complex **1**.

The electronic absorption spectra of **1**, recorded at different concentrations with fixed concentration of CT-DNA or without it, are shown in Fig. S-1A of the Supplementary material. It was found that the absorption maximum of the complex was centered at 358 nm. After the interaction with CT-DNA, the changes in spectra were detected. Analysis of the absorption changes induced upon binding of **1** to CT-DNA is shown in the inset in Fig. S-1A. By comparison of the sum of absorbances at 258 nm of free complex **1** and free CT-DNA and the observed absorbance of the **1**-CT-DNA, it can be concluded that there was a concentration-dependent difference between them. The bands which correspond to CT-DNA showed the broadening of the peak at 258 nm in concentration-dependent way, and the hypochromism of 1.87, 6.67 and 8.58 % for 1, 5 and 10 μM of the complex, respectively (Fig. S-1A, inset). Significant changes in spectra of **1** after the interaction with CT-DNA were observed for bands at 358 nm, as evidenced by hypochromism of 42.31, 23.26 and 18.79 % (for 1, 5 and 10 μM of the complex, respectively). Hypochromism and red shift are common evidence for intercalation. Given that no shifts in the spectrum were detected and considering the positive charge on molecule of the complex, the obtained results indicate that the electrostatic interaction is the probable mode of binding.

In order to obtain more information on interaction of the complex with DNA, spectroscopic titration of the solution of the complex the concentration of which was kept constant (10 μM) with the solutions of increasing concentrations of CT-DNA was performed. The results are shown in Fig. S-1B. A quantitative determination of the binding strength of the compound to DNA is made by calculation of binding constants K_B of the compound from Eq. (1).²⁴ The intrinsic binding constant K_B of **1** (inset in Fig. S-1B) was calculated as $2.9 \times 10^3 \text{ M}^{-1}$. The obtained value was lower than the value reported for a classical intercalator (ranged 10^6 to 10^7 M^{-1})³². The value of K_B was comparable to those for metal complexes binding in the minor groove of DNA.³³ However, non-linearity of the curve showed that at least two types of binding sites are available for the interaction of complex **1** with DNA, suggesting different binding modes.

In order to further investigate the binding mode, fluorescence spectroscopy was performed by the fluorescence displacement experiments carried out with two different dyes: ethidium bromide (EB), a typical intercalator, and Hoechst 33258 (H), a minor groove binder. While EB fluoresces weakly, its fluorescence yield increases significantly in the presence of CT-DNA (Fig S-2A). Binding of EB to CT-DNA was followed by the excitation at 500 nm with fluorescence maximum at 600 nm. The addition of increasing concentrations of **1** to EB-CT-DNA system caused reduction in the fluorescence intensity of the band at 600 nm by 32 % with the maximal applied concentration of the complex. The criterion for fluorescence quenching by a typical strong intercalator is the fluorescence value reduction of more than 50 %.³⁴⁻³⁶ This means that that the mech-

anism of fluorescence of EB quenching by complex **1** is different from intercalation. The extent of this quenching of EB by **1** was estimated using Stern–Volmer Equation (2). The fluorescence quenching constant (K) was calculated from the ratio of the slope to the intercept from the plot I_0/I versus c_1 as shown in the inset in Fig. S 2A. The plot is linear and gives a K of $3.07 \times 10^3 \text{ M}^{-1}$.

Hoechst 33258 recognizes at least four AT base pairs and binds strongly and selectively with high affinity to double-stranded B-DNA structure by the combination of hydrogen bonding, van der Waals contacts with the walls of the minor groove, and the electrostatic interactions between its cationic structure and the DNA.³⁷ As the emission spectra showed (Fig. S-2B), the fluorescence of H increased significantly upon the interaction with CT-DNA. A successive addition of **1** to H-CT-DNA solution caused appreciable reduction in the fluorescence intensity of the band at 443 nm (about 60 % with maximal applied concentration of **1**), accompanied by a small blue shift of emission maximum to 441 nm. The quenching constant calculated by the linear regression of a plot I_0/I against c_1 (inset in Fig. S-2B) was $K = 4.16 \times 10^4 \text{ M}^{-1}$. The plot displayed a good linear relationship for the investigated concentration ranges of **1**, indicating the displacement of H33258 from H–CT-DNA. By comparing the results, it can be concluded that the competition of **1** with H 33258 was more efficient than in case of ethidium bromide in binding to DNA.

In view of fluorescence and UV–Vis absorption spectral results, it can be deduced that the interaction of the complex **1** with DNA occurred *via* minor groove binding and electrostatic interactions between a positively charged quarternary ammonium group and negatively charged phosphate groups of DNA backbone.

For effects of Cu(II) complex on intracellular ROS levels, BSA fluorescence measurements and DNA cleavage experiments, see Supplementary Material.

CONCLUSIONS

The ligand **HLCI** and Cu(II) complex **1** have been characterized by elemental analysis and IR spectroscopy. The five-coordination geometry of the Cu(II) ion (mononuclear complex **1**) can be described as distorted square-based pyramidal. Cu(II) ion is coordinated through NNO set of donor atoms, of formally neutral zwitter-ionic form, of **HLCI** ligand, one nitrogen atom of the azide ligand, while fifth remaining coordination site is occupied by the oxygen atom from methanol. The effects of Cu(II) complex on cell cycle phase distribution showed a small increase in the percentages of HeLa cells in subG1 and S phases and also a pronounced increase in the percentage of cells in G2/M phase of the cell cycle. The results of effects of Cu(II) complex on ROS generation suggested the antioxidant properties of the tested complex at lower concentration. The results obtained *via* DNA interaction studies indicate that minor groove binding and electrostatic interactions are the probable mode of binding for complex **1**. The

lower value of intrinsic binding constant K_B of **1** and nonlinearity of the curve indicates that at least two types of binding sites are responsible for the interaction of the complex with DNA. Of a particular interest is anti-angiogenetic activity of the complex, since the formation of blood vessels is crucial for tumor growth.

SUPPLEMENTARY MATERIAL

Additional data and information are available electronically at the pages of journal website: <https://www.shd-pub.org.rs/index.php/JSCS/article/view/11447>, or from the corresponding author on request.

Acknowledgement. The authors are grateful to the Ministry of Education, Science and Technological Development of the Republic of Serbia for the financial support (Grant numbers: 451-03-9/2021-14/200043, 451-03-9/2021-14/200026, 451-03-9/2021-14/200168 and 451-03-9/2021-14/200288).

ИЗВОД

ИСПИТИВАЊЕ АНТИТУМОРСКОГ ПОТЕНЦИЈАЛА КОМПЛЕКСА CU(II) СА ХИДРАЗНОМ 2-АЦЕТИЛТИАЗОЛА И ЖИРАРОВОГ Т-РЕАГЕНСА

НЕВЕНА СТЕВАНОВИЋ¹, МИМА ЈЕВТОВИЋ², ДРАГАНА МИТИЋ², ИВАНА З. МАТИЋ³, МАРИЈА ЂОРЂИЋ ЦРНОГОРАЦ³, МИРОСЛАВА ВУЧИЋ⁴, ДУШАН СЛАДИЋ¹, БОЖИДАР ЧОБЕЉИЋ¹ и КАТАРИНА АНЂЕЛКОВИЋ¹

¹Универзитет у Београду-Хемијски факултет, Студентски брџи 12–16, 11000 Београд, ²Иновациони центар, Хемијски факултет, Студентски брџи 12–16, 11000 Београд, ³Универзитет у Београду-Институт за онкологију и радиологију Србије, 11000 Београд и ⁴Универзитет у Београду-Институт за хемију, технологију и металургију, Центар за хемију, Њевошева 12, 11000 Београд

У овом раду урађена је карактеризација и детаљно испитивање биолошке активности претходно синтетисаног комплекса Cu(II) са *N,N,N*-триметил-2-оксо-2-(2-(1-(тиазол-2-ил)етилиден)хидразинил)етан-1-аминијум-хлоридом. Комплекс Cu(II) састоји се из депротонаног, формално неутралног, лиганда координаног преко NNO атома у цвтер-јонском облику, једног азидо лиганда и једног молекула метанола. Комплекс Cu(II) одабран је на основу резултата претходно испитиване цитотоксичне активности, урађених тестова на рачићима *Artemia salina* и DPPH теста. У циљу одређивања механизма антитуморског дејства, урађена је анализа ћелијског циклуса аденокарцинома грлића материце. Мерењем продукције реактивних оксидативних врста проучаван је њихов утицај и улога у цитотоксичној активности. Испитивана су и потенцијална анти-инвазивна и анти-ангиогена својства комплекса Cu(II). Ради одређивања типа интеракција између комплекса метала и ДНК урађена су испитивања: интеракција са ДНК, флуоресценције и цепања ДНК ланца.

(Примљено 3. децембра, ревидирано 17 децембра, прихваћено 20. децембра 2021)

REFERENCES

1. M. Çınarlı, Ç. Yüksektepe Ataoğlu, E. Çınarlı, Ö. İdil, *J. Mol. Struct.* **1213** (2020) 128 (<http://dx.doi.org/10.1016/j.molstruc.2020.128152>)
2. F. I. Abouzayed, S. M. Emam, S. A. Abouel-Enein, *J. Mol. Struct.* **1216** (2020) 128 (<http://dx.doi.org/10.1016/j.molstruc.2020.128314>)
3. K. Rishu, K. Harpreet, K. Brij Kishore, *Sci. Rev. Chem. Comm.* **3** (2013) 1 (<https://www.tsjournals.com/articles/applications-of-copper--schiffs-base-complexes--a-revie.pdf>)

4. S. Jiang, H. Ni, F. Liu, S. Gu, P. Yu, Y. Gou, *Inorg. Chim. Acta* **499** (2020) 119186 (<http://dx.doi.org/10.1016/j.ica.2019.119186>)
5. S. Yousef Ebrahimipour, I. Sheikhshoaie, A. Crochet, M. Khaleghi, K. M. Fromm, *J. Mol. Struct.* **1072** (2014) (<http://dx.doi.org/10.1016/j.molstruc.2014.05.024>)
6. M. Sutradhar, Rajeshwari, T. Roy Barman, A. R. Fernandes, F. Paradinha, C. Roma-Rodrigues, M. F. C. Guedes da Silva, A. J. L. Pombeiro, *J. Inorg. Biochem.* **175** (2017) (<http://dx.doi.org/10.1016/j.jinorgbio.2017.07.034>)
7. Q. Mo, J. Deng, Y. Liu, G. Huang, Z. Li, P. Yu, Y. Gou, F. Yang, *Eur. J. Med. Chem.* **156** (2018) (<http://dx.doi.org/10.1016/j.ejmech.2018.07.022>)
8. S. Y. Ebrahimipour, I. Sheikhshoaie, M. Mohamadi, S. Suarez, R. Baggio, M. Khaleghi, M. Torkzadeh-Mahani, A. Mostafavi, *Spectrochim. Acta, A* **142** (2015) 410 (<http://dx.doi.org/10.1016/j.saa.2015.01.088>)
9. M. M. Fousiamol, M. Sithambaresan, K. K. Damodaran, M. R. P. Kurup, *Inorg. Chim. Acta* **501** (2020) 119301 (<http://dx.doi.org/10.1016/j.ica.2019.119301>)
10. P. H. O. Santiago, M. B. Santiago, C. H. G. Martins, C. C. Gatto, *Inorg. Chim. Acta* **508** (2020) 119632 (<http://dx.doi.org/10.1016/j.ica.2020.119632>)
11. P. H. O. Santiago, F. S. Tiago, M. S. Castro, P. E. N. Souza, J. B. L. Martins, C. C. Gatto, *J. Inorg. Biochem.* **204** (2020) 110949 (<http://dx.doi.org/10.1016/j.jinorgbio.2019.110949>)
12. Y. Gou, J. Li, B. Fan, B. Xu, M. Zhou, F. Yang, *Eur. J. Med. Chem.* **134** (2017) (<http://dx.doi.org/10.1016/j.ejmech.2017.04.026>)
13. D. K. Sau, R. J. Butcher, S. Chaudhuri, N. Saha, *Mol. Cell. Biochem.* **253** (2003) 21 (<http://dx.doi.org/10.1023/A:1026041032078>)
14. O. Palamarcu, M. N. M. Milunović, A. Sirbu, E. Stratulat, A. Pui, N. Gligorijevic, S. Radulovic, J. Kožisek, D. Darvasiova, P. Rapta, E. A. Enyedy, G. Novitchi, S. Shova, V. B. Arion, *New. J. Chem.* **43** (2019) 134 (<http://dx.doi.org/10.1039/C8NJ04041A>)
15. M. R. Milenković, A. T. Papastavrou, D. Radanović, A. Pevec, Z. Jagličić, M. Zlatar, M. Gruden, G. C. Vougioukalakis, I. Turel, K. Anđelković, B. Čobeljić, *Polyhedron* **165** (2019) 22 (<http://dx.doi.org/10.1016/j.poly.2019.03.001>)
16. T. Keškić, B. Čobeljić, M. Gruden, K. Anđelković, A. Pevec, I. Turel, D. Radanović, M. Zlatar, *Cryst. Growth Des.* **19** (2019) 4810 (<http://dx.doi.org/10.1021/acs.cgd.9b00760>)
17. N. Stevanović, P. P. Mazzeo, A. Bacchi, I. Z. Matić, M. Đorđić Crnogorac, T. Stanojković, M. Vujčić, I. Novaković, D. Radanović, M. Šumar-Ristović, D. Sladić, B. Čobeljić, K. Anđelković, *J. Biol. Inorg. Chem.* (2021) (<http://dx.doi.org/10.1007/s00775-021-01893-5>)
18. T. T. Adejumo, N. v. Tzouras, L. P. Zorba, D. Radanović, A. Pevec, S. Grubišić, D. Mitić, K. K. Anđelković, G. C. Vougioukalakis, B. Čobeljić, I. Turel, *Molecules* **25** (2020) 4043 (<http://dx.doi.org/10.3390/molecules25184043>)
19. N. Stevanović, M. Zlatar, I. Novakovic, A. Pevec, D. Radanović, I. Matić, M. Djordjic Crnogorac, T. Stanojkovic, M. Vujčić, M. Gruden, D. Sladić, K. Anđelković, I. Turel, B. Čobeljić, *Dalton Trans.* (2021) (<http://dx.doi.org/10.1039/D1DT03169D>)
20. Michael G. Ormerod, *Flow cytometry. A practical approach*. 3rd ed., Oxford University Press, Oxford, 2000
21. E. Aranda, G. I. Owen, *Biol. Res.* **42** (2009) 377 (<http://dx.doi.org/10.4067/S0716-97602009000300012>)
22. I. Z. Matić, I. Aljančić, V. Vajs, M. Jadranin, N. Gligorijević, S. Milosavljević, Z. D. Juranić, *Nat. Prod. Commun.* **8** (2013) 1291 (<https://doi.org/10.1177%2F1934578X1300800927>)

23. M. Č. Romanović, B. Čobeljić, A. Pevec, I. Turel, S. Grubišić, D. Radanović, K. Anđelković, M. Milenković, M. R. Milenković, *J. Coord. Chem.* **70** (2017) 3702 (<http://dx.doi.org/10.1080/00958972.2017.1405262>)
24. R. Vijayalakshmi, M. Kanthimathi, V. Subramanian, B. U. Nair, *Biochem. Biophys. Res. Commun.* **271** (2000) 731 (<http://dx.doi.org/10.1006/bbrc.2000.2707>)
25. P. Nagababu, A. K. Barui, B. Thulasiram, C. S. Devi, S. Satyanarayana, C. R. Patra, B. Sreedhar, *J. Med. Chem.* **58** (2015) 5226 (<http://dx.doi.org/10.1021/acs.jmedchem.5b00651>)
26. M. v. Rodić, V. M. Leovac, L. S. Jovanović, V. Spasojević, M. D. Joksović, T. Stanojković, I. Z. Matic, L. S. Vojinović-Ješić, V. Marković, *Eur. J. Med. Chem.* **115** (2016) 75 (<http://dx.doi.org/10.1016/j.ejmech.2016.03.003>)
27. R. I. Teleanu, C. Chircov, A. M. Grumezescu, D. M. Teleanu, *J. Clin. Med.* **9** (2019) 84 (<http://dx.doi.org/10.3390/jcm9010084>)
28. L. Streckowski, B. Wilson, *Mutat. Res.-Fund. Mol. M.* **623** (2007) 3 (<http://dx.doi.org/10.1016/j.mrfmmm.2007.03.008>)
29. F. R. Keene, J. A. Smith, J. G. Collins, *Coord. Chem. Rev.* **253** (2009) 2021 (<http://dx.doi.org/10.1016/j.ccr.2009.01.004>)
30. S. E. Sherman, Dan. Gibson, A. H. J. Wang, S. J. Lippard, *J. Am. Chem. Soc.* **110** (1988) 7368 (<http://dx.doi.org/10.1021/ja00230a017>)
31. I. Turel, J. Kljun, *Curr. Top. Med. Chem.* **11** (2011) 2661 (<http://dx.doi.org/10.2174/156802611798040787>)
32. M. Cory, D. D. McKee, J. Kagan, Henry D. W., J. A. Miller, *J. Am. Chem. Soc.* **107** (1985) 2528 (<http://dx.doi.org/10.1021/ja00294a054>)
33. J. Wang, L. Shuai, X. Xiao, Y. Zeng, Z. Li, T. Matsumura-Inoue, *J. Inorg. Biochem.* **99** (2005) 883 (<http://dx.doi.org/10.1016/j.jinorgbio.2004.12.018>)
34. F. Dimiza, S. Fountoulaki, A. N. Papadopoulos, C. A. Kontogiorgis, V. Tangoulis, C. P. Raptopoulou, V. Psycharis, A. Terzis, D. P. Kessissoglou, G. Psomas, *Dalton Trans.* **40** (2011) 8555 (<http://dx.doi.org/10.1039/c1dt10714c>)
35. E. S. Koumoussi, M. Zampakou, C. P. Raptopoulou, V. Psycharis, C. M. Beavers, S. J. Teat, G. Psomas, T. C. Stamatatos, *Inorg. Chem.* **51** (2012) 7699 (<http://dx.doi.org/10.1021/ic300739x>)
36. S. Mardanya, S. Karmakar, D. Maity, S. Baitalik, *Inorg. Chem.* **54** (2015) 513 (<http://dx.doi.org/10.1021/ic502271k>)
37. R. Kakkar, R. Garg, Suruchi, *J. Mol. Struct.: THEOCHEM* **584** (2002) 37 ([http://dx.doi.org/10.1016/S0166-1280\(02\)00026-X](http://dx.doi.org/10.1016/S0166-1280(02)00026-X)).



SUPPLEMENTARY MATERIAL TO

**Evaluation of antitumor potential of Cu(II) complex with
hydrazone of 2-acetylthiazole and Girard's T reagent**

NEVENA STEVANOVIĆ¹, MIMA JEVTIČIĆ², DRAGANA MITIĆ², IVANA Z. MATIĆ³,
MARIJA ĐORĐIĆ CRNOGORAC³, MIROSLAVA VUJČIĆ⁴, DUŠAN SLADIĆ¹,
BOŽIDAR ČOBELJIĆ¹ and KATARINA ANĐELKOVIĆ^{1*}

¹University of Belgrade-Faculty of Chemistry, Studentski trg 12–16, 11000 Belgrade,
Serbia, ²Innovative centre of the Faculty of Chemistry, Studentski trg 12–16, 11000 Belgrade,
Serbia, ³Institute of Oncology and Radiology of Serbia, 11000 Belgrade, Serbia and
⁴University of Belgrade-Institute of Chemistry, Technology and Metallurgy,
Department of Chemistry, Njegoševa 12, 11000 Belgrade, Serbia

J. Serb. Chem. Soc. 87 (2) (2022) 181–192

SPECTROSCOPIC DATA OF SYNTHESIZED COMPOUNDS

Ligand HLCI

IR (ATR): 3387w, 3128w, 3091m, 3017m, 2955s, 1701vs, 1612w, 1550vs,
1486s, 1401m, 1300w, 1201s, 1135w, 976w, 944w, 914m, 786w, 748w, 684w,
585w, 551w. (**HL**¹Cl -E). ¹H NMR (500 MHz, DMSO-*d*₆, δ): 2.41 (*s*, 3H, H-5),
3.30 (*s*, 9H, H-8), 4.60 (*s*, 2H, H-7), 7.85 (*d*, 1H, *J* = 5.0, H-2), 7.93 (*d*, 1H, *J* =
5.0, H-3), 11.61 (*s*, 1H, N-H). ¹³C NMR (125 MHz, DMSO-*d*₆, δ): 13.90 (C-5),
53.65 (C-8), 63.01 (C-7), 123.33 (C-2), 143.94 (C-3), 146.98 (C-4), 161.23 (C-
1), 167.04 (C-6). (**HL**¹Cl -Z). ¹H NMR (500 MHz, DMSO-*d*₆, δ): 2.53 (*s*, 3H, H-
5), 3.34 (*s*, 9H, H-8), 4.82 (*s*, 2H, H-7), 7.85 (*d*, 1H, *J* = 5.0, H-2), 7.93 (*d*, 1H, *J* =
5.0, H-3), 11.86 (*s*, 1H, N-H). ¹³C NMR (125 MHz, DMSO-*d*₆, δ), : 15.05 (C-
5), 53.89 (C-8), 63.76 (C-7), 123.65 (C-2), 143.97 (C-3), 150.80 (C-4), 166.78
(C-1), 167.34 (C-6).

The Cu(II) complex 1

Yield: 42 mg (36 %). Combustion analysis for C₁₁H₂₀BCuF₄N₇O₂S:
Calculated. C 28.43, H 4.34, N 21.10, S 6.90; found C 28.53, H 4.15, N 21.17, S
6.89. IR (ATR): 3352w, 3317w, 3077m, 3050s, 2970m, 2940w, 2047vs, 1829w,
1698w, 1604w, 1522s, 1477m, 1444m, 1413m, 1395m, 1325m, 1287m, 1239w,
1159w, 1124w, 1088w, 1053m, 1007m, 961w, 939w, 917m, 878w, 783m, 735w,
656w, 631w, 563w.

*Corresponding author. E-mail: kka@chem.bg.ac.rs

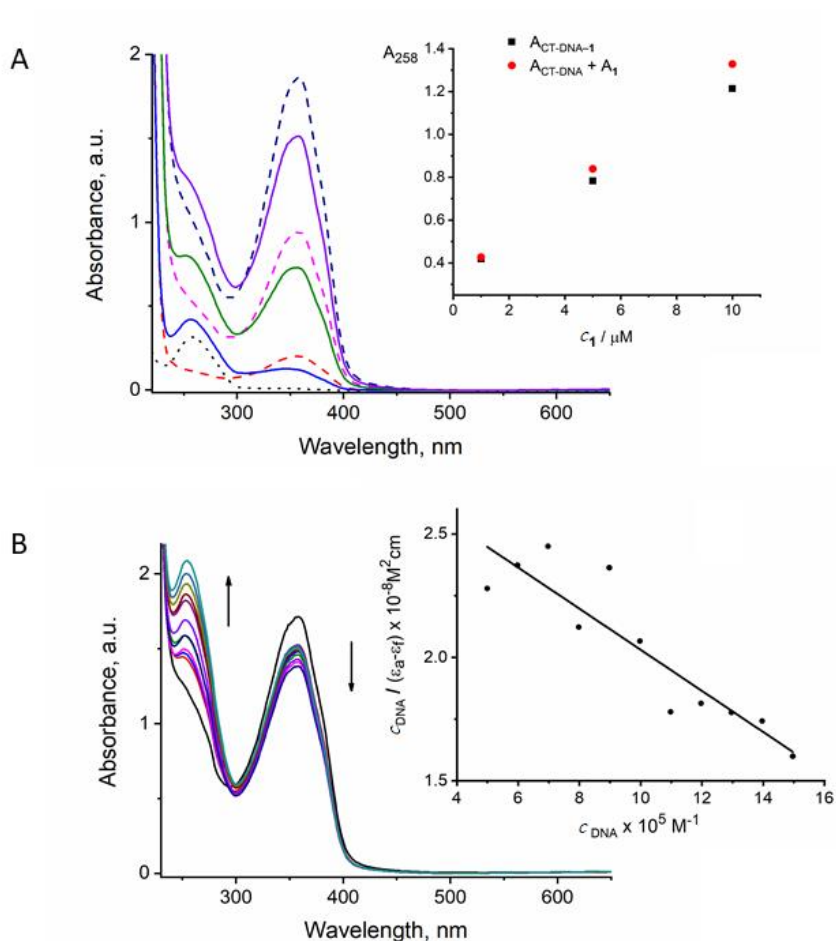


Fig. S-1. DNA-binding activity: (A) UV-Vis absorption spectra of CT-DNA (49.9 μM , dotted line), complex **1** (1, 5, and 10 μM , dashed lines) and **1**-CT-DNA after the interaction (solid lines); in the inset comparison of absorption at 258 nm between the CT-DNA-**1** and the sum of the values of CT-DNA and **1**; (B) – The absorbance titration of the compound **1** (10 μM) by gradually increasing the concentration of double stranded CT-DNA (4.99, 5.98, 6.98, 7.98, 8.98, 9.98, 10.98, 11.97, 12.97, 13.97 and 14.97 $\times 10^{-5}$ M); the arrows show the changes in absorbance with increasing amounts of CT-DNA; in the inset is shown the plot of $c_{\text{DNA}} / (\epsilon_A - \epsilon_F)$ versus c_{DNA} .

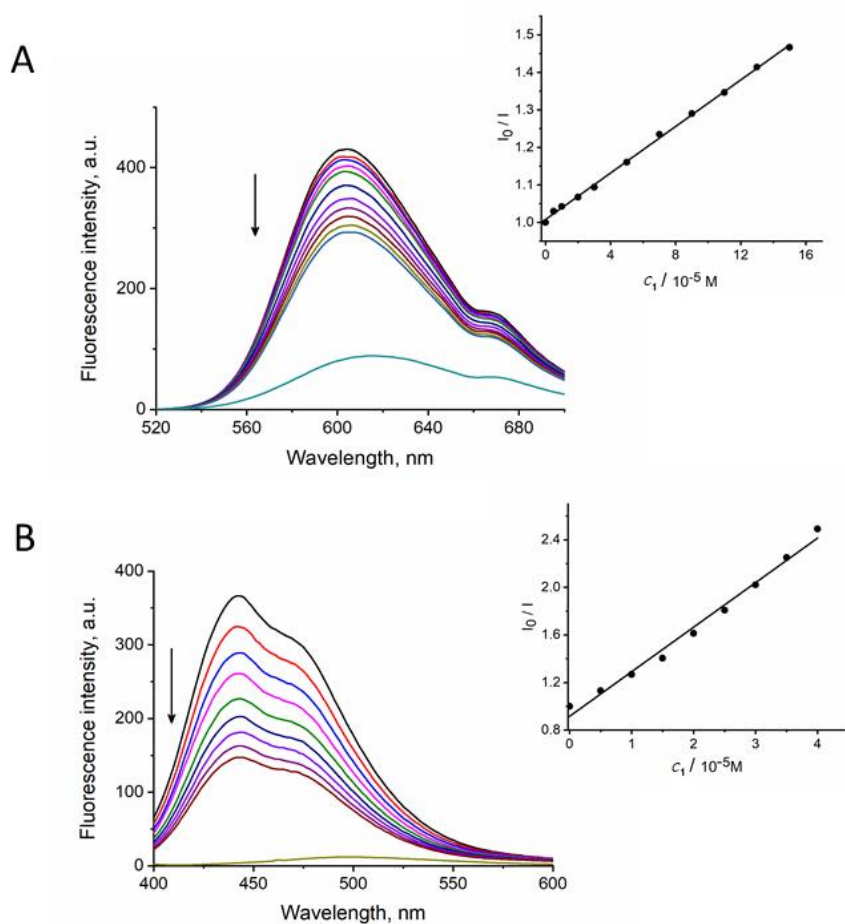


Fig. S-2. Fluorescence displacement study: (A) – changes in emission spectra of ethidium bromide ($2.5 \times 10^{-5} \text{ M}$) bound to CT-DNA ($9.7 \times 10^{-5} \text{ M}$) and quenching of EB–CT-DNA system by increasing concentrations of **1** (B) – Changes in emission spectra of Hoechst 33258 ($2.8 \times 10^{-5} \text{ M}$) bound to CT-DNA ($9.7 \times 10^{-5} \text{ M}$) and quenching H–CT-DNA system by increasing concentrations of **1**. The arrows show that fluorescence intensity decreased with increasing concentration of the complex. The insets in panels (A) and (B) show fluorescence quenching curves of EB bound to DNA at $\lambda_{\text{max}} = 600 \text{ nm}$ by **1**, and H bound to DNA at $\lambda_{\text{max}} = 443 \text{ nm}$ by **1**, respectively.

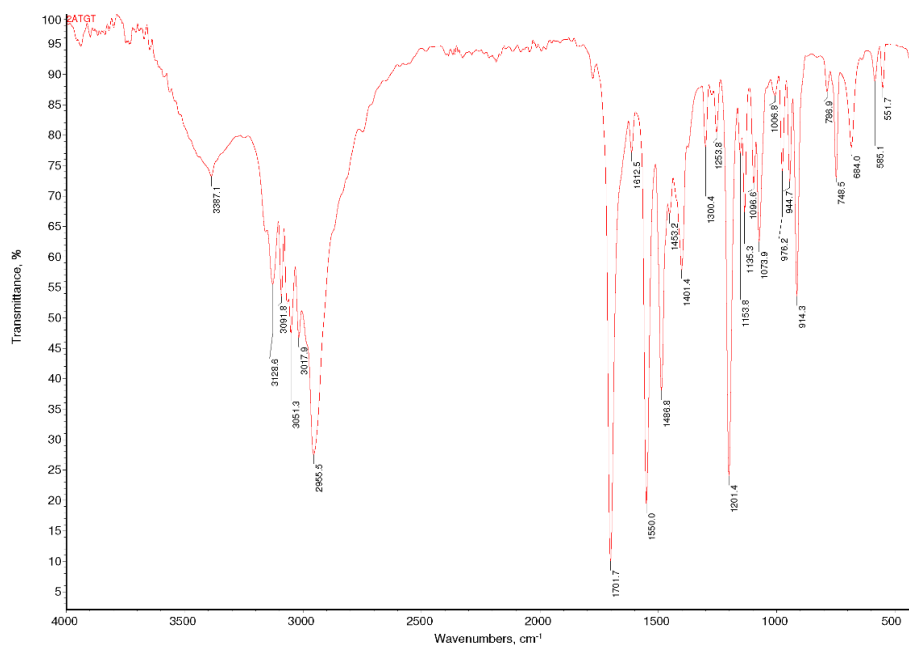


Fig. S-3. IR spectra of ligand HLCl

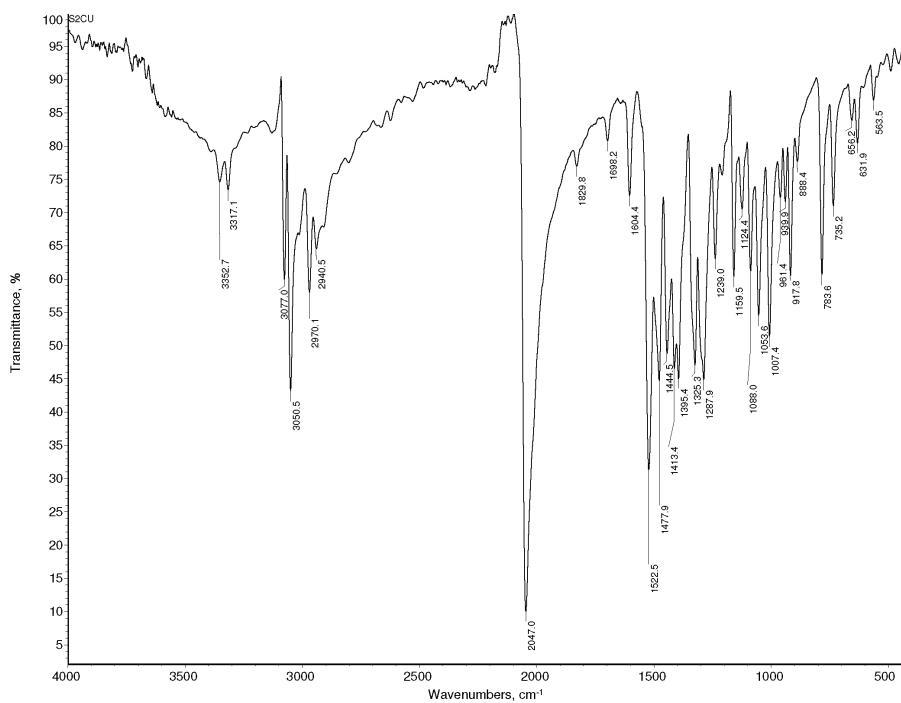


Fig. S-4. IR spectra of complex 1

BIOLOGICAL ACTIVITY

Measurement of intracellular reactive oxygen species (ROS) levels in HeLa and HaCaT cell lines

HeLa cells were incubated with IC_{50} concentration of Cu(II) complex for 24 h. After the incubation, the cells were collected by trypsinization, washed with PBS and incubated again in a solution of 30 μ M 2',7'-dichlorodihydrofluorescein diacetate in PBS for 45 min at 37 °C, according to the previously described procedure.¹ The cells were then washed with PBS and intracellular ROS levels were assessed by flow cytometry.

HaCaT cells were incubated with subtoxic IC_{20} concentration of Cu(II) complex for 24 h (applied concentration was 20 μ M, as assessed by MTT test for 24 h treatment). Afterwards, the cells were collected, washed and incubated in a solution of 30 μ M 2',7'-dichlorodihydrofluorescein diacetate in PBS for 45 min at 37 °C. After the incubation and washing, the cell samples were exposed to 4 mM hydrogen peroxide solution (H_2O_2) to induce the generation of ROS for 30 min at 37 °C. After 30 min, these cells were washed with PBS and analyzed.

The intensity of green fluorescence emitted by dichlorofluorescein in HeLa and HaCaT cells was measured by flow cytometry. Data are presented as mean \pm S.D. of two independent experiments.

Effects of Cu(II) complex on intracellular ROS levels

In order to explore the possible role of ROS generation in mediating cytotoxic effects of novel Cu(II) complex (**1**), the intracellular ROS level in HeLa cells treated with IC_{50} concentration of the complex for 24 h was measured by flow cytometry using 2',7'-dichlorodihydrofluorescein diacetate as a fluorescent probe. The effects of the complex on intracellular ROS levels in HeLa cells are presented in Fig. S-5. The tested Cu(II) complex **1** remarkably decreased the intracellular ROS level in HeLa cells, when compared with basal intracellular ROS level in untreated control cell samples, suggesting the antioxidant properties of tested complex at lower sub-toxic concentration.

Due to potential radical-scavenging activity of the novel complex, applied at subtoxic concentration, the effect of the complex on generation of intracellular ROS induced by H_2O_2 in normal keratinocytes HaCaT was examined, as it can be seen in Fig. S-6. Preincubation of normal HaCaT cells with subtoxic IC_{20} concentration of the complex for 24 h induced an increase in the intracellular ROS level triggered by exogenously added H_2O_2 , in comparison with this level in untreated control cells exposed only to H_2O_2 , pointing to prooxidant activity of **1** in the presence of H_2O_2 in normal cells. This is in accordance with the studies reporting an increase in intracellular ROS production induced by some copper complexes.²⁻⁴ Therefore, it is possible that higher toxic concentrations of

the investigated Cu(II) complex **1** may modulate differently intracellular ROS levels in cancer cells.

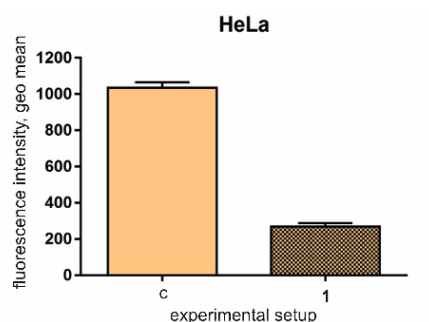


Fig. S-5. Effects of 24 h pretreatment of HeLa cells with IC_{50} concentration of the Cu(II) complex (**1**) on intracellular ROS level.

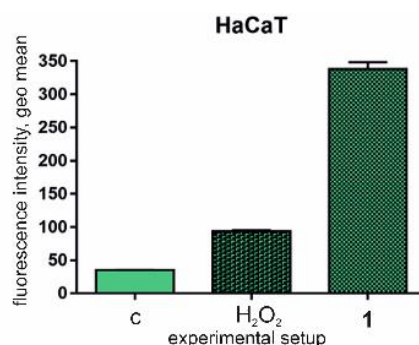


Fig. S-6. Effects of 24 h pretreatment of HaCaT cells with IC_{20} concentration of Cu(II) complex **1** on intracellular ROS production induced by hydrogen peroxide.

BSA fluorescence measurements

For BSA fluorescence measurements, BSA concentration in 40 mM bicarbonate buffer was kept constant in all samples, while the concentration of the compounds was increased: into 1 mL of buffer 10 μ L of stock solution of BSA (1 mg/mL) and 0.5 μ L of stock solution of the compound (10 mM) were added and incubated for 10 min. The emission spectra in range 295 to 500 nm were recorded (excitation wavelength 280 nm). Another 0.5 μ L of the solution of **1** was successively added at final concentrations of **1**: 5×10^{-6} M, 1, 1.5, 2, 2.5, 3, 3.5, 4, 4.5, 5, 5.5 and 6×10^{-5} M. The change in the fluorescence intensity was measured.

BSA interaction studies

BSA has often been used as a model protein to measure the albumin-binding ability of drugs and metal complexes. Fig. S-7 shows that BSA exhibited an

intense fluorescence emission band at 335 nm when excited at 296 nm, due to presence of tryptophan residues Trp-134 and Trp-212.⁵ The addition of increasing concentrations of **1** to BSA solution resulted in a significant quenching of fluorescence intensity, indicating the interaction of the complex with the protein. The obtained strong decrease in fluorescence intensity at maximum wavelength (by 65 %) and a blue shift (about 14 nm) suggested that the complex caused significant conformational changes in the secondary structure of albumin. The fluorescence quenching data were further analyzed with the Stern-Volmer equation (S-1).⁶

$$I_0/I = 1 + K_q\tau_0c_Q = 1 + K_{sv}c_Q \quad (\text{S-1})$$

$$K_q = K_{sv} / \tau_0 \quad (\text{S-2})$$

where I and I_0 are the steady state fluorescence intensities in presence and absence of a quencher, respectively. K_{sv} is the Stern-Volmer constant and c_Q is concentration of the quencher; τ_0 is the average lifetime of the protein without the quencher. As shown in insets in Fig. S-7, good linear fitting linearity of the plot suggests that the Stern-Volmer model is appropriate for studying the binding mechanism between **1** and BSA. The Stern-Volmer constant K_{sv} and the quenching constant K_q were calculated using the equations (S-1) and (S-2), respectively. K_{sv} for **1** was calculated from the plot of I_0/I versus c_1 as $2.75 \times 10^4 \text{ M}^{-1}$. Assuming that average lifetime of the biomolecule is around 10^{-8} s^{-1} K_q value for **1** was calculated to be $2.75 \times 10^{-12} \text{ M}^{-1}\text{s}^{-1}$, indicating static quenching, *i.e.* the formation of a nonfluorescent complex between the compound and BSA.

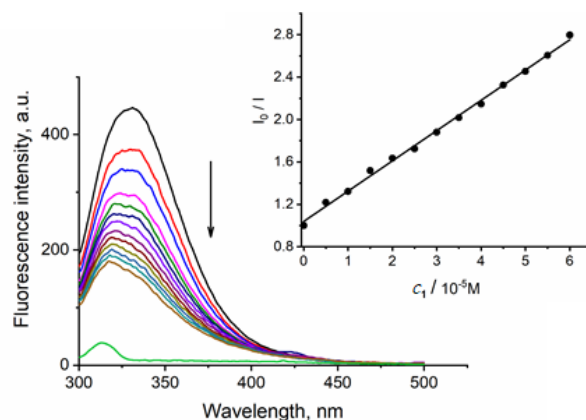


Fig. S-7. Fluorescence spectra of BSA in the absence and presence of increasing concentrations of **1**. Value of K_{sv} was calculated from the plot I_0/I versus c_1 shown in inset. The arrow shows the decrease in fluorescence intensities with increasing concentrations of the complex.

DNA cleavage experiments. For DNA cleavage experiments, plasmid pUC19 (pUC19, 2686 bp, purchased from Sigma-Aldrich, USA) was prepared by its

transformation in chemically competent cells *Escherichia coli* strain XL1 blue. Amplification of the clone was done according to the protocol for growing *E. coli* culture overnight in LB medium at 37 °C⁸ and purification was performed using Qiagen Plasmid plus Maxi kit. Finally, DNA was eluted in 10 mM Tris-HCl buffer and stored at –20 °C. The concentration of plasmid DNA (550 ng/μL) was determined by measuring the absorbance of the DNA-containing solution at 260 nm. One optical unit corresponds to 50 μg/mL of double stranded DNA.

The cleavage reaction of supercoiled pUC19 DNA (550 ng) with complex **1** (1, 2, 3, 4, 5, 6 and 7 mM) was performed in a 20 μL reaction mixture in 40 mM bicarbonate buffer pH 8.4 at 37 °C, for 90 minutes. The reaction mixtures were vortexed from time to time. The reaction was terminated by short centrifugation at 10000 rpm and addition of 5 μL of loading buffer (0.25 % bromophenol blue, 0.25 % xylene cyanol FF and 30 % glycerol in TAE buffer, pH 8.24 (40 mM Tris-acetate, 1 mM EDTA)). The samples were subjected to electrophoresis on 1 % agarose gel (Amersham Pharmacia-Biotech, Inc) prepared in TAE buffer pH 8.24. The electrophoresis was performed at a constant voltage (80 V) until bromophenol blue had passed through 75 % of the gel. A Submarine Mini-gel Electrophoresis Unit (Hoeffer HE 33) with an EPS 300 power supply was used. After electrophoresis, the gel was stained for 30 min by soaking it in an aqueous ethidium bromide solution (0.5 μg/mL). The stained gel was illuminated under a UV transilluminator Vilber-Lourmat (France) at 312 nm and photographed with a Nikon Coolpix P340 Digital Camera through filter DEEP YELLOW 15 (TIFFEN, USA).

DNA cleavage. The type of DNA interactions with the metal complex has been further established by the investigation of damage to circular DNA. The nuclease efficiency of the Cu(II) complexes is usually investigated using different activators for initiating the DNA cleavage.⁹ In this work, the ability of **1** to cleave double-stranded plasmid DNA in the absence of reducing agents was investigated using an agarose electrophoretic assay by monitoring the conversion of supercoiled form (FI) plasmid DNA into the nicked (FII) and the linear form (FIII). As shown in Fig. S-8 (lane 1), plasmid pUC19 consisted mainly of FI and FII. Upon the addition of an increasing concentration of complex **1** to the plasmid, a gradual diminishing of the amount of supercoiled form FI, followed by the formation of nicked form FII, occurred. In addition, the bands corresponding to FI and FII forms smeared at a much higher concentration of **1** (5, 6 and 7 mM, lanes 6, 7 and 8, respectively), indicating the nuclease activity of the complex, which converts DNA to shorter fragments. The form FIII was not observed at the applied concentration range of **1**, indicating that the double strand scission did not occur upon the interaction of complex Cu(II) with circular DNA.

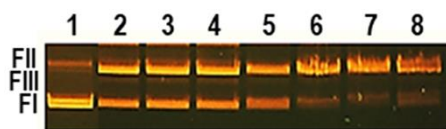


Fig. S-8. DNA cleavage activity of **1**: the agarose gel electrophoretic pattern of supercoiled form FI, open form FII and linear form FIII of pUC19 (0.32 μ M; lane 1) after an interaction with **1** (1, 2, 3, 4, 5, 6 and 7 mM, lanes 2–8, respectively).

REFERENCES

1. N. Mihailović, V. Marković, I. Z. Matic, N. S. Stanisavljević, Ž. S. Jovanović, S. Trifunović, L. Joksović, *RSC Advances* **7** (2017) 8550 (<http://dx.doi.org/10.1039/C6RA28787E>)
2. C. R. Kowol, P. Heffeter, W. Miklos, L. Gille, R. Trondl, L. Cappellacci, W. Berger, B. K. Keppler, *J. Biol. Inorg. Chem.* **17** (2012) 409 (<http://dx.doi.org/10.1007/s00775-011-0864-x>)
3. A. Sirbu, O. Palamarciuc, M. v. Babak, J. M. Lim, K. Ohui, E. A. Enyedy, S. Shova, D. Darvasiová, P. Rapta, W. H. Ang, V. B. Arion, *Dalton Trans.* **46** (2017) 3833 (<http://dx.doi.org/10.1039/C7DT00283A>)
4. C. Shobha Devi, B. Thulasiram, R. R. Aerva, P. Nagababu, *J. Fluoresc.* **28** (2018) 1195 (<http://dx.doi.org/10.1007/s10895-018-2283-7>)
5. C. Protogeraki, E. G. Andreadou, F. Perdih, I. Turel, A. A. Pantazaki, G. Psomas, *Eur. J. Med. Chem.* **86** (2014) 189 (<http://dx.doi.org/10.1016/j.ejmech.2014.08.043>)
6. K. Ghosh, S. Rathi, D. Arora, *J. Lumin.* **175** (2016) 135 (<http://dx.doi.org/10.1016/j.jlumin.2016.01.029>)
7. P. Banerjee, S. Pramanik, A. Sarkar, S. C. Bhattacharya, *J. Phys. Chem. B* **113** (2009) 11429 (<http://dx.doi.org/10.1021/jp811479r>)
8. W. J. Dower, J. F. Miller, C. W. Ragsdale, *Nucleic Acids Res.* **16** (1988) 6127 (<http://dx.doi.org/10.1093/nar/16.13.6127>)
9. K. Ghosh, P. Kumar, N. Tyagi, U. P. Singh, V. Aggarwal, M. C. Baratto, *Eur. J. Med. Chem.* **45** (2010) 3770 (<http://dx.doi.org/10.1016/j.ejmech.2010.05.026>).



J. Serb. Chem. Soc. 87 (2) 193–203 (2022)
JSCS–5515

Density functional theory calculations and molecular docking of 2-phenylbenzimidazoles with estrogen receptor for quantitative structure–activity relationship studies

NOSRAT MADADI MAHANI^{1*}, SAYED ZIA MOHAMMADI¹
and KHADIJE ANJOMSHOA²

¹Department of Chemistry, Payame Noor University, 19395-4697, Tehran, Iran and
²Chemistry Department, ValiAsr University of Rafsanjan, P.O. Box 518 Rafsanjan, Iran

(Received 2 March, revised 16 May, accepted 31 May 2021)

Abstract: Benzimidazole derivatives, especially 2-phenylbenzimidazole with various substituents on the C-5, C-2 and C-6 positions, are so important in pharmaceutical chemistry. Multiple linear regression was applied to predict the activity of 27 novel 2-phenylbenzimidazole derivatives as anticancer agents. At first, we made an effort to create a QSAR model for a selected series of novel 2-phenylbenzimidazole with density functional theory and molecular docking descriptors. Then, we tried to investigate the nature of the interactions between 2-phenylbenzimidazole derivatives and the estrogen receptor using the molecular docking method. Six descriptors of MATS4e, GATS5e, R6v, R1v+, dipole moment, and torsional free energy were selected for modelling. Due to docking results, increase in the binding energy, and decrease in the dipole moment could increase inhibitor activity.

Keywords: dipole moment; torsional free energy; breast cancer; biological activity.

INTRODUCTION

Cancer is one of the most serious diseases created by unusual cell growth invading and spreading to different organs of the human body. Estrogen receptor (ER) is a therapeutic target and crucial prognostic sign of breast cancer.¹ Estrogen advances breast cancer propagation through several appointed paths. Binding estrogen with estrogen receptors irritates the estrogen responsive element of DNA. This complex causes duplication of cells and result in breast cancer.² Many studies have been performed in design and discovery research of novel selective estrogen receptor modulators. Thus, the design and synthesis of novel anticancer agents with further improvement and fewer side effects is necessary.

*Corresponding author. E-mail: nmmdady@gmail.com
<https://doi.org/10.2298/JSC210302044M>

Benzimidazole is aromatic heterocycle found in extensive number of natural and biologically active molecules and considered to be significant pharmacophore.³ Derivatives of novel benzimidazole replaced with various functional groups can be used as an antibacterial,⁴ antimicrobial,⁵ anti-inflammatory,⁶ analgesic,⁷ anthelmintic⁸ and antitumor⁹ agents. The benzimidazole is particularly one of the most effective compounds used in therapy of several cancer cell lines. The existence of substituents, such as hydroxyl groups and carbonyl in the C-5 position, besides substituents in the C-2 position, could remarkably increase the novel compounds' anticancer activity.¹⁰ Huynh and co-workers synthesized several new derivatives of 2-phenylbenzimidazole with a various range of substituents on the C-5, C-2 and C-6 positions of 2-phenylbenzimidazole with the condensation of o-phenylenediamines and different aldehydes and afterwards illustrated their structure–activity relationship (SAR) upon three cancer cell lines: PC3, MDA-MB-231 and A54.¹¹

On the other hand, quantitative structure–activity relationship studies have obtained a fundamental position within medicine chemistry. In QSAR analysis, one or more molecular descriptors described the molecular activity using statistical analysis. The basic goal of this analysis is the development of statistical models for prediction of the biological activity of novel compounds that have not been synthesized or their biological activity have not been determined. Several statistical methods suitable for chemometric analysis include multiple linear regression, partial least squares regression, principal component regression, and different types of artificial neural networks,¹² which can be used to create a correlation model between molecular descriptors and the related properties. Molecular descriptors can be calculated with molecular docking and DFT calculations.

Molecular docking may be a simulation approach for planning drug which can predict the compliance of a receptor–ligand complex. The receptor is regularly a protein or a nucleic acid molecule (DNA or RNA) and the ligand could be a small particle or drug.¹³ Besides, molecular docking is one of main instruments for virtual screening strategies. Docking research and examination of the larvicidal action of some 2-phenylbenzimidazole derivatives were handled by Escal *et al.*¹⁴ Novel benzimidazole subsidiaries as cholinesterase inhibitors were synthesized by Yoon *et al.* and their docking examination were explored.¹⁵ Mizuno *et al.* explored docking atomic of novel benzimidazoles for the treatment of metabolic disorder.¹⁶ Molecular docking research on a set of bisphenylbenzimidazole derivatives have been examined to identify the compounds binding orientations inside the HIV-1 reverse transcriptase non-nucleoside binding pocket.¹⁷ A suitable correlation between the computed binding free energies and the experimental inhibitory activities proposes that the distinguished binding conformations of these inhibitors are reputable. This model may be utilized for a new non-nucleoside HIV-1 reverse transcriptase inhibitors due to the 1-benzyl-2-arylbenzim-

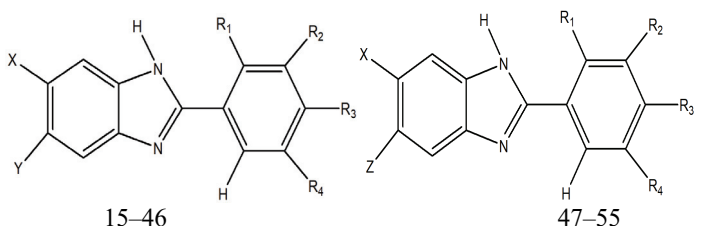
imidazole scaffold. An appropriate QSAR model due to radial distribution performance descriptors and docking have been displayed for a few 4-anilinoquinazoline derivatives as potent EGFR inhibitors by Beglari *et al.*¹⁸

We investigated the binding mode of new 2-phenylbenzimidazole derivatives (chemical structures are shown in Table I) with estrogen receptor offering a QSAR model which could predict the biological activity of novel 2-phenylbenzimidazole. Multiple linear regressions were used to predict the activities of novel 2-phenylbenzimidazole. At first, we made an effort to create a QSAR for a selected series of novel 2-phenylbenzimidazole with DFT and molecular docking descriptors. Then, we attempted to investigate the nature of interactions between 2-phenylbenzimidazole derivatives and estrogen receptor using the molecular docking method.

EXPERIMENTAL

The dataset, involving 2-phenylbenzimidazole derivatives with inhibitory activity IC_{50} was provided from the literature. The structure of studying compounds is indicated in Table I.

TABLE I. Structures of the compounds used in inhibitory activity modelling and their IC_{50} ¹¹



Compd.	X	Y	Z	R1	R2	R3	R4	IC_{50} / μ M
15	H	Cl	–	OH	H	H	H	>100
16	H	Cl	–	H	OH	H	H	18.20
17	H	Cl	–	H	H	OH	H	36.56
19	H	Cl	–	OCH ₃	H	H	OCH ₃	85.11
20	H	Cl	–	H	OCH ₃	OCH ₃	OCH ₃	21.88
21	H	Cl	–	H	H	N(CH ₃) ₂	H	18.62
22	H	Cl	–	NO ₂	H	H	H	33.11
23	H	Cl	–	CF ₃	H	H	H	6.92
24	H	Cl	–	H	OCH ₃	OH	I	39.26
25	H	Cl	–	H	H	OCH ₂ Ph	H	19.95
28	Cl	Cl	–	H	H	OH	H	60.26
30	Cl	Cl	–	OCH ₃	H	H	OCH ₃	69.18
31	Cl	Cl	–	H	OCH ₃	OCH ₃	OCH ₃	>100
32	Cl	Cl	–	H	H	N(CH ₃) ₂	H	60.26
34	Cl	Cl	–	CF ₃	H	H	H	>100
36	Cl	Cl	–	H	H	–O–CH ₂ –Ph	H	52.48
37	H	Ph–CO–	–	OH	H	H	H	>100
38	H	Ph–CO–	–	H	OH	H	H	5.50
40	H	Ph–CO–	–	H	H	OCH ₃	H	>100

TABLE I. Continued

Compd.	X	Y	Z	R1	R2	R3	R4	IC_{50} / μ M
41	H	Ph-CO-	-	H	OCH ₃	OCH ₃	OCH ₃	>100
45	H	Ph-CO-	-	H	OCH ₃	OH	I	54.95
47	H	-	Ph-CH(OH)-	OH	H	H	H	17.78
48	H	-	Ph-CH(OH)-	H	OH	H	H	17.38
49	H	-	Ph-CH(OH)-	H	H	OH	H	33.88
50	H	-	Ph-CH(OH)-	H	H	OCH ₃	H	53.70
51	H	-	Ph-CH(OH)-	H	OCH ₃	OCH ₃	OCH ₃	>100
53	H	-	Ph-CH(OH)-	CF ₃	H	H	H	47.86

Drawing of the structure of pharmaceutical derivatives was done with Gauss View software. The computation of optimization and frequency of the structure of 2-phenylbenzimidazole derivatives as ligand were with density functional hypothesis (DFT) approach¹⁹ utilizing G09 software.²⁰ In these calculations, the B3LYP level of theory²¹ and with 6-311G* standard basis set for all atoms except iodine (I) atom with LANL2Z, basis set²² has been used. Some of the computed descriptors used in this research consisted the lowest unoccupied molecular orbital and the highest occupied molecular orbital energies, electron affinity, and dipole moment, enthalpy, and log *P* and electrophilicity index. Frontier molecular orbitals of HOMO and LUMO were acquired from the population analysis calculations and visualized using Gauss View. These parameters play an influential and important role in illustrated ligands interaction in the binding pocket of the Estrogen receptor. Using the analytic second derivatives, harmonic vibrational wavenumbers were computed to corroborate the convergence to minima on the potential surface.

Docking calculations between new 2-phenylbenzimidazole derivatives as ligand and estrogen receptor have been performed using Auto Dock 4.2.²³ Estrogen receptor crystal structure (PDB ID: 3OS8) has been gained from Protein Data Bank (www.rcsb.org). This receptor has four chains A, B, C, and D but three B, C and D were omitted. Then, molecular docking was accomplished using the Lamarckian genetic algorithm.¹³ To identify the binding sites in estrogen receptor, blind docking has been done, by the grid size set to 60, 60, and 60 Å³ along with X-, Y- and Z-axis with 9.526, 22.699 and -23.362 Å grid space. The conformation with the lowest binding free energy and low inhibition constants was employed for better analysis. Dragon, Gaussian and Auto Dock softwares were utilized to create molecular descriptors. By stepwise MLR approach, the linear relationship between a dependent variable, p*IC*₅₀ (-log *IC*₅₀), and independent variables, like electronic, constitutional, topological, and steric descriptors, is displayed as a linear equation, which makes it a potent method for QSAR modelling.

RESULTS AND DISCUSSION

The reactivity of compounds was foretold, and several energy descriptors were investigated in detail. In usual, the frontier molecular orbitals are utilized to study the interactions 2-phenylbenzimidazole derivatives. In addition, HOMO and LUMO orbitals indicate the reactivity of 2-phenylbenzimidazole derivatives and their possible interactions with estrogen receptor.²⁴ HOMO and LUMO orbitals of one of the foremost biological activity are indicated in Fig. 1.

HOMO-LUMO's red and green colours, respectively, indicate positive and negative orbitals. HOMO is delocalized over the complete molecule, whereas

LUMO is delocalized but within the monosubstituted phenyl ring. It shows the charge transfer inside the molecules. Electronic descriptors are revealed in Tables II and III. The energy gap values were computed for these compounds which build up the stability and bioactivity of the molecules. For all molecules, energy gap over 3eV and chemical potentials are equal or higher than -3.9 eV. The computed higher hardness value, moreover, shows the stability of the molecules. All the molecules have high electrophilicity index values for the sake of which are assessed as dynamic biological system. For the foremost portion, the higher electronegative potential surface was found over C=O, which illustrates that it ought to be susceptible to nucleophilic attacks.

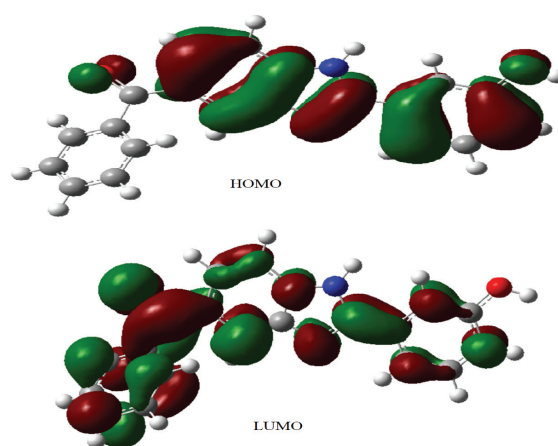


Fig. 1. Frontier orbitals of 2-phenylbenzimidazole derivatives (**38**).

TABLE II. Values of the descriptors of HOMO, LUMO, energy gap, ionization potential ($I = -E_{\text{HOMO}}$), electron affinity ($A = -E_{\text{LUMO}}$) global hardness ($\eta = (I-A)/2$) and softness ($S = 1/\eta$) at the B3LYP/6-31G level

Comp.	HOMO, eV	LUMO, eV	Energy gap, eV	I / eV	A / eV	η / eV	S / eV
15	-6.1613	-1.6491	-4.5122	6.1613	1.6491	2.2561	163.9640
16	-6.3158	-1.7791	-4.5366	6.3158	1.7791	2.2683	163.0793
17	-6.1112	-1.6192	-4.4920	6.1112	1.6192	2.2460	164.6987
19	-5.9200	-1.6167	-4.3033	5.9200	1.6167	2.1516	171.9233
20	-5.9750	-1.5533	-4.4216	5.9750	1.5533	2.2108	167.3228
21	-5.4443	-1.3610	-4.0832	5.4443	1.3610	2.0416	181.1883
22	-6.7023	-3.6883	-3.0140	6.7023	3.6883	1.5070	245.4652
23	-6.6471	-2.2714	-4.3756	6.6471	2.271	2.1878	169.0806
24	-6.2105	-1.7756	-4.4349	6.2105	1.7756	2.2174	166.8199
28	-6.2568	-1.8376	-4.4191	6.2568	1.8376	2.2095	167.4155
30	-6.0566	-1.8196	-4.2369	6.0566	1.8196	2.1184	174.6164
32	-5.4897	-1.5074	-3.9823	5.4897	1.5074	1.9911	185.7796
36	-6.1439	-1.7614	-4.3824	6.1439	1.7614	2.1912	168.8182
38	-6.2565	-1.9263	-4.3302	6.2565	1.9263	2.1651	170.8542

TABLE II. Continued

Comp.	HOMO, eV	LUMO, eV	Energy gap, eV	I / eV	A / eV	η / eV	S / eV
45	-6.1648	-1.9507	-4.2140	6.1648	1.9507	2.1070	175.5631
25	-1.5297	-4.4588	5.9886	-0.0562	6.0231	0.0830	-2.9661
31	-1.8765	-4.2820	6.1586	-0.0689	6.2003	0.08064	-3.0448
34	-2.2714	-5.9619	8.2334	-0.0835	8.2669	0.0604	-4.0749
37	-1.8248	-4.2793	6.1042	-0.0670	6.1382	0.08145	-3.0185
40	-1.8528	-4.1088	5.9616	-0.0681	5.9967	0.08337	-2.9467
41	-1.9094	-4.1020	6.0114	-0.0702	6.0114	0.08317	-2.9706

TABLE III. Values of the descriptors of chemical potential ($\mu = -(I + A)/2$), electronegativity ($\chi = -\mu$), electrophilicity index ($\omega = 2\mu/2\eta$), enthalpy, dipole moment and solubility ($\log P$) at the B3LY P/6-31G level

Comp.	μ / eV	χ / eV	$\omega = 2\mu/2\eta$	$\log P$	Enthalpy, kcal* mol ⁻¹	Dipole moment, D
15	-3.9052	3.9052	0.0232	-0.61	-1145.5221	7.8058
16	-4.0474	4.0474	0.0251	-0.61	-1145.5151	5.9407
17	-3.8652	3.8652	0.0226	-0.61	-1145.5152	7.1983
19	-3.7684	3.7684	0.0206	-1.57	-1299.2709	6.6226
20	-3.7642	3.7642	0.0211	-2.56	-1413.7352	3.9989
21	-3.4027	3.4027	0.0159	-0.53	-1204.1882	8.7549
22	-5.1953	5.1953	0.0274	-2.33	-1274.7754	4.0937
23	-4.4593	4.4593	0.0294	0.99	-1407.3609	4.7797
24	-3.9930	3.9930	0.0238	-1.08	-1270.7727	5.2597
28	-4.0472	4.0472	0.0244	-0.83	-1605.1209	7.5822
30	-3.9381	3.9381	0.0222	-1.79	-1758.8770	7.4367
32	-3.4986	3.4986	0.0164	-0.75	-1663.7944	10.1408
36	-3.9527	3.9527	0.0231	0.22	-1875.3535	8.3441
38	-4.0914	4.0914	0.0244	0.7	-1030.1764	5.6543
45	-4.0578	4.0578	0.0234	0.22	-1155.4341	5.1256
25	2.9661	-1.5297	-4.4588	0.44	-1415.7479	7.1679
31	3.0448	-1.8765	-4.2820	-2.78	-1873.3408	4.893
34	4.0749	-2.2714	-5.9619	0.99	-1407.3609	6.8421
37	3.0185	-1.824	-4.2793	0.7	-1030.1834	4.5896
40	2.9467	-1.852	-4.1088	0.73	-1069.4472	3.1936
41	2.9706	-1.9094	-4.1020	-1.26	-1298.3963	3.8498

For this research, interactions among 2-phenylbenzimidazole derivatives as ligand and estrogen receptor were performed by docking approach. As shown in Table III, docking descriptors involve binding energy, inhibition constant, Van der Waals energy, hydrogen bond and dehydration, total internal energy, ultimate intra-molecular energy, torsional free energy, and nonbinding energy. The inhibitory activity of ligands **38**, **19** and **30** is great. The inhibitory activity of ligands **17** and **15** is small. As shown in Fig. 2, docking of medicinal ligand **38** with estrogen receptor (3OS8) were detailed with Discovery Studio visualizer 4.1

* 1 kcal = 4184 J

(2014) software. For the protein 3OS8 (A), the exchanges are the residues of estrogen inhibitor; Arg 394, Met 357 and Glu 353 form π -sigma exchange with OH and C=O for ligand **38**. The ligand forms stable complex and has good binding affinity values (-9.2 kcal/mol for the complex with 3OS8 (A), all derivatives give high binding energy values, -8.9 , -8.6 , -9.6 and -9.02 kcal/mol for ligands of **48**, **53**, **49** and **37**, respectively. Therefore, the 2-phenylbenzimidazole derivatives display activity against estrogen inhibitor. Ligands of **17** and **15** displayed the maximum of inhibition constant (k_i) which have least activity because they have only OH substituent on the benzene ring.

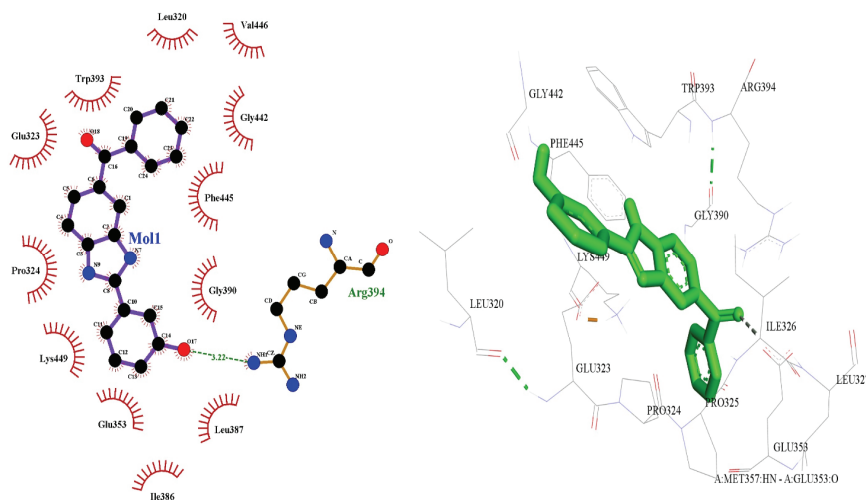


Fig. 2. Docking of ligand **38** with protein 3OS8 (A).

Ligands of **38** and **20** displayed the least of inhibition constant for they have Ph-C=O functional group. This evidence indicated that appropriate functional groups on the benzene ring were necessary for increases and better antibacterial activities in drug design. Therefore, these results indicate that electron-withdrawing groups play an important role in the anticancer activities of 2-phenylbenzimidazole derivatives.

The data set composed of 27 molecules is offered to an advanced multiple regression analysis until designing a MLR model. This method used the coefficients R , R^2 and the standard deviation to select the best regression performance. The correlation coefficient is $R = 0.931$, $R^2 = 0.866$, and $F = 14.047$. These values are related to assess the best model. The values of pIC_{50} of training and test sets, were predicted using MLR model. Statistical parameters of the best QSAR model, are shown in Table IV.

QSAR methods were performed on 2-phenylbenzimidazole derivatives to predict their biological activities. The values of predicted pIC_{50} , calculated with

statistical parameters and the graph of experimental pIC_{50} values against calculated pIC_{50} values using MLR method are seen in Fig. 3.

TABLE IV. Values of the chemical descriptors were obtained using molecular docking

Compd.	Energy, kcal mol ⁻¹							k_i μM
	Bind- ing	Torsion al free	Final total internal	Final inter- molecular	Unbound systems	Electro- static	vdW + Hbond + desolv	
15	-6.5	0.6	-0.78	-7.13	-0.78	-0.3	-6.84	16.2
16	-7	0.6	-0.17	-7.63	-0.17	-0.37	-7.63	7.01
17	-6.4	0.6	-0.2	-6.97	-0.2	-0.1	-6.86	21.2
19	-7.9	0.89	-0.31	-8.75	-0.31	-0.37	-8.38	1.76
20	-7.1	1.19	-0.63	-8.33	-0.63	-0.13	-8.2	5.86
21	-6.7	0.6	-0.32	-7.32	-0.32	-0.1	-7.22	11.8
22	-7.8	0.6	-0.94	-8.43	-0.94	-1.14	-7.29	1.81
23	-6.7	0.6	-0.56	-7.28	-0.56	-0.02	-7.26	12.6
24	-7.2	0.89	-0.99	-8.07	-0.99	0	-8.07	5.53
28	-6.6	0.6	-0.19	-7.18	-0.19	-0.12	-7.06	15
30	-7.8	0.89	-0.31	-8.73	-0.31	-0.33	-8.39	1.82
32	-6.9	0.6	-0.32	-7.5	-0.32	-0.1	-7.4	8.71
36	-8.7	1.19	-0.84	-9.86	-0.84	0.09	-9.94	0.45
38	-9.2	1.19	-0.62	-10.4	-0.62	-0.4	-10.03	0.17
45	-9	1.49	-1.44	-10.5	-1.44	-0.01	-10.52	0.24
47	-8.7	1.49	-1.11	-10.2	-1.11	-0.34	-9.81	0.45
48	-8.9	1.49	-0.61	-10.4	-0.61	-0.39	-10	0.3
49	-9.6	1.49	-0.54	-9.81	-0.54	-0.19	-9.61	0.8
50	-8.7	1.49	-0.58	-10.2	-0.58	-0.23	-9.96	0.42
51	-8.7	2.09	-0.99	-10.8	-0.99	-0.29	-10.52	0.41
53	-8.6	1.49	-0.96	-10.1	-0.96	-0.19	-9.93	0.47
25	-8.42	1.19	-0.86	-9.61	-0.86	0.07	-9.68	0.67
31	-7.03	1.19	-0.65	-8.22	-0.65	-0.13	-8.09	7.05
34	-6.68	0.6	-0.56	-7.28	-0.56	-0.02	-7.26	12.60
37	-9.02	1.19	-1.23	-10.21	-1.23	-0.38	-9.83	0.24
40	-8.45	1.19	-0.69	-9.64	-0.69	-0.03	-9.61	0.64
41	-8.49	1.79	-1.08	-10.28	-1.08	-0.09	-10.2	0.59

This study proposed the role of atomic features (mass, van der Waals volume and Sanderson electronegativities) due to weighted 2D-autocorrelations (MATS4e and GATS5e) and descriptors due to the elements of leverage matrix obtained by centered atomic coordinates considering weighted by van der Waals volume (GETAWAY descriptors: R6v and R1v+). In MLR models (Table V), R6V descriptor has a negative correlation with pIC_{50} . The small values of dipole moment indicate a high degree of anticancer activity, e.g., compounds **20** and **38** (8.7549 and 5.6543 D) compared to the compounds **32** (10.1408 D). As a result, ligands **38** and **20** have better inhibitory activity than the ligands **32**. R1v+ and MATS4e descriptors have a positive correlation with pIC_{50} .

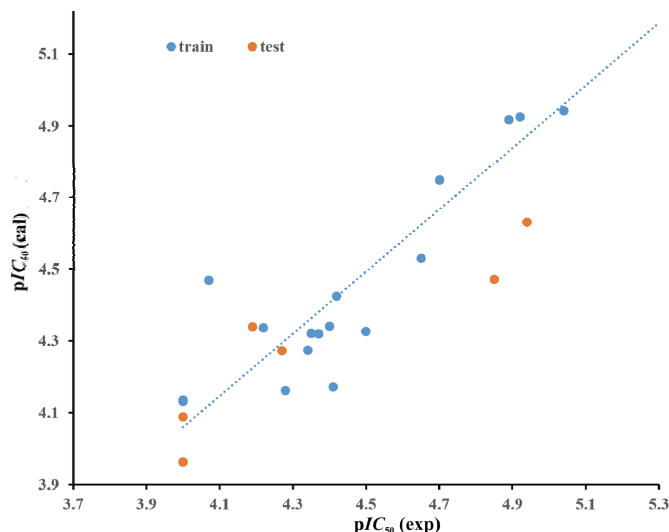


Fig. 3. Plot of experimental pIC_{50} of 2-phenylbenzimidazole derivatives against the calculated values of pIC_{50} using MLR model.

TABLE V. MLR model for of 2-phenylbenzimidazoles

Descriptor definition	Descriptor type	Regression coefficient	Standard deviation
Dipole moment	Electronic	0.065	0.033
Torsional free energy	Docking property	0.077	0.121
MATS4e	2D-autocorrelations	3.001	0.609
GATS5e	2D-autocorrelations	0.675	0.228
R6v	GETAWAY descriptors	-7.976	1.190
R1v+	GETAWAY descriptors	14.295	3.604
Constant	—	5.430	0.495

CONCLUSION

Regarding the results of QSAR, the prediction of 2-phenylbenzimidazole derivatives data in MLR method was acceptable. Hydrogen and hydrophobic interactions were investigated by molecular docking. Results showed that raising binding energy values and decreasing the constant inhibition reduce the inhibitory activity of 2-phenylbenzimidazole derivatives. Arg 394, Met 357 and Glu 353 amino acids of estrogen receptor have an important role in interaction. These results could prepare an important structural intuitions required to optimize 2-phenylbenzimidazole-sensitive inhibitors of the estrogen receptor. Considering DFT calculation compound **38** is susceptible to nucleophilic attacks due to higher electronegative potential surface. Ligands **20** and **38** are introduced for later research because they displayed the minimum value of inhibition constant and the highest electronegative surface potential.

Acknowledgement. The authors are grateful to the Payame Noor University for encouragements.

ИЗВОД

ТЕОРИЈА ФУНКЦИОНАЛА ГУСТИНЕ И МОЛЕКУЛСКИ ДОКИНГ ЗА ПРОУЧАВАЊЕ
КВАНТИТАТИВНЕ РЕЛАЦИЈЕ СТРУКТУРА–АКТИВНОСТ У ИНТЕРАКЦИЈИ
2-ФЕНИЛБЕНЗИМИДАЗОЛА И РЕЦЕПТОРА ЕСТРОГЕНА

NOSRAT MADADI MAHANI¹ SAYED ZIA MOHAMMADI¹ и KHADIJE ANJOMSHOA²

¹Department of Chemistry, Payame Noor University, 19395-4697, Tehran, Iran u ²Chemistry Department, ValiAsr University of Rafsanjan, P.O. Box 518 Rafsanjan, Iran

Деривати бензимидазола, нарочито 2-фенилбензимидазола са разним супституентима на положајима С-5, С-2 и С-6, су веома значајни у фармацеутској хемији. Примењена је вишеструка линеарна регресија за предвиђање активности 27 нових 2-фенилбензимидазолских деривата као антиканцерских агенаса. Направљен је QSAR модел за одабрану серију нових 2-фенилбензимидазола помоћу дескриптора из теорије функционала густине и молекулског докинга. За природу интеракција између деривата 2-фенил+бензимидазола и рецептора естрогена, коришћен је метод молекулског докинга. За моделовање је одабрано шест дескриптора: MATS4e, GATS5e, R6v, R1v+, диполни моманат и торзиона слободна енергија. Према резултатима доковања, пораст енергије везивања и опадање диполног момента може повећати активност инхибитора.

(Примљено 2. марта, ревидирано 16. маја, прихваћено 31. маја 2021)

REFERENCES

1. J. M. Hall, J. F. Couse, K. S. Korach, *J. Biol. Chem.* **296** (2001) 1642 (<https://doi.org/10.1074/jbc.R100029200>)
2. J. D. Yager, N. E. Davidson, *New Engl. J. Med.* **354** (2006) 270 (<https://doi.org/10.1056/NEJMra050776>)
3. R. Abonia, E. Cortes, B. Insuasty, J. Quiroga, M. Nogueras, J. Cobo, *Eur. J. Med. Chem.* **46** (2011) 4062 (<https://doi.org/10.1016/j.ejmech.2011.06.006>)
4. H. Kkbay, R. Durmazt, N. Sirecitt, S. Gnalt, *Asian J. Chem.* **21** (2009) 6181
5. P. T. Nguyen, J. D. Baldeck, J. Olsson, R. E. Marquis, *Oral Microbiol. Immunol.* **20** (2005) 93 (<https://doi.org/10.1111/j.1399-302X.2004.00197.x>)
6. N. C. Desai, A. M. Dodiya, N. R. Shihory, *Med. Chem. Res.* **21** (2012) 2579 (<https://doi.org/10.1007/s00044-011-9782-2>)
7. S. Dixit, P. Kumar Sharma, N. Kaushik, *Med. Chem. Res.* **22** (2013) 900 (<https://doi.org/10.1007/s00044-012-0083-1>)
8. L. Townsend, D. Wise, *Parasitol. Today* **6** (1990) 107 ([https://doi.org/10.1016/0169-4758\(90\)90226-T](https://doi.org/10.1016/0169-4758(90)90226-T))
9. S. A. Galal, A. S. Abdelsamie, M. L. Rodriguez, S. M. Kerwin, H.I. El Diwani, *Eur. J. Chem.* **1** (2010) 67 (<http://doi.org/10.5155/eurjchem.1.2.67-72.1>)
10. C. Karthikeyan, V. R. Solomon, H. Lee, P. Trivedi, *Arabian J. Chem.* **10** (2017) S1788 (<https://doi.org/10.1016/j.arabjc.2013.07.003>)
11. T. Huynh, T. Nguyen, T. Nguyen, T. Hoang, *RSC Adv.* **10** (2020) 20543 (<https://doi.org/10.1039/D0RA02282A>)

12. H. Hadni, M. Mazigh, E. Charif, A. Bouayad, M. Elhallaoui, *Biochem. Res. Int.* **2018** (2018) 1 (<https://doi.org/10.13171/mjc93190924930hh>)
13. R. Dias, W. Filgueira de Azevedo Jr., *Curr. Drug Targets* **9** (2008) 1040 (<https://doi.org/10.2174/138945008786949432>)
14. N. Escala, E. Valderas-Garcia, M. Alvarez Bardon, V. Castilla Gomez de Agüero, R. Escarcena, J. LuisLopez-Perez, F. A. Rojo-Vazquez, A. Feliciano, R. Balaña-Fouce, M. Martínez-Valladares, E. del Olmo, *Eur. J. Med. Chem.* **208** (2020) 112554 (<https://doi.org/10.1016/j.ejmech.2020.112554>)
15. Y. K. Yoon, M. A. Ali, A. C. Wei, T. S. Choon, K. Y. Khaw, V. Murugaiyah, H. Osman, V. H. Masand, *Bioorg. Chem.* **49** (2013) 33 (<https://doi.org/10.1016/j.bioorg.2013.06.008>)
16. C. S. Mizuno, A. G. Chittiboyina, F. H. Shah, A. Patny, T. W. Kurtz, H. A. Pershadsingh, R. C. Speth, V. T. Karamyan, P. B. Carvalho, M. A. Avery, *J. Med. Chem.* **53** (2010) 1076 (<https://doi.org/10.1021/jm901272d>)
17. C. F. Lagos, J. Caballero, F. D. Gonzalez-Nilo, C. D. Pessoa-Mahana, T. Perez-Acle, *Chem. Biol. Drug Des.* **72** (2008) 360 (<https://doi.org/10.1111/j.1747-0285.2008.00716.x>)
18. M. Beglari, N. Goudarzi, D. Shahsavani, M. Arab Chamjangali, Z. Mozafari, *Struct. Chem.* **31** (2020) 1481 (<https://doi.org/10.1007/s11224-020-01505-z>)
19. R. Parr, W. Yang, *Density functional theory of atoms and molecules*, Oxford University Press, New York, 1989
20. *Gaussian 09, Revision A.02*, Gaussian, Inc., Wallingford CT, 2016
21. A. D. Becke, *J. Chem. Phys.* **98** (1993) 5648 (<https://doi.org/10.1063/1.464913>)
22. A. Siiskonen, A. Priimagi, *J. Mol. Model.* **23** (2017) 3112 (<https://doi.org/10.1007/s00894-017-3212-4>)
23. G. Morris, R. Huey, W. Lindstrom, M. F. Sanner, R. K. Belew, D. S. Goodsell, A. J. Olson, *J. Comput. Chem.* **30** (2009) 2785 (<https://doi.org/10.1002/jcc.21256>)
24. Y. S. Mary, H. T. Varghese, C. Y. Panicker, M. Girisha, B. K. Sagar, H. S. Yathirajan, A. A. Al-Saadi, C. Van Alsenoy, *Spectrochim. Acta, A* **150** (2015) 543 (<https://doi.org/10.1016/j.saa.2015.05.090>).



J. Serb. Chem. Soc. 87 (2) 205–217 (2022)
JSCS–5516

Beech sawdust based adsorbents for solid-phase extraction of pesticides and pharmaceuticals

MARIJA M. VUKČEVIĆ^{1*#}, MARINA M. MALETIĆ^{2#}, TATJANA M. ĐURKIĆ¹,
BILJANA M. BABIĆ³ and ANA M. KALIJDIS⁴

¹Faculty of Technology and Metallurgy, University of Belgrade, Karnegijeva 4, 11000 Belgrade, Serbia, ²Innovation Center of the Faculty of Technology and Metallurgy, Karnegijeva 4, 11000 Belgrade, Serbia, ³Institute of Physics – National Institute of the Republic of Serbia, University of Belgrade, Pregrevica 118, 11080 Belgrade, Serbia and ⁴Department of Materials, VINČA Institute of Nuclear Sciences - National Institute of the Republic of Serbia, University of Belgrade, Mike Petrovica Alasa 12–14, 11000 Belgrade, Serbia

(Received 14 June, revised 14 July, accepted 15 July 2021)

Abstract: Carbonaceous solid-phase extraction (SPE) sorbent, efficient in isolation and enrichment of multiclass pesticides and pharmaceuticals from water, was synthesized starting from cheap waste beech sawdust and using KOH as the activated agent. The first step in carbon material preparation was hydrothermal carbonization of the waste beech sawdust. Following hydrothermal treatment, the obtained material was activated, using different amounts of KOH. It was found that applied activation leads to changes in material structure, an increase in specific surface area, and a decrease in the number of surface oxygen groups compared to carbonized sample. SPE procedure of multiclass pesticides and pharmaceuticals from water using activated carbonized beech sawdust (AcSD) was optimized by selecting the appropriate elution solvents, the sample pH, and the sample volume to obtain the highest enrichment efficiency. The optimized SPE procedure was applied for water analysis using different AcSD samples as a sorbent for analyte preconcentration. Activated carbon sorbent, obtained with the highest amount of KOH, showed the highest recoveries regarding the most analytes, which were comparable with the recoveries obtained by commercial cartridges.

Keywords: waste sawdust; hydrothermal synthesis; surface properties; method optimization; organic pollutants analysis.

* Corresponding author. E-mail: marijab@tmf.bg.ac.rs

Serbian Chemical Society member.

<https://doi.org/10.2298/JSC210614051V>

INTRODUCTION

Over the last few decades, due to their increased use and application, pharmaceuticals and pesticides have been frequently detected in the aquatic environment. Intensive application of pesticides in agriculture brings significant pollution of surface water and groundwater and become an increasing environmental problem.^{1–4} Pharmaceuticals used in human and veterinary medicine also contribute to pollution of the aquatic environment, due to their occurrence in the water system as a consequence of frequent use, improper disposal, as well as the inability of wastewater treatment plants to eliminate them. The presence of pesticides and pharmaceuticals in water may have a huge negative impact on human health, as well as the aquatic ecosystem and therefore it is necessary to develop appropriate methods for their constant monitoring.^{5–9}

Residues of pesticides and pharmaceuticals are usually present at low concentrations in surface water and groundwater, and therefore the methods for their determination must include an enrichment step, before analysis. For this purpose, a commonly used sample preparation technique is solid-phase extraction (SPE), since it provides analytes isolation, concentration, and the extract clean-up in a single step. The choice of the sorbent is critically important in SPE because it controls parameters such as selectivity, affinity, and extraction capacity.¹⁰ In addition to the commonly used commercially available polymeric or silica-based SPE cartridges, such as poly(styrene-divinylbenzene), C18, and zeolite, various tailor-made carbon materials are increasingly used as SPE sorbents.^{8,11–13} Since the type of carbon sorbent, its structure, and the nature of the interaction between the carbon surface and the analyte greatly influence the preconcentration efficiency, the selection of suitable carbon sorbent is a crucial step in order to achieve high recoveries of the SPE method. However, sometimes, in addition to the good analytical performance of the carbon sorbent, it is also necessary to consider its cost, and the potential way to reduce the cost is using waste biomass as a starting material for obtaining cheap SPE sorbents.¹⁴ The usage of different types of biomass waste represents an environmentally sound conversion process, and a current trend in the field of material production. In addition, as an alternative to dry pyrolysis which is carried out in an inert atmosphere at high temperatures, the wet pyrolysis process (hydrothermal carbonization) allows obtaining the carbonaceous solids with relatively high yields at mild temperatures (120–180 °C). The obtained carbon materials are suitable for further modification by different methods of activation or functionalization, and in this way, it is possible to tailor the desired characteristics depending on the potential application.^{15–17}

In this work, beech sawdust, obtained as a waste from the wood industry, was used as a starting material for the production of SPE carbon sorbents. Carbon sorbents were obtained starting from sawdust and using hydrothermal carbonization, followed by activation in the presence of KOH as an activating agent. By

varying the activation parameters, activated carbonized beech sawdust (AcSD) samples with different characteristics were obtained. To achieve the highest possible recoveries, the SPE method was optimized in terms of selecting the appropriate type of organic extraction solvent, as well as the volume and pH of the water sample. The possibility of using activated carbonized beech sawdust samples as an adsorbent in the solid phase extraction method was tested using an aqueous solution of pharmaceuticals and pesticide mixtures. Additionally, recoveries obtained by AcSD samples were compared with the recoveries obtained by commercial cartridges. Four pharmaceuticals: carbamazepine, lorazepam, diazepam (sedatives), clopidogrel (cardiovascular) and two metabolites of metamizole (4-acetylaminoantipyrine, 4-AAA, and 4-formylaminoantipyrine, 4-FAA), as well as seven pesticides: atrazine, propazine (triazine), imidacloprid, acetamiprid (neonicotinoid), dimethoate, malathion (organophosphate) and tebufenozide (diacylhydrazine) were selected for this study.

EXPERIMENTAL

Sample preparation

Beech sawdust obtained as waste from the wood industry was used as the starting material for the preparation of hydrothermal carbon (HTC). Hydrothermal carbonization of sawdust was carried out into Teflon lined stainless steel autoclave at a temperature of 180 °C and self-generated pressure for 24 h. The carbonization reaction mixture consisted of 6 g of sawdust, 40 cm³ of distilled water, and 0.015 g of citric acid, which was used as a catalyst. After hydrothermal carbonization, the solid product was filtered and washed with methanol and distilled water. In order to improve the sorption characteristics of the material, HTC was activated using KOH as an activating agent. Activation was carried out in an electric furnace under the constant nitrogen flow (150 cm³ min⁻¹), up to a temperature of 900 °C, with a heating rate of 5 °C min⁻¹. By varying the mass ratios of KOH and HTC, different carbon sorbent samples were obtained and denoted as: AcSD₀ (KOH/HTC = 0/1), AcSD_{0.5} (KOH/HTC = 0.5/1) and AcSD₁ (KOH/HTC = 1/1).

Sample characterization

The surface morphology on examined samples and the influence of activating agent on surface morphology was examined by scanning electron microscopy (Mira Tescan 3X, Tescan Orsay Holding, Czech Republic).

Nitrogen adsorption and desorption isotherms were measured on activated carbonized beech sawdust samples at -196 °C. The specific surface area and the pore size distribution (PSD) of AcSDs samples were analyzed using the Surfer (Thermo Fisher Scientific, USA). PSD was estimated by applying the BJH method¹⁸ to the desorption branch of isotherms and mesopore surface and micropore volume were estimated using the t-plot method.¹⁹

The type of functional groups present on the activated carbonized beech sawdust surface was examined by Fourier transform infrared spectroscopy (FTIR). FT-IR spectra were recorded in the range from 400 to 4000 cm⁻¹ (Bomem MB-Series, Hartmann Braun, Germany).

The nature and thermal stability of activated carbonized beech sawdust surface oxygen groups were examined by temperature-programmed desorption (TPD) in combination with mass spectrometry. The TPD profiles were obtained using a custom-built set-up, consisting of a quartz tube placed inside an electrical furnace, as it is described in the literature.²⁰ The

sample was outgassed in the quartz tube and subjected to TPD at a constant heating rate of $10\text{ }^{\circ}\text{C min}^{-1}$ up to $900\text{ }^{\circ}\text{C}$, under a high vacuum. The amounts of CO and CO_2 released from the carbon sample (0.1 g) were monitored using an Extorr 300 quadrupole mass spectrometer (Extorr Inc., USA).

Solid-phase extraction procedure

SPE cartridges were prepared by filling empty SPE columns with 0.05 g of activated carbonized beech sawdust, and two polyethylene frits were used to hold the adsorbent packing in the cartridge. The aqueous solution of selected pharmaceuticals and pesticides was prepared by spiking deionized water to the concentration of 1 ng cm^{-3} per each analyte. The following parameters that may affect the SPE procedure efficiency were optimized: volume and pH of the water sample and type of elution solvents. The optimal volume of the aqueous solution of the analyte mixture was selected based on the SPE method recoveries using 50, 100 and 200 cm^3 of the aqueous solution, without pH adjustment. To select the optimal pH of the aqueous solution, pH values were adjusted on 4, 5, 6, 7 and 8, prior to extraction. An appropriate elution solvent was selected based on the method recoveries obtained using: methanol, dichloromethane–methanol (1:1) and acetonitrile. For SPE optimization experiments, the SPE cartridges were preconditioned with 5 cm^3 of selected elution solvent followed by 5 cm^3 of deionized water. Spiked water samples were loaded at a flow rate of $1\text{ cm}^3\text{ min}^{-1}$. The cartridges were then dried under vacuum for 10 min and analytes were eluted with selected elution solvent to extract a volume of 15 cm^3 . Extracts were evaporated to dryness under N_2 and reconstituted with 1 cm^3 of methanol. The final extracts in methanol were filtered through $0.45\text{ }\mu\text{m}$ polyvinylidene fluoride (PVDF) filters, into the autosampler vials and analyzed using high performance liquid chromatography–tandem mass spectrometry (LC–MS/MS, Thermo Scientific). Recoveries ($R / \%$) were calculated as ratio between peak area of analyte in methanol extract (PAext), and peak area of analyte in standard solution (PAstd):

$$R = 100 \frac{\text{PAext}}{\text{PAstd}} \quad (1)$$

Relative standard deviation ($RSD / \%$) was calculated as ratio between recovery standard deviation $\text{std}(R)$, and average recovery ($\text{average}(R)$):

$$RSD = 100 \frac{\text{std}(R)}{\text{average}(R)} \quad (2)$$

LC–MS/MS method conditions are given in Supplementary material to this paper. The optimized SPE procedure was applied to test the possibility of using different activated carbonized beech sawdust samples as SPE adsorbents for the extraction of selected pesticides and pharmaceuticals from water. Additionally, recovery values obtained using the AcSD₁ sample were compared with the recoveries obtained by commercial cartridges: Supelclean Envi-Carb, Supelclean Envi-18, Supelclean LC-SCX, Supelclean LC-18 (Sigma–Aldrich) and Oasis HLB (Waters, USA).

RESULTS AND DISCUSSION

Surface characteristics of activated carbonized beech sawdust samples

Morphology of hydrothermally treated and activated carbonized beech sawdust samples were analyzed by scanning electron microscopy (Fig. 1). Morphologies of AcSD samples are more or less featured by the presence of clearly defined carbon spheres with a smooth surface, which is characteristic of hydro-

thermal carbons.^{15–17,21} It can be noted that the surface of the AcSD₀ sample is completely covered with spherical particles of different diameters, ranging from 50 up to 700 nm. The differences in surface structure caused by activation in the presence of KOH are reflected in the decrease of the carbon spheres diameters, or, in the case of more aggressive treatment, their disappearance. In that way, sample AcSD_{0.5} is characterized by the presence of carbon spheres with diameters lower than 200 nm, while the AcSD₁ surface contains spheres with diameters lower than 50 nm, and only a few with diameters up to 200 nm. Additionally, activation in the presence of KOH leads to the smoothing of the surface of hydrothermally treated beech sawdust, along with the formation of large pores.

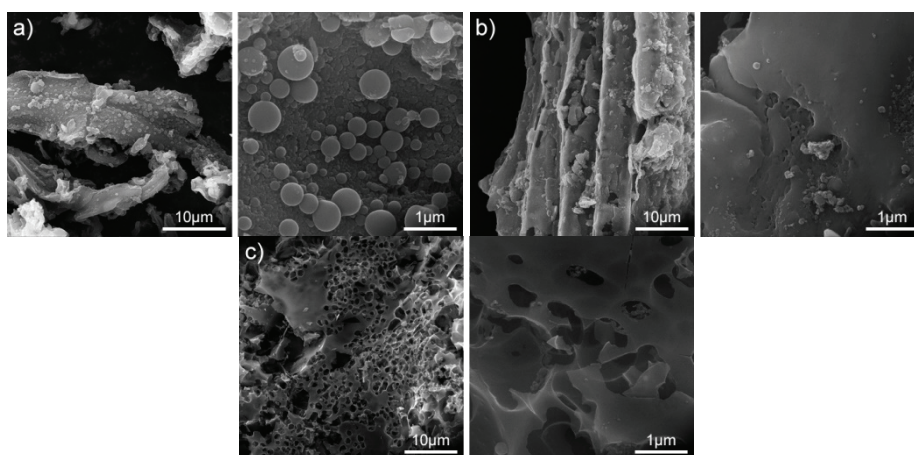


Fig. 1. FESEM photographs of activated carbonized beech sawdust samples: a) AcSD₀, b) AcSD_{0.5} and c) AcSD₁.

Calculated porosity parameters of AcSD samples are given in Table I.

TABLE I. Porous properties and amount of CO (Q_{CO}) and CO₂ (Q_{CO_2}) evolving surface groups of activated carbonized beech sawdust samples

Sample	AcSD ₀	AcSD _{0.5}	AcSD ₁
$S_{BET} / m^2 g^{-1}$	213	514	729
$S_{meso} / m^2 g^{-1}$	3	3	6
$S_{mic} / m^2 g^{-1}$	210	511	723
$V_{mic} / cm^3 g^{-1}$	0.187	0.255	0.375
r_{med} / nm	1.5	1.6	1.9
$Q_{CO} / mmol g^{-1}$	68.15	26.25	10.39
$Q_{CO_2} / mmol g^{-1}$	585.78	545.94	338.25
$Q_{CO} + Q_{CO_2} / mmol g^{-1}$	653.93	572.19	338.64

Specific surface areas (S_{BET}) ranged from 213 (AcSD₀) to 729 (AcSD₁) m² g⁻¹, while the mean pore diameters (r_{med}) were below 2 nm for all samples and

increases with increasing the amount of activating agent. Hydrothermal carbonization of sawdust followed by activation in the presence of KOH yielded microporous materials with a low proportion of mesoporosity. The increased amount of KOH opens up the porous surface structure, increasing the volume of micropores and strongly increasing the specific surface area of the activated carbonized beech sawdust.

Fourier transform infrared spectroscopy and temperature-programmed desorption were used to determine the nature and amount of AcSD surface oxygen groups and to evaluate the influence of the activation process on AcSD surface chemistry. The FTIR spectra displayed in Fig. 2. give qualitative information about functional groups present on the surface of the AcSD samples.

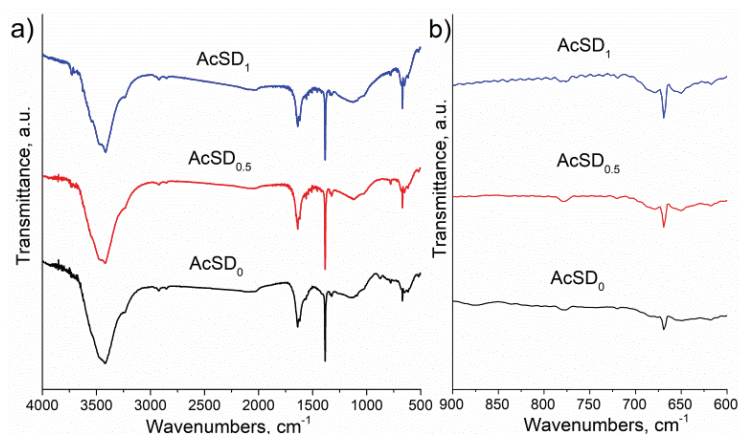


Fig. 2. FTIR spectra of AcSD samples (a) and enlarged section from 600 to 900 cm^{-1} (b).

All tested samples showed very similar FTIR spectra with slight differences in peak intensity, indicating that activation in the presence of KOH had no significant effect on the nature of the surface functional groups. The intense broad band, in the 3600–3300 cm^{-1} region, is characteristic of stretching vibrations of the O–H bond in hydroxyl or carboxyl groups. Two low-intensity bands with maxima at 2850 and 2920 cm^{-1} , observed for all tested samples, are attributed to the symmetrical and asymmetrical deformation vibrations of C–H groups in methyl and methylene groups (CH_3 , CH_2 , $\text{CH}_2\text{–OH}$).²² The moderate-intensity band at 1640 cm^{-1} may originate from the bending vibration of the O–H bond, or the stretching vibration of the aliphatic C=C bond, while the shoulder at 1620 cm^{-1} originates from the vibrations of the aromatic C=C bond.^{15,23–25} The intense peak at 1384 cm^{-1} corresponds to the deformation vibration of the C–O bond in the carboxyl group.²⁶ A low-intensity band in the range of 1300–1000 cm^{-1} may derive from the stretching vibrations of the C–OH, or bending vibrations of the O–H bond, indicating the presence of hydroxyl groups.²⁷ The low-

intensity peak at 875 cm^{-1} originates from the vibration of the aromatic C–H bond twist, while the peak at 669 cm^{-1} originates from deformation vibrations of the aromatic ring. These two peaks are affected by KOH activation: peak at 875 cm^{-1} observed for AcSD₀ sample disappears upon KOH activation, while the intensity of the peak at 669 cm^{-1} increase with the increase in the amount of KOH.

The TPD profiles of CO and CO₂, released during thermal decomposition of the surface oxygen groups, were recorded and shown in Fig 3. TPD analysis of sample AcSD₀ showed pronounced evolution of CO at a relatively low temperature of 465 K, which may originate from thermal decomposition of carbonyl groups in α -substituted ketones and aldehydes,^{15,28} as well as slightly weaker CO release up to a temperature of 1000 K, which can be assigned to phenols, ethers, carbonyls and quinones.^{28,29} TPD profile of CO₂ for sample AcSD₀ showed a peak at 580 K, along with the shoulders at 420 and 520 K, which can originate from thermal decomposition of carboxylic and lactone groups,^{30,31} while the peak displayed around 820 K may originate from lactones or carboxylic anhydride groups.³² CO decomposition profiles showed maxima around 541 K, for sample AcSD_{0.5}, and maxima around 640 and 1000 K, for sample AcSD₁, while CO₂ decomposition profiles showed maxima around 625 K for sample AcSD_{0.5}, and 580 K, for sample AcSD₁. TPD profiles of CO showed that the increase in activating agent amount, shifts temperature maxima to higher values, while temperature, at which CO₂-releasing oxygen groups decompose, remains the same or increases with increase in KOH amount. This temperature increase indicates the stabilization the oxygen groups on materials surface. Additionally, an increased amount of KOH decreases the peak intensity of TPD profiles, which indicates a decrease in the number of surface groups.

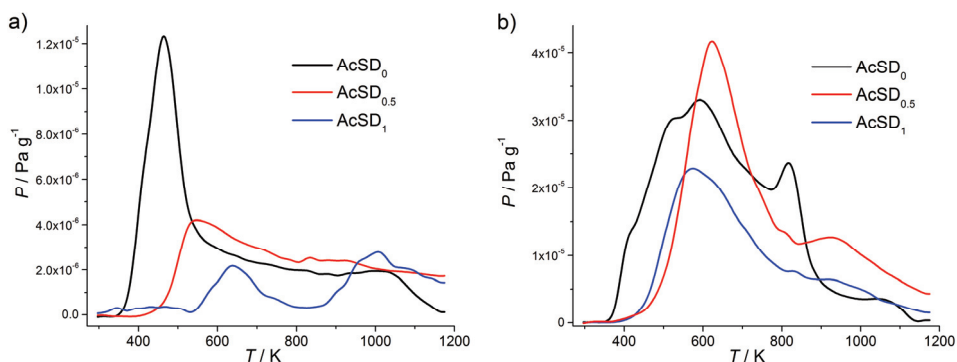


Fig. 3. TPD spectra of AcSD samples: a) CO and b) CO₂ desorption profiles.

The amounts of CO and CO₂ evolving groups (Table I) were obtained by the integration of the appropriate TPD profile. Obtained results indicate that AcSD samples contain a significant amount of CO₂ evolving groups and carboxyl, lac-

tone, and anhydride groups are mainly present on the surface of the material. Changes in the amounts of CO and CO₂ evolving groups along with the temperature maxima shifts, both induced by different amount of KOH used for activation, indicate that during the activation process the reduction of oxygen groups already existing on the carbon material surface occurs, with the simultaneous formation of the more stable oxygen groups.²⁰

Activated carbonized beech sawdust samples as an adsorbent in solid-phase extraction

The parameters that determine the recoveries of the SPE method have to be optimized to achieve the highest efficiency of the method. Optimization of the SPE method was performed using a sample with the largest specific surface area, AcSD₁, as an SPE adsorbent. The SPE recoveries obtained by optimization of water sample volume, initial pH value and elution solvent are presented in Fig. 4. The SPE method is considered to be efficient if the obtained recovery values fall within 70–120 %, with relative standard deviation (*RSD*) ≤ 20 %.^{14,33–36} The most suitable recoveries of selected analytes were obtained for 100 cm³ of water samples, and for all analytes, except dimethoate, diazepam, and atrazine, obtained recoveries ranged from 70 to 119 % (Fig. 4a).

The following step in SPE optimization was to select the most appropriate pH value of the water sample of selected analytes. Therefore, initial pH values were adjusted to 4, 5, 6, 7 and 8. The best recoveries (71–111 %) were obtained at the pH value of 6 (Fig. 4b), and this pH value was chosen as the optimal for extraction of selected analytes from water samples. The optimization of elution solvents (Fig. 4c) led to the selection of a mixture of dichloromethane-methanol (1:1) as an optimal solvent, since obtained recoveries were better than those obtained using methanol and acetonitrile.

After the optimization, the SPE procedure for the enrichment of selected pesticides and pharmaceuticals in water samples implies the usage of 100 cm³ of the water sample, with the pH value adjusted to 6, along with the usage of dichloromethane-methanol (1:1) mixture for elution of analytes. This procedure was applied to examine the possibility of using different samples of activated carbonized beech sawdust as SPE adsorbents. Recoveries obtained in this way (Fig. 5) showed that sample AcSD₀ can be used for the enrichment of only six of thirteen tested analytes, including imidacloprid, diazepam, clopidogrel, atrazine, malathion and tebufenozide, with recoveries ranging from 72 to 88 %. Sample AcSD_{0.5} showed high performance for eleven tested analytes, with recoveries ranging from 72 to 100 %, while recoveries obtained for dimethoate and carbamazepine were insufficient. Additionally, good recoveries (71–111 %) for all tested analytes, except atrazine (65 %) were obtained using sample AcSD₁.

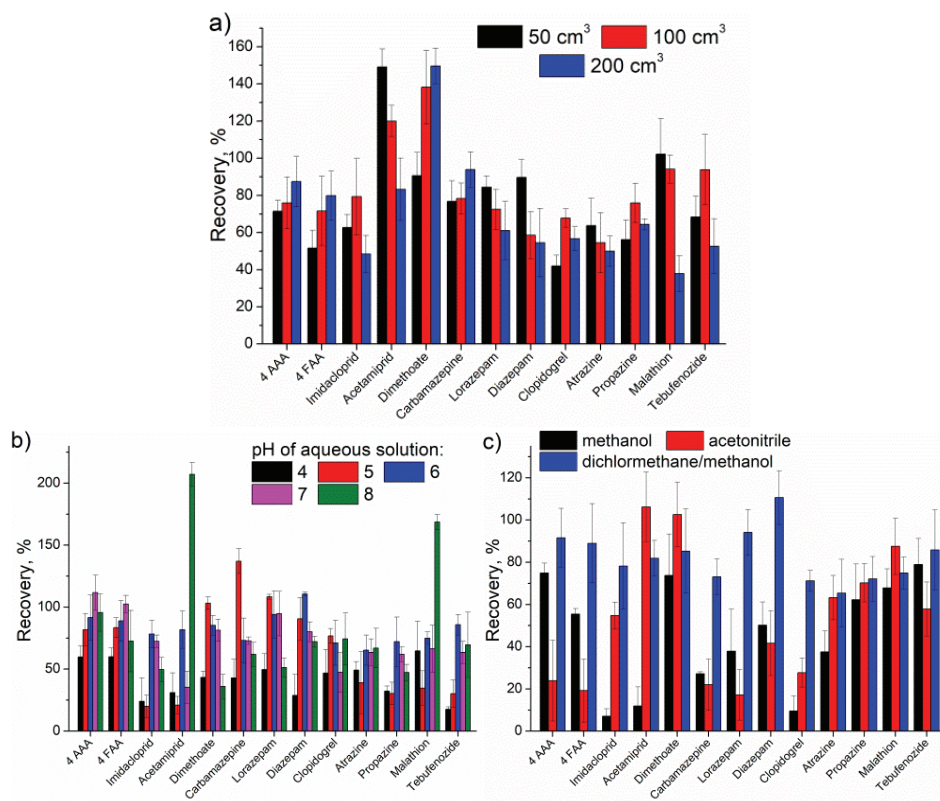


Fig. 4. Recoveries of selected analytes on AcSD₁ for different: a) sample volumes, b) initial pH values, c) elution solvents obtained for the water samples spiked at 1 ng cm⁻³ per each analyte.

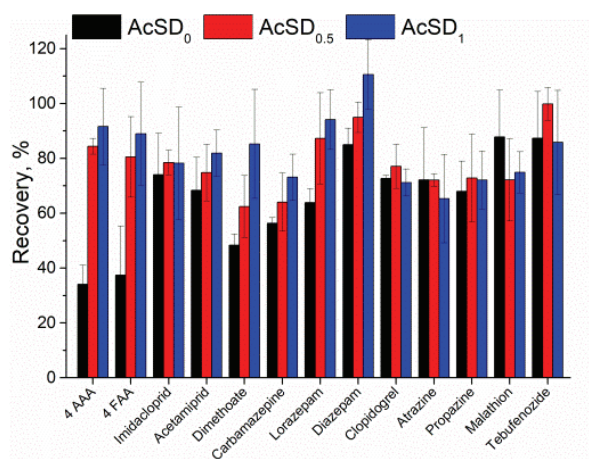


Fig 5. Recoveries of selected pesticides and pharmaceuticals obtained using different AcSD samples as SPE cartridges.

These results imply that the extraction efficiency of activated carbonized beech sawdust is highly affected by the surface characteristics of the material. An increase in specific surface area and mean pore diameter enhance extraction efficiency of activated carbonized beech sawdust. The lowest recoveries obtained for sample AcSD₀ can be the consequence of low specific surface area, along with the negative influence that surface oxygen groups may have on SPE efficiency. It was noted that presence of surface oxygen groups has detrimental effect on extraction efficiency of activated carbonized beech sawdust. Carboxyl groups present on the surface of activated carbonized beech sawdust, as electron acceptor groups, may withdraw π -electrons from the graphene layers, decreasing in that way dispersive interactions between adsorbate (aromatic organic compounds) and adsorbent (carbon surface) and leading to reduced adsorption.^{8,29} Also, hydrophilic carboxyl groups intensify adsorption of water onto carbon surface, along with the formation of water clusters that reduce the availability of carbon surface for adsorption of organic compounds.³⁷

Comparing the recovery values obtained for commercial cartridges and AcSD₁ (Table II), it was shown that the AcSD₁ sample could be successfully applied as a solid-phase adsorbent for the analysis of selected pharmaceuticals and pesticides in water samples. Additionally, for 4 AAA and lorazepam, recoveries obtained by tested material were higher than the ones obtained by commercial cartridges.

TABLE II. Recoveries of selected analytes obtained using commercial cartridges and SPE cartridges filled with AcSD₁ as a sorbent

Analyte	Recovery (<i>RSD</i>), %					
	AcSD ₁	Envi-18	Envi Carb	LC-18	LC-SCX	Oasis HLB
4 AAA	92 (14)	44 (6)	86 (2)	91 (7)	19 (4)	90 (9)
4 FAA	89 (19)	64 (7)	76 (15)	100 (9)	13 (26)	86 (6)
Imidacloprid	78 (20)	97 (9)	99 (9)	105 (18)	50 (7)	83 (6)
Acetamiprid	82 (8)	96 (7)	95 (11)	100 (7)	60 (3)	82 (5)
Dimethoate	85 (20)	70 (6)	90 (6)	87 (4)	12 (19)	71 (10)
Carbamazepine	73 (8)	93 (5)	91 (11)	95 (5)	90 (4)	78 (6)
Atrazine	65 (16)	77 (6)	88 (13)	85 (16)	82 (7)	78 (9)
Lorazepam	94 (11)	91 (9)	80 (7)	90 (11)	90 (6)	73 (7)
Propazine	72 (11)	75 (2)	78 (9)	75 (22)	78 (7)	75 (17)
Diazepam	111 (13)	100 (2)	91 (2)	97 (6)	39 (10)	80 (9)
Malathion	75 (8)	62 (11)	86 (9)	85 (10)	76 (2)	77 (2)
Tebufenozide	86 (19)	97 (16)	97 (12)	103 (18)	98 (12)	85 (11)
Clopidogrel	71 (5)	70 (20)	77 (18)	69 (18)	-	77 (19)

CONCLUSION

Activation of hydrothermally treated beech sawdust using potassium hydroxide induced changes in material morphology and surface chemistry and pro-

sity. The increase in KOH amount led to the increase in specific surface area, while maintaining the high microporosity of the surface. The clearly defined carbon spheres, characteristic for hydrothermally treated material, disappeared upon KOH activation, along with the decrease in the number of surface oxygen groups. In this way, the efficient carbon sorbent for isolation and enrichment of multi-class pesticides and pharmaceuticals was obtained. The results showed that it is possible to synthesize solid-phase extraction sorbents, starting from cheap waste beech sawdust material and using KOH as the activated agent. Furthermore, cartridges obtained with a larger amount of KOH showed the highest efficiency in analyte preconcentration, comparable to the efficiency of much more expensive commercial cartridges.

SUPPLEMENTARY MATERIAL

Additional data and information are available electronically at the pages of journal website: <https://www.shd-pub.org.rs/index.php/JSCS/article/view/10859>, or from the corresponding author on request.

Acknowledgement. The research was funded by the Ministry of Education, Science and Technological Development of the Republic of Serbia (Contract No. 451-03-9/2021-14/200135, Contract No. 451-03-9/2021-14/200287 and Contract No. 451-03-9/2021-14/200017).

ИЗВОД

УГЉЕНИЧНИ АДСОРБЕНТИ НА БАЗИ БУКОВЕ ПИЉЕВИНЕ ЗА ПРЕДКОНЦЕНТРИСАЊЕ ПЕСТИЦИДА И ЛЕКОВА У МЕТОДИ ЕКСТРАКЦИЈЕ НА ЧВРСТОЈ ФАЗИ

МАРИЈА М. ВУКЧЕВИЋ¹, МАРИНА М. МАЛЕТИЋ², ТАТЈАНА М. ЂУРКИЋ¹, БИЉАНА М. БАБИЋ³
и АНА М. КАЛИЈАДИС⁴

¹Технолошко–металурички факултет, Универзитет у Београду, Карнегијева 4, 11000 Београд,

²Иновациони Центар Технолошко–металуричког факултета, Карнегијева 4, 11000 Београд,

³Институт за физику–Институт од националног значаја, Универзитет у Београду, Претривица 118, 11080 Београд и ⁴Лабораторија за материјале, Институт за нуклеарне науке Винча–Институт од националног значаја, Универзитет у Београду, Мике Пејровића Аласа 12–14, 11000 Београд

Предмет овог рада био је испитивање могућности примене активног угља на бази хидротермално третиране пиљевине као адсорбента у методи екстракције на чврстој фази (енгл. solid phase extraction, SPE) при анализи остатака лекова и пестицида из површинских и подземних вода. У циљу добијања нових SPE адсорбента, отпадна пиљевина је најпре хидротермално карбонизована, а затим је активирана коришћењем KOH као активирајућег агенса. Варирањем количине активирајућег агенса добијени су различити узорци активiranог хидротермалног угљеника (AcSD). Површина добијених материјала окарактерисана је одређивањем специфичне површине, пречника и запремине пора, као и врсте и количине површинских група. У циљу постизања максималних приноса лекова и пестицида, извршена је оптимизација SPE методе одабиром одговарајуће запремине и pH вредности узорка воде, као и органског растварача за елуирање. Оптимизована SPE метода примењена је за анализу воде коришћењем различитих узорака AcSD као SPE адсорбента, а добијени приноси су упоређени са приносима ове методе на комерцијалним кертрицима. Добијени резултати су показали да се активи-

рани хидротермални угљеник на бази пиљевине може успешно користити за предко-
нцентрисање лекова и пестицида из воде.

(Примљено 14. јуна, ревидирано 14. јула, прихваћено 15. јула 2021)

REFERENCES

1. K. S. Rajmohan, R. Chandrasekaran, S. Varjan, *Indian J. Microbiol.* **60** (2020) 125 (<http://dx.doi.org/10.1007/s12088-019-00841-x>)
2. T. Radović, S. Grujić, A. Petković, M. Dimkić, M. Laušević, *Environ. Monit. Assess.* **187** (2015) 4092 (<http://dx.doi.org/10.1007/s10661-014-4092-z>)
3. T. Reemtsmaa, L. Alder, U. Banasiak, *J. Chromatogr., A* **1271** (2013) 95 (<http://dx.doi.org/10.1016/j.chroma.2012.11.023>)
4. F. A. Swartjes, M. Van der Aa, *Sci. Total Environ.* **699** (2020) 134186 (<https://doi.org/10.1016/j.scitotenv.2019.134186>)
5. S. Teixeira, R. Gurke, H. Eckert, K. Kuhn, J. Fauler, G. Cuniberti, *J. Environ. Chem. Eng.* **4** (2016) 287 (<http://dx.doi.org/10.1016/j.jece.2015.10.045>)
6. S. Grujić, T. Vasiljević, M. Laušević, *J. Chromatogr., A* **1216** (2009) 4989 (<https://doi.org/10.1016/j.chroma.2009.04.059>)
7. Y. Li, J. Ding, L. Zhang, X. Liu, G. Wang, *Sci. Total Environ.* **696** (2019) 133991. (<https://doi.org/10.1016/j.scitotenv.2019.133991>)
8. B. Lalović, T. Đurkić, M. Vukčević, I. Janković-Častvan, A. Kalijadis, Z. Laušević, M. Laušević, *Environ. Sci. Pollut. Res.* **24** (2017) 20784 (<http://dx.doi.org/10.1007/s11356-017-9748-0>)
9. J. Rivera-Utrilla, M. Sánchez-Polo, M.Á. Ferro-García, G. Prados-Joya, R. Ocampo-Pérez, *Chemosphere* **93** (2013) 1268 (<https://doi.org/10.1016/j.chemosphere.2013.07.059>)
10. D. Mutavdžić Pavlović, S. Babić, A.J.M. Horvat, M. Kaštelan-Macan, *Trend Anal. Chem.* **26** (2007) 1062 (<https://doi.org/10.1016/j.trac.2007.09.010>)
11. F. Maya, C. Palomino Cabello, M. Ghani, G. Turnes Palomino, V. Cerdà, *J. Sep. Sci.* **4** (2018) 262 (<https://doi.org/10.1002/jssc.201700836>)
12. J. Płotka-Wasyłka, N. Szczepanska, M.d.L. Guardia, J. Namiesnik, *Trend. Anal. Chem.* **77** (2016) 23 (<http://dx.doi.org/10.1016/j.trac.2015.10.010>)
13. A. H. El-Sheikh, J. A. Sweileh, Y. S. Al-Degs, A. A. Insisi, N. Al-Rabady, *Talanta* **74** (2008) 1675 (<http://dx.doi.org/10.1016/j.talanta.2007.09.005>)
14. M. Vukcevic, A. Kalijadis, M. Radisic, B. Pejic, M. Kostic, Z. Lausevic, M. Lausevic, *Chem. Eng. J.* **211–212** (2012) 224 (<https://doi.org/10.1016/j.cej.2012.09.059>)
15. A. Kalijadis, J. Đorđević, T. Trtić-Petrović, M. Vukčević, M. Popović, V. Maksimović, Z. Rakočević, Z. Laušević, *Carbon* **95** (2015) 42 (<http://dx.doi.org/10.1016/j.carbon.2015.08.016>)
16. C. Falco, N. Baccile, M. M. Titirici, *Green Chem.* **13** (2011) 3273 (<https://doi.org/10.1039/C1GC15742F>)
17. Q. Wu, W. Li, J. Tan, Y. Wu, S. Liu, *Chem. Eng. J.* **266** (2015) 112 (<https://doi.org/10.1016/j.cej.2014.12.089>)
18. E. P. Barrett, L. G. Joyner, P. P. Halenda, *J. Am. Chem. Soc.* **73** (1951) 373 (<http://dx.doi.org/10.1021/ja01145a126>)
19. K. Kaneko, C. Ishii, M. Ruike, H. Kuwabara, *Carbon* **30** (1992) 1075 ([http://dx.doi.org/10.1016/0008-6223\(92\)90139-N](http://dx.doi.org/10.1016/0008-6223(92)90139-N))

20. M. M. Vukčević, A. M. Kalijadis, T. M. Vasiljević, B. M. Babić, Z. V. Laušević, M. D. Laušević, *Micropor. Mesopor. Mat.* **214** (2015) 156 (<https://doi.org/10.1016/j.micromeso.2015.05.012>)
21. M. M. Titirici, M. Antonietti, N. Baccile, *Green Chem.* **10** (2008) 1204 (<http://dx.doi.org/10.1039/b807009a>)
22. S. Mihajlović, M. Vukčević, B. Pejić, A. Perić Grujić, M. Ristić, *Environ. Sci. Pollut. Res.* **27** (2020) 35769 (<https://doi.org/10.1007/s11356-020-09811-z>)
23. M. Maletić, M. Vukčević, A. Kalijadis, I. Janković-Častvan, A. Dapčević, Z. Laušević, M. Laušević, *Arab. J. Chem.* **12** (2019) 4388 (<http://dx.doi.org/10.1016/j.arabj.2016.06.020>)
24. C. Cheng-Meng, Z. Qiang, Y. Mang-Guo, H. Chun-Hsien, Y. Yong-Gang, W. Mao-Zhang, *Carbon* **50** (2012) 3572 (<http://dx.doi.org/10.1016/j.carbon.2012.03.029>)
25. M. Sevilla, A.B. Fuertes, *Carbon* **47** (2009) 2281 (<https://doi.org/10.1016/j.carbon.2009.04.026>)
26. J. H. Zhou, Z. J. Sui, J. Zhu, P. Li, D. Chen, Y. C. Dai, W. k. Yuan, *Carbon* **45** (2007) 785 (<https://doi.org/10.1016/j.carbon.2006.11.019>)
27. S. C. Lyu, J. H. Han, K. W. Shin, J. H. Sok, *Carbon* **49** (2011) 1532 (<https://doi.org/10.1016/j.carbon.2010.12.012>)
28. G. S. Szymanski, Z. Karpinski, S. Biniak, A. Swiatkowski, *Carbon* **40** (2002) 2627 ([https://doi.org/10.1016/S0008-6223\(02\)00188-4](https://doi.org/10.1016/S0008-6223(02)00188-4))
29. M. Vukčević, A. Kalijadis, B. Babić, Z. Laušević, M. Laušević, *J. Serb. Chem. Soc.* **78** (2013) 1617 (<http://dx.doi.org/10.2298/JSC131227006V>)
30. G. Peng, F. Gramm, C. Ludwig, F. Vogel, *Catal. Sci. Technol.* **5** (2015) 3658 (<https://doi.org/10.1039/c5cy00352k>)
31. S. Rincón Prat, C. Schneider, T. Kolb, *Fuel* **267** (2020) 117179 (<https://doi.org/10.1016/j.fuel.2020.117179>)
32. T. Ishii, T. Kyotani, in *Materials Science and Engineering of Carbon: Characterization*, F. Kang, M. Inagaki, Eds., Elsevier Inc., Oxford, 2016, p. 287 (<https://doi.org/10.1016/B978-0-12-805256-3.00014-3>)
33. H. H. Noh, C. J. Kim, H. Kwon, D. Kim, B. C. Moon, S. Baek, M.S. Oh, K.S. Kyung, *PLoS ONE* (2020) (<https://doi.org/10.1371/journal.pone.0235526>)
34. J. A. Oliveira, L. J. P. Izeppi, R. F. Loose, D. K. Muenchen, O. D. Prestes, R. Zanella, *Anal. Methods* **11** (2019) 2333 (<https://doi.org/10.1039/c9ay00289h>)
35. E. Rutkowska, B. Łozowicka, P. Kaczyński, *Food Anal. Methods* **11** (2018) 709 (<https://doi.org/10.1007/s12161-017-1047-3>)
36. S. Y. Wang, E. K. Fodjo, C. Kong, H. J. Yu, *Water* **12** (2020) 1238 (<https://doi.org/10.3390/w12051238>)
37. O. Guven Apul, T. Karanfil, *Water Res.* **68** (2015) 34 (<http://dx.doi.org/10.1016/j.watres.2014.09.032>).



J. Serb. Chem. Soc. 87 (2) S47–S49 (2022)

SUPPLEMENTARY MATERIAL TO
**Beech sawdust based adsorbents for solid-phase extraction of
pesticides and pharmaceuticals**

MARIJA M. VUKČEVIĆ^{1*#}, MARINA M. MALETIĆ^{2#}, TATJANA M. ĐURKIĆ¹,
BILJANA M. BABIĆ³ and ANA M. KALIJADIS⁴

¹Faculty of Technology and Metallurgy, University of Belgrade, Karnegijeva 4, 11000 Belgrade, Serbia, ²Innovation Center of the Faculty of Technology and Metallurgy, Karnegijeva 4, 11000 Belgrade, Serbia, ³Institute of Physics - National Institute of the Republic of Serbia, University of Belgrade, Pregrevica 118, 11080 Belgrade, Serbia and ⁴Department of Materials, VINČA Institute of Nuclear Sciences - National Institute of the Republic of Serbia, University of Belgrade, Mike Petrovica Alasa 12–14, 11000 Belgrade, Serbia

J. Serb. Chem. Soc. 87 (2) (2022) 205–217

LC–MS/MS ANALYSIS

Separation of the analytes was performed on a reverse-phase column, Zorbax Eclipse XDB-C18 75 mm long, 4.6 mm *i.d.* and 3.5 μm particle size (Agilent Technologies, USA) of Surveyor HPLC system (Thermo Fisher Scientific, USA). The gradient of the mobile phase consisted of methanol (A), water (B), and 10 % acetic acid (C) are shown in Table S-I. Quadrupole ion trap mass spectrometer, LCQ Advantage (Thermo Fisher Scientific, USA), was used for the detection and quantification of selected pesticides and pharmaceuticals. The electrospray ionization technique was used, and all analytes were analyzed in the positive ionization mode. Selected reaction monitoring (SRM) chromatograms of selected pesticides and pharmaceuticals are given in Figure S-1, and LC/MS-MS quantification parameters are presented in Table S-II.

* Corresponding author. E-mail: marijab@tmf.bg.ac.rs

TABLE S-I. Gradient and flow rate of the mobile phase

Time, min	Flow rate, cm ³ min ⁻¹	Content, %		
		A	B	C
0	0.5	33	66	1
20.00	0.5	100	0	0
20.01	1	100	0	0
30.00	1	100	0	0
30.01	0.5	33	66	1
40.00	0.5	33	66	1

TABLE S-II. LC-MS/MS quantification parameters for selected pesticides and pharmaceuticals

Analyte	Retention time, min	<i>m/z</i>	Collision energy, a.u.*	<i>m/z</i>
		Precursor ion		Product ion
4-AAA	3.27	246	28	228
4-FAA	3.10	232	30	204
Imidacloprid	5.11	256	28	210
Acetamiprid	6.76	223	36	126
Dimethoate	6.95	230	26	199
Carbamazepine	12.96	237	34	194
Atrazine	14.28	216	38	174
Lorazepam	14.61	321	32	303
Propazine	16.29	230	36	188
Diazepam	16.61	285	40	257
Malathion	17.21	331	28	285
Tebufenozide	18.85	375	34	225
Clopidogrel	20.25	322	28	212

*arbitrary units defined by LCQ system

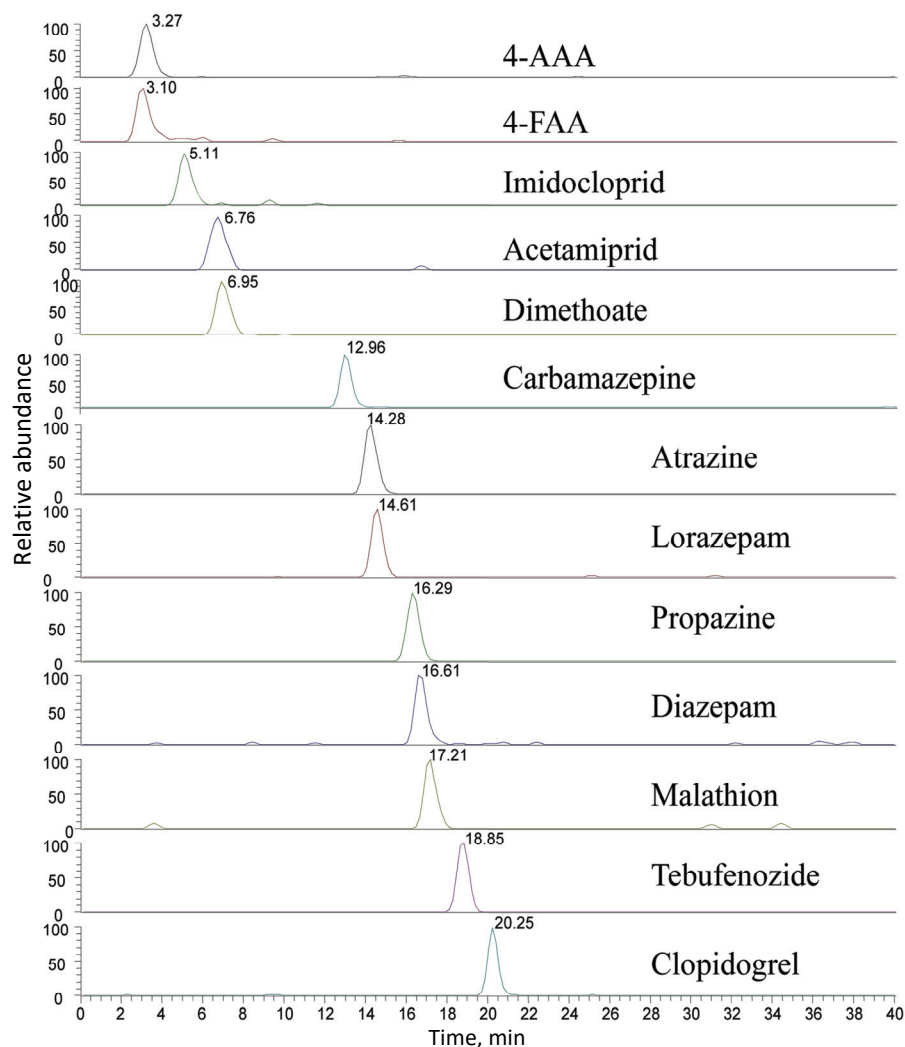


Fig. S-1. SRM chromatograms of selected pesticides and pharmaceuticals.



J. Serb. Chem. Soc. 87 (2) 219–232 (2022)
JSCS–5517

Urea as a complexing agent for selective removal of Ta and Cu in sodium carbonate based alumina chemical–mechanical planarization slurry

ARPITA SHUKLA, NOYEL VICTORIA SELVAM
and MANIVANNAN RAMACHANDRAN*

*Department of Chemical Engineering, National Institute of Technology Raipur,
Chhattisgarh-492010, India*

(Received 20 December 2020, revised 25 June, accepted 29 June 2021)

Abstract: This work reports urea as a promising complexing agent in sodium carbonate-based alumina slurry for chemical–mechanical planarization (CMP) of tantalum and copper. Ta and Cu were polished using Na_2CO_3 (1 wt. %) with alumina (2 wt. %) in the presence and absence of urea. The effect of slurry pH, urea concentration, applied downward pressure and platen rotational speed were deliberated and the outcomes conveyed. Prior to the addition of urea, the Ta removal rate (RR) was observed to increase with pH from acidic to alkaline, having a maximum RR at pH 11. However, Cu RR decreases with increasing pH with minimum RR at pH 11. With the addition of urea in the slurry, a Cu to Ta removal rate selectivity of nearly 1:1 was encountered at pH 11. The addition of urea simultaneous boosts the Ta RR and suppresses Cu RR at pH 11, as it adsorbs on the metal surface. Potentiodynamic polarization was conducted to determine the corrosion current (I_{corr}) and the corrosion potential (E_{corr}). Electrochemical impedance spectroscopy of both metals was carried out in the proposed formulation and the obtained outcomes are elaborated.

Keywords: chemical mechanical planarization; corrosion potential; electrochemical study; electrochemical impedance spectroscopy; corrosion current.

INTRODUCTION

In the realm of integrated circuit (IC) industries, chemical mechanical planarization (CMP) has acquired immense attention to date.¹ There are different applications of CMP in the process of IC fabrication, among which front-end-of-line (FEOL) and back-end-of-line (BEOL) processes hold significant importance.² The materials used for gap-filling, such as silicon dioxide, are polished during the FEOL stage. The BEOL stage includes the formation of metallic interconnects and

* Corresponding author. E-mail: rmani.che@nitrr.ac.in
<https://doi.org/10.2298/JSC201220049S>

a barrier layer. Copper and tantalum are widely used as interconnect and barrier materials, respectively.³ Cu having extremely promising characteristics, such as low resistivity and high electron migration resistance, has been given precedence over aluminum for interconnects.⁴ Due to its higher mobility, Cu poses a tendency to diffuse in silicon and Si-based materials. A diffusion barrier layer made up of Ta or TaN is incorporated to hinder Cu diffusion between Cu and adjacent Si-based material.⁵ Currently, in the integrated circuits fabrication, Cu is employed for BEOL along with materials having a lower value of dielectric constant, such as Ta and nitrides of Ta.⁶

In IC manufacturing industries, it is vital to maintain the polishing rate of Ta as well as Cu consistent.⁷ Moreover, a Cu to Ta polishing selectivity ratio of nearly 1:1 is preferable for efficient polishing. The formulation of the polishing slurry is of significant importance in metal CMP. The polishing slurry is mainly a combination of an abrasive, oxidizer dispersed in distilled water. Various additives, such as complexing agents, surfactants, corrosion inhibitor, dispersants *etc.*, may be present in the polishing slurry depending on the desired metal to be polished. Fumed silica, colloidal silica, alumina are some of the frequently studied abrasives for metal polishing.^{8–11} Numerous oxidizers, such as potassium iodate, quinones, and their derivatives *etc.*, have been intricately studied, among which hydrogen peroxide (H_2O_2) is the most prominent one. A slurry containing H_2O_2 as oxidizer is not stable as it has a decomposition nature. A stabilizer, such as phosphoric acid, must be used in the formulated slurry to overcome the decomposition issue.^{12–14} Many researchers have worked on Ta and Cu CMP, but only a few literature reports are available on 1:1 Cu to Ta removal rate selectivity. Jindal *et al.* reported 1:1.7 selectivity in a slurry containing 3 wt. % fumed silica, 5 wt. % H_2O_2 and 1 wt. % glycine as complexing agent at pH 12.¹⁵ Babu *et al.* reported approximately 1:1 selectivity using a slurry formulation of 5 wt. % colloidal silica, 5 wt. % H_2O_2 and 0.13 M tartaric acid at pH 6.¹⁶ Kaufman *et al.* investigated Ta and Cu CMP with slurry comprising of 2 wt.% alumina, 5 wt.% H_2O_2 and 0.5 wt.% tartaric acid at pH 10 and reported a selectivity of 1:1.9.¹⁷ Carter *et al.* studied a Cu and Ta CMP using a slurry composition of 0.5 wt. % fumed silica, 0.5 wt. % cesium carbonate and 5 mM of various organic and inorganic quinon containing compounds as oxidizers at pH 2.2 and obtained a range of selectivity with different oxidizer, *i.e.*, 1,8-disulfonic acid dipotassium salt ($\approx 3:1$), 1,5-disulfonic acid disodium salt ($\approx 1.5:1$), H_2O_2 (0.17:1) and potassium persulfate ($\approx 1:1$).¹⁴ Although few researches has been performed on Ta and Cu CMP incorporating various competent abrasives, oxidizers, and complexing agents, the mechanism of the removal rate selectivity is still not well understood. This study targets the achievement of a Cu to Ta removal rate selectivity of 1:1. Cu and Ta differ highly in their chemical and physical properties, being a mild and hard metal, respectively. The addition of an additive is needed, which can enhance the Ta RR and simultaneously suppress

Cu RR. Organic acids, such as citric acid, tartaric acid and urea, were tested and better synergy for both the metals with urea was obtained. Hence, urea was selected for further selectivity study in the alkaline region and has also previously been studied as an inhibitor for Cu CMP.¹⁸ Particularly, sodium carbonate as oxidizer and urea as complexing agent have not been studied in any literature to date and this is the first report which uses the above formulation for Ta and Cu CMP.

In this research work, Ta and Cu CMP experiments were performed using a polishing slurry containing alumina as abrasive, sodium carbonate as oxidizer and urea as complexing agent dispersed in distilled water. Static etch rate experiments were performed for both metals in the oxidizer solution at various pH to understand the chemical dissolution behavior. However, the static etch rate of tantalum was found to be practically zero. The influence of numerous parameters, such as pH of the polishing slurry, alteration in the concentration of the complexing agent, increasing the applied downward pressure and increase in rotational platen speed on metal removal rate was studied and the results are conveyed. A metal polishing selectivity of nearly 1:1 is reported, which is desirable for a CMP involving more than one type of metal. Electrochemical analysis, potentiodynamic polarization and electrochemical impedance spectroscopy (EIS) of both the metal were performed in 1 wt. % sodium carbonate solution in the presence and absence of urea. An electrical equivalent circuit (EEC) was proposed for the EIS results, and the EIS data were also validated using the Kramer–Kronig transformation.

EXPERIMENTAL

Polishing experiments were executed using a benchtop polisher assembly of Labopol 5 and Laboforce 3 purchased from Struers Denmark. A Suba IV polishing pad, constructed of polyurethane, obtained from Eminess Technology, USA, was used for the CMP experiments. All the experiments were performed using Ta ($\approx 99.9\%$ pure) and Cu ($\approx 99.9\%$ pure) coupons, which were purchased from Alfa Aesar and Industrial Engineering Store, India, respectively. Both the coupons had 2.5 cm diameter and 1.25 cm thickness. Polishing slurry composed of alumina as abrasive along with sodium carbonate as oxidizer, with and without urea as the complexing agent dispersed in distilled water was employed for the CMP experiments. All the used chemicals were of analytical reagent grade and obtained from Loba Chemie. Unless otherwise stated, the concentration of abrasive, oxidizer and complexing agent were maintained at 2, 1 and 0.1 wt. %, respectively. The speed of the coupon holder was fixed at 250 rpm. The platen rotational speed and downward pressure were kept at 100 rpm and 40680 Pa, respectively, unless specified otherwise. The flow rate of the polishing slurry was maintained at 100 ml min^{-1} with the help of a peristaltic pump throughout the experiment. Potassium hydroxide or nitric acid was used to regulate and reach the desired slurry pH. All the polishing experiments were conducted at ambient temperature. The polishing pad was hand conditioned using 600 grade silicon carbide paper employing the same slurry prior to each polishing cycle to ensure consistency of the polishing pad surface. Both the coupons were washed with distilled water and subsequently air dried. The samples were weighed before and after polishing using an analytical balance (Sartorius, BSA 2245-CW). The rate of material removal was calculated from weight loss of the specimen, metal density, area and the polishing time. The

average removal rate and the standard deviation were calculated from three polishing runs performed under identical conditions.

A PARSTAT MC 1000 electrochemical workstation (Ametek, USA) was used for all the electrochemical experiments. Open circuit potential (OCP), potentiodynamic polarization (Tafel) and electrochemical impedance spectroscopy (EIS) were executed and the outcomes were studied. The cell consisted of the studied metal electrode (Cu/Ta), a saturated Ag/AgCl electrode and a platinum wire, employed as the working, reference and counter electrode, respectively. All potentials in the paper refer to Ag/AgCl scale. The working electrode for both the metals was prepared by covering small cylindrical metal sample with a Teflon casing giving a circular cross section of the exposed surface. The electrical connection between the electrochemical cell system and working electrode were established with the aid of copper. The working electrodes were polished with 0.3 μm alumina powder followed with 0.05 μm alumina powder procured from Buehler (USA). Both the electrodes were then washed and sonicated with distilled water. The electrolyte used in this study was Na_2CO_3 , HNO_3 or KOH were used to maintain the pH of the electrolyte solution. Open circuit potential (OCP) measurements were performed for 3 min to stabilize the electrochemical system preceding all the electrochemical experiments. A potential range of -250 – 250 mV was applied with respect to the value obtained from the OCP for the Tafel experiments at a scan rate of 1 mV s^{-1} . After extrapolation of the anodic and cathodic branches of the Tafel curves using PARSTAT software, the E_{corr} and I_{corr} values were found. A frequency range of 0.1 Hz to 100 kHz with respect to the OCP value was applied for the EIS studies. An EEC was identified using ZSimpWin (Princeton Applied Research, USA) software which gives more insight into the results obtained from EIS.

RESULTS AND DISCUSSION

Effect of pH on material removal rate

The effect caused by change in pH of the slurry on the removal rate of Ta and Cu is illustrated in Fig. 1a and b. The CMP experiments were executed using a slurry containing 2 wt. % alumina and 1 wt. % sodium carbonate (Fig. 1a) without urea (Fig. 1b) with 0.1 wt. % urea. Without urea, the Ta removal rate increases when the pH moves from acidic to alkaline side with maximum metal removal rate at pH 11.¹⁹ Ta reacts with the water present in polishing slurry forming a stable Ta_2O_5 layer, which is challenging to remove from metal surface. This oxide layer is relatively weaker at alkaline pH values than at acidic ones.²⁰

The Ta removal rate was enhanced at all the pH with the introduction of urea to the polishing slurry. The resulting enhancement was perhaps because urea forms a complex with the formed oxide layer. In the absence of urea, the Cu removal rate decreases with increasing pH, with a maximum removal rate at pH 3. In the presence of urea, Cu removal rate was suppressed at all the pH values. This behavior could be attributed to the adsorption of urea on the surface of polished metal. Enhancement in Ta removal rate and suppression in Cu removal rate with the addition of urea yields nearly 1:1 Cu removal rate to Ta removal rate selectivity at pH 11, which is desirable for barrier layer CMP. Henceforth, all the further experiments were conducted at pH 11.

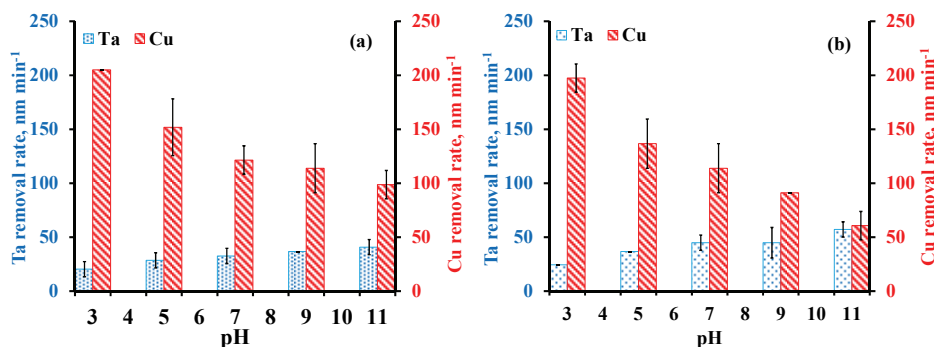


Fig. 1. Effect of pH on material removal rate of Ta and Cu using 2 wt. % alumina and 1 wt. % Na_2CO_3 ; a) without and b) with urea.

A Cu dissolution study was also performed with and without urea in the solution. A 2 wt. % sodium carbonate solution, a 0.1 wt. % urea and a 2 wt. % sodium carbonate along with 0.1 wt. % urea solution were taken for the dissolution study. Cu showed no dissolution with urea. A decrease in the dissolution rate of copper was observed with increasing pH, $\approx 12 \text{ nm min}^{-1}$ at pH 3 to 3 nm min^{-1} at pH 11 in 2 wt. % sodium carbonate + 0.1 wt. % urea. Nearly the same dissolution was encountered prior to the introduction of urea.

Effect of urea concentration

Effect of urea concentration with 2 wt. % alumina slurry containing 1 wt. % Na_2CO_3 on the Ta and Cu metal removal rate at pH 11 were studied and the outcomes are presented in Fig. 2. As the urea concentration increases from 0.05 to 0.5 wt. %, an increase in the Ta removal rate was observed. A similar trend was also observed for the Cu removal rate. On increasing the urea concentration, the ratio of the Cu to Ta removal rate was observed to decrease initially from 1.5:1 to 1.1:1 and then increases from 1.1:1 to 4:1. The desired polishing selectivity of $\sim 1:1$ was observed with 0.1 wt. % urea concentration. Polishing experiments were not performed beyond 0.5 wt. % urea concentration, as the selectivity ratio between Ta and Cu removal rate was higher than the desired range.

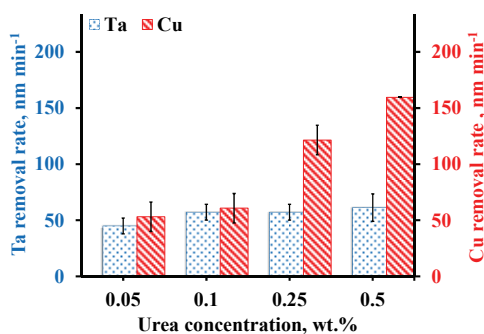


Fig. 2. Effect of urea concentration on material removal rate of Ta and Cu.

Effect of pressure and platen speed

The influence of the applied downward pressure and platen rotational speed on the removal rate of Ta and Cu are portrayed in Fig. 3a and b, respectively. The experiments were conducted with 2 wt. % alumina + 1 wt. % Na₂CO₃ + 0.1 wt. % urea slurry and a constant pH of 11 was maintained throughout. The applied downward pressure ranged from 19995 to 81359 Pa.

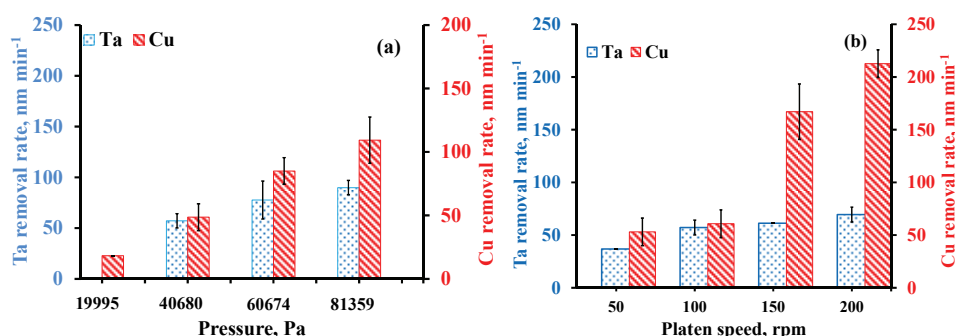


Fig. 3. Effect of: a) applied pressure and b) platen speed on material removal rate of Ta and Cu.

The selectivity of the removal rate was noticed to enhance from 0 to 1.5:1 with increasing applied downward pressure. This could possibly be due to increase in the contact area between metal surface and polishing pad.²¹ The rotational speed of the platen was varied from 50 rpm to 200 rpm having same polishing slurry composition mentioned earlier, with a constant pressure of 40680 Pa and the results are reported in Fig. 3b. The removal rate selectivity ratio increased from 1.5:1 to 3:1.

Potentiodynamic polarization study (Tafel)

Tafel experiments were conducted with an electrolytic solution containing 1 wt. % Na₂CO₃ with and without 0.1 wt. % urea for both the metal coupons (Ta and Cu). The studies were performed for various odd pH values from 3 to 11. The results are shown in Fig. 4a and b, which depict the Tafel plot for Ta without and with the addition of urea, respectively. It can clearly be seen that the shift in anodic current density towards the left with increasing pH from 3 to 11 confirms the maximum dissolution at pH 11 for both cases.³ However, the obtained current density in the latter case is slightly increased. The obtained pattern matches well with the results obtained from the CMP experiments with and without incorporation of urea.

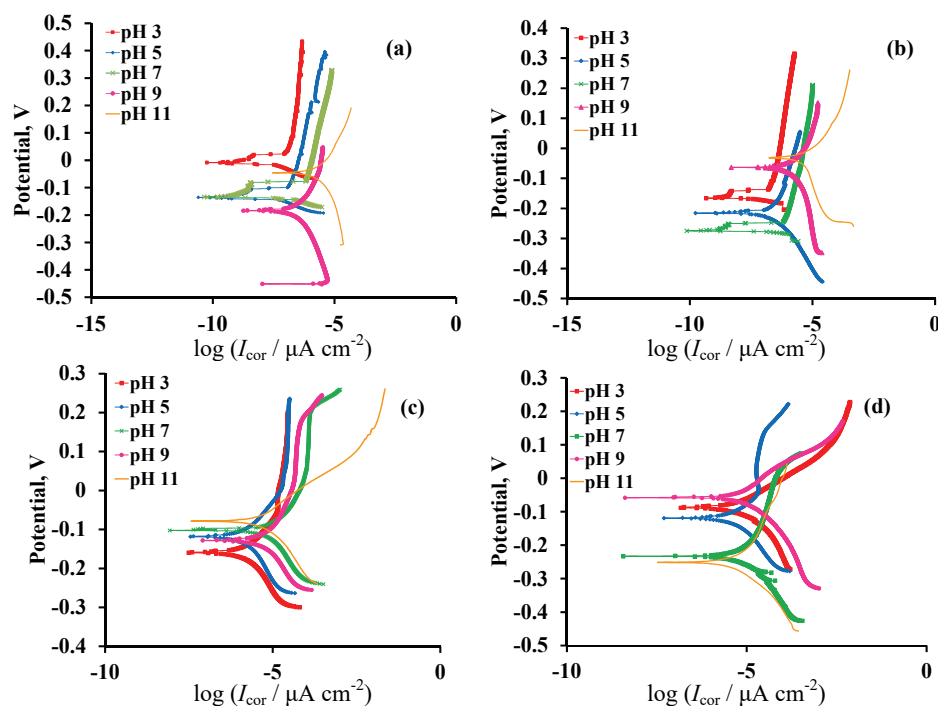


Fig. 4. Potentiodynamic polarization curves of Ta and Cu in the presence of 1 wt. % Na_2CO_3 at various pH values: a) Ta without urea, b) Ta with 0.1 wt. % urea, c) Cu without urea and d) Cu with 0.1 wt. % urea.

On extrapolation of the anodic and cathodic branches, I_{corr} values are obtained for without and with urea and the values are presented in Table I. In the absence of urea, I_{corr} values of tantalum increased from 0.059 to $1.78 \mu\text{A cm}^{-2}$ with increasing pH value from 3 to 11. After the addition of urea, an increase in I_{corr} value of Ta from $0.07 \mu\text{A cm}^{-2}$ at pH 3 to $2.84 \mu\text{A cm}^{-2}$ at pH 11 was observed. This could be due to the adsorption of urea in the Ta surface. The Tafel plot for Cu with the same composition of electrolyte as reported earlier without and with 0.1 wt.% urea are depicted in Fig. 4c and d, respectively.

TABLE I. Tafel parameters for Ta in the presence of 1 wt. % Na_2CO_3 with and without urea at various pH values

pH	Without urea		With urea	
	$E_{\text{corr}} / \text{mV vs. Ag/AgCl}$	$I_{\text{corr}} / \mu\text{A cm}^{-2}$	$E_{\text{corr}} / \text{mV vs. Ag/AgCl}$	$I_{\text{corr}} / \mu\text{A cm}^{-2}$
3	-3.13	0.059	-169.71	0.07
5	-128.58	0.07	-211.83	0.156
7	-139.17	0.202	-265.28	0.321
9	-187.17	0.232	-70.73	1.14
11	-48.78	1.78	-37.15	2.84

The I_{corr} values obtained from extrapolating the anodic and cathodic branches without urea and with urea for both the metals are given in Table II. In the absence of urea, the I_{corr} value decreases from 2.34 to 1.14 $\mu\text{A cm}^{-2}$ with increasing pH value from 3 to 11. However, in the presence of urea, the I_{corr} value decreases from 1.66 $\mu\text{A cm}^{-2}$ at pH 3 to 0.988 $\mu\text{A cm}^{-2}$ at pH 11. With the addition of urea, an inhibition mechanism occurs which causes a reduction in the I_{corr} value over the entire pH range, which corroborates with the CMP results. Galvanic corrosion arises when different electrochemical materials come into electrical contact after they are immersed in an electrolyte. Further optimization of the slurry is required based on the galvanic corrosion potential difference, which could be considered as future plan of this work.

TABLE II. Tafel parameters for Cu in the presence of 1 wt. % Na_2CO_3 with and without urea at various pH values

pH	Without urea		With urea	
	$E_{\text{corr}} / \text{mV vs. Ag/AgCl}$	$I_{\text{corr}} / \mu\text{A cm}^{-2}$	$E_{\text{corr}} / \text{mV vs. Ag/AgCl}$	$I_{\text{corr}} / \mu\text{A cm}^{-2}$
3	-162.948	2.342	-89.331	1.633
5	-121.284	2.009	-115.205	1.375
7	-101.106	1.614	-226.11	1.216
9	-126.762	1.369	-53.003	1.142
11	-84.603	1.142	-252.897	0.988

Electrochemical impedance spectroscopy

The electrochemical impedance spectroscopy results of Ta and Cu metal coupons performed in the sodium carbonate solution with and without urea at different pH values are shown in Fig. 5a–d.

EIS results were modelled using Zsimpwin software and the best fit is shown in Fig. 5a–d. Each trend shows a solid line and marker. The solid line refers to the modelled data while the marker show the corresponding experimental data.

As shown in Fig. 6, a combination of three resistance (R) and two constant phase element (CPE), electrical equivalent circuit (EEC) was employed. R_{sol} , R_{film} and CPE_{film} signifies electrolyte solution resistance, the oxide layer pseudo-resistance and its corresponding constant phase element, respectively. R_{ct} and CPE_{dl} signifies the charge transfer resistance and the constant phase element of electrical double layer, respectively.^{22,23}

The shaped semicircles are due to the formation of a thin oxide film after the adsorption of sodium carbonate on the metal surface. As an outcome of this conduct, the above stated both CPE s are assimilated in the EEC. The CPE arises from the distribution in the current density along the electrode surface because of surface heterogeneity and surface roughness of the electrode.²⁴

EEC fit parameters for Ta and Cu in the presence of 2 wt. % alumina, 1 wt. % Na_2CO_3 with and without 0.1 wt. % urea at various pH are given in Table III.

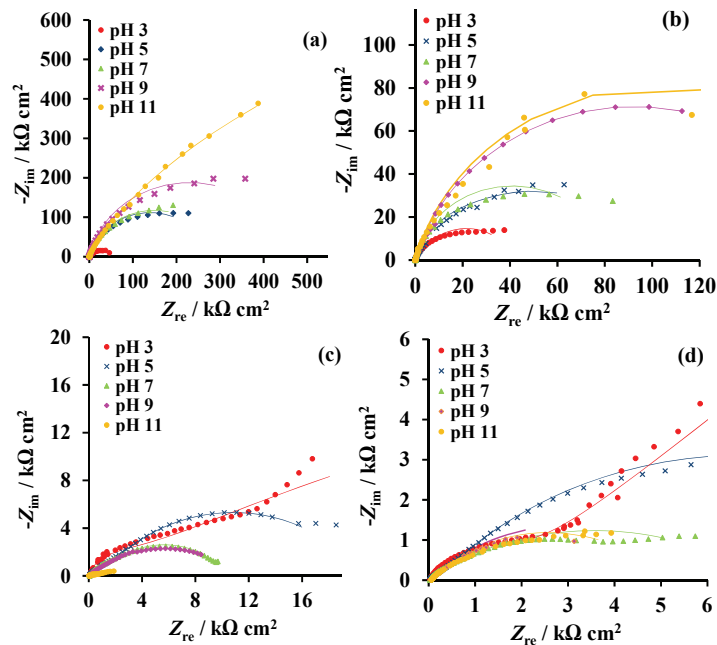


Fig. 5. EIS spectra of Ta and Cu in the presence of 1 wt. % Na_2CO_3 at various pH: a) Ta without urea, b) Ta with 0.1 wt. % urea, c) Cu without urea and d) Cu with 0.1 wt. % urea.

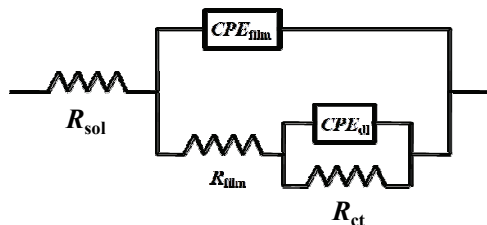


Fig. 6. Electrical equivalent circuit to analyze the experimental data.

As shown in Table III, the values of R_{sol} and R_{film} for Ta decrease as the pH changes from the acidic to the alkaline range. With the addition of urea, a declination in both the resistances is observed for all the pH range, caused by the adsorption of urea on the Ta surface. The variation in resistance is per chance associated with the change in the passive film thickness. R_{sol} and R_{film} for Cu increases with increasing pH, having minimum resistance at pH 3, as shown in Table IV. After addition of urea, the value increases for all the pH range. The pattern obtained in resistance variation matches well with the MRR resulting from the CMP experiments.

The Kramers–Kronig transformation (KKT) was employed to check the electrochemical impedance data for stability, linearity and causality²⁵ and the equations are reported elsewhere.²⁶

TABLE III. EEC fit parameters for Ta in the presence of 2 wt. % alumina, 1 wt. % Na₂CO₃ with and without 0.1 wt. % urea at various pH values

Parameter	pH									
	Without urea					With urea				
	3	5	7	9	11	3	5	7	9	11
$R_{sol} / \Omega \text{ cm}^2$	29.4	29.3	28.9	27.2	26.5	18.7	16.7	15.7	15.5	14.3
$Y_{film} \times 10^5$	0.6	2.1	0.4	0.7	1.6	5.9	2	5.2	2.8	2.5
$\Omega^{-1} \text{ s}^n \text{ cm}^{-2}$										
n_{film}	0.8	0.8	1	0.9	0.9	0.9	0.8	0.8	0.8	0.9
$R_{film} / \Omega \text{ cm}^2$	29090	20080	253.2	71.9	22.9	184700	68450	20810	1847	634.6
$Y_{dl} \times 10^5$	0.5	4.6	2.3	1.7	0.2	51.2	0.2	10.1	0	0.8
$\Omega^{-1} \text{ s}^n \text{ cm}^{-2}$										
n_{dl}	0.8	1	0.8	0.8	1	1	1	0.8	0.8	0.9
$R_{ct} / \text{k}\Omega \text{ cm}^2$	3007.0	461.00	295.30	279.30	18.30	208.5	82.16	21.78	20.05	4.512

TABLE IV. EEC fit parameters for Cu in the presence of 2 wt. % alumina, 1 wt. % Na₂CO₃ with and without 0.1 wt. % urea at various pH values

Parameter	pH									
	Without urea					With urea				
	3	5	7	9	11	3	5	7	9	11
$R_{sol} / \Omega \text{ cm}^2$	49.6	59.0	67.5	73.8	76.8	46.3	51.9	26.9	27.6	26.2
$Y_{dl} \times 10^5$	12.5	1.5	1.5	0.2	1.5	0.4	0.0	15.9	248.8	1.6
$\Omega^{-1} \text{ s}^n \text{ cm}^{-2}$										
n_{film}	0.6	0.8	0.8	0.8	0.8	0.5	0.8	0.8	0.8	0.8
$R_{film} / \Omega \text{ cm}^2$	419.3	778.2	17280	1540	1875	300.5	309.1	1994	5060	5913
$Y_{dl} \times 10^5$	185.5	9.1	11.5	7.5	0.1	429.6	305.0	22.2	20.9	31.8
$\Omega^{-1} \text{ s}^n \text{ cm}^{-2}$										
n_{dl}	0.7	0.8	0.8	0.8	0.8	0.2	0.8	0.4	0.8	0.5
$R_{ct} / \Omega \text{ cm}^2$	134100	10380	18720	8486	11590	1008	20200	6870	13240	18520

The recorded experimental data were used to calculate the value of $Z(\omega)$ for a finite frequency range from ω_{min} to ω_{max} using the equations. This ensures adequate integration accuracy with small integration steps dx on interpolation.²⁷ Once the imaginary part is known for entire frequency range the real part is assessed using KKT. The KKT plots for Ta and Cu in 1 wt. % Na₂CO₃ with 0.1 wt. % urea, Z_{re} vs. frequency and $-Z_{im}$ vs. frequency are shown in Fig. 7. The electrochemical system is found to be stable and linear, as the experimental and fitted data matched well.

Proposed Ta and Cu removal mechanism

In order to explain Ta and Cu removal mechanism using sodium carbonate as oxidizer and urea as complexing agent, the following chemical reactions are proposed at alkaline pH values. Initially, the Na₂CO₃ present in the slurry reacts with water and dissociates into sodium hydroxide (NaOH) and carbon dioxide as given in Eq. (1).²⁸ Ta has a tendency to cover itself with an oxide layer of tanta-

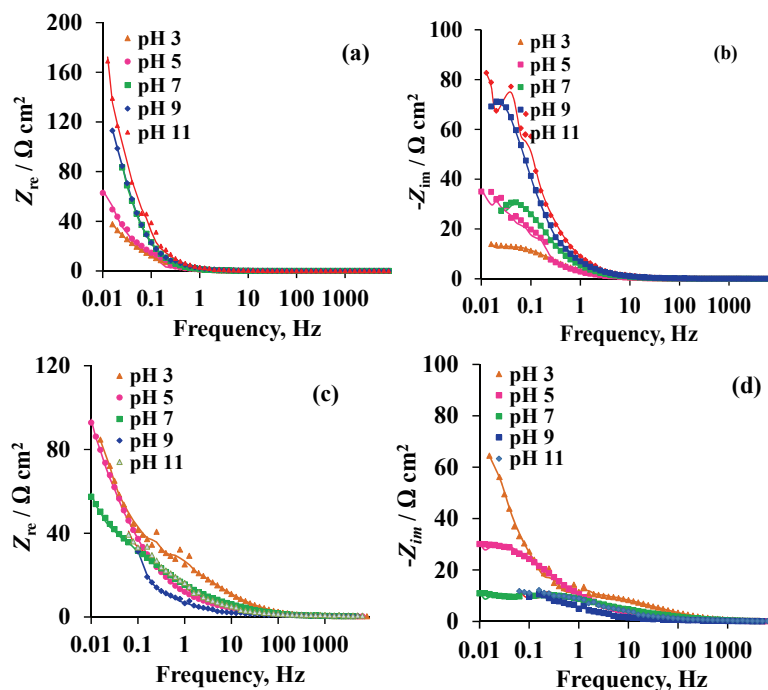
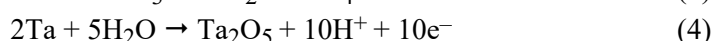
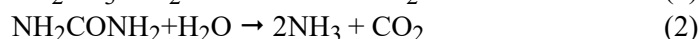
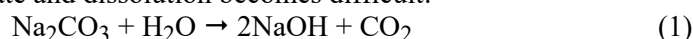


Fig.7. KKT fits for Ta: a) Z_{re} vs. frequency, b) $-Z_{im}$ vs. frequency, and for Cu: c) Z_{re} vs. frequency and d) Z_{im} vs. frequency, in 1 wt. % Na_2CO_3 with 0.1 wt. % urea.

lum pentoxide (Ta_2O_5). Ta_2O_5 is the only formed hard stable oxide, due to which the material removal rate and dissolution becomes difficult:²⁹



Urea reacts with water and produces ammonia and carbon dioxide (Eq. (2)), further NH_3 molecule encounters self-dissociation when comes in contact with water. It dissociates into its conjugate acid and conjugate base which are NH_4^+ and NH_2^- , shown in Eq. (3). In the next step (Eq. (4)), Ta undergoes oxidation, *i.e.*, reacts with atmospheric water molecules and Ta_2O_5 is formed at all pH and concentrations.³⁰ The formed Ta_2O_5 reacts with NaOH at alkaline pH,²⁸ which results in a polytantalate compound $\text{Na}_8\text{Ta}_6\text{O}_{19}$, depicted in Eq. (5), which is less stable³¹ and easy to remove. The formed ammonium ions form a complex with the polytantalate compound, which is perhaps unstable and easier to abrade, hence an enhanced removal rate is observed.

Cu metal reacts with the O₂ present in the atmosphere/aqueous environment and becomes oxidized into cupric oxide, as shown in Eq. (6). Formation of cupric oxide is confirmed from the presence of blue color on the metal surface during Cu CMP:³²



The formed cupric oxide further reacts with the formed sodium hydroxide (Eq. (1)) and produces sodium tetrahydroxocuprate, a more stable compound, as shown in Eq. (7). The ammonium ions from Eq. (3) along with the formed oxide compound, further form a complex due to which the material removal rate is suppressed.

CONCLUSIONS

Urea was confirmed as a complexing agent for Ta and Cu CMP in a sodium carbonate based alumina slurry. Metal removal rates of Ta and Cu were measured with different urea concentrations, at varying pH, increasing applied pressure and increasing the rotating speed of platen. The Ta removal rate increases as the pH increases from 3 to 11, having a maximum removal rate at pH 11 without urea. Whereas, a reduction in Cu RR was observed with increasing hydrogen ion concentration from pH 3 to 11, having a maximum removal rate at pH 3. With the addition of urea, the Ta removal rate was enhanced and suppression in Cu removal rate was seen, which gives desired nearly 1:1 polishing selectivity. Urea enhances the Ta RR at the same time suppresses the Cu RR, which results in the desired selectivity. The trend obtained in the I_{corr} values from Tafel plots for both the metals resembles well the results obtained from the CMP experiments for both the metals. The variation in both R_{sol} and R_{film} with pH shows an alteration in the passive film thickness and variation in dissolution rate, which enhances the removal for Ta and at same time, suppresses the Cu RR.

Acknowledgement. We gratefully acknowledge the Department of Science and Technology-Science and Engineering Research Board (DST-SERB), India, for providing funds for research work under Grant No SB/FTP/ETA-0351/2013.

ИЗВОД

УРЕА КАО КОМПЛЕКСИРАЈУЋЕ СРЕДСТВО ЗА СЕЛЕКТИВНО УКЛАЊАЊЕ Та И Cu У БИКАРБОНАТНОЈ СУСПЕНЗИЈИ ГЛИНИЦЕ ЗА ХЕМИЈСКО–МЕХАНИЧКУ ПЛАНАРИЗАЦИЈУ

ARPITA SHUKLA, NOYEL VICTORIA SELVAM и MANIVANNAN RAMACHANDRAN

Department of Chemical Engineering, National Institute of Technology Raipur, Chhattisgarh-492010, India

Овај рад приказује улогу урее као комплексирајућег средства у бикарбонатној суспензији глинице која се користи за хемијско–механичку планаризацију тантала и бакра. Та и Cu су полирани коришћењем суспензије глинице (2 мас. %) и Na₂CO₃ (1 мас. %) са и без додатка урее. Разматрани су ефекти рН вредности суспензије, концентрације

урее, примењеног притиска и брзине ротирања цилиндричне плоче. Без додатка урее је запажено да брзина уклањања Та расте са променом рН суспензије од киселе ка алкалној уз постизање максимума на рН 11, док брзина уклањања Си опада са повећањем рН са минимумом на рН 11. Међутим, у присуству урее брзине уклањања Си и Та су биле једнаке на рН 11. Додатак урее је повећао брзину уклањања Та и истовремено смањило брзину уклањања Си на рН 11, јер се уреа адсорбовала на површини метала. За одређивање корозионе струје и корозионог потенцијала примењена је потенциодинамичка поларизација. Урађена је и спектроскопија електрохемијске импеданције оба метала у суспензији предложеног састава и дискутовани су добијени резултати.

(Примљено 20. децембра 2020, ревидирано 25. јуна, прихваћено 29. јуна 2021)

REFERENCES

1. H. J. Kim, Y. J. Jang, J. Choi, B. Kwon, K. Lee, Y. Ko, *Met. Mater. Int.* **335** (2013) 19 (<https://doi.org/10.1016/j.jieec.2016.06.011>)
2. M. Krishnan, J. W. Nalaskowski, L. M. Cook, *Chem. Rev.* **178** (2010) 110 (<https://doi.org/10.1021/cr900170>)
3. J. Seo, U. Paik, in *Advances in Chemical Mechanical Planarization (CMP)*, S. Babu, Ed., Woodhead Publishing, Singapore, 2016, pp. 273–298 (<https://doi.org/10.1016/B978-0-08-100165-3.00011-5>)
4. J. M. Steigerwald, S. P. Murarka, R. J. Gutmann, *Chemical Mechanical Planarization of Microelectronic Materials*, John Wiley and Sons, Berlin, 2008 (ISBN-13: 978-00471-13827-3)
5. S. G. Pyo, *Met. Mater. Int.* **293** (2010) 2 (<https://doi.org/10.1007/s12540-010-0420-1>)
6. K. Maex, M. R. Baklanov, D. Shamiryan, F. Lacopi, S. H. Brongersma, Z. S. Yanovitskaya, *J. Appl. Phys.* **8793** (2003) 11 (<https://doi.org/10.1063/1.1567460>)
7. J. Cheng, T. Wang, L. Jiang, X. Lu, *Appl. Surf. Sci.* **401** (2015) 351 (<https://doi.org/10.1016/j.apsusc.2015.05.150>)
8. A. Vijayakumar, T. Du, K. B. Sundaram, *Microelectron. Eng.* **93** (2003) 70 ([https://doi.org/10.1016/S0167-9317\(03\)00398-8](https://doi.org/10.1016/S0167-9317(03)00398-8))
9. R. Govindarajan, S. Siddiqui, M. Keswani, S. Raghavan, D. R. P. Singh, N. Chawla, *Electrochem. Solid-State Lett.* **10** (2011) 14 (<https://doi.org/10.1149/1.3535269>)
10. Z. Lu, S. H. Lee, S. V. Babu, E. Matijević, *J. Colloid Interface Sci.* **55** (2003) 1 ([https://doi.org/10.1016/S0021-9797\(02\)00166-2](https://doi.org/10.1016/S0021-9797(02)00166-2))
11. T. Du, D. Tamboli, V. Desai, V. S. Chathapuram, K. B. Sundaram, *J. Mater. Sci. Mater. Electron.* **87** (2004) 15 (<https://doi.org/10.1023/B:JMSE.0000005381.96813.0f>)
12. M. Christopher Sulym, D. Roy, *Appl. Surf. Sci.* **2583** (2010) 256 (<https://doi.org/10.1016/j.apsusc.2009.10.108>)
13. N. H. Kim, J. H. Lim, S. Y. Kim, E. G. Chang, *Mater. Lett.* **4601** (2003) 57 ([https://doi.org/10.1016/S0167-577X\(03\)00368-9](https://doi.org/10.1016/S0167-577X(03)00368-9))
14. P. W. Carter, J. Zhang, J. Wang, S. Li, *J. Electrochem. Soc.* **H378** (2008) 155 (<https://doi.org/10.1149/1.2898683>)
15. A. Jindal, Y. Li, S. V. Babu, *Mater. Res. Soc. Symp. Proc.* **8** (2001) 671 (<https://doi.org/10.1149/1.1792871>)
16. S. V. S. B. Janjam, S. Peddeti, D. Roy, S. V. Babu, *Electrochem. Solid-State Lett.* **H327** (2008) 11 (<https://doi.org/10.1149/1.2980345>)
17. V. B. Kaufman, R. C. Kistler, S. Wang, (Cabot Corporation) US006063306A (2000)

18. F. Altaf, R. Qureshi, S. Ahmed, A. Y. Khan, A. Naseer, *J. Electroanal. Chem.* **642** (2010) 98 (<https://doi.org/10.1016/j.jelechem.2010.02.011>)
19. A. Shukla, S. N. Victoria, R. Manivannan, *J. Indian Chem. Soc.* **97** (2020) 1021 (https://indianchemicalsociety.com/portal/uploads/journal/2020_07_11_Extended_16055_11486.pdf)
20. A. Jindal, S. V. Babu, *J. Electrochem. Soc.* **G709** (2004) 151 (<https://doi.org/10.1149/1.1792871>)
21. S. Kim, N. Saka, J. H. Chun, *Procedia CRIP* **42** (2014) 14 (<https://doi.org/10.1109/TSM.2014.2335156>)
22. K. Yadav, M. Ramachandran, S.N. Victoria, *ECS Trans.* **59** (2018) 6 (<https://doi.org/10.1149/08506.0059ecst>)
23. H. Yang, S. Yang, Y. Cai, G. Hou, M. Tang, *Electrochim. Acta* **2829** (2010) 55 (<https://doi.org/10.1016/j.electacta.2009.12.074>)
24. G. J. Brug, A. L. G. van den Eeden, M. Sluyters-Rehbach, J. H. Sluyters, *J. Electroanal. Chem. Interf. Electrochem.* **275** (1984) 176 ([https://doi.org/10.1016/S0022-0728\(84\)80324-1](https://doi.org/10.1016/S0022-0728(84)80324-1))
25. R. P. Venkatesh, S. Ramanathan, *J. Appl. Electrochem.* **767** (2010) 40 (<https://doi.org/10.1007/s10800-009-0055-4>)
26. K. Yadav, R. Manivannan, S. N. Victoria, *ECS J. Solid State Sci. Technol.* **P879** (2017) 6 (<https://doi.org/10.1149/2.0301712jss>)
27. K. Yadav, R. Manivannan, S. N. Victoria, *Mater. Today Proc.* **1220** (2019) 18 (<https://doi.org/10.1016/j.matpr.2019.06.584>)
28. A. Robin, *J. Appl. Electrochem.* **37** (2003) 33 (<https://doi.org/10.1023/A:1022982320438>)
29. T. Du, J. Chen, D. Cao, *J. Mater. Sci.* **3903** (2001) 36 (<https://doi.org/10.1023/A:1017909919388>)
30. M. Pourbaix, *Mater. Sci. Forum* **43** (1974) <http://sunlight.caltech.edu/aic/pourbaix.pdf>
31. Y. H. Chen, T. H. Tsai, S. C. Yen, *Microelectron. Eng.* **174** (2010) 87 (<https://doi.org/10.1016/j.mee.2009.07.009>)
32. M. C. Turk, S. E. Rock, H. P. Amanapu, L. G. Teugels, D. Roy, *ECS J. Solid State Sci. Technol.* **P205** (2013) 5 (<https://doi.org/10.1149/2.009305jss>).



J. Serb. Chem. Soc. 87 (2) 233–245 (2022)
JSCS–5518

Development of a method for the derivatization of ethanalamines and its application to sand samples

TOMAS ROZSYPAL*

*Nuclear, Biological and Chemical Defense Institute, University of Defense, Vita Nejedleho
691, 68203 Vyskov, Czech Republic*

(Received 12 March, revised 12 May, accepted 13 June 2021)

Abstract: Nitrogen mustards are dangerous and available blistering chemical warfare agents. In the presented study, six derivatization methods are compared for the analysis of degradation products of the most important blistering nitrogen mustards (ethyl diethanolamine, methyl diethanolamine and triethanolamine) by gas chromatography coupled with mass spectrometry. Five silylation methods (using BSTFA and BSA) and one trifluoroacetylation method (using TFAA) were tested. The derivatization reactions were performed in acetonitrile. As the method with optimal results, trifluoroacetylation by TFAA was selected. Analytes reacted with the corresponding reagent rapidly, quantitatively, with stable kinetics and at room temperature. Calibration curves for quantitative analysis of ethanalamines after TFAA derivatization were created. The corresponding detection limits varied between 9×10^{-3} and 7×10^{-5} $\text{mmol} \cdot \text{dm}^{-3}$ for the tested analytes. The developed method was applied for the analysis of ethanalamines after extraction from sand using acetonitrile. Limits of detection were 11.4 to 12.3 μg of the analyte in 1 g of sand. The use of the developed method in military deployable laboratories designated for the rapid identification of chemical warfare agents and corresponding degradation products is encouraged.

Keywords: nitrogen mustard; gas chromatography; mass spectrometry; chemical warfare agents; deployable laboratory.

INTRODUCTION

Nitrogen mustards bis(2-chloroethyl)amine (HN-1), bis(2-chloroethyl)methylamine (HN-2), and tris(2-chloroethyl)amine (HN-3) are harmful blistering chemical warfare agents (CWA) scheduled in the 1A Chemical Weapons Convention Schedule.¹ These are chemicals with similar effects to sulfur mustard are persistent toxic chemicals, only slightly soluble in water and with slow hydrolysis rates.² Nitrogen mustards are specific by their potent alkylating effects³ and

* E-mail: tomas.rozsygal@unob.cz
<https://doi.org/10.2298/JSC210312047R>

they interact with a number of biomolecules and a characteristic manifestation of poisoning is severe blister formation.⁴ These are controlled substances, however, the synthetic pathways are quite simple, precursors are available, and nitrogen mustards therefore still pose an actual threat. The hydrolysis degradation products are ethyl diethanolamine (EDEA), methyl diethanolamine (MDEA) and triethanolamine (TEA).

For identification of CWA military deployable laboratories have often been employed. These laboratories search not only for intact CWA but also for degradation products to exclude false negatives. Liquid chromatography (LC) coupled with mass spectrometry (MS) or nuclear magnetic resonance (NMR) techniques were successfully used for the identification of nitrogen mustards and corresponding degradation products in different matrices, such as water and decontamination mixtures,⁵ organic samples,⁶ wipes and solid samples,⁷ urine and serum.^{8,9} These methods ensure the identification of analytes at very low concentrations (ng ml^{-1}). However, military deployable laboratories mostly do not possess a NMR detector, nor a LC/MS system because of their high purchase price and vibration sensitivity during military transport.

For nitrogen mustard identification, gas chromatography (GC) coupled with a number of detectors is often used.¹⁰ Hydrolysis products could be derivatized with trimethylsilyl (TMS) or *tert*-butyldimethylsilyl (TBDMS) reagents, such as trimethylsilyl iodide (TMSI) + trimethylsilyl chloride (TMCS),¹¹ *N,O*-bis(trimethylsilyl)trifluoroacetamide (BSTFA) + TMCS¹² or *N-tert*-butyldimethylsilyl-*N*-methyltrifluoroacetamide (MTBSTFA).¹³ A rapid method using trifluoroacetylation by *N*-trifluoroacetylbenzimidazole and *N*-trifluoroacetylimidazole (TFAI) was developed.¹⁴ However, no quantitative data were demonstrated. Methods for sample-applied derivatization of partially hydrolyzed nitrogen mustards were created using silylation,¹⁵ trifluoroacetylation using TFAI and heptafluorobutyrylation.¹⁶ In the last case, better results were obtained in comparison to silylation. Formation of fluorinated derivatives is recommended also for GC coupled with Fourier transform infrared spectrometry (FTIR) analysis because of the high absorptivity of these derivatives in their IR spectrum.¹⁷ Directly for military deployable laboratories, derivatization of ethanolamines by BSTFA in acetonitrile at 60° for 30 min is recommended.¹⁸

Various matrices contaminated by ethanolamines have been analyzed. A GC/FPD-NPD (flame photometric detection and nitrogen phosphorus detection) method was developed for the determination of nitrogen mustards and ethanolamines in water, soil, organic solvents and PVC.¹⁹ Nerve agent degradation products in soil are derivatized using methylation by trimethyloxonium tetrafluoroborate.²⁰ Arsenic CWAs in sand samples are identified after thermal desorption.²¹ Popiel and Sankowska²² recommended solid phase microextraction (SPME) as a universal extraction technique for CWA degradation products in

different sample matrices. A simple method for extraction, derivatization, and GC/MS analysis of ethanolamines in sand samples was not presented.

In the current praxis of military deployable chemical laboratories, rugged methods are used that do not suffer from long distance transport of the container. The identification method of choice is GC/MS. The aim of this paper is the development of a simple, quick, reliable, and universal method for the identification of nitrogen mustards ethanolamines EDEA, MDEA and TEA in sand samples using GC/MS, a method usable in military deployable laboratories.

EXPERIMENTAL

Chemicals and equipment

N-ethyl-diethanolamine 98 % (EDEA), *N*-methyl-diethanolamine 99 % (MDEA) and triethanolamine 99 % (TEA) were used as standards of ethanolamines. As the internal standard, tributyl phosphate 99 % was used. As derivatization reagents, *N,O*-bis(trimethylsilyl)trifluoroacetamide 99 % (BSTFA), *N,O*-bis(trimethylsilyl)acetamide 98.5 % (BSA), trifluoroacetic anhydride 99 % (TFAA) and trimethylchlorosilane 99 % (TMCS) were used. Acetonitrile gradient grade was used as the extraction solvent (all Sigma Aldrich, Schnellendorf, Germany). Sodium carbonate anhydrous *p.a.* and annealed copper sulfate (both Penta, Prague, Czech Republic) were also used. As the sample matrix, sea sand pure (Lachema, Brno, Czech Republic) was used.

Gas chromatography with mass spectrometry was conducted using the mobile GC/MS system Griffin 465 (FLIR, Wilsonville, USA, electron ionization, ion trap, *m/z* 40–425, split injection, standard DB-5MS column (15 m×0.18 mm×0.18 μm). For data acquisition and interpretation, software packages, Griffin System software (FLIR, Wilsonville, OR, USA) and AMDIS 2.72 were used. The chromatographic method was 13.65 min long. The start temperature was 40 °C, held for 1 min. Then a gradient of 30 °C min⁻¹ was applied, and the final temperature was 300 °C, which was held for 4 min. The split was set to 1:4 ratio.

For injections micro syringes, Hamilton (Chromservis, Prague, Czech Republic) were used. Extractions were conducted using a Multi Reax shaker (Heidolph, Schwabach, Germany). For temperature control during the derivatization reactions, HD-4 thermostat (Julabo, Seelbach, Germany) was used. Samples were extracted into Supelco 7 mL clear glass vials with screw caps with a solid top and PTFE liner (Sigma Aldrich, Schnellendorf, Germany). For sonication, an ultrasonic bath Sonorex (Bandelin, Germany) was used. X-ray fluorescence (XRF) analysis of the sand matrix was conducted with an ElvaX Mobile (Elvatech, Kyiv, Ukraine). Characterization of the sand grain size distribution was conducted using an AS 200 vibratory sieve shaker (Retsch, Haan, Germany).

Sand characterization

The sand was washed with distilled water, dried and stored in a desiccator prior to analysis. The elemental composition was determined by XRF spectrometry. For this purpose, 5 g of the matrix was added to a XRF vial and it was analyzed in the spectrometer chamber for 1 min using a method developed for soils (35 kV voltage).

Grain distribution of the sand was determined by adding 5 g of the sand into the vibratory sieve shaker and the shaking method proceeded for 2 min. Then the individual sizes of sand grains (from individual sieves) were weighed.

Derivatization of ethanolamines

Six derivatization methods were tested. Silylation by BSTFA at 30 °C, silylation by BSTFA at 60 °C, silylation by BSTFA + 1 % TMCS, silylation by BSA, silylation by BSA + TMCS (5:1) and trifluoroacetylation by TFAA.

A 0.5 mmol dm⁻³ solutions of the corresponding ethanolamine (EDEA, MDEA or TEA) in acetonitrile with internal standard (1.83×10⁻⁴ mmol dm⁻³) were created. Then, 1 mL of the solution was added into a vial and the derivatization reagent (or solution) was added in a volume specified in Table I for each derivatization procedure. The vial content was sonicated for 1 min, and then the vial was placed into the thermostat set to the temperature specified for each derivatization procedure in Table I. Then, aliquots of the reaction mixture were taken over time and analyzed by GC/MS to determine the time dependence of the derivatives formation. In a similar way, blank samples (TBP in solvent with derivatization reagent) were always analyzed (with all derivatization methods).

TABLE I. Parameters of the derivatization procedures tested for the derivatization of ethanolamines

Derivatization procedure	BSTFA at 30 °C	BSTFA at 60 °C	BSTFA + TMCS	BSA	BSA + TMCS	TFAA
Volume of the reagent added, μL	20	20	20	20	20	30
Derivatization temperature, °C	30	60	30	30	30	30

Test of the effect of solvent on derivatization by TFAA

A 0.5 mmol dm⁻³ solution of MDEA in hexane with internal standard (1.83×10⁻⁴ mmol dm⁻³) was created. Then, 1 mL of the solution was added into a vial and 30 μL of TFAA were added. The vial content was sonicated for 1 min, and then the vial was placed into a thermostat at 30 °C for 30 min. After the specified reaction time, the sample was analyzed by GC/MS. Then, ethyl acetate was tested as the reaction solvent in the same manner.

Calibration curves formation

For each ethanolamine (EDEA, MDEA and TEA), calibration solutions were prepared with a concentration of 0.05, 0.25 and 0.50 mmol dm⁻³ in acetonitrile with TBP internal standard (1.83×10⁻⁴ mmol dm⁻³). To each of these solutions, 30 μL of TFAA was added sequentially, and each mixture was derivatized at 30 °C for 30 min. After the specified reaction time, each sample was analyzed by GC/MS. Each calibration dependence was determined five times and each time, it was verified that the instrument was turned on. From the obtained responses, calibration dependences for individual ethanolamines were created to compare the extraction yields from sand samples in the following steps.

Extraction of kind regards ethanolamines from sand

For each ethanolamine (EDEA, MDEA and TEA), calibration solutions were prepared with concentration of 0.5, 2.5 and 5.0 mmol dm⁻³ in acetonitrile with TBP as the internal standard (1.83×10⁻⁴ mmol dm⁻³). These concentrations were chosen so that the resulting maximum concentrations after extraction from the sand corresponded to the calibration concentrations from the previous paragraph. Then, 1 g of sand was dosed into 7 mL vials for each sample. Then, 300 μL of the ethanolamine solutions described above were then added into the individual sand samples. Thus, 3 samples of analyte in sand with increasing concentration for each ethanolamine were created. The solvent was allowed to freely evaporate from the samples to the dry state of the sand (90 min). Then, 3 mL of acetonitrile with internal standard

(1.83×10^{-4} mmol dm⁻³) were added to each sample. The samples were extracted for 5 min on a shaker at 1600 rpm. The sample was then centrifuged and 1 mL of the liquid was collected in a vial. To the solution was added 30 μ L of TFAA and the mixture was derivatized at 30 °C for 30 min. After the specified reaction time, the sample was analyzed by GC/MS. Each sample was generated and analyzed five times.

RESULTS AND DISCUSSION

Sand characterization

The elemental composition (weight-to-weight) of the sand was determined by XRF spectrometry: light elements (up to Na) 98.8 %, Ca 0.27 %, Ti 0.25 %, Rh 0.22 %, Ag 0.20 %, Cd 0.11 %, Fe 0.05 %, Ni 0.03 %, Zr 0.02 %. The results of the determination of the grain size distribution of the matrix are given in Table II.

TABLE II. Matrix characterization by determination of the grain size distribution

Grain size, μ m	Contribution, %	Grain size, μ m	Contribution, %
500	0.70	150	24.10
400	2.48	100	3.94
300	15.60	50	0.40
200	52.72	–	–

Derivatization of ethanolamines by BSTFA at 30 °C

In the derivatization of ethanolamines by BSTFA, trimethylsilylated ethers were formed *via* nucleophilic substitution of the hydroxy groups. The substitution proceeded fairly readily, only fully silylated derivatives were recorded on the chromatograms. In the GC/MS method, it was necessary to shift the MS data acquisition to retention time (*RT*) by 2.57 min due to the late elution of BSTFA, which interfered in the chromatogram.

In the case of EDEA, an artifact co-eluted with the derivatized analyte, which caused an increase in the intensity of the background signal and a deterioration in the resolution of the analyte peak. The peak was low and wide and ranged from *RT* 5.10 to 5.25 min. A similar phenomenon has been reported with MDEA. A small broad peak formed in the *RT* range of 4.85–4.95 min. In the case of TEA, the chromatogram was not disrupted by artifacts, however, silylated TEA was characterized by an *RT* very close to the TBP used as the internal standard. The chromatograms obtained by silylation of ethanolamines are shown in the Fig. 1. The retention indices of the individual silylated derivatives and the EI-MS data of the most abundant fragment ions are given in the Table III.

The graph (Fig. 2) records the kinetics of the formation of the silylated derivatives, *i.e.*, the concentration of the final products as a function of the reaction time with BSTFA. It is evident that the final products were formed relatively quickly and after 30 min, the yields did not increase much, so even at ambient temperature the desired products were formed relatively rapidly.

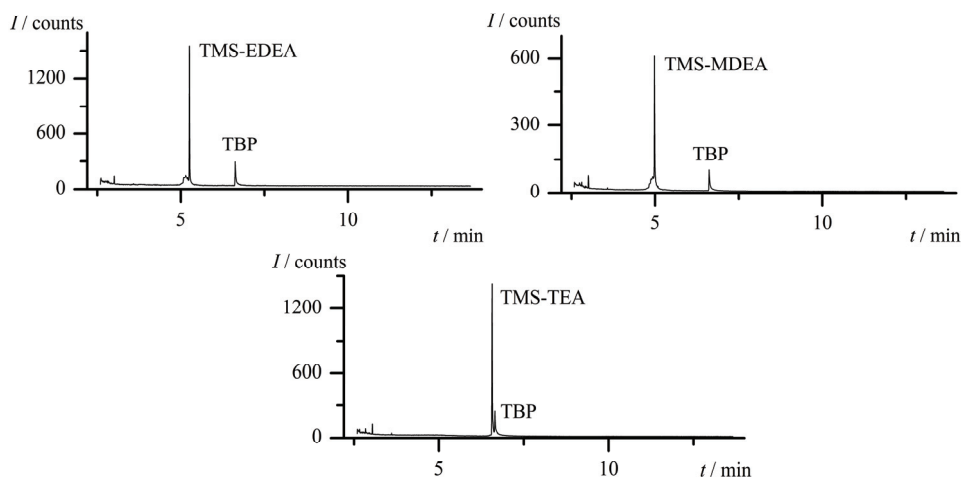


Fig. 1. Chromatograms of TMS derivatives of ethanolamines spiked with the internal standard tributyl phosphate (TSB).

TABLE III. Retention times (*RT*) and corresponding retention indexes (*RI*) of trimethylsilylated analytes – EDEA, MDEA and TEA and internal standard tributyl phosphate, and the most abundant fragment ions (the first most abundant ion was used for quantification)

Parameter	EDEA	MDEA	TEA	TBP
<i>RT</i> -min	5.26	4.98	6.57	6.64
<i>RI</i>	1348	1298	1629	1647
Relative abundance of fragment ions, %	174 (100.0) 73 (45.0) 117 (10.6)	160 (100.0) 73 (51.1) 161 (6.8)	263 (100.0) 73 (52.0) 264 (11.5)	99

Derivatization of ethanolamines by BSTFA at 60 °C

When derivatizing ethanolamines at higher temperatures, similar results were obtained as in the previous case. With silylated EDEA and MDEA, the same artifacts eluted with *RT* values close to the analytes. In the case of MDEA, this interfering peak was wider than in the case of derivatization at 30 °C. Fig. 2 A and B shows the resulting silylated ethanolamine products as a function of the reaction time. Compared to the course of the reaction at a lower temperature, the results were characterized by higher deviations and were thus more difficult to quantify. As at 30 °C, the maximum values were reached after a reaction time of 30 minutes and thus, the increase in temperature did not have a significant effect on the acceleration of the derivatization.

Derivatization of ethanolamines by BSA

BSA, like BSTFA, derivatives alkoxy groups by trimethylsilylation. The silylated derivatives formed relatively quickly and the maximum yield was reached after only 30 min. In addition, higher peak signals were observed for TEA, indi-

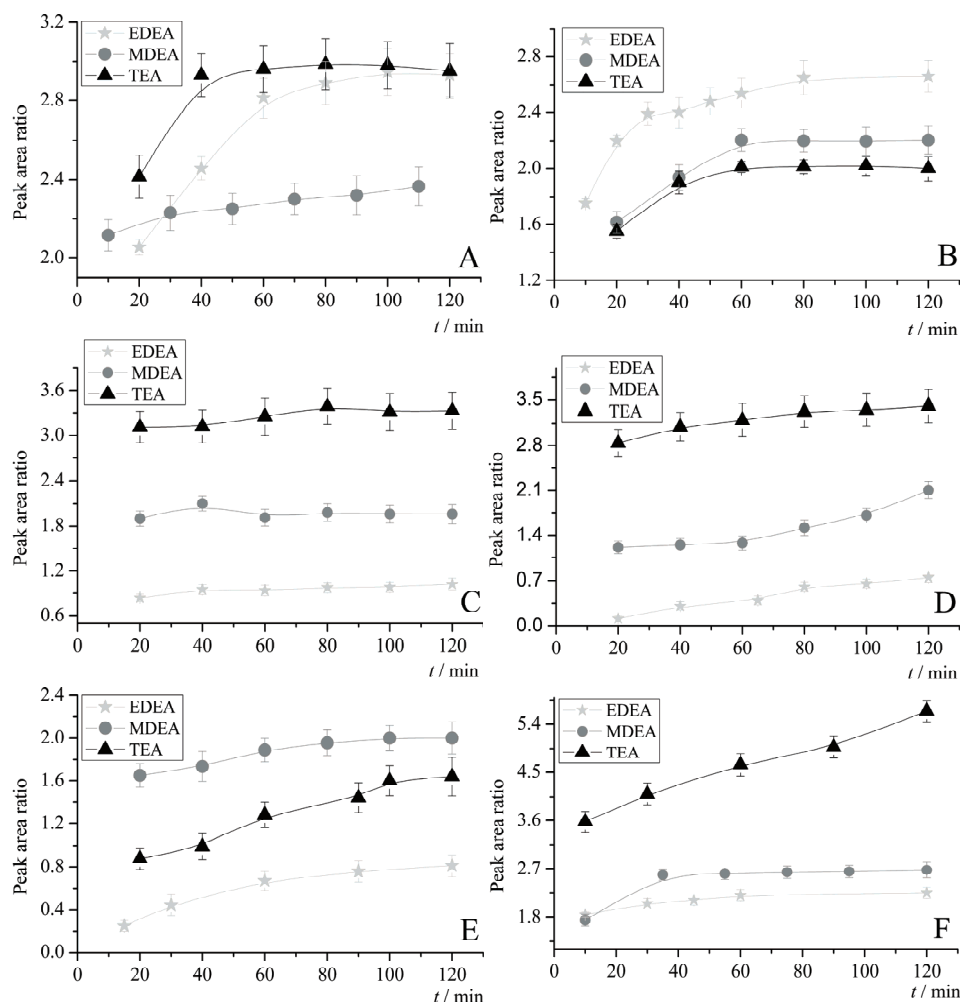


Fig. 2. Kinetics of the formation of trimethylsilyl derivatives after derivatization of ethanolamines by BSTFA at 30 (A) and at 60 °C (B); BSA (C), BSA + TMCS (D), BSTFA + TMCS (E) and the formation of trifluoroacetyl derivatives after derivatization by TFAA (F). The y-axis denotes area ratio between analyte and tributyl phosphate peaks.

cating higher yields compared to BSTFA derivatization. The results were characterized by higher deviations compared to BSTFA and were thus less suitable for quantitative purposes. A graphical representation of the formation of the derivatization products as a function of the reaction time is given in Fig. 2C and D.

Derivatization of ethanolamines by BSA + TMCS

TMCS-catalyzed BSA derivatization (5:1 BSA + TMCS mixture) showed worse results than BSA alone, probably due to the high TMCS content. Reaction

yields were lower, with slower kinetics, and were also characterized by high deviations, which had a negative impact on quantitative evaluation. The chromatograms were full of peaks that interfered with identification, in the case of EDEA the derivatized analyte co-eluted an artifact with a broad peak base in the region of RT 5.00–5.24 min. In the case of MDEA, an artifact also eluted with a broad base in front of the analyte peak in the RT 4.70–4.96 min region. In the case of TEA, the derivatized analyte eluted very close to the internal standard. A graphical representation of the formation of derivatization products as a function of the reaction time is depicted in Fig. 2C and D.

Derivatization of ethanolamines by BSTFA + TMCS

BSTFA with TMCS (1 %), a mixture used to derivatize poorly derivatizable substances was also tested. Trimethylsilylated ethers of ethanolamines were formed with the same parameters as in the previous cases, together with artifacts similar to those produced by derivatization of ethanolamines only by BSTFA alone. However, the trimethylsilylated products formed with slower kinetics, as can be seen in Fig. 2E and F.

Previous studies dealing with the silylation of ethanolamines^{11–13} have shown low detection limits, however, in none of the studies did the authors mention a relatively large number of artifacts in the resulting chromatograms, nor the co-elution of other substances with derivatized ethanolamines. This article also points out the low long-term stability of the resulting TMS derivatives.

Derivatization of ethanolamines by TFAA

The reaction of TFAA with ethanolamines resulted in trifluoroacetylation of hydroxy groups. Esters with trifluoroacetylated all possible hydroxy groups were formed readily (Fig. 3). Unlike silylating agents, TFAA did not create a peak of the unreacted reagent in the chromatogram, and MS could be acquired immediately after elution of the solvent. There were also no artifacts recorded on the chromatograms that would interfere with the identification or quantification, happened in previous cases. Chromatograms of the trifluoroacetylated ethanolamines spiked with TBP are depicted in Fig. 4. The retention indices of the derivatized analytes together with the EI-MS data (the most abundant fragment ions) are given in Table IV.

Perfluoroacylation was tested by Chandra *et al.*¹⁶ in the derivatization of half-nitrogen mustards to determine fragmentation pathways. When compared to silylation under similar conditions,¹⁵ perfluoroacylation was preferred as the derivatization technique for half-nitrogen mustards due to more intense molecular ion peaks. In the case of the fully hydrolyzed nitrogen mustards studied by us, this hypothesis was also confirmed. Moreover, trifluoroacetylated products were formed relatively rapidly and with stable kinetics. In the case of EDEA and

MDEA, the products were formed in maximum yield after only 30 minutes and it was not necessary to extend the reaction time.

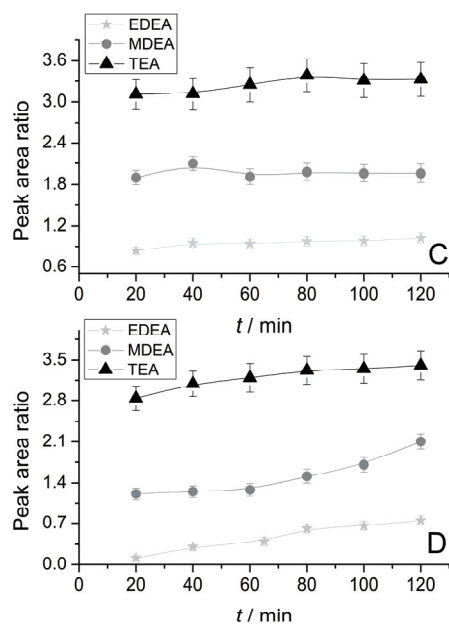


Fig. 3. Trifluoroacetyl derivatives of ethanolamines–bis(2-trifluoroacetoxyethyl)ethanamine (A), bis(2-trifluoroacetoxyethyl)methanamine (B) and tris(trifluoroacetyl)triethanolamine (C).

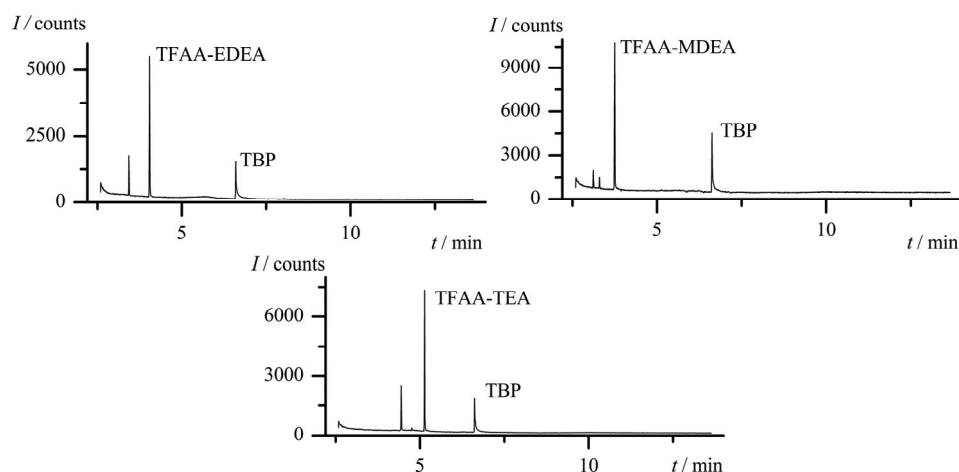


Fig. 4. Chromatograms of trifluoroacetyl derivatives of ethanolamines spiked with the internal standard tributyl phosphate.

In the case of TEA, there was a linear increase in yields throughout the observed reaction (120 min). This fact can be explained by the need to esterify 3 hydroxy groups compared to 2 groups in EDEA and MDEA. TEA derivatives with 1 and 2 substituted hydroxy groups were not recorded in the chromato-

grams, probably due to the high polarity of these substances. There was also no change in the ratios of trifluoroacetylated product and the internal standard when the samples were left and reanalyzed after several hours. Due to the stable kinetics and low deviations, the optimal reaction time of 30 min was chosen for the experiments in the next phase. A graphical representation of the formation of the derivatization products as a function of the reaction time is given in Fig. 4.

TABLE IV. Retention times (*RT*) and retention indexes (*RI*) of trifluoroacetylated analytes – EDEA, MDEA and TEA and internal standard tributyl phosphate, and the most abundant fragment ions (the first most abundant ion was used for quantification)

Parameter	EDEA	MDEA	TEA	TBP
<i>RT</i> / min	4.07	3.75	5.15	6.64
<i>RI</i>	1135	1083	1326	1647
Relative abundance of fragment ions, %	141 (100.0)	141 (100.0)	141 (100.0)	99
	198 (89.2)	184 (81.4)	311 (33.9)	
	69 (28.5)	69 (37.0)	69 (32.3)	

In comparison to the results given by Pardasani *et al.*,¹⁴ acetonitrile was found suitable and there is no need to use *n*-heptane, which is not commonly used in a mobile laboratory. TFAA is also a cheaper variant for trifluoroacetylation. The results were quantitative after 30 min reaction and it took place at room temperature, unlike some of the methods presented by the cited authors.

Calibration curves

Trifluoroacetylation by TFAA was chosen as the optimal method for the derivatization of nitrogen mustard ethanolamines due to stable kinetics, low deviations, fast reaction time and the absence of interfering or other peaks in the chromatogram. The chromatograms did not even contain peaks of the reagent alone.

Calibration curves were generated as dependences of the size ratio of the chromatographic peak areas of the respective derivatized analyte and TBP on the analyte concentration. The analyte concentrations were chosen so that the theoretical maximum yields fell within the calibrated ranges during the subsequent formation of contaminated sand samples. Each calibration curve was measured five times and gross errors were ruled out using the Q-test. The parameters of the linear regression equation for the respective dependencies are listed in Table V.

The results were mainly characterized by high values of the correlation coefficient for EDEA and TEA. The table also shows the values of the average standard deviation of individual points in the calibration dependences.

An experiment was also conducted to exchange the derivatization solvent, acetonitrile for hexane and ethyl acetate. In this case, about 10 % of the derivatization efficiency value compared to acetonitrile (in the case of hexane) and 50 % of the efficiency value in the case of ethyl acetate were achieved.

TABLE V. Analytical parameters of the calibration curves for the determination of nitrogen mustard ethanolamines (EDEA, MDEA and TEA); *x*-axis – analyte concentration, mmol dm^{-3} ; *y*-axis – absolute value of the ratio of the peaks of the derivatized analyte and TBP

Compound	$k^a / \text{dm}^3 \text{mmol}^{-1}$	q^a	$s_{y/x}^b$	R^{2c}	$SD^d / \%$
EDEA	4.2833	-0.0848	0.016	0.9999	2
MDEA	5.5462	-0.2691	0.265	0.9780	4
TEA	8.3431	-0.1299	0.001	1.000	1

^aParameters of the regression equation according to $y = kc + q$; ^bstandard deviation of *y* for each value of *x*; ^cvalue of the reliability of linear regression; ^drelative standard deviation of the calibration points

Limit of detection and quantification

Signal to noise (*S/N*) ratios were recorded for all peaks of trifluoroacetylated analytes (EDEA, MDEA and TEA) and the corresponding TBP peaks, from which calibration curves were constructed. Then, the analyte concentrations at *S/N* 3 (limit of detection) and 10 (limit of quantification) were estimated. The values obtained are given in the Table VI. Control samples for verification were also created for the determined concentration values.

TABLE VI. Limits of detection and quantification of the developed methods for quantitative analysis of nitrogen mustard ethanolamines (EDEA, MDEA and TEA) after trifluoroacetylation, limits of detection of the methods applied to sand samples

Compound	<i>LOD</i> $\mu\text{mol dm}^{-3}$	<i>LOQ</i> $\mu\text{mol dm}^{-3}$	<i>LOD</i> in sand $\mu\text{mol dm}^{-3}$	<i>LOD</i> in sand $\mu\text{g g}^{-1}$
EDEA	0.08	0.50	30	11.4
MDEA	9.00	11.00	30	11.4
TEA	0.07	0.30	30	12.3

Extraction of ethanolamines from sand

Ethanolamines were extracted from the sand with acetonitrile due to the suitability of this solvent for derivatization as well as the considerable polarity compared to other organic solvents. In addition to the limits of detection and quantification of the calibration methods, Table VI also lists the detection limits of the respective developed methods for the extraction of ethanolamines from sand. The limits of detection are comparable for all ethanolamines. Due to the high extraction efficiency, this technique is more suitable for field conditions than thermal desorption²¹ or SPME.²²

CONCLUSIONS

It was found that silylation, which is a commonly recommended technique for the field identification of alcohols related to the Chemical Weapons Convention, is not the most suitable derivatization technique for ethanolamines. However, TFAA reacted with ethanolamines at room temperature and within 30 minutes and the results were quantitative and accurate. The identified trifluoro-

acetylated derivatives were not disturbed by the presence of other substances in the chromatogram, the derivatizing reagent itself did not generate a signal in the chromatogram, which in comparison with silylating agents allows the acquisition of MS immediately after elution of the solvent (acetonitrile) and thus possible additional analytes with low *RT* values can be identified in the mixture. In addition, the trifluoroacetylated derivatives were stable in the solvent and did not decompose gradually. The method was applied to sand samples of ethanolamines, where the limits of detection in tens of $\mu\text{g g}^{-1}$ were reached.

The high efficiency, robustness and low price of this liquid–liquid extraction procedure make it more suitable compared to thermal desorption or SPME and it is recommended for application in the field analysis of chemical warfare agents.

ИЗВОД

РАЗВОЈ МЕТОДЕ ЗА ДЕРИВАТИЗАЦИЈУ ЕТАНОЛАМИНА И ЊЕНУ ПРИМЕНУ НА УЗОРКЕ ПЕСКА

TOMAS ROZSYPAL

Nuclear, Biological and Chemical Defense Institute, University of Defense, Vita Nejedleho 691, 68203 Vyskov, Czech Republic

Азотни иперити су опасни и доступни хемијски бојни отрови из групе пликаваца. У овом раду је упоређено шест метода дериватизације за анализу производа деградације најважнијих азотних иперита пликаваца (етил-диетаноламин, метил-диетаноламин и три-диетаноламин) применом гасне хроматографије спрегнуте са масеном спектрометријом. Тестирано је пет метода силиловања (коришћењем BSTFA и BSA) и једна метода трифлуороацетиловања (коришћењем TFAA). Реакције дериватизације изведене су у ацетонитрилу. Метода која даје оптималан резултат је метода трифлуороацетиловања. Аналити су са одговарајућим реагентом реаговали брзо, квантитативно, са стабилном кинетиком и на собној температури. Конструисане су калибрационе криве за квантитативну анализу етаноламина после дериватизације помоћу TFAA. Детекциони лимити за тестиране анализе су варирали између 9×10^{-3} и 7×10^{-5} $\text{mmol} \cdot \text{dm}^{-3}$. Развијена метода је примењена за анализу етаноламина после екстракције из песка помоћу ацетонитрила. Лимити детекције су били у опсегу 11,4–12,3 $\mu\text{g/g}$ песка. Охрабрујућа је могућност примене развијене методе у мобилним војним теренским лабораторијама, за брзу идентификацију бојних отрова и одговарајућих производа деградације.

(Примљено 12. марта, ревидирано 12. маја, прихваћено 13. јуна 2021)

REFERENCES

1. *Convention on the Prohibition of the Development, Production, Stockpiling and Use of Chemical Weapons and on their Destruction*, OPCW, Paris 2020 (https://www.opcw.org/sites/default/files/documents/CWC/CWC_en.pdf)
2. T. Rozsypal, *JPC-J. Planar Chromatogr.* **33** (2020) 669 (<https://doi.org/10.1007/s00764-020-00072-7>)
3. Y.-H. Jan, D. E. Heck, D. L. Laskin, J. D. Laskin, *Toxicol. Lett.* **326** (2020) 78 (<https://doi.org/10.1016/j.toxlet.2020.03.008>)

4. N. Tewari-Singh, R. Agarwal, *Ann. NY Acad. Sci.* **1374** (2016) 184 (<https://doi.org/10.1111/nyas.13099>)
5. H.-C. Chua, H.-S. Lee, M.-T. Sng, *J. Chromatogr., A* **1102** (2006) 214 (<https://doi.org/10.1016/j.chroma.2005.10.066>)
6. A. Mazumder, A. Kumar, A. K. Purohit, D. K. Dubey, *J. Chromatogr., A* **1217** (2010) 2887 (<https://doi.org/10.1016/j.chroma.2010.02.071>)
7. S. A. Willison, *J. Chromatogr., A* **1270** (2012) 72 (<https://doi.org/10.1016/j.chroma.2012.11.013>)
8. M. Otsuka, H. Miyaguchi, M. Uchiyama, *J. Chromatogr., A* **1625** (2020) 461306 (<https://doi.org/10.1016/j.chroma.2020.461306>)
9. M. Otsuka, H. Miyaguchi, M. Uchiyama, *J. Chromatogr., A* **1602** (2019) 199 (<https://doi.org/10.1016/j.chroma.2019.05.015>)
10. Z. Witkiewicz, M. Mazurek, J. Szulc, *J. Chromatogr., A* **503** (1990) 293 ([https://doi.org/10.1016/S0021-9673\(01\)81514-4](https://doi.org/10.1016/S0021-9673(01)81514-4))
11. R. M. Black, B. Muir, *J. Chromatogr., A* **1000** (2003) 253 ([https://doi.org/10.1016/S0021-9673\(03\)00183-3](https://doi.org/10.1016/S0021-9673(03)00183-3))
12. L. Kenar, O. Alp, *J. Chromatogr. Sci.* **49** (2011) 631 (<https://doi.org/10.1093/chromsci/49.5.361>)
13. I. Ohsawa, Y. Seto, *J. Chromatogr., A* **1122** (2006) 242 (<https://doi.org/10.1016/j.chroma.2006.04.076>)
14. D. Pardasani, M. Palit, A. K. Gupta, P. K. Kanaujia, D. K. Dubey, *J. Chromatogr., A* **1059** (2004) 157 (<https://doi.org/10.1016/j.chroma.2004.10.039>)
15. B. Chandra, K. Sinha Roy, M. Shaik, C. Waghmare, M. Palit, *Rapid Commun. Mass Spectrom.* **34** (2020) 1 (<https://doi.org/10.1002/rcm.8586>)
16. B. Chandra, K. Sinha Roy, M. Shaik, C. Waghmare, M. Palit, *Rapid Commun. Mass Spectrom.* **34** (2020) 1 (<https://doi.org/10.1002/rcm.8777>)
17. P. Garg, A. Purohit, V. K. Tak, D. K. Dubey, *J. Chromatogr., A* **1216** (2009) 7906 (<https://doi.org/10.1016/j.chroma.2009.09.032>)
18. C. A. Valdez, R. N. Leif, S. Hok, A. K. Vu, E. P. Salazar, A. Alcaraz, *Sci. Total Environ.* **683** (2019) 175 (<https://doi.org/10.1016/j.scitotenv.2019.05.205>)
19. R. B. Sousa, P. F. P. M. Alves, S. F. Cavalcante, L. B. Bernardo, C. S. Barros, C. N. Ferreira, A. L. S. Lima, *Rev. Virtual Quím.* **6** (2014) 601 (<https://doi.org/10.5935/1984-6835.20140039>)
20. P. Vanninen, *Recommended operating procedures for analysis in the verification of chemical disarmament*, University of Helsinki, Helsinki, 2017 (ISBN 978-951-51-3917-7)
21. D. T. D. Qadah, J. H. Aldstadt, *Anal. Lett.* **51** (2018) 1321 (<https://doi.org/10.1080/00032719.2017.1379531>)
22. S. Popiel, M. Sankowska, *J. Chromatogr., A* **1218** (2011) 8457 (<https://doi.org/10.1016/j.chroma.2011.09.066>).



J. Serb. Chem. Soc. 87 (2) 247–261 (2022)
JSCS–5519

Homogeneous microwave-assisted carboxymethylation from totally chlorine free bleached olive tree pruning residues pulp

IMEN LANDOLSI^{1*}, NARJES RJIBA¹, MOHAMED HAMD AOUI¹,
OMAR ANIS HARZALLAH² and CHEDLY BOUDOKHANE^{3,4}

¹Textile Materials and Processes Research Unit (MPTEX), National Engineering School of Monastir, University of Monastir, Monastir, Tunisia, ²Laboratory of Physics and Mechanics Textile (LPMT), ENSISA – University of Haute Alsace, Mulhouse, France, ³Laboratory of Dyeing Services and Textile Treatments, Chimitex Plus, Sousse, Tunisia and ⁴Research Unit of Applied Chemistry and Environment, Faculty of Science of Monastir, University of Monastir, Monastir, Tunisia

(Received 1 April, revised 10 June, accepted 11 June 2021)

Abstract: This study deals with a new methodology for the production of carboxymethyl cellulose (CMC) from olive pruning residues, agricultural by-products. Cellulose was extracted by the soda–anthraquinone pulping process, and the pulp bleaching was performed using totally chlorine free (TCF) bleaching. Then, CMC microwave-assisted synthesis was performed in a homogeneous media, using DMA/LiCl as a cellulose solvent. A Box–Behnken design was applied in order to evaluate which parameters of the carboxymethylation process (*viz.* reaction time, reaction temperature, and amount of monochloroacetic acid) affect the degree of substitution and the yield of the synthesis reaction of this cellulose derivative. Optimized conditions to yield CMC were determined based on the desirability function approach. The prepared materials under synthesis using the optimal conditions were characterized using several analytical tools, *i.e.*, FTIR, TGA, DSC and SEM. This cellulose derivative was successfully fabricated by a fast and efficient microwave-assisted method and thus would provide many opportunities for diverse applications.

Keywords: agricultural by-product; cellulose; pulping; carboxymethyl cellulose synthesis.

INTRODUCTION

Cellulose is the principal constituent of all plant cell walls. It is the most abundant and important biopolymer on earth, almost inexhaustible, renewable material, and environmentally benign. It still possesses high potential for future applications; it can be easily modified to more natural and sustainable alter-

*Corresponding author. E-mail: andolsi-imen@hotmail.com
<https://doi.org/10.2298/JSC210401046L>

natives compared to synthetic products. The main raw material of cellulose derivative is cellulose from wood pulp (containing 40–50 % cellulose) and cotton linters (contain 90 % cellulose). However, nowadays uses of these raw materials of cellulose resources are discouraged because of the cost of production and increasing environmental concerns.^{1,2} The attention is focused on the recovery of waste (“waste-to-value”).

The global agriculture sector produces annually billions of tons of agricultural biomass. However, this progress has also led to the generation and accumulation of agricultural wastes of little commercial value. Only a small fraction of agricultural wastes are used, as animal feeds and for energy production.³ In particular, pruning of olive trees generates a large amount of biomass that is burned, causing severe environmental concern, or left in farmland as a source of food for animals. Therefore, the transformation of this agricultural residue into value-added products is interesting. Note that according to estimates from many countries, 25 kg of leaves and twigs are produced per year per tree.⁴

Moreover, carboxymethyl cellulose (CMC) is one of the most important water-soluble derivatives of cellulose. It is available in several grades (technical, semi-purified, purified, and extra purified) and it is widely employed in many areas of industry and human life, such as detergents, paper coating, textile sizing and printing, ceramic, food, toothpaste, pharmaceuticals, *etc.*⁵ It is formed by the carboxymethylation of the hydroxyl group in cellulose.⁶ In this context, the valorization of olive pruning residues, a widely available agriculture by-product in Tunisia, was realized by the synthesis of CMC. Indeed, as raw materials for CMC synthesis, cleaned and crushed olive tree pruning residues was delignified using the soda–anthraquinone pulping process. Then, the obtained pulp was bleached using totally chlorine-free bleaching sequences (TCF), the most environmentally bleaching process that uses only oxygen-based bleaching chemicals.

The commercial production of carboxymethyl cellulose (CMC) is carried out by using a heterogeneous slurry of cellulose in a solvent that swells but neither dissolves the starting polymer nor the CMC obtained. Under these reaction conditions, the CMCs thus obtained have a non-uniform distribution of substituents within the anhydroglucose unit. On the other hand, homogeneous carboxymethylation reactions offer reaction uniformity and should produce a more even distribution of substituents than heterogeneous processes.⁷

As known, cellulose is a homopolysaccharide that is formed from linearly connecting D-glucose units condensed through $\beta(1-4)$ glycosidic bonds. It possesses a highly crystalline structure due to the presence of extensive intra- and intermolecular hydrogen bonding. Consequently, this natural polymer is insoluble in water and typical organic solvents and can only be dissolved if the intra- and intermolecular hydrogen bonds are effectively disrupted.⁸ Thus, the dissolution of cellulose destroys the highly organized hydrogen-bonding system sur-

rounding the polyglucan chain. Salt systems in non-aqueous solvents are widely used to dissolve cellulose.⁹ Here, the dissolution of the obtained bleached pulp was carried out, using LiCl/DMAc (lithium chloride in *N,N*-dimethylacetamide). It is a non-derivatizing solvent, *i.e.*, one that causes dissolution without forming covalent bonds. This step was followed by a reaction with a derivatizing agent (monochloroacetic acid (MCA)) to obtain the desired product (CMC).

By combining major green chemistry principles, *viz.*, the use of renewable biomass materials and the choice of a rapid method allows a high value-added application of biomass. Indeed, herein a fast microwave-assisted method for CMC synthesis is reported. In recent years, microwave chemistry has become increasingly popular within organic synthesis.^{10,11} Compared with conventional heating, microwave-assisted heating, under controlled conditions, is an advanced technology in reducing reaction time besides increasing product yield and purity.^{12–14} Microwave irradiation-assisted synthesis has been widely used in the chemical functionalization of polymer materials. It has been developed for cellulose modification processes including acetylation¹⁵ and carboxymethylation.¹⁶ Therefore, microwave irradiation is a promising method to modify the physico-chemical properties of cellulose.

Herein, an attempt was made to exploit a lignocellulosic material widely available in Tunisia as a source of cellulose fibers to develop a new microwave-assisted method for preparing CMC from totally chlorine free-bleached pulp in a homogeneous media using LiCl/*N,N*-dimethylacetamide as a solvent. The optimal conditions for unconventional CMC preparation were predicted by the response surface regression model, and the CMC product was characterized.

EXPERIMENTAL

Raw materials

The olive tree pruning residues used in this work were collected from the province of Monastir-Tunisia. Leaves and stems were separated in order to study each material separately. Cleaned and crushed raw materials were then used for cellulose extraction.

Pulping procedure

Soda-anthraquinone pulping experiments were performed in a rotating system and heated under controlled temperature. The following cooking conditions were employed: liquor ratio was 10:1, temperature 140 °C for leaves and 110 °C for stems, and cooking time of 1 h for leaves and 3 h for stems. The alkali charge was 8 mass % for leaves and 16 mass % for stems with freshly prepared caustic soda, and the amount of anthraquinone was 0.1 mass % based on the oven-dry weight of the raw materials. After cooking, the pulp obtained through filtration was extensively washed with water until free of residue alkali. The pulp yield was determined after oven drying to constant weight.

Bleaching procedure

The obtained pulp was bleached by TCF (totally chlorine free) bleaching processes, using only a peroxide that has the role to eliminate chromophores in the lignin structures. It was selected due to its least hazardous and oxidative damaging potential. Thus, pulp bleaching

was carried out by a simple stage peroxide sequence QP (where Q-chelating treatment and P-hydrogen peroxide bleaching stage). The following chelating stage (Q) conditions were employed: 10 % consistency, 0.25 % EDTA during 2 h at 70 °C in a slightly acidic medium (pH regulation by H₂SO₄). Then, the last peroxide stage (P) conditions were employed: 10 % consistency, 0.2 % EDTA, 0.2 % MgSO₄ during 3 h (1 h) at 90 °C (75 °C) with 2.25 % of H₂O₂ (5 %) for olive stems (respectively for olive leaves). The final brightness of 84 was attained for both pulps, leaves, and stems.

Carboxymethylation of cellulose in DMAc LiCl medium

The microwave-assisted synthesis of CMCs under homogeneous reaction conditions of the obtained bleached pulps was carried out in two steps, *i.e.*, cellulose dissolution and etherification. For cellulose dissolution, DMAc/LiCl was selected as a non-derivatizing solvent, *i.e.*, one that causes dissolution without forming covalent bonds. This step was followed by a reaction with a derivatizing agent (monochloroacetic acid (MCA)) to obtain the desired product (CMC). Thus, the oven-dried bleached pulp of cellulose (0.1 g) was kept at 130 °C under magnetic stirring in 6 ml of *N,N*-dimethylacetamide (DMAc) for 2 h. After cooling to 100 °C, 0.3 g of anhydrous LiCl was added to the slurry. Then the slurry was cooled down to room temperature under stirring and left standing overnight. The next day, a suspension of the desired amount of MCA in 2 ml of DMAc was added and stirred for 10 min at room temperature, followed by a suspension of NaOH 40% (2 ml) in 2 ml DMAc. Afterwards, microwave irradiation in a monomode microwave reactor (CEM discover automated reactor) was applied on the suspension with stirring under pressure according to the conditions of the experimental plan presented in Table I. Finally, the reaction mixture was precipitated into 30 ml of ethanol. After filtration, the solid product obtained as CMC was washed extensively with ethanol to remove undesirable by-products and dried at 50 °C.

TABLE I. Box–Behnken experimental design (BBD) for the carboxymethylation process

Run order	Factors			Responses			
	τ / min (X_1)	t / °C (X_2)	Amount of MCA, g per g of cellulose (X_3)	Olive leaves		Olive stems	
				DS ^a	Yield ^b , %	DS ^a	Yield ^b , %
1	5 (-1)	70 (-1)	4.5 (0)	0.87	157.21	0.95	160.63
2	15 (1)	70 (-1)	4.5 (0)	0.63	150.88	0.64	154.62
3	5 (-1)	90 (1)	4.5 (0)	0.74	152.11	0.68	155.66
4	15 (1)	90 (1)	4.5 (0)	1.32	174.87	1.39	177.21
5	5 (-1)	80 (0)	3 (-1)	0.42	146.14	0.47	149.74
6	15 (1)	80 (0)	3 (-1)	0.98	158.32	1.03	162.23
7	5 (-1)	80 (0)	6 (1)	1.18	168.81	1.25	171.14
8	15 (1)	80 (0)	6 (1)	1.68	192.48	1.87	196.27
9	10 (0)	70 (-1)	3 (-1)	0.81	155.04	0.83	159.24
10	10 (0)	90 (1)	3 (-1)	1.36	176.24	1.47	177.96
11	10 (0)	70 (-1)	6 (1)	1.44	180.02	1.55	182.22
12	10 (0)	90 (1)	6 (1)	1.15	166.13	1.22	170.08
13	10 (0)	80 (0)	4.5 (0)	1.43	179.34	1.55	182.14
14	10 (0)	80 (0)	4.5 (0)	1.42	177.95	1.57	181.01
15	10 (0)	80 (0)	4.5 (0)	1.41	178.4	1.55	181.42

^aDegree of substitution of carboxymethyl groups; ^byield of carboxymethylation

Experimental design and statistical analysis

A Box–Behnken response surface design was used to analyze the main effects and interactions of the variables (*viz.*, time, temperature of the microwave irradiation, and the amount of monochloroacetic acid (MCA) per g of cellulose) in the response variables average, degree of substitution (DS), and reaction yield.

As this design is suitable for the exploration of quadratic response surfaces and constructs a second-order polynomial model,¹⁷ it was used to optimize the conditions for CMC microwave-assisted synthesis from olive tree pruning residue from a small number of experimental runs.

Fifteen experiment runs were performed with different combinations of three factors with three replicates at the center point to estimate the pure error. For each run, the experimental responses are shown in Table I.

Characterization

The prepared materials thus synthesized under optimal conditions were then characterized.

Determination of the degree of substitution of carboxymethyl groups. In this work, to determine the DS of the prepared CMC samples, a titration method was used. This technique is widely described in the literature.¹⁸ Firstly, the sample was mineralized at 600 °C for 4 h. Before the titration, the obtained ash which contained Na₂O was dissolved in hot water at 80 °C. Next, the solution was titrated with 0.1 N (0.05 M) H₂SO₄ in the presence of Methyl Orange as the titration indicator. The reddish solution thus obtained was subsequently heated to remove dissolved CO₂ until it became yellow. So, a ratio *B* can be defined, and the *DS* estimated using:¹⁸

$$B = \frac{0.1V}{m_{\text{CMC}}} \quad (1)$$

where 0.1 is the normality of the sulfuric acid solution, *V* is the total volume of the titrating solution added to neutralize the ash solution, and *m*_{CMC} is the oven-dried weight of the initial sample and:

$$DS = \frac{0.162B}{1 - 0.08B} \quad (2)$$

where 0.162 and 0.08 are, respectively, the molar masses (kg·mol⁻¹) of the glucose units and CHCOO⁻Na⁺ groups substituted on the cellulose.

These measurements were duplicated and the difference between the two values was within an experimental error of 5 %.

The yield of carboxymethylation. The yield of carboxymethylation reaction was measured on a dry basis by dividing the dry weight of carboxymethyl cellulose (*m*_{CMC}) by the dry weight of the bleached pulp of olive tree branch cellulose (*m*_{cellulose}), as shown:

$$\text{Yield} = 100 \frac{m_{\text{CMC}}}{m_{\text{cellulose}}} \quad (3)$$

Scanning electron microscopy (SEM). The morphological variations were studied using a high-resolution SEM instrument. The dry sample was spread on a double-sided conducting adhesive tape, pasted on a metallic stub, coated with gold in an anion sputter coating unit for 2 min, and observed in a JEOL-JSM-IT100 electron probe micro-analyzer at 15 kV.

FTIR studies. FTIR spectra were used to characterize the samples, which were recorded with an FTIR-8400S Shimadzu Fourier transform infrared spectrophotometer, at room temperature in the range of 4000–500 cm^{-1} .

Thermogravimetric analysis (TGA). Thermal stabilities of samples were recorded using TGA Q500 V20.10 Build 36 instrument to measure the weight loss at different temperatures with a heating range 35 to 800 $^{\circ}\text{C}$ at a rate of 10 $^{\circ}\text{C min}^{-1}$.

Differential scanning calorimetric analysis (DSC). The thermal behavior of CMC was studied using DSC Q200 V24.4 Build 116 thermal analyzer. The sample was inserted into the aluminum pan and a DSC scan was first made from 25 to 180 $^{\circ}\text{C}$ at a heating rate of 10 min^{-1} under nitrogen atmosphere at a flow rate of 50 mL. Then it was cooled to clear the thermal history of the sample. The second scan is then carried out from 25 to 250 $^{\circ}\text{C}$ at a speed of 10 $^{\circ}\text{C min}^{-1}$. The results were recorded and analyzed.

RESULTS AND DISCUSSION

Statistical analysis and the optimization of carboxymethylation conditions

Regression analysis presented in Table II indicates that the model equations can adequately be used to describe the microwave-assisted CMC synthesis under a wide range of operating conditions. The coefficient of determination (R^2) is a measure of the degree of fit and a good model fit should yield an R^2 of at least 0.8.^{19,20} This means that the response model evaluated in this study can explain very well the CMC microwave-assisted synthesis for the two studied raw materials, olive tree leaves and olive tree stems.

TABLE II. Regression analysis of a full second-order polynomial model for optimization of microwave-assisted synthesis of CMCs

Terms	Olive leaves				Olive stems			
	DS^a		Yield ^b , %		DS^a		Yield ^b , %	
	Coeff ^c	p^d	Coeff ^c	p^d	Coeff ^c	p^d	Coeff ^c	p^d
Constant	1.420	0.000	178.56	0.000	1.557	0.000	181.52	0.000
X_1	0.175	0.061	6.53	0.058	0.197	0.053	6.65	0.054
X_2	0.102	0.218	3.28	0.274	0.098	0.263	3.03	0.305
X_3	0.235	0.023	8.96	0.020	0.261	0.021	8.82	0.021
$X_1 \times X_1$	-0.327	0.028	-11.36	0.034	-0.377	0.022	-11.01	0.037
$X_2 \times X_2$	-0.202	0.117	-8.44	0.085	-0.265	0.070	-8.48	0.081
$X_3 \times X_3$	-0.027	0.807	-0.77	0.853	-0.025	0.840	-0.67	0.871
$X_1 \times X_2$	0.205	0.103	7.27	0.112	0.255	0.070	6.89	0.125
$X_1 \times X_3$	-0.015	0.890	2.87	0.481	0.015	0.898	3.16	0.437
$X_2 \times X_3$	-0.210	0.097	-8.77	0.068	-0.242	0.080	-7.71	0.094
R^2	88.51		89.03		89.83		88.62	

^aDegree of substitution of carboxymethyl groups; ^byield of carboxymethylation; ^cregression coefficients;

^d p -value used to measure the significance of each parameter

The p -value was used as a tool to check the significance of each parameter. A value lower than 0.05 indicates that the term is statistically significant, whereas a value higher than 0.10 indicates that the term is not significant. Regarding the

responses of DS and yields for the two raw materials thus studied, the time of microwave irradiations (X_1) was a significant parameter as p -value was less than 0.05 and the amount of MCA (X_3) was slightly significant because the p -value was less than 0.1. Whereas the temperature (X_2) was not a significant factor since the p -value was more than 0.1. By applying response surface methodology, the predictive equations for homogeneous microwaves assisted synthesis of CMC without the non-significant terms and in uncoded units were expressed as follows:

For olive tree leaves:

$$DS = 1.420 + 0.175X_1 + 0.235X_3 - 0.327X_1^2 - 0.210X_2X_3 \quad (4)$$

$$Y = 178.56 + 6.53X_1 + 8.96X_3 - 11.36X_1^2 - 8.44X_2^2 - 8.77X_2X_3 \quad (5)$$

For olive tree stems:

$$DS = 1.557 + 0.1975X_1 + 0.2612X_3 - 0.377X_1^2 - 0.265X_2^2 + 0.255X_1X_2 - 0.242X_2X_3 \quad (6)$$

$$Y = 181.52 + 6.65X_1 + 8.82X_3 - 11.01X_1^2 - 8.48X_2^2 - 7.71X_2X_3 \quad (7)$$

Optimization of carboxymethylation conditions

The optimal process parameters were found by using optimization choice in Minitab software to maximize the responses yield and DS which were listed in Table III. The composite desirability index calculated were 0.95 and 0.94 for olive tree leaves and olive tree stems respectively, so highly desirable. To verify the suitability of these predicted optimal values, additional experiments were performed. Experimental results obtained under the same conditions were in agreement with the predicted results, with differences smaller than 5 %.

TABLE III. Predicted optimum values and experimental results in optimum conditions for the microwave-assisted synthesis of CMCs; * – value of mean deviation

Origin	Variables		Yield ^a , %		DS^b	
			Predicted	Experimental	Predicted	Experimental
Leaves	τ / min	11	188.83	193.17 ± 0.12*	1.65	1.69 ± 0.071*
	t / °C	80				
	Amount of MCA, g per g of cellulose	6				
Stems	τ / min	11	191.85	195.73 ± 0.18*	1.82	1.86 ± 0.094*
	t / °C	80				
	Amount of MCA, g per g of cellulose	6				

^aYield of carboxymethylation; ^bdegree of substitution of carboxymethyl groups

Morphological analysis by SEM

The SEM micrographs of olive tree raw materials (leaves and stems), celluloses (bleached and unbleached), and CMCs produced by homogeneous microwave-assisted synthesis are presented in Fig. 1.

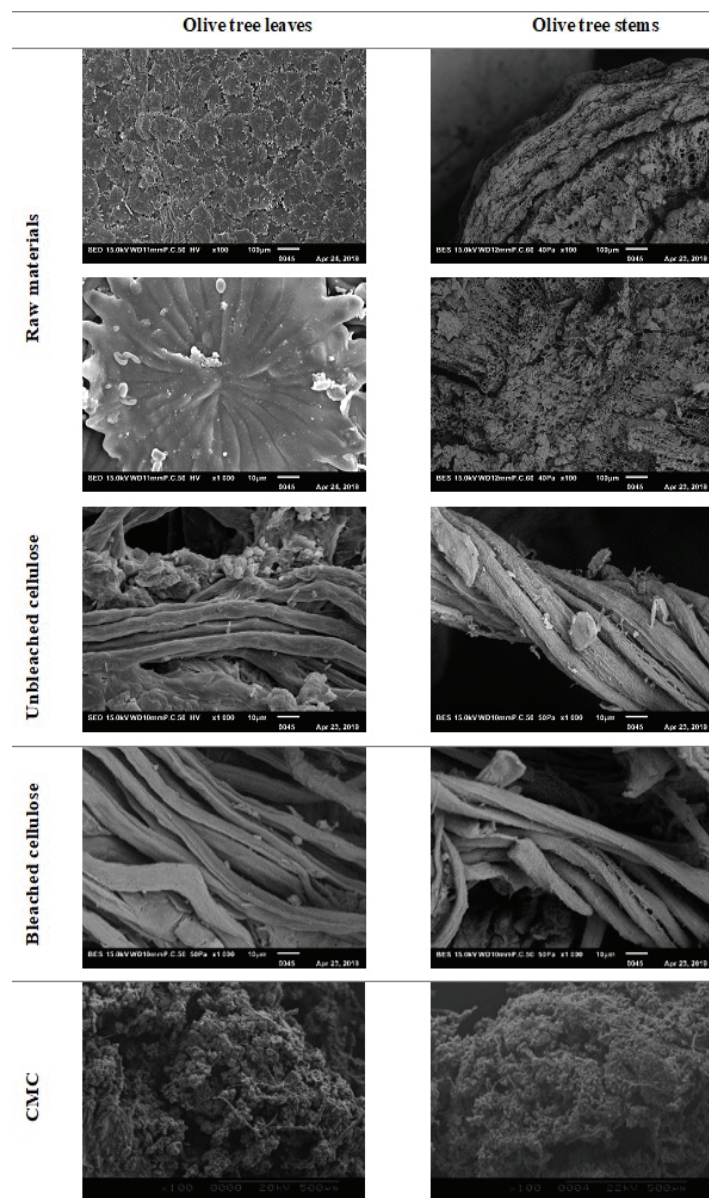


Fig. 1. SEM micrographs of olive tree raw materials (leaves and stems), celluloses, and CMCs produced by homogeneous microwave-assisted synthesis.

The olive tree is an evergreen tree that has foliage throughout the year. As shown in Fig. 1, its leaves are composed of an organized layer of star-shaped cells densely distributed, called trichomes. For stems, the observation of a cross-section shows a multicellular structure and several porous fibers. In fact, it is well

recognized that the cellulose chains of natural fibers are linked by lignin and hemicellulose, forming multicellular fibers.

After the soda-anthraquinone delignification process, cellulose was isolated, giving individual fibers while some others remain quite compact because of the amount of residual lignin not removed which hangs up. During the bleaching process, the amount of residual lignin decreases further and fibers become more individualized.

The SEM micrographs of various CMCs powdered samples revealed that the dissolution of the cellulose was successfully carried out, except for a few fibers.

FTIR

After various treatments, FTIR spectroscopy presents an appropriate tool to specify the variations on the chemical structure of the resulting samples. The infrared spectra of bleached celluloses isolated from olive tree leaves and stems as well as different synthesized CMCs are shown in Fig. 2.

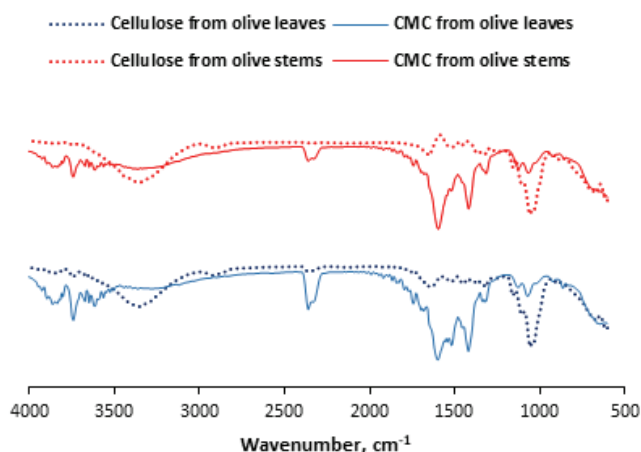


Fig. 2. FTIR spectra of bleached celluloses and CMCs samples prepared from olive tree leaves and olive tree stems.

For both bleached celluloses, as shown in Fig 2, the peaks around 3341 cm^{-1} correspond to the O–H stretching vibration of the –OH groups in cellulose molecules.^{21–23} Moreover, the other strong peaks observed at 1034 and 1057 cm^{-1} can be attributed to the C–O–C glycosidic ring skeletal vibration.^{24,25}

In the case of all carboxymethylated derivatives thus synthesized, the appearance of an intense absorption band around 1620 cm^{-1} confirms the presence of the carboxylate group ($-\text{COO}^{-}\text{Na}^{+}$). Thereby giving evidence that during the modification process hydroxyl groups of cellulose are replaced with carboxyl groups. The absorption bands at 1318 and 1420 cm^{-1} are attributed respectively to the COO stretching in CO_2H and binding in OCH_2 .²⁶

Thermogravimetric analysis (TGA)

The thermal decomposition of different samples, cellulose and carboxymethyl cellulose (CMC), prepared from olive stems and olive leaves were studied under a nitrogen atmosphere. Their thermogravimetric analysis (TGA) curves are shown in Fig. 3 and their mass losses were evaluated and listed in Table IV.

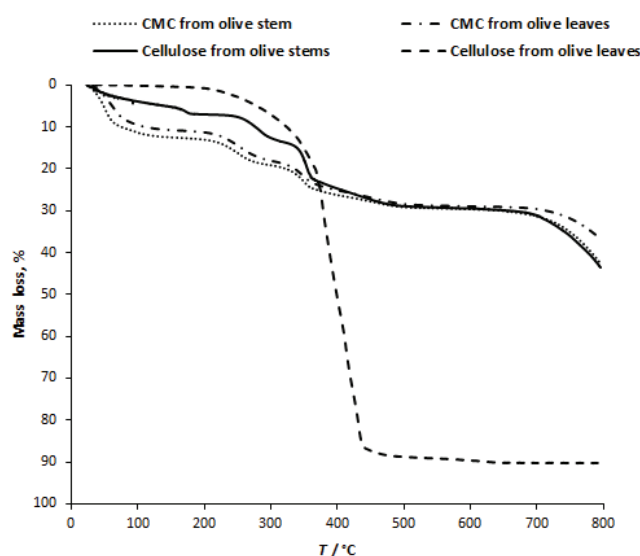


Fig.3. TGA curves of the bleached celluloses and CMCs samples prepared from olive tree leaves and stems.

For the cellulose samples, the onset temperatures are respectively 278 °C for cellulose olive leaves and 141 °C for cellulose from olive stems. Concerning the temperatures of maximum mass loss, a shift of 28 °C was observed between the two samples. According to Zickler *et al.*,²⁷ cellulose was hardly degraded at temperatures below 310 °C, whereas the kinetics became too fast above 360 °C and the thermal degradation mechanisms differed along and across the cellulose fibrils. A highest weight loss at temperatures higher than 380–400 °C and a sharply lower residual mass after the decomposition step was observed for cellulose from olive leaves (56.45 for cellulose from olive stems *vs.* 9.65 for cellulose from olive leaves). It was observed that the residual mass of cellulose from olive leaves was very low; this indicates their high purity and absence of inorganic residues.

It is well known that the thermal behavior of cellulose can be influenced by its physical properties. So, these results are probably due to the difference in crystallinity, degree of polymerization, and moisture contents.²⁸ Additionally, these differences might be attributed to the presence of different amounts of residual lignin in the two celluloses after extraction. Whereas, smaller differences appear between the two carboxymethylcelluloses (CMC) samples.

TABLE IV. TGA/DTA thermal parameters for the degradation of different samples prepared from olive tree leaves and stems.

Sample	$t_{5\%}^a$ °C	t_{max}^b °C	Mass loss at t_{max} , %	Total mass loss, %	Residue %
Cellulose from olive stems	141	352	18.6	43.55	56.45
Cellulose from olive leaves	278	380	32	90.35	9.65
CMC from olive stems	48	355	24	42.7	57.3
CMC from olive leaves	60	353	21	36.9	63.1

^aOnset temperature; ^btemperature of maximum degradation rate

The thermogravimetric analysis (TGA) and the first derivative thermogravimetric (DTG) curves for the two CMCs studied in a nitrogen atmosphere are shown in Fig. 4.

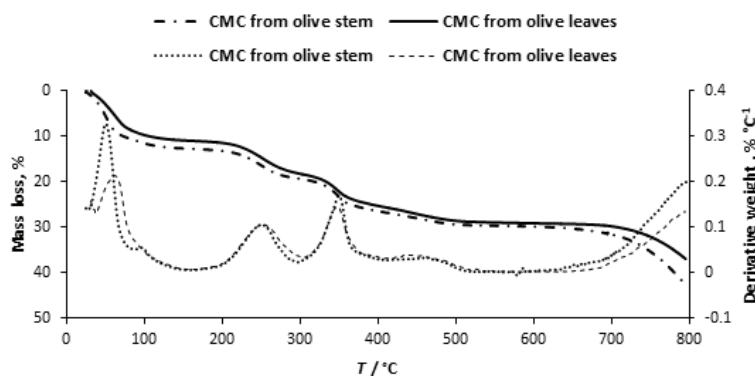


Fig. 4. TGA and DTA curves of the CMCs samples prepared from olive tree leaves and stems.

They have almost the same pace of thermal decomposition. In fact, within 100 °C, weight reduction can be due to moisture loss. The onset temperature ($t_{5\%}$) of both obtained CMC were respectively 48 °C for CMC from olive stems and 60 °C for CMC from olive leaves. At around 353 °C, the residual weight was about 75 %. Beyond 350 °C, the rate of mass loss decreased, revealing the appearance of another pyrolysis mechanism. Increasing temperature more than 700 °C, losing weight proceeded at a slower rate. When the temperature reached 800 °C, the residual mass was about 63 % for CMC obtained from olive tree leaves and 57 % for CMC from olive tree stems. From where complete decomposition of CMC did not occur.

Differential scanning calorimetric analysis (DSC)

Usually, DSC allows the determination of first- and second-order thermal transitions, such as melting, crystallization, and glass transition phenomena.²⁹ The glass transition temperature, as a second-order transition, is often observed in polymeric systems and is considered as the change between the glassy and rubbery state.

As mentioned above, two heating scans were carried out on each sample. The heating runs of CMCs samples up to 250 °C are shown in Figs. 5 and 6.

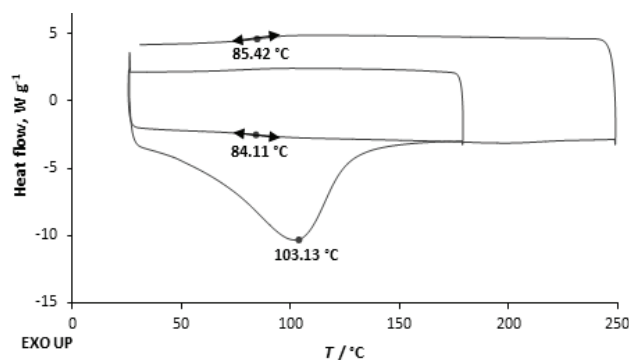


Fig. 5. DSC thermogram of carboxymethyl cellulose prepared from olive tree leaves.

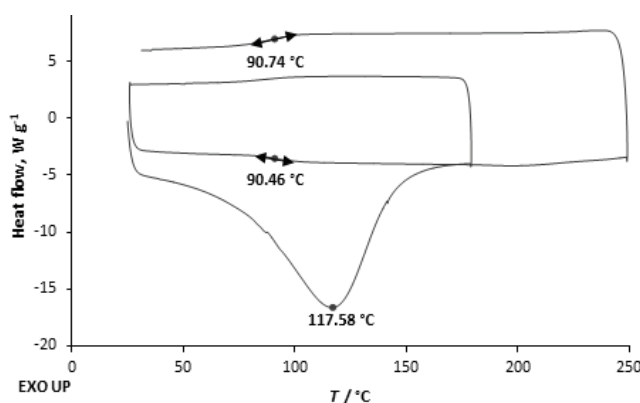


Fig. 6. DSC thermogram of carboxymethyl cellulose prepared from olive tree stems.

The DSC thermograms in the first scan exhibit a sharp peak at around 117 and 103 °C for olive tree stems and olive tree leaves, respectively, which are not apparent in the second scan. Thereby, they might be assigned to the dehydration of cellulose. Then, enthalpy changes were observed in the second scan at around 85 and 90 °C for the samples from olives leaves and olive stems, respectively. These enthalpy changes have obviously been attributed to the glass transition temperatures. In addition, no exothermic peak appeared in the thermograms, which implies that the melting temperature of the CMCs samples would be greater than 250 °C.

CONCLUSIONS

The present work shows that celluloses extracted from olive pruning residues leaves and stems, which were totally chlorine-free bleached, were suitable

for the production of carboxymethyl cellulose. The results obtained suggest that it is an agriculture by-product with great potential to be a feedstock for producing this derivative.

Moreover in this work, the development and the optimization of a new methodology for homogeneous carboxymethylation using DMA/LiCl as a cellulose solvent system in a monomode microwave reactor was successfully achieved.

According to surface methodology Box–Behnken design, several reaction conditions were tested to be optimized and different average degrees of substitution were thus obtained. Applying the optimized set conditions: 6 g of monochloroacetic acid per g of cellulose; reaction time of 11 min and temperature of 80 °C, CMCs having a DS of 1.69 and 1.86 can be prepared from olive leaves and stems, respectively. The obtained CMCs were characterized using different tools. The formation of the carboxymethyl group was confirmed by FT-IR spectroscopy. SEM images confirmed that the prepared CMC has a powdered aspect and the dissolution of the cellulosic structure was done successfully.

The obtained results can be considered promising. A highly substituted carboxymethyl cellulose was obtained by a new production process, suitable for use in several fields of application, such as a yarn sizing agent in textile industries.

Acknowledgements. This project was carried out under the MOBIDOC scheme, funded by the EU through the EMORI program and managed by the ANPR.

ИЗВОД

МИКРОТАЛАСНО ПОТПОМОГНУТА ХОМОГЕНА КАРБОКСИМЕТИЛАЦИЈА ИЗБЕЉЕНИХ ОСТАТАКА ЦЕЛУЛОЗЕ ИЗ ОСТАТАКА ОРЕЗИВАЊА МАСЛИНА ПОСТУПКОМ БЕЗ УПОТРЕБЕ ХЛОРА

IMEN LANDOLSI¹, NARJES RJIBA¹, MOHAMED HAMDAOUI¹, OMAR ANIS HARZALLAH²
и CHEDLY BOUDOKHANE^{3,4}

¹*Textile Materials and Processes Research Unit (MPTEX), National Engineering School of Monastir, University of Monastir, Monastir, Tunisia,* ²*Laboratory of Physics and Mechanics Textile (LPMT), ENSISA – University of Haute Alsace, Mulhouse, France,* ³*Laboratory of Dyeing Services and Textile Treatments, Chimitex Plus, Sousse, Tunisia* и ⁴*Research Unit of Applied Chemistry and Environment, Faculty of Science of Monastir, University of Monastir, Monastir, Tunisia*

Ова студија се бави новом методологијом за производњу карбоксиметил-целулозе (СМС) из остатака орезивања маслина, нуспроизвода из пољопривреде. Целулоза је екстрахована поступком пулповања сода-антрахиноном, а избеливање пулпе је изведено без хлора (ТСФ). Затим је изведена микроталасно потпомогнута синтеза СМС у хомогеном медијуму, користећи DMA/LiCl као растварач за целулозу. Примењен је *Box–Behnken* дизајн како би се проценило који параметри процеса карбоксиметилације (односно време реакције, температура реакције и количина монохлорсирћетне киселине) утичу на степен супституције и принос реакције синтезе овог деривата целулозе. Оптимизовани услови за добијање СМС одређени су на приступом функције пожељности. Синтеза припремљених материјала под оптималним условима окарактерисана је употребом неколико аналитичких техника као што су FTIR, TGA, DSC и SEM. Овај дериват

ват целулозе успешно је произведен брзом и ефикасном методом потпомогнутом микророталасном пећницом, што ће пружити бројне могућности за различите примене.

(Примљено 1. априла, ревидирано 10. јуна, прихваћено 11. јуна 2021)

REFERENCES

1. A. Bono, P. H. Ying, yan yan Farm, C. L. Muei, R. Sarbatly, D. Krishnaiah, *ANAS* **3** (2009) 5 (https://www.researchgate.net/publication/279598236_Synthesis_and_characterization_of_carboxymethyl_cellulose_from_palm_kernel_cake)
2. R. K. Singh, A. K. Singh, *Waste Biomass Valor.* **4** (2013) 129 (<https://doi.org/10.1007/s12649-012-9123-9>)
3. M. Sain, S. Panthapulakkal, *Ind. Crops Prod.* **23** (2006) 1 (<https://doi.org/10.1016/j.indcrop.2005.01.006>)
4. A. Nefzaoui, in *Fourrages et Sous-Produits Méditerranéens*, X. Alibés, J.-L. Tisserand, Eds., CIHEAM, Zaragoza, 1991, pp. 101–108 (<http://om.ciheam.org/om/pdf/a16/91605051.pdf>)
5. T. Heinze, A. Koschella, *Macromol. Symp.* **223** (2005) 13 (<https://doi.org/10.1002/masy.200550502>)
6. G. Zhang, L. Zhang, H. Deng, P. Sun, *J. Chem. Technol. Biotechnol.* **86** (2011) 584 (<https://doi.org/10.1002/jctb.2556>)
7. T. Heinze, U. Erler, I. Nehls, D. Klemm, *Angew. Makromol. Chem.* **215** (1994) 93 (<https://doi.org/10.1002/apmc.1994.052150108>)
8. S. Sen, J. D. Martin, D. S. Argyropoulos, *ACS Sustain. Chem. Eng.* **1** (2013) 858 (<https://doi.org/10.1021/sc400085a>)
9. S. Fischer, H. Leipner, E. Brendler, W. Voigt, K. Fischer, in *Polysaccharide Applications*, American Chemical Society, Washington, DC, 1999, pp. 143–150 (<https://10.1021/bk-1999-0737.ch010>)
10. M. B. Gawande, S. N. Shelke, R. Zboril, R. S. Varma, *Acc. Chem. Res.* **47** (2014) 1338 (<https://doi.org/10.1021/ar400309b>)
11. J. D. Moseley, C. O. Kappe, *Green Chem.* **13** (2011) 794 (<https://doi.org/10.1039/C0GC00823K>)
12. S. Caddick, R. Fitzmaurice, *Tetrahedron* **65** (2009) 3325 (<https://doi.org/10.1016/j.tet.2009.01.105>)
13. M. Nüchter, B. Ondruschka, W. Bonrath, A. Gum, *Green Chem.* **6** (2004) 128 (<https://doi.org/10.1039/B310502D>)
14. Y.-J. Zhu, F. Chen, *Chem. Rev.* **114** (2014) 6462 (<https://doi.org/10.1021/cr400366s>)
15. J. Li, L.-P. Zhang, F. Peng, J. Bian, T.-Q. Yuan, F. Xu, R.-C. Sun, *Molecules* **14** (2009) 3551 (<https://doi.org/10.3390/molecules14093551>)
16. A. Biswas, S. Kim, G. W. Selling, H. Cheng, *Ind Crops Prod.* **60** (2014) 259 (<https://doi.org/10.1016/j.indcrop.2014.06.004>)
17. B. Martín-García, S. Pimentel-Moral, A. M. Gómez-Caravaca, D. Arráez-Román, A. Segura-Carretero, *Ind Crops Prod.* **154** (2020) 112741 (<https://doi.org/10.1016/j.indcrop.2020.112741>)
18. T. Salmi, D. Valtakari, E. Paatero, B. Holmbom, R. Sjöholm, *Ind. Eng. Chem. Res.* **33** (1994) 1454 (<https://doi.org/10.1021/ie00030a004>)

19. A. M. Joglekar, A. T. May, *CFW* **32** (1987) 857
(<https://www.semanticscholar.org/paper/Product-excellence-through-design-of-experiments-Joglekar-May/927ffd1c557062b82f407ad08d82122af959827c>)
20. L. Manzato, M. L. Takeno, W. A. G. Pessoa-Junior, L. A. M. Mariuba, J. Simonsen, *Fibers Polym.* **19** (2018) 289 (<https://doi.org/10.1007/s12221-018-1123-8>)
21. P. Penjumras, R. B. A. Rahman, R. A. Talib, K. Abdan, *Agric. Agric. Sci. Proc.* **2** (2014) 237 (<https://doi.org/10.1016/j.aaspro.2014.11.034>)
22. X. F. Sun, F. Xu, R. C. Sun, P. Fowler, M. S. Baird, *Carbohydr. Res.* **340** (2005) 97
(<https://doi.org/10.1016/j.carres.2004.10.022>)
23. A. Mandal, D. Chakrabarty, *Carbohydr. Polym.* **86** (2011) 1291
(<https://doi.org/10.1016/j.carbpol.2011.06.030>)
24. N. Laribi, S. Maatoug, Z. Jebali, R. Zouari, H. Majdoub, M. Cheikhrouhou, *Cellul. Chem. Technol.* **54** (2020) 225 (<https://doi.org/10.35812/CelluloseChemTechnol.2020.54.24>)
25. S. M. L. Rosa, N. Rehman, M. I. G. de Miranda, S. M. B. Nachtigall, C. I. D. Bica, *Carbohydr. Polym.* **87** (2012) 1131 (<https://doi.org/10.1016/j.carbpol.2011.08.084>)
26. M. Adinugraha, D. Marseno, Haryadi, *Carbohydr. Polym.* **62** (2005) 164
(<https://doi.org/10.1016/j.carbpol.2005.07.019>)
27. G. A. Zickler, W. Wagermaier, S. S. Funari, M. Burghammer, O. Paris, *J. Anal. Appl. Pyrolysis* **80** (2007) 134 (<https://doi.org/10.1016/j.jaap.2007.01.011>)
28. A. N. Shebani, A. J. van Reenen, M. Meincken, *Thermochim. Acta* **471** (2008) 43
(<https://doi.org/10.1016/j.tca.2008.02.020>)
29. C. Leyva-Porras, P. Cruz-Alcantar, V. Espinosa-Solís, E. Martínez-Guerra, C. I. Piñón-Balderrama, I. Compean Martínez, M. Z. Saavedra-Leos, *Polymers (Basel)* **12** (2019) 5
(<https://doi.org/10.3390/polym12010005>).



J. Serb. Chem. Soc. 87 (2) 263–273 (2022)
JSCS–5520

Solid–liquid phase equilibria in the ternary systems $\text{H}_2\text{O}+\text{ZnCl}_2+\text{NaCl}$ at temperatures of 298, 313 and 333 K

SEVILAY DEMIRCI¹, VEDAT ADIGUZEL^{1*} and OMER SAHIN²

¹Department of Chemical Engineering, Kafkas University, Kars 36100, Turkey and

²Department of Chemical Engineering, Siirt University, Siirt 56100, Turkey

(Received 19 April, accepted 15 July 2021)

Abstract: In this study, an economic separation method is suggested with the use of phase equilibria in order to ensure the recycling of ZnCl_2 , the industrial waste amount of which is very high, and to prevent it from an environmental pollutant. Sodium chloride–zinc chloride–water systems were examined by the isothermal method at temperatures of 298, 313 and 333 K. The analyses of the liquid and solid phases were used to determine the composition of the solid phase using the Schreinemaker’s graphic method. The solid–liquid phase equilibrium and viscosity data belonging to all the ternary systems were identified and the solubility and viscosity changes with temperature were compared. The viscosity values were inversely proportional to the temperature as the amount of ZnCl_2 in the solution increased. NaCl , $2\text{NaCl} \cdot \text{ZnCl}_2 \cdot n\text{H}_2\text{O}$ ($n: 2, 0$), ZnCl_2 salts were observed at 298, 313 and 333 K in the solid phases that are in equilibrium with the liquid phase at the invariant point.

Keywords: crystallization region; invariant point; Schreinmakers method; solubility; viscosity.

INTRODUCTION

The solid-liquid phase equilibrium method is widely used, which includes increasing the yield of valuable chemicals and products in the salt industry. Moreover, this method makes the waste less harmful for the environment by increasing the rate of recycling and waste disposal. Thirdly, it enables a researcher to economically obtain valuable chemicals in fewer reaction steps in a lab setting.^{1–3}

ZnCl_2 is widely applied in industry, such as for the production of paper, the metal industry, textiles, the synthesis of important chemicals, agriculture, water refinement, cosmetics and the drug industry.^{4,5} However, industrial ZnCl_2 waste brings about economic and environmental problems especially in the steel ind-

* Corresponding author. E-mail: vedatnursen@gmail.com
<https://doi.org/10.2298/JSC210419053D>

ustry. In this industry, one of the most effective and oldest methods is the hot-dip galvanizing method in order to increase the corrosion resistance of steel.⁵ In the galvanizing process, the metal is cleaned from undesirable substances, such as rust and impurities in the acid bath. The amount of iron and zinc increases together in the acid reaction in the acid bath. The content of this impure solution is reported as 5–200 g L⁻¹ zinc, 60–150 g L⁻¹ iron and 10–80 g L⁻¹ HCl.^{6–9}

The issue of waste disposal is gaining significance in industry day by day together with the increase in environmental awareness and toughness of legislation. In this study, a separation process is suggested for ZnCl₂ with the change in solid–liquid phase equilibrium at different temperatures by benefiting from the ternary system H₂O+ZnCl₂+NaCl.

EXPERIMENTAL

Apparatus and reagents

NaCl (≥99.5 %) and ZnCl₂ (98 %) were purchased from Merck and used without further purification. The solution condition was provided for by pure water of pH 6.6 and conductivity <10⁻⁴ S m⁻¹.

Viscosity analyses were realized using a Brookfield DV2T viscometer (accuracy ±1.0 % of the full-scale range).

Titration measurements were conducted with Hirschmann Solarus automatic burette (accuracy ±0.2 %). A stable experimental temperature was provided by a Polyscience branded cooler and mixer water bath (accuracy ±0.05 K).

Experimental methods

Phase equilibria were determined by the isothermal solubility saturation method.^{10–13} Sealed insulated tubes containing saturated ZnCl₂ solutions dissolved in 40mL pure water were placed on the disc.¹³ NaCl salts were added to these tubes subsequently in increasing amounts until the invariant point was reached. The disc was mixed for one day in a heater and cooler circulator which is stable at the desired temperature (298, 313 and 333 K). The tubes were kept in the circulator until the phase separation was clearly seen. The samples were taken from the solid and liquid phases of all the tubes for ion analysis and viscosity determination. The solid phase compositions at all temperatures were detected according to the Schreinmaker's wet residue method.^{10–14}

The same processes were repeated by adding ZnCl₂ salts to the saturated solutions of NaCl in increasing amounts until the invariant point was reached. All the tests were repeated three times for reliability of the test results. Results were expressed as ± standard deviation value.

The tables and graphics were formed after conducting the mathematical calculations necessary for interpretation all the data and results.

Analytical methods

Cl⁻ and Zn²⁺ concentrations were determined respectively with Mohr and EDTA according to complexometric titration methods.¹⁵ Na⁺ amounts were calculated according to the total ion balance.

RESULTS AND DISCUSSION

Solubility data of H₂O–ZnCl₂–NaCl system at 298 K

The solubility and viscosity values of NaCl–H₂O and ZnCl₂–H₂O binary systems were detected respectively as 26.42 % NaCl and 80.13 % ZnCl₂, 1.55 mPa s and 156.84 mPa s at 298 K. The solid phases belonging to these compositions were found as NaCl and ZnCl₂.

NaCl, ZnCl₂ and H₂O compositions and viscosity in the invariant points of H₂O+ZnCl₂+NaCl system at 298 K were, respectively, F: 17.99, 39.70 and 42.31 % and 5.78 mPa s; E₁: 4.68, 67.68 and 27.64 % and 31.92 mPa s. The solid phase of invariant point consisted of NaCl, ZnCl₂ and 2NaCl ZnCl₂ 2H₂O salts.

The solubility and viscosity data belonging to this ternary system are given in Table I and Figs. 1 and 2.

TABLE I. SLE data for the ternary H₂O–ZnCl₂–NaCl system at 298 K and 0.102 MPa; standard uncertainties *u* are $u(\rho) = 0.001 \text{ g cm}^{-3}$, $u(T) = 0.05 \text{ K}$, $u_r(P) = 5 \%$ and $u(w) = 0.01$; NC: NaCl, DS: 2NaCl ZnCl₂ 2H₂O, ZC: ZnCl₂

No.	Content, mass. %				Content, mol. %		$\eta / \text{mPa s}$	Equilibrium salt
	Liquid phase		Solid phase		NaCl	ZnCl ₂		
	NaCl	ZnCl ₂	NaCl	ZnCl ₂				
1	26.42	0.00	95.08	0.00	100	0.00	1.55	NC
2	24.50	14.81	89.04	2.60	79.50	20.50	1.79	NC
3	22.61	25.70	95.04	1.28	67.24	32.76	3.07	NC
4	20.36	33.95	93.05	3.45	58.29	41.71	4.18	NC
5	19.20	36.94	82.37	8.04	54.75	45.25	4.85	NC
6F	17.99	39.70	34.05	44.50	51.34	48.66	5.78	NC+DS
7	14.15	47.03	34.00	47.30	41.22	58.78	8.12	DS
8	10.77	53.40	31.44	48.37	32.00	68.00	11.53	DS
9	8.04	59.30	30.08	50.70	23.95	76.05	17.43	DS
10	6.75	62.20	29.46	52.35	20.17	79.83	21.10	DS
11E ₁	4.68	67.68	17.48	66.36	13.88	86.12	31.92	DS+ZC
12	3.46	70.71	2.87	76.07	10.24	89.76	45.18	ZC
13	2.56	73.22	2.17	76.97	7.57	92.43	78.55	ZC
14	0.00	80.13	0.00	86.18	0.00	100	156.84	ZC

There are three crystallization areas in Fig. 1: 1) CAF corresponding to the crystallization area of NaCl; 2) FPE₁ corresponding to the crystallization area of 2NaCl ZnCl₂ 2H₂O; 3) E₁BD corresponding to crystallization area of ZnCl₂. Point A and B are the invariant points of the binary systems NaCl–H₂O and ZnCl₂–H₂O. Point E₁ and F represent an invariant of the ternary systems. The curves AF, FE₁ and E₁B represent the saturation curves. *X* and *Y* points correspond to the percent amount of ZnCl₂ and NaCl in the double salt, respectively.

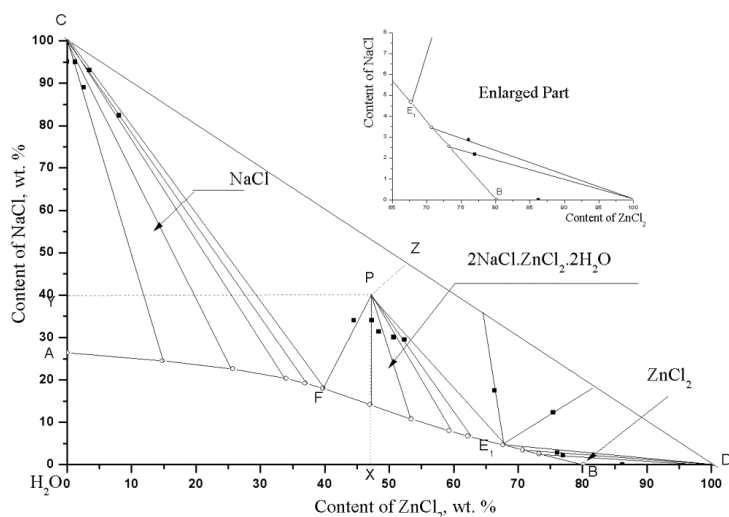


Fig. 1. SLE diagram for the ternary H_2O - ZnCl_2 - NaCl system at 298 K and 0.102 MPa.

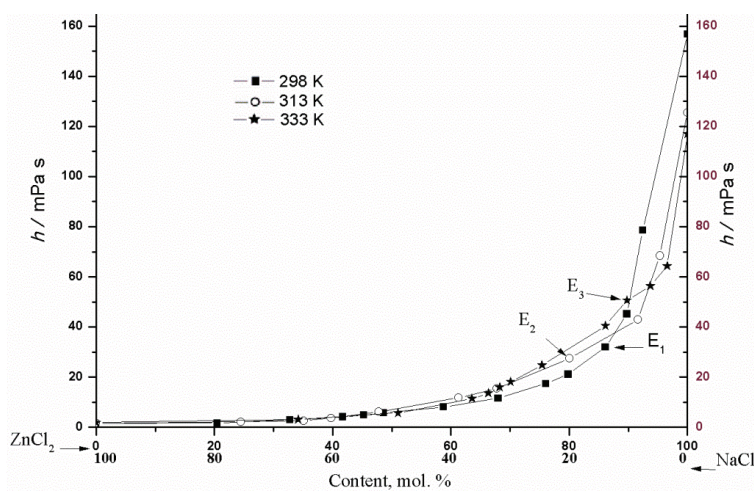


Fig. 2. Viscosity diagram for the ternary H_2O - ZnCl_2 - NaCl system at 298–333 K and 0.102 MPa.

Solubility data of H_2O - ZnCl_2 - NaCl system at 313 K

The solubility and viscosity values of NaCl - H_2O and ZnCl_2 - H_2O binary systems were determined respectively as 27.25 % NaCl and 81.10 % ZnCl_2 , 1.62 and 117 mPa s at 313 K. The solid phases belonging to these compositions were found as NaCl and ZnCl_2 .

NaCl , ZnCl_2 and H_2O compositions and viscosity in the invariant point of H_2O + ZnCl_2 + NaCl system at 313 K were, respectively, F: 19.16, 40.89 and 39.95

% and 6.20 mPa s; E_2 : 6.86, 64.15 and 28.99 % and 27.42 mPa s. The solid phase of invariant point consists of NaCl, $ZnCl_2$ and $2NaCl \cdot ZnCl_2$ salts.

The solubility and viscosity data belonging to this ternary system are given in Table II and Figs. 2 and 3.

TABLE II. SLE data for the ternary $H_2O-ZnCl_2-NaCl$ system at 313 K and 0.102 MPa; standard uncertainties u are $u(\rho) = 0.001 \text{ g/cm}^3$, $u(T) = 0.05\text{K}$, $u_t(P) = 5\%$ and $u(w) = 0.01w$
NC: NaCl, DS2: $2NaCl \cdot ZnCl_2$, ZC: $ZnCl_2$

No.	Content, mass. %				Content, mol. %		$\eta / \text{mPa s}$	Equilibrium salt
	Liquid phase		Solid phase		NaCl	$ZnCl_2$		
	NaCl	$ZnCl_2$	NaCl	$ZnCl_2$				
1	27.25	0.00	96.08	0.00	100	0.00	1.62	NC
2	22.92	17.33	87.01	2.80	75.52	24.48	2.14	NC
3	21.78	27.46	80.74	6.80	64.91	35.09	2.60	NC
4	20.97	32.27	91.32	3.60	60.24	39.76	3.64	NC
5F	19.16	40.89	38.90	50.15	52.21	47.79	6.20	NC+DS2
6	13.5	49.88	35.62	52.51	38.69	61.31	11.81	DS2
7	11.26	55.29	32.00	52.72	32.20	67.80	15.50	DS2
8 E_2	6.86	64.15	29.57	60.00	19.96	80.04	27.42	DS2+ZC
9	2.78	70.05	2.90	76.60	8.38	91.62	43.00	ZC
10	1.52	72.7	2.04	77.00	4.65	95.35	68.40	ZC
11	0.00	81.1	0.00	83.12	0.00	100	125.5	ZC

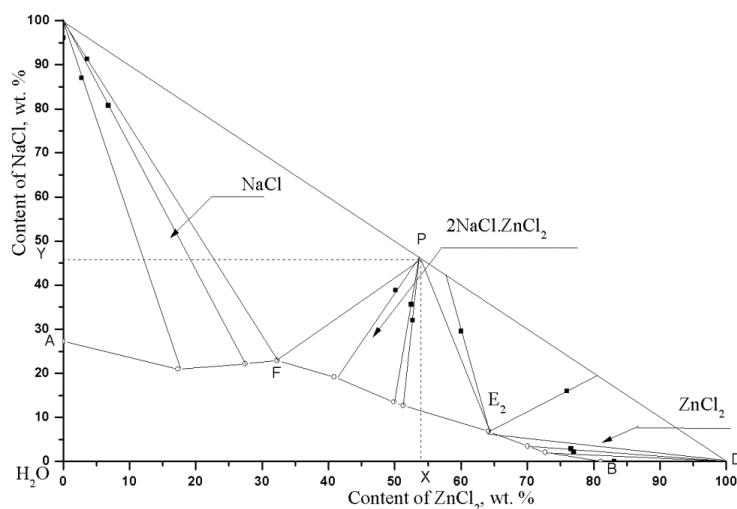


Fig. 3. SLE diagram for the ternary $H_2O-ZnCl_2-NaCl$ system at 313 K and 0.102 MPa.

There are three crystallization areas in Fig. 3: 1) CAF corresponding to the crystallization area of NaCl; 2) FPE_2 corresponding to the crystallization area of $2NaCl \cdot ZnCl_2$; 3) E_2BD corresponding to crystallization area of $ZnCl_2$. Point A and B are the invariant points of the binary systems NaCl- H_2O and $ZnCl_2-H_2O$.

The point E₂ and F represent an invariant of the ternary systems. The curves AF, FE₂ and E₂B represent the saturation curves.

X and Y points correspond to the percent amount of ZnCl₂ and NaCl in the double salt, respectively.

Solubility data of the H₂O–ZnCl₂–NaCl system at 333 K

When the temperature was brought to 333 K, it was observed that NaCl whose solubility value is 27.24 % in the NaCl–H₂O system decreases to 18.99 (F), 3.57 % (E₃) and the solubility of ZnCl₂ whose solubility is 83.2 % in ZnCl₂–H₂O system decreases to 46.22 (F), 73.03 % (E₃). It is also determined that the viscosity values change respectively from 1.92 mPa s to 5.76 (F), 50.67 mPa s (E₃) and from 125.5 mPa.s to 5.76 (F), 50.67 mPa s (E₃) when the invariant point is reached. The solid phase of the invariant point consists of NaCl, ZnCl₂ and 2NaCl·ZnCl₂ salts.

The solubility and viscosity data belonging to this ternary system are given in Table III and Figs. 2 and 4.

TABLE III. SLE data for the ternary H₂O–ZnCl₂–NaCl system at 333 K and 0.102 MPa; standard uncertainties *u* are *u*(*p*) = 0.001 g/cm³, *u*(*T*) = 0.05K, *u*_r(*P*) = 5% and *u*(*w*) = 0.01; NC: NaCl, DS2: 2NaCl·ZnCl₂, ZC: ZnCl₂

No.	Content, mass. %				Content, mol. %		<i>η</i> / mPa s	Equilibrium salt
	Liquid phase		Solid phase		NaCl	ZnCl ₂		
	NaCl	ZnCl ₂	NaCl	ZnCl ₂				
1	27.24	0.00	89.22	0.00	100	0.00	1.92	NC
2	23.00	27.83	88.63	3.78	65.84	34.16	3.11	NC
3F	18.99	46.22	31.66	49.38	48.93	51.07	5.76	NC+DS2
4	14.16	57.61	29.66	55.49	36.43	63.57	11.42	DS2
5	13.01	59.80	32.84	56.03	33.66	66.33	13.60	DS2
6	12.33	61.80	29.19	57.27	31.75	68.25	16.08	DS2
7	11.54	63.03	28.29	58.23	29.92	70.08	18.12	DS2
8	9.42	67.38	30.06	59.98	24.58	75.42	24.78	DS2
9	4.99	72.24	28.75	61.47	13.86	86.14	40.50	DS2
10E ₃	3.57	73.03	19.28	70.59	10.22	89.78	50.67	DS2+ZC
11	2.17	75.50	1.87	82.12	6.28	93.72	56.40	ZC
12	1.19	78.30	0.82	81.11	3.41	96.59	64.33	ZC
13	0.00	83.20	0.00	88.89	0.00	100	117	ZC

There are three crystallization areas in Fig. 4: 1) CAF corresponding to the crystallization area of NaCl, 2) FPE₃ corresponding to the crystallization area of 2NaCl·ZnCl₂, 3) E₃BD corresponding to the crystallization area of ZnCl₂. Point A and B are the invariant points of the binary systems NaCl–H₂O and ZnCl₂–H₂O. Point E₃ and F represent invariants of the ternary systems. The curves AF, FE₃ and E₃B represent the saturation curves.

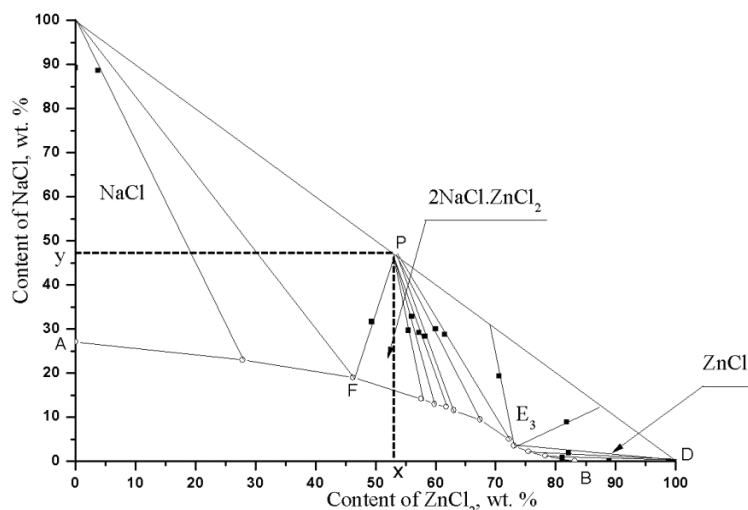


Fig. 4. SLE diagram for the ternary $\text{H}_2\text{O}-\text{ZnCl}_2-\text{NaCl}$ system at 333 K and 0.102 MPa.

The points X and Y correspond to the percent amount of ZnCl_2 and NaCl in double salt, respectively.

Comparison of $\text{H}_2\text{O}-\text{ZnCl}_2-\text{NaCl}$ systems between 273 and 373 K

The composition change belonging to six temperatures in total were compared also by using the data between the temperatures 273 and 373 K, belonging to the ternary system $\text{NaCl}-\text{ZnCl}_2-\text{H}_2\text{O}$ from the literature.^{12,16–18}

When the binary systems of $\text{NaCl}-\text{H}_2\text{O}$ were examined between 273 and 373 K, the mass percentage composition change of the solubility of NaCl shows a low value of 2 %. However, it could be seen that mass percentage composition change of temperature and solubility was a noteworthy value of 19.32 % in the binary system of ZnCl_2 .

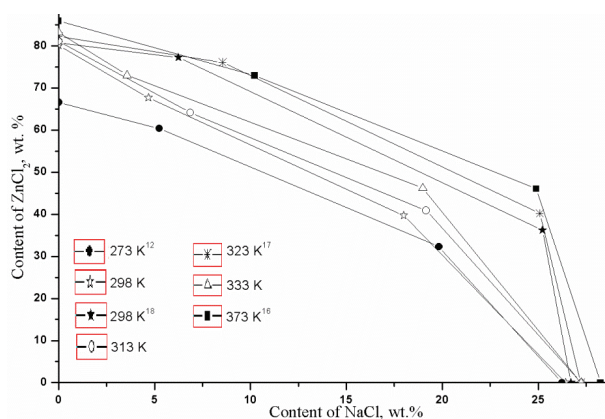
In addition, it was observed that the solubility of NaCl was between 3.57–10.21 % and the solubility of ZnCl_2 was between 60.37–77.25 % when the invariant point data of the ternary systems were examined (Table IV, Fig. 5).

The solubility of NaCl and ZnCl_2 increased with increasing temperature. All the ternary systems contained the double salt. The structure of the double salt was of the form $2\text{NaCl}\cdot\text{ZnCl}_2\cdot 2\text{H}_2\text{O}$ at low temperatures (273 and 298 K). Nevertheless, it turned into a double salt $2\text{NaCl}\cdot\text{ZnCl}_2$ above 313 K (313–373 K) as the temperature increased. Obviously, the hydrated double salt turned into an anhydrous double salt with increasing temperature.

Comparing the present study with data from Zhang *et al.*¹⁸ at 298 K, it was observed that the solubility of the solid phase compositions and double salts were compatible with each other.

TABLE IV. SLE data for the ternary $\text{H}_2\text{O}-\text{ZnCl}_2-\text{NaCl}$ systems at 273–333 K

T / K	Invariant point, mass %		Solid phase	Reference
	NaCl	ZnCl_2		
273	26.25	0.00	NaCl	Adiguzel <i>et al.</i> ¹²
	19.83	32.27	$\text{NaCl}+2\text{NaCl} \cdot \text{ZnCl}_2 \cdot 2\text{H}_2\text{O}$	
	5.24	60.37	$\text{ZnCl}_2 \cdot 2\text{H}_2\text{O}+2\text{NaCl} \cdot \text{ZnCl}_2 \cdot 2\text{H}_2\text{O}$	
	0.00	66.60	$\text{ZnCl}_2 \cdot 2\text{H}_2\text{O}$	
298	26.71	0.00	NaCl	Zhang <i>et al.</i> ¹⁸
	25.22	36.23	$\text{NaCl}+2\text{NaCl} \cdot \text{ZnCl}_2 \cdot 2\text{H}_2\text{O}$	
	6.24	77.25	$\text{ZnCl}_2+2\text{NaCl} \cdot \text{ZnCl}_2 \cdot 2\text{H}_2\text{O}$	
	0.00	80.77	ZnCl_2	
298	26.42	0.00	NaCl	In this study
	17.99	39.70	$\text{NaCl}+2\text{NaCl} \cdot \text{ZnCl}_2 \cdot 2\text{H}_2\text{O}$	
	4.68	67.68	$\text{ZnCl}_2+2\text{NaCl} \cdot \text{ZnCl}_2 \cdot 2\text{H}_2\text{O}$	
	0.00	80.13	ZnCl_2	
313	27.25	0.00	NaCl	In this study
	19.16	40.89	$\text{NaCl}+2\text{NaCl} \cdot \text{ZnCl}_2$	
	6.86	64.15	$\text{ZnCl}_2+2\text{NaCl} \cdot \text{ZnCl}_2$	
	0.00	81.10	ZnCl_2	
323	27.22	0.00	NaCl	Zhang <i>et al.</i> ¹⁷
	25.08	40.17	$\text{NaCl}+2\text{NaCl} \cdot \text{ZnCl}_2$	
	8.55	76.09	$\text{ZnCl}_2+2\text{NaCl} \cdot \text{ZnCl}_2$	
	0.00	82.25	ZnCl_2	
333	27.24	0.00	NaCl	In this study
	18.99	46.22	$\text{NaCl}+2\text{NaCl} \cdot \text{ZnCl}_2$	
	3.57	73.03	$\text{ZnCl}_2+2\text{NaCl} \cdot \text{ZnCl}_2$	
	0.00	83.20	ZnCl_2	
373	28.25	0.00	NaCl	Zhang <i>et al.</i> ¹⁶
	24.90	46.07	$\text{NaCl}+2\text{NaCl} \cdot \text{ZnCl}_2$	
	10.21	72.97	$\text{ZnCl}_2+2\text{NaCl} \cdot \text{ZnCl}_2$	
	0.00	85.92	ZnCl_2	

Fig. 5. Comparison between the SLE diagrams for the ternary $\text{H}_2\text{O}-\text{ZnCl}_2-\text{NaCl}$ system at 273–373 K.

CONCLUSIONS

It was stated that the solubility of ZnCl_2 decreases from 66.6 to 60.37 % and the solubility of NaCl decreases sharply from 26.25 to 5.24 % to the invariant point as shown in the ternary system of $\text{NaCl-ZnCl}_2\text{-H}_2\text{O}$ at 273 K, as conducted by Adiguzel *et al.*¹²

Zhang *et al.* implied that the solubility of ZnCl_2 decreases from 80.77 % to 77.25 % to the invariant point and the solubility of NaCl decreases from 26.71 to 6.24 %. These results show a sharper drop compared to that of ZnCl_2 in the ternary system at 298 K.¹⁸

It was observed in the ternary system at 298 K that the solubility of ZnCl_2 decreases from 80.13 to 67.68 % to the invariant point. On the other hand, the solubility of NaCl decreases significantly from 26.42 to 4.68 % compared to that of ZnCl_2 .

It was concluded in the ternary system at 313 K that the solubility of ZnCl_2 decreases from 81.1 to 64.15 % to the invariant point and the solubility of NaCl decreases from 27.25 to 6.86 % and show a similar change with ZnCl_2 .

The solubility of ZnCl_2 at 333 K changed from 83.2 to 73.03 % to the invariant point. The solubility of NaCl decreased 27.04 to 3.57 %. The solubility change of NaCl is greater at this temperature.

It was reported that the solubility of ZnCl_2 decreases from 82.25 to 76.09 % and the solubility of NaCl decreases from 27.22 to 8.55 % according to the ternary system of $\text{NaCl-ZnCl}_2\text{-H}_2\text{O}$ at 323 K as studied by Zhang *et al.*¹⁷

It was found that the solubility of ZnCl_2 decreases from 85.92 to 72.97 % and the solubility of NaCl decreases from 28.25 to 10.21 % in the study regarding the ternary system of $\text{NaCl-ZnCl}_2\text{-H}_2\text{O}$ at 373 K, which was conducted by Zhang *et al.*¹⁶

When the solubility change data of the ternary system of $\text{H}_2\text{O+ZnCl}_2\text{+NaCl}$ between 273–373 K temperature was compared, it could be clearly seen that ZnCl_2 had a salting-out effect on NaCl. In addition, it was seen that the viscosity values are inversely proportional to the temperature as the amount of ZnCl_2 in the solution increased when the viscosity values of the ternary systems are compared in this study.

In conclusion, this study and literature data suggest that the process for the separation of ZnCl_2 by adding NaCl in the calculated amount to the solution and/or by decreasing the temperature of the solution of NaCl and ZnCl_2 occur at temperatures between 273 and 373 K. Therefore, an economic separation method could be developed by the method of phase equilibrium using NaCl, which is cheap and easily accessible, in order to provide or the recycling of ZnCl_2 , the industrial waste amount of which is very high and to prevent it from posing a threat for the environment.

Acknowledgement. This work was supported by The Scientific and Technological Research Council of Turkey (TUBITAK) under Project No. 114Z651.

ИЗВОД

РАВНОТЕЖА ФАЗА ЧВРСТО–ТЕЧНО ТЕРМЕРНОГ СИСТЕМА $H_2O+ZnCl_2+NaCl$ НА
ТЕМПЕРАТУРАМА ОД 298, 313 И 333 КSEVILAY DEMIRCI¹, VEDAT ADIGUZEL¹ и OMER SAHIN²¹Department of Chemical Engineering, Kafkas University, Kars 36100, Turkey u ²Department of Chemical Engineering, Siirt University, Siirt 56100, Turkey

У овом раду је предложена сепарациона метода заснована на фазној равнотежи, којом се постиже економски оправдана рециклажа $ZnCl_2$, присутног у значајним количинама у индустријском отпаду, а у циљу спречавања загађења животне средине. Растворљивост систему натријум-хлорид + цинк-хлорид + вода је испитивана у изотермским условима на температурама 298, 313 и 333 К. Schreinemakers графичка метода је коришћена за анализу течне и чврсте фазе и за одређивање састава испитиваног система. У раду су дати подаци за равнотежу чврсто–течно, као и подаци за вискозност и растворљивост тернарног система. Такође испитиван је утицај температуре на вискозност и растворљивост. Вредности вискозности су биле обрнуто пропорционалне температуре, како се количина $ZnCl_2$ у раствору повећавала.

(Примљено 19. априла, прихваћено 15. јула 2021)

REFERENCES

1. H. Civelekoğlu, R. Tolun, N. Bulutçu, *Inorganic Technology*, İTÜ Maden Fakültesi Ofset Atölyesi, İstanbul, 1987, pp. 80–103 (<https://www.ituyayinlari.com.tr/kitap/34/inorganik-Teknolojiler>) (in Turkish)
2. A. Olcay, *Chemical Technology*, Gazi Kitabevi, Ankara, 1998, pp. 10–38 (<https://www.gazikitabevi.com.tr/urun/kimyasal-teknolojiler>) (in Turkish)
3. Y. Mastai, *Advances in Crystallization Processes*, InTech, Rijeka, 2012, pp. 400–413 (<https://dx.doi.org/10.5772/2672>)
4. P. Patnaik, *Handbook of Inorganic Chemicals*, McGraw-Hill Professional, New York, 2002, pp. 50–200 (<https://dx.doi.org/10.5860/choice.40-6428>)
5. A. R. Marder, *Prog. Mater. Sci.* **45** (2000) 191 ([https://dx.doi.org/10.1016/S0079-6425\(98\)00006-1](https://dx.doi.org/10.1016/S0079-6425(98)00006-1))
6. K. H. Lum, G. W. Stevens, S. E. Kentish, *Hydrometallurgy* **142** (2014) 108 (<https://dx.doi.org/10.1016/j.hydromet.2013.11.016>)
7. J. Carrillo-Abad, M. García-Gabaldón, V. Pérez-Herranz, *Desalination* **343** (2014) 38 (<https://dx.doi.org/10.1016/j.desal.2013.11.040>)
8. K. H. Lum, G. W. Stevens, J. M. Perera, S. E. Kentish, *Hydrometallurgy* **133** (2013) 64 (<https://dx.doi.org/10.1016/j.hydromet.2012.12.001>)
9. S. Bao, L. Tang, K. Li, P. Ning, J. Peng, H. Guo, T. Zhu, Y. Liu, *J. Colloid Interface Sci.* **462** (2016) 235 (<https://dx.doi.org/10.1016/j.jcis.2015.10.011>)
10. V. Alişoğlu, V. Adıguzel, *C. R. Chim.* **11** (2008) 938 (<https://dx.doi.org/10.1016/j.crci.2007.12.001>)
11. H. Erge, V. Adıguzel, V. Alişoğlu, *Fluid Phase Equilib.* **344** (2013) 13 (<https://dx.doi.org/10.1016/j.fluid.2012.12.033>)

12. V. Adıgüzel, H. Erge, V. Alişoğlu, H. Necefoğlu, *J. Chem. Thermodyn.* **75** (2014) 35 (<https://dx.doi.org/10.1016/j.jct.2014.04.014>)
13. S. Demirci, V. Adıgüzel, Ö. Şahin, *J. Chem. Eng. Data* **61** (2016) 2292 (<https://dx.doi.org/10.1021/acs.jced.5b00988>)
14. H. Schott, *J. Chem. Eng. Data* **6** (1961) 324 (<https://dx.doi.org/10.1021/je00103a002>)
15. T. Gündüz, *Laboratory Book of Quantitative Analysis*, Gazi Büro Kitabevi, Ankara, 2012, pp. 280–282 (ISBN 9799757313457) (in Turkish)
16. X. Zhang, W. Zhang, D. Wang, H. Zhang, S. Sang, *Russ. J. Inorg. Chem.* **62** (2017) 995 (<https://dx.doi.org/10.1134/S0036023617070245>)
17. X. Zhang, S. Zhou, Y. Mu, *J. Chem. Eng. Data* **64** (2019) 4330 (<https://dx.doi.org/10.1021/acs.jced.9b00422>)
18. X. Zhang, L. Zhao, W. Wang, S. Sang, *J. Chem. Eng. Data* **65** (2020) 4475 (<https://dx.doi.org/10.1021/acs.jced.0c00313>).



J. Serb. Chem. Soc. 87 (2) 275–290 (2022)
JSCS–5521

The influence of active learning and submicrorepresentations on 14-year-old students' understanding of the alkaline earth metal concepts

KATARINA SENTA WISSIAK GRM* and IZTOK DEVETAK

University of Ljubljana, Faculty of Education, Kardeljeva pl. 16, 1000 Ljubljana, Slovenia

(Received 28 March, revised 20 July, accepted 3 September 2021)

Abstract: This study aimed to examine the impact of two different approaches on students' understanding of selected chemical concepts. The first treatment group was taught by a method comprising guided active learning demonstrations, and the second treatment group was exposed to guided active learning demonstrations with explanations at the submicroscopic level. In a control group, the selected topic was taught without guided active learning demonstrations and without explanations at the submicroscopic level. The instruments used in this research included the test of logical thinking (TOLT), knowledge pre-test (KPT), two achievement tests (AT-1 and AT-2) and a questionnaire for students. One hundred and seventy-one students (average age 13.9 years) participated in the study. The results indicate that both approaches (*i.e.*, guided active learning demonstrations and guided active learning demonstrations with explanations at submicroscopic level) are more effective than only symbolic teaching. It can be concluded from the results that students' knowledge, obtained by either method that includes guided active learning, is retained in the students' long-term memory. Some suggestions for implications for the primary science curriculum are also discussed.

Keywords: chemistry; lower secondary school; cooperative learning; student centred-learning; triple nature of chemical concepts.

INTRODUCTION

The teaching and learning of chemistry have undergone many changes, and different strategies have been introduced in recent years to reduce students' misconceptions. Research papers published internationally discuss the more or less positive effects of educational strategies using the three levels of chemical representations (*i.e.*, macro, submicro and symbolic level).^{1–11}

* Corresponding author. E-mail: katarina.wissiak@pef.uni-lj.si
<https://doi.org/10.2298/JSC210328071W>

Students' should be engaged in a more active role during teaching and learning in the classroom, where they are more or less guided during the learning process.¹¹ Active learning strategies, such as POGIL developed in the US or the PARSEL, PROFILES and GALC strategies introduced in Europe emphasize students' central role in their learning. In this context, teachers are leaders of the learning process, and they do not have a central role in teaching.^{12,13}

The main purpose of the present research is to investigate the effect of two different teaching approaches: 1) a guided active learning strategy with macroscopic demonstration and 2) a guided active learning strategy including macroscopic demonstration supported by the sub-microlevel explanations of selected chemical concepts regarding alkaline earth metals.

Theoretical background

For years, chemistry education researchers have been exploring how three levels of chemical representations help students develop the conceptual understanding of chemical phenomena.^{14–23} In comparison with the triangle of three levels of chemical representations, which was introduced by Alex Johnstone (1982), other authors have attempted to upgrade Johnstones' model, showing different levels of connections between triple nature of chemical concepts and also attempt to put the Johnstones' triangle into the new perspective.^{21,24,25} The interdependence of three levels of science concepts representations (ITLS) model shows different levels of the interdependence of chemical representations in connection with the visualization method used in the science classroom and mental models of chemical phenomena that this model helps students to develop (Fig. 1).²⁵

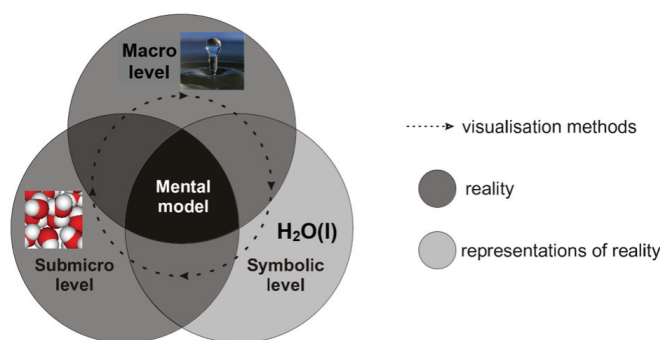


Fig. 1. Model representing interdependence of three levels of science concepts – ITLS model.²⁵

The ITLS model connects the concrete (*i.e.*, sensory, experimental, *etc.*) macro level with the abstract (*i.e.*, particulate) sub-microlevel and abstract (mathematical, diagrams, pictures, chemical symbols and equations, *etc.*) symbolic levels. Macro- and sub-microlevels are present in natural phenomena. The pre-

sentations of the sub-microlevel, including the particulate model, are mental constructs to explain and predict macro phenomena. The symbolic one is the simple representation of it and helps people communicate about the phenomena and conduct further research. All three levels should cover and supplement each other in a specific way so that adequate mental models of the natural phenomena should be developed in students' long-term memory. These mental models should be as far as possible understandable for students, without misconceptions. For these mental models to be created; students should be actively engaged in different educational strategies. These strategies should incorporate appropriate visualization elements to illustrate the abstract submicrolevel of natural phenomena (*i.e.*, submicrorepresentations, physical models, *etc.*) Understanding of the phenomena is established when all three levels of the concepts representations are adequately integrated into students' long-term memory, where the concept structure can influence students' chemical (scientific) literacy.^{9,25} Since students confront problems when integrating new knowledge into their long-term memory, research in science education in the previous two decades, has emphasized using different educational strategies to overcome the gap between students' perception of the natural phenomena and their mental models formed in their long term memory.^{2,5,15,26}

Research also shows that students have considerable difficulty understanding the submicro and symbolic levels of chemical representations and that previous knowledge of a specific topic influences the integration of new science concepts into students' mental structure.^{5,9,17,24,25,27,28} It is also necessary to emphasize that teachers use mostly the symbolic level of chemical concepts representations to teach chemistry at the primary, secondary, and university levels.²⁴ Using only the symbolic level of chemical concepts does not lead students to understand chemical phenomena at the particulate level.²⁹ The integration of the three levels of chemical representations according to the ITLS model, and students' exposure to the submicrorepresentations during the educational process, positively influence their more adequate understanding of the nature of the particles' interactions compared to those who learned the same concepts only by reading texts.^{2,30} It is reasonable to believe that the use of different models (*e.g.*, submicrorepresentations, physical models) could improve the quality of the educational process and students' knowledge (*e.g.*, to visualize chemical equations, the correlation between structure and properties, *etc.*) and should therefore be more widely used.

Research has consistently shown that traditional lecture methods, in which teachers talk and students listen, dominate college and university classrooms.³¹ To past passive learning to active learning and to find better ways of engaging students in the learning process, a Model of Active Learning has been developed, which suggests how teachers can develop a meaningful set of active learning activities (Fig. 2).¹³

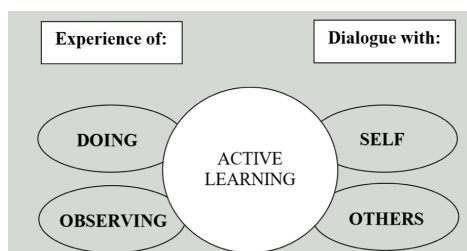


Fig. 2. Model of Active Learning (modified by Dee Fink¹³).

This model suggests that all learning activities involve some kind of experience or some kind of dialogue. The two main kinds of dialogue are “Dialogue with Self” and “Dialogue with Others”. Two main kinds of experience are “Observing” and “Doing”. Each of the four modes of learning described in the model above has its value, and using them can add variety to lessons and thus be more interesting for the learner. Furthermore, properly connected, the various learning activities can have an impact that is more than additive or cumulative; they can be interactive and thereby multiply the educational impact. Likewise, other research suggests that students must be actively involved in the learning process; they must do more than merely listen, they must read, write, discuss, do hands-on activities (*e.g.*, chemical experiments, constructing models, etc.) and must be engaged in solving problems.¹³ Most importantly, students must be actively involved in the learning and teaching process, so that they become engaged in such higher-order thinking tasks as analysis, synthesis, and evaluation.

Use of the techniques and strategies that promote active learning in the classroom is vital because of their powerful impact on students’ learning.³¹ Many important activities that support active learning include teaching practices that focus on sense-making, self-assessment, and reflection on what worked and what needs improving.

These practices have been shown to increase the degree to which students transfer their learning to new settings and events. Subsequently, students also prefer strategies promoting active learning to traditional lectures. Those students who actively engage with the material are more likely to recall information later, and be able to use that information in different contexts.³²

The term “active learning” means involving students in practicing important skills and in applying new knowledge.³³ However, the important elements of this active learning process can be described as follows: 1) reviews of previous learning, 2) point of showing how (where the teacher shows how to do), 3) a process of controlled practice (where the meaning and the process of the work are stressed), 4) a process of individual work, which is the heart of the learning process, 5) check of the work being done, 6) evaluation (assignments including review questions) and 7) final review: “What have we learned?”

A very good example of an active learning process, with a very positive effect on the observers, in the chemistry teaching process is demonstrations, which are widely published and used by chemistry teachers at all levels. In addition to those, a long and distinguished history of demonstrations exists, with Faraday's lectures perhaps being the first real, lasting example of the impact of the chemical demonstrations on the audience. In short, there appears to be little doubt that the demonstrations excite and 'charm' the students and do have educational benefits.^{34,35}

However, there are different opinions about the didactic approaches, even when conducting chemical demonstrations in the classroom. The literature asserts that guided and minimally guided instructional approaches are popular; yet, authors point out that approaches that ignore both structures and constitute human cognitive architecture are likely to be ineffective.³⁵⁻³⁷ In this context, it is clear how important it is to incorporate the guided active learning approach into chemistry teaching, *e.g.*, chemistry experimental work, especially guided experimental work, in order to make the most of the use of chemical demonstration as a teaching tool in general. Undoubtedly, chemical demonstrations seem to have a significant effect on observers, if extended with the guided learning approach, at best the essence of the chemical content presented could be extracted.

For this reason, in our study we decided to implement the method of actively guided experimental work in the chemistry learning and teaching process.

METHODOLOGY

Research problem and research questions

Accepting the well-known recognition that students frequently have difficulty in learning science because they do not understand how macroscopic, particulate, and symbolic representations of matter are related, we attempted to introduce the context by applying the active learning method, in order to help the students understand these important relationships. With this in mind, a specially designed guided active learning method was developed to help students connect the macro- with the submicro-levels of chemistry, taking into account the well-known fact that demonstrations and experiments can contribute to active and meaningful conceptual learning.³⁶ Namely, learning theory and research on guided-learning instructions suggests that, unless students' concepts are linked in long-term memory, they will have an incomplete understanding of a given subject and that students are more likely to learn concepts when learning is active.^{13,38,39} Accordingly, to follow the trends, the realisation of the active learning process – in our case, a method comprising guided active learning demonstrations (Experimental group 1 – EXP1) and guided active learning demonstrations with explanations at submicro level (Experimental group 2 – EXP2) was designed as a specific teaching approach that was incorporated into the educational process.

The main purpose of the study is therefore, to investigate the effect of two different teaching approaches (EXP1 and EXP2) on students' understanding of selected chemical concepts. Accordingly, we designed a guided active learning demonstration worksheet and presented it to students in (intervention) chemistry classes. The essence of this approach is represented in precisely divided and predicted steps that allow students to identify, analyze and exp-

lain each step of the experiment. In this way, each specific macroscopic observation (previously identified by the teacher as important for understanding the nature of the chemical concept) was explained in detail, including sub-micro and symbolic level explanation. However, this was not the case in the control group, as this is not the usual practice of Slovenian teachers. Namely, the national chemistry curriculum in Slovenia does not prescribe a chemical experiment as a compulsory part when the teacher introduces chemical concepts to the students. In this sense, our chemistry teachers are free to decide whether or not to include a chemistry experiment in their lessons when a new chemistry topic is introduced in chemistry classes. However, Slovenian teachers often use chemical demonstrations, but only to increase students' interest in the chemistry topic, which leads students into the passive role. Therefore, we tried to overcome this by introducing the method of guided active learning demonstrations to change from passive to active role of students. Ergo, instead of students just admiring the chemical demonstration performed by the teacher, students were given an immediate opportunity to focus on and explain the essential parts of the experiment. Namely, by using the students' worksheet for guided active learning demonstrations, we enable students to realize the importance of each step, and also give them the opportunity to lean on the steps and follow the chemical experiment easily. In this sense, we give students the important time and place to analyze the crucial steps that are important to understand and further explain chemical phenomena introduced by the conducted chemical experiment.

These specific concepts (alkaline earth metal properties – AEMP) were selected because they are included in the school curriculum at all levels of education, and also because the Slovenian land is mostly composed out of limestone (calcium carbonate) and thus could be interesting for students.

According to the purpose of the research, one basic research question could be addressed: What is the influence of (EXP1) and (EXP2) on students' understanding of selected chemical concepts?

Based on the research question, four hypotheses could be formed:

H1: Students participating in EXP1 and EXP2 will score significantly higher on an achievement test than those students who were taught only at the symbolic level of the AEMP concepts.

H2: Students experiencing EXP2 will score significantly higher on the achievement test than those who participated in a EXP1.

H3: Students participating in EXP1, and in EXP2 will score significantly higher on a delayed achievement test than those students who were taught only the symbolic level of the AEMP concepts.

H4: Students experiencing EXP2 will score significantly higher on the delayed achievement test than those who experienced EXP1.

Participants

The research sample consisted of 171 students from four Slovene primary schools (94 males; 55.0 % and 77 females; 45.0 %). The average age of students involved in the research was 13.9 years ($SD = 0.37$ year). Sixty students (35.1 %) taught using only the symbolic representation of the selected chemistry content (CONT). A further fifty-one students (29.8 %) were involved in EXP1 and sixty-three students (36.8 %) in EXP2.

Experimental and control groups were compared according to some independent variables (general and science school success in the previous year, formal reasoning abilities, and pre-test achievements). These variables were selected because they can influence students' understanding of future chemical concepts to be taught. The one-way between-group analysis

of variance (ANOVA) was conducted to explore the differences between the groups of students exposed to different teaching strategies (CONT, EXP1 or EXP2) in selected independent variables. The analysis of independent variables (the degrees of freedom (df (groups), df (students) = 2, 171) and significance of the differences between the groups ($Sig.$)) shows that the three groups were not statistically significantly different according to the selected independent variables (Table I).

TABLE I. ANOVA between groups of students exposed to three different educational strategies

Variable	Group	<i>M</i>	<i>SD</i>	<i>F</i> value	<i>Sig.</i>
General school success	CONT	4.3	0.66	0.195	0.823
	EXP1	4.4	0.64		
	EXP2	4.3	0.76		
Science school achievements	CONT	3.9	0.78	1.085	0.340
	EXP1	4.1	0.86		
	EXP2	4.2	0.77		
Formal reasoning abilities	CONT	3.3	2.25	1.498	0.226
	EXP1	2.9	2.58		
	EXP2	2.6	2.26		
Knowledge pre-test (KPT) achievement	CONT	3.8	1.61	2.115	0.072
	EXP1	4.0	1.72		
	EXP2	3.7	1.92		

Instruments

The instruments used in this research included the test of logical thinking (TOLT) and the knowledge pre-test (KPT) and two achievement tests: the achievement test applied immediately after educational strategy (AT-1), and a delayed achievement test (AT-2) administered two weeks later. All chemistry achievement tests were designed specifically for this study. The description of the instruments is presented in the Supplementary material to this paper.

Research design

The selected chemistry content (alkaline earth metals properties – AEMP) was presented to two treatment groups using different teaching approaches: 1) the first treatment group received a guided active learning demonstrations (EXP1), and 2) the second treatment group guided active learning demonstrations with explanations at submicro level (EXP2).

Both teaching strategies also included symbolic representations using chemical formulae and equations. However, the (CONT) was taught using only the symbolic representation of chemical concepts, introduced without conducting a chemical experiment during the lesson and explaining it with submicrorepresentations.

Indeed, this is the normal practice used by Slovenian teachers since the national chemistry curriculum does not prescribe a chemical experiment as a compulsory part when the teacher introduces chemical concepts to the students. In this sense, our chemistry teachers are free to decide whether to include a chemical experiment in their lessons when a new chemical topic is presented in the chemistry room.

This design provided an opportunity to examine the effect of different teaching approaches on students' knowledge, specifically the main difference between the treatments and control groups. All the teachers involved in this study were familiar with the specific teaching approach, which they had to apply to their educational process. All teaching approaches were

discussed in detail with the teachers, and specific modifications to the teaching strategy were made. More detailed description of teaching approaches is explained in the Supplementary material to this paper.

The instructions took 45 min in each group. All the students took the same set of instruments, administered at simultaneous intervals. The TOLT and knowledge pre-test (KPT) were administered two days before applying a specific educational strategy introducing AEMP to the students. After applying selected pedagogical strategies, the achievement test (AT-1) was administered at the end of the class and after fourteen days, according to Ebbinghaus theory, which states that forgetting occurs as a function of time. The rate of decay is highest in the first few days after learning the specific material; between days 6 and 31, learned material decays by only about 4 %⁴¹ and 14 days after intervention it is useful to test knowledge retention. The delayed achievement test (AT-2) was used to collect data on students' knowledge stored in long-term memory about the AEMP. These instruments were used to control variables (formal reasoning skills, prior knowledge) that have been described in the research literature^{4,9,42} as influential independent variables in the process of teaching chemistry using SMRs.

Descriptive statistics were obtained for illustrating the TOLT, KPT, AT-1 and AT-2 characteristics. Pearson's correlation coefficients for determining the correlation between chemistry knowledge tests were calculated. Also, the one-way between-groups analysis of variance (ANOVA) was conducted to explore the differences between groups of students exposed to different teaching strategies, and to explore the differences in total success on achievement tests between the groups of students exposed to different educational strategies presenting AEMP.

RESULTS AND DISCUSSION

The results are presented on two levels: 1) results, obtained immediately after the applied educational strategy, and 2) results obtained after a 14-day period, to assess the level of knowledge retention. The results show students' better understanding of chemical concepts regarding AEMP when the educational strategy is applied by using active learning chemical demonstration or is even upgraded by explanation at the submicroscopic level, as when the symbolic representation of the same chemical concepts is applied.

It can be seen from Fig. 3, comparing the chemistry achievement scores from pre-test, test and post-test, that students experiencing EXP2 achieve the highest scores on both achievement tests (AT-1 and AT-2). The lowest scores were achieved by the students in the control group, where the alkaline earth metals were taught only by symbolic explanations of their properties. It can also be concluded from the results presented in this chart that students who had not experienced the submicro level explanations of the experimental observations did not reach the highest scores on achievement tests. More detailed results are presented below.

The influence of EXP1 and EXP2 on students' knowledge about AEMP immediately after the application of educational strategies

The first level of results shows students' achievements immediately after the specific educational strategy was applied.

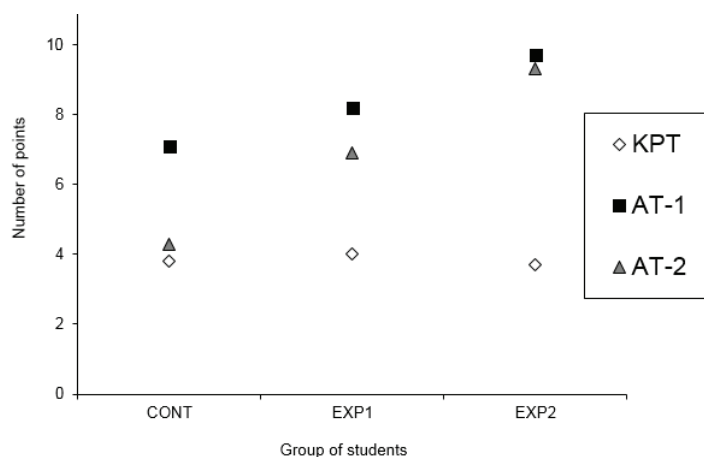


Fig. 3. Comparing the students' average achievements on three chemistry knowledge tests regarding AEMP.

It can be concluded from Table II that students exposed to the guided active learning demonstration supported by sub-microrepresentations were the most successful in solving the test. The lowest achievements were recorded in the control group.

TABLE II. Average achievement scores of students at AT-1 test (possible points 0–12); significances: CONT–EXP1, $p = 0.350$; CONT–EXP2, $p \leq 0.000$; EXP1–EXP2, $p = 0.004$

Group/number of students	Average AT-1 score	SD
CONT/60	7.07	1.72
EXP1/51	8.18	2.15
EXP2/63	9.73	2.04

The one-way between-groups analysis of variance (ANOVA) was conducted to explore the differences in total success on achievement AT-1 between the groups of students exposed to different educational strategies. The differences between the three groups of students are statistically significant ($F(2, 171) = 12.35, p < 0.001$). Post hoc comparisons using Tukey HSD showed a statistically significant difference ($p < 0.001$) between the mean scores for students in the control group and students involved in the EXP2 strategy. There is also a statistically significant difference ($p = 0.004$) in the AT-1 score between groups of students participating in the EXP1 and EXP2 strategy. There is no statistically significant difference ($p = 0.350$) between the control group of students and the EXP1 group.

The effect of EXP1 and EXP2 on students' long-term knowledge about AEMP

The second part of the results shows students' achievements on AT-2 obtained 14 days after the specific educational strategy was applied. The results

can be interpreted as students' retained knowledge of the AEMP integrated into their-long-term memory.

Based on the results presented in Tables II and III, it can be concluded that students in the control group retained the lowest level of assessed knowledge; students received on average 2.77 (7.07–4.30) points less on AT-2 than on AT-1. However, the average score obtained by students in both experimental groups compared to the control group at AT-1 and AT-2 test was diminished by less than 2 points; 1.31 (8.18–6.87) points in the EXP1 group and 0.39 (9.73–9.34) points in EXP2 group. Table III shows that students participating in the experimental groups scored higher on the knowledge test than the control group 14 days after the educational strategies were applied. The highest average score was recorded in the EXP2 group.

TABLE III. Average achievement scores of students in the AT-2 test (possible points 0–12); significances: CONT–EXP1, $p \leq 0.000$; CONT–EXP2, $p = 0.001$; EXP1–EXP2, $p = 0.002$

Group/number of students	Average AT-2 score	SD
CONT/60	4.30	1.69
EXP1/51	6.87	1.83
EXP2/63	9.34	2.12

The ANOVA was also conducted to explore the differences in total success on achievement AT-2 between the groups of students participating in the specific strategy. The differences between the three groups of students are statistically significant ($F(2, 171) = 23.54, p < 0.001$). Post hoc comparisons using Tukey HSD showed that there is a statistically significant difference ($p < 0.001$) between the mean scores of students using only chemical symbolic language (CONT) and the EXP1 group of students. There is also a statistically significant difference ($p < 0.001$) between the CONT and the EXP2 group of students. The difference between the group of students participating in the EXP1 educational process and the group of students involved in the EXP2 educational strategy is statistically significant ($p = 0.002$).

This study was carried out to confirm the four hypotheses that were derived from the main purpose of the study and the research question, which was to investigate the effect of two different teaching approaches (EXP1 and EXP2) on students' understanding of AEMP immediately after the application of the educational strategy and after 14 days (effect of the teaching on students' long-term memory knowledge about AEMP).

The first hypothesis was: "Students participating in EXP1 and EXP2 will score significantly higher on an achievement test than those students who were taught only at the symbolic level of the AEMP concepts." The hypothesis cannot be confirmed. It can be concluded that a guided active learning demonstration (EXP1) for supporting the macroscopic level is not statistically significantly

more effective on students' chemical knowledge than teaching the alkaline earth metal concepts only at the symbolic level. In contrast, a positive effect of explaining selected chemistry concepts at the submicroscopic level in combination with a guided active learning method demonstration (EXP2) on students' chemistry knowledge can be recorded, compared to the achievement test results of students that were taught only the symbolic level of chemical concepts. From this result, it can be summarized that a chemical demonstration alone, even though it is upgraded with students' active observations, does not improve the students' knowledge better than teaching chemistry only by the symbolic level written and explained by the teacher on the blackboard. It is important to emphasize that these findings support the findings of other researchers,^{24,42,43} who concluded that symbolic teaching of chemistry is not effective, yet teachers mainly use the symbolic level of chemical concepts to teach chemistry. Even smaller impact on student understanding of chemical concepts can be expected if teachers do not use the guided active learning method in explaining selected chemical concepts at the submicroscopic level. The results obtained in the present study can be compared with several research studies. Namely, when students learn science in classrooms with minimal feedback, they are often lost and frustrated, and their confusion can lead to misconceptions, in particular when learning situations are unguided.^{44,45}

The second hypothesis relates to the comparison between the achievement test scores of students experiencing a guided active learning demonstration followed by the AEMP concepts representations at submicroscopic level (EXP2) and those who participated in a guided active learning demonstration (EXP1). This hypothesis is confirmed. There is a significant difference in the achievement test (AT-1) scores between students exposed to the (EXP1) and students exposed to the (EXP2). These results are consistent with the conclusions of other researchers.^{8,15,16,27} Gabel,² for example, reported that those students who were exposed to the submicrorepresentations during the educational process more adequately understand the nature of the particles' interactions compared to those that learned the same concepts only by textbook reading. From the results obtained in this study, it can be concluded that explaining the macroscopic phenomena by submicroscopic representations is an important step while constructing adequate chemical knowledge because the knowledge obtained by submicroscopic explanations is more sufficient.

The third hypothesis is 'Students participating in (EXP1) and in (EXP2) will score significantly higher on a delayed achievement test than those students who were taught only the symbolic level of the AEMP concepts.

The third hypothesis is confirmed. Knowledge obtained by the active learning in both cases is more persistent than knowledge constructed only by teaching chemical concepts at the symbolic level. This finding is interpreted as indicating

that both treatments resulted in effective learning by the groups that experienced them: the students in both treatment groups learned more, and their knowledge was retained longer. These findings are in accordance with those of Kirschner *et al.*,³⁴ who claimed that, based on current knowledge of human cognitive architecture, minimal guidance during instruction is significantly less effective and efficient than guidance specifically designed to support the cognitive processing necessary for learning. The fact is that long-term memory is viewed as the central, dominant structure of human cognition, so everything we see, hear and think about is critically dependent on and influenced by our long-term memory.

The last hypothesis “Students experiencing (EXP2) will score significantly higher on the delayed achievement test than those who experienced (EXP1)” is also confirmed.

It can be concluded that learning chemical concepts at the submicroscopic level can influence constructing more persistent concept structure in students’ long-term memory and that this adequately incorporated data can be recalled more easily when needed for solving new chemical problems. By achieving more stable chemical knowledge in students’ long-term memory, we could enable students to build knowledge on a sound basis. This finding is a very important aspect of chemistry teaching and learning, because research shows that those students often do not have a proper knowledge base that would make it possible to upgrade their knowledge of more and more abstract chemical concepts when they make progress on the educational vertical.⁵ Chittleborough and Treagust⁴³ also found that students’ abilities to use and interpret chemical models (submicrorepresentations can also be regarded as models of particles) do influence their abilities to understand chemical concepts. These modelling skills should be taught (rather than left to be an incidental consequence of the teaching of chemical concepts) by being incorporated into instruction and by students being given practice in the application of multiple representations of chemicals and their interactions. According to these aspects and findings reported by Davidowitz *et al.*,¹⁷ students need to model (draw) submicrorepresentations during their chemical education. Teachers should be aware of these activities so that they can use them when trying to explain specific phenomena at the submicroscopic level also to the students without properly developed modelling abilities.

CONCLUSION

The main conclusion of the study is that teaching the chemistry content – alkaline earth metals – to primary school students aged 14 years by guided active learning demonstrations and/or by guided active learning demonstrations with explanations at the submicroscopic level is more effective than traditional (blackboard – chalk symbolic) chemistry teaching. It can be concluded from the results that students’ knowledge, obtained by either method, is more persistent and rem-

ains stored in the students' long-term memory for longer periods. Knowledge stored in the long-term memory should be scientifically correct, and individual pieces of information should be vertically and horizontally connected into the adequate concept structure. For a student, such processed information is applicable to new educational situations and aids them in constructing new knowledge.

Further studies are needed to accurately interpret how a guided active learning demonstration supported by submicrorepresentations influences the students' long-term knowledge and how the guided active learning chemistry (GALC) strategy influences students' knowledge.⁴⁶

In the future, the research should be applied on a larger scale in elementary school and transmitted at the secondary and university level. It is also important to stress that submicrorepresentations of chemical concepts affect students' proper knowledge development, as reported by some researchers, which is why the extra treatment group involving only submicrorepresentations in the teaching approach was not included in the "present study."^{15,17,47} In future research, the influence of this variable to the students' knowledge incorporated into the active learning strategies, can also be explored. Other chemistry content can also be used for these teaching strategies. It is also important to emphasize that students lose knowledge after 14 days from learning concepts if they do not use it. AT-2 should, for that reason, be applied at the same sample a few times after the teaching, so that the dynamic of concept structure change in the students' long-term memory can be followed.

Overall, the data of this study seem to provide evidence that teachers should incorporate in their educational strategies either guided active learning demonstrations or even more effective guided active learning demonstrations with explanations at the submicroscopic level. In such a way, students could be prepared to challenge new science problems with adequate in-depth scientific knowledge in their further education, which may lead to more persistent and meaningful learning, based on the problem-solving approach.

SUPPLEMENTARY MATERIAL

Additional data and information are available electronically at the pages of journal website: <https://www.shd-pub.org.rs/index.php/JSCS/article/view/10580>, or from the corresponding author on request.

ИЗВОД

УТИЦАЈ АКТИВНОГ УЧЕЊА И РЕПРЕЗЕНТАЦИЈА СУБМИКРОСКОПСКОГ НИВОА НА РАЗУМЕВАЊЕ 14-ГОДИШЊИХ УЧЕНИКА О ЗЕМНОАЛКАЛНИМ МЕТАЛИМА

KATARINA SENTA WISSIAK GRM и IZTOK DEVETAK

University of Ljubljana, Faculty of Education, Kardeljeva pl. 16, 1000 Ljubljana, Slovenia

Циљ истраживања је био да се испита утицај два различита приступа на ученичко разумевање изабраних хемијских појмова. Прва група ученика у истраживању је подучавана методом активног учења вођеног демонстрацијама, а друга група је уз активно

учење вођено демонстрацијама dobila и објашњења субмикроскопског нивоа. У контролној групи одабрана тема је обрађена без активног учења вођеног демонстрацијама и без објашњења субмикроскопског нивоа. У истраживању су коришћени следећи инструменти: тест логичког мишљења (TOLT), пред-тест знања (KPT), два теста постигнућа (AT-1 и AT-2) и упитник за ученике. У истраживању је учествовао сто седамдесет један ученик (просечне старости 13,9 година). Резултати указују да су оба приступа (тј. активно учење вођено демонстрацијама, са и без објашњења субмикроскопског нивоа) ефикаснији од наставе искључиво на симболичком нивоу. Из резултата се може закључити да се знање ученика, стечено било којом методом која укључује вођено активно учење, задржава у дугорочном памћењу ученика. У раду су дискутоване импликације резултата истраживања на основношколски наставни програм у области природних наука.

(Примљено 28. марта, ревидирано 20. јула, прихваћено 3. септембра 2021)

REFERENCES

1. A. H. Johnstone, *Sch. Sci. Rev.* **64** (1982) 377
2. D. Gabel, *J. Chem. Educ.* **76** (1999) 548 (<https://doi.org/10.1021/ed076p548>)
3. D. F. Treagust, A. G. Harrison, G. J. Venville, *J. Sci. Teacher Educ.* **9** (1998) 85 (<https://doi.org/10.1023/A:1009423030880>)
4. H. K. Wu, J. S. Krajcik, E. Soloway, *J. Sci. Teacher Educ.* **38** (2001) 821 (<https://doi.org/10.1002/tea.1033>)
5. A. G. Harrison, D. F. Treagust, *Chemical Education: Towards Research-Based Practice*, Kluwer Academic Publishers, Dordrecht, 2002, pp. 189–212 (https://www.academia.edu/5488505/Chemical_education_towards_research_based_practice_science_technology)
6. D. F. Treagust, G. Chittleborough, T. Mamiala, *Int. J. Sci. Educ.* **25** (2003) 1353 (<https://doi.org/10.1080/0950069032000070306>)
7. J. E. Upahi, U. Ramnarain, *Chem. Educ. Res. Pract.* **20** (2019) 146 (<https://doi.org/10.1039/C8RP00191J>)
8. R. M. Kelly, L. L. Jones, *J. Chem. Educ.* **85** (2008) 303 (<https://doi.org/10.1021/ed085p303>)
9. I. Devetak, S. A. Glažar, *Int. J. Sci. Educ.* **32** (2010) 1561 (<https://doi.org/10.1080/09500690903150609>)
10. J. M. Nyachwaya, M. Gillaspie, *Chem. Educ. Res. Pract.* **17** (2016) 58 (<https://doi.org/10.1039/C5RP00140D>)
11. N. Becker, C. Stanford, M. Towns, R. Cole, *Chem. Educ. Res. Pract.* **16** (2015) 769 (<https://doi.org/10.1039/C5RP00064E>)
12. D. D. Rodić, T. N. Rončević, M. D. Segedinac, *Acta Chim. Slov.* **65** (2018) 394 (<http://dx.doi.org/10.17344/acsi.2017.4139>)
13. L. Dee Fink, *Creating significant learning experiences: An integrated approach to designing college courses*. Calif: Jossey-Bass, San Francisco, CA, 2003, pp. 102–154 (<https://www.wiley.com/ensi/Creating+Significant+Learning+Experiences%3A+An+Integrated+Approach+to+Designing+College+Courses%2C+Revised+and+Updated-p-9781118416327>)
14. K. L. Adams, J. A. Luft, *Int. J. Sci. Educ.* **13** (2018) 69
15. G. Papageorgiou, P. Johnson, *Int. J. Sci. Educ.* **27** (2005) 1299 (<https://doi.org/10.1080/09500690500102698>)
16. M. Stains, V. Talanquer, *Int. J. Sci. Educ.* **29** (2007) 643 (<https://doi.org/10.1080/09500690600931129>)

17. B. Davidowitz, G. Chittleborough, E. Murray, *Chem. Educ. Res. Pract.* **11** (2010) 154 (<https://doi.org/10.1039/C005464J>)
18. V. Talanquer, *Int. J. Sci. Educ.* **33** (2011) 179 (<https://doi.org/10.1080/09500690903386435>)
19. K. de Berg, *Chem. Educ. Res. Pract.* **13** (2012) 8 (<https://doi.org/10.1039/C1RP90056K>)
20. U. Ramnarain, U. A. Joseph, *Chem. Educ. Res. Pract.* **13** (2012) 462 (<https://doi.org/10.1039/C2RP20071F>)
21. K. S. Taber, *Chem. Educ. Res. Pract.* **14** (2013) 151 (<https://doi.org/10.1039/C3RP00012E>)
22. M. M. W. Cheng, J. K. Gilbert, *Int. J. Sci. Educ.* **39** (2017) 1173 (<http://dx.doi.org/10.1080/09500693.2017.1319989>)
23. D. D. Trivić, V. D. Milanović, *J. Serb. Chem. Soc.* **83** (2018) 1177 (<http://doi.org/10.2298/JSC171220055T>)
24. G. Chittleborough, *Learning with Understanding in the Chemistry Classroom*, Springer, Dordrecht, 2014, pp. 25–40 (<https://www.springer.com/gp/book/9789400743656>)
25. I. Devetak, J. Vogrinc, S. A. Glažar, *Res. Sci. Educ.* **39** (2009) 157 (<https://doi.org/10.1007/s11165-007-9077-2>)
26. J. D. Bradley, M. Brand, G. G. Gerrans, *S. Afr. J. Sci. Educ.* **37** (1998) 85
27. N. Solsona, M. Izquierdo, M. O. De Jong, *Int. J. Sci. Educ.* **25** (2003) 3
28. E. Adadan, K. C. Trundle, K. E. Irving, *J. Res. Sci. Teach.* **47** (2010) 1004 (<https://doi.org/10.1002/tea.20366>)
29. A. L. Kerna, N. B. Woodb, G. H. Roehrig, J. Nyachwayac, *Chem. Educ. Res. Pract.* **11** (2010) 165 (<https://doi.org/10.1039/C005465H>)
30. O. Lee, D. C. Eichinger, C. W. Anderson, G. D. Berkheimer, T. D. Blakeslee, *J. Res. Sci. Teach.* **30** (1993) 249 (<https://doi.org/10.1002/tea.3660300304>)
31. C. Bonwell, J. Eison, *Active Learning: Creating Excitement in the Classroom*, George Washington University, Washington, DC, 1991 (<https://eric.ed.gov/?id=ED336049>)
32. J. S. Bruner, *Harv. Educ. Rev.* **31** (1961) 21
33. D. Muijs, D. Reynolds, *Effective teaching: Evidence Based Practice*, Sage Publications, London, 2017
34. P. A. Kirschner, J. Sweller, R. E. Clark, *Educ. Psychol.* **41** (2006) 75 (https://doi.org/10.1207/s15326985ep4102_1)
35. P. H. Walton, *Univ. Chem, Educ.* **6** (2002) 22
36. G. Tsaparlis, *Learning with Understanding in the Chemistry Classroom*, Springer, Dordrecht, 2014, pp. 41–61 (<https://www.springer.com/gp/book/9789400743656>)
37. National Research Council, *How People Learn: Brain, Mind, Experience, and School: Expanded Edition*, The National Academies Press, Washington, DC. 2000. pp. 3–23 (<https://www.nap.edu/catalog/9853/how-people-learn-brain-mind-experience-and-school-expanded-edition>)
38. R. Moreno, *Instr. Sci.* **32** (2004) 99 (<https://doi.org/10.1023/B:TRUC.0000021811.66966.1d>)
39. L. Deslauriers, L. S. McCarty, K. Miller, K. Callaghan, G. Kestin, *PNAS* **116** (2019) 19251 (<https://doi.org/10.1073/pnas.1821936116>)
40. K. G. Tobin, W. Capie, *Educ. Psychol. Meas.* **41** (1981) 413 (<https://doi.org/10.1177/001316448104100220>)
41. B. Marentič Požarnik, *Psychology of learning and instruction*, DZS, Ljubljana, 2000 (<https://doi.org/10.4312/as.6.4.150-152>) (in Slovenian)

42. V. M. Williamson, M. R. Abraham, *J. Res. Sci. Teach.* **32** (1995) 521 (<https://doi.org/10.1002/tea.366032050843>)
43. G. Chittleborough, D. F. Treagust, *Chem. Educ. Res. Pract.* **8** (2007) 274 (<https://doi.org/10.1039/B6RP90035F>)
44. J. S. Chall, *The academic achievement challenge*, Guilford Press, New York, 2000
45. D. Klahr, M. Nigam, *Psychol. Sci.* **15** (2004) 661 (<https://doi.org/10.1111/j.0956-7976.2004.00737.x>)
46. I. Devetak, S. A. Glažar, *Facilitating effective student learning through teacher research and innovation*, University of Ljubljana, Faculty of Education, Ljubljana, 2010, pp. 399–414 (<http://www.pef.uni-lj.si/ceps/knjiznica/doc/zuljan-vogrinc.pdf>)
47. D. M. Bunce, D. Gabel, *J. Res. Sci. Teach.* **39** (2002) 911 (<https://doi.org/10.1002/tea.10056>).



J. Serb. Chem. Soc. 87 (2) S50–S57 (2022)

SUPPLEMENTARY MATERIAL TO
**The influence of active learning and submicrorepresentations on
14-year-old students' understanding of the alkaline earth metal
concepts**

KATARINA SENTA WISSIAK GRM* and IZTOK DEVETAK

University of Ljubljana, Faculty of Education, Kardeljeva pl. 16, 1000 Ljubljana, Slovenia

J. Serb. Chem. Soc. 87 (2) (2022) 275–290

DETAILED DESCRIPTION OF THE INSTRUMENTS

Pre-tests (TOLT and KPT)

The level of students' formal reasoning abilities was obtained with the Test of Logical Thinking (TOLT).⁴⁰ The TOLT is a ten-item group paper-pencil test. The authors of the test reported a strong correlation ($r = 0.82$; $p < 0.0001$) between performance on tasks during Piagetian clinical interviews, which are considered to be a traditionally preferable method in measuring individuals' formal reasoning abilities, and the results on TOLT. The TOLT has high internal consistency reliability (Cronbach's alpha was 0.85). The test consists of ten items, two for each of the five modes of reasoning to be measured (*i.e.* controlling variables, proportional, correlational, probabilistic, and combinatorial reasoning). The test scores from 0-1 point (concrete reasoners), 2-3 points (transitional reasoners) and 4-10 points (formal reasoners) were used as a basis for classifying the students. Students spent 38 minutes solving the test.

TOLT – sample items

Sample question No. 1: Vegetable seeds

The gardener has bought a bag of three pumpkin seeds and three bean seeds. If the gardener takes only one seed from the bag, what is the probability that this seed is a bean?

A. $1/2$ B. $1/3$ C. $1/4$ D. $1/6$ E. $4/6$

1. four trials are required because three pumpkin seeds can be selected in a row.
2. one bean seed must be selected from the six seeds.
3. one bean seed must be selected from a total of three seeds.
4. half of the seeds are beans.

*Corresponding author. E-mail: katarina.wissiak@pef.uni-lj.si

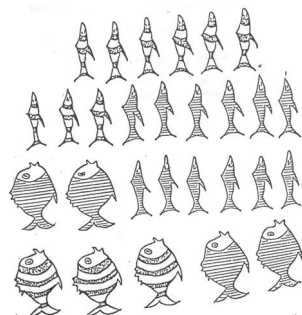
5. in addition to one bean seed, three pumpkin seeds can be selected from all six seeds.

Sample question No. 2: Shopping mall

On the ground floor of the shopping mall, there are four spaces for new stores. TRADE IN COSMETICS (K), TRADE ALL 3 EUR (E), TRADE IN FOOD (H) and TRADE IN ANIMALS (Ž) want to move into these four rooms. Each shop can choose one of the four rooms. One way the shops could occupy the rooms is KEHŽ. List all the other possible ways the shops could be arranged in the rooms.

Write all possible answers on the lines below; more lines are drawn than there are possible answers. Possible combinations of shops KEHŽ _____

Sample question No. 3: Fish



Do fat fish have broad stripes rather than slender fish have broad stripes?

- A. yes
- B. no

Reason:

1. some fat fish have wide stripes and some have narrow stripes.
2. 3/7 of a fat fish has broad stripes.
3. 12/28 fish have broad stripes and 16/28 have narrow stripes.

4. 3/7 thick fish have broad stripes and 9/21 slender fish have broad stripes.
5. some fish with wide stripes are slim and some are fat.

The Knowledge Pre-Test (KPT) is a seven-item group paper-pencil test, composed of open-ended and multiple-choice items. All concepts tested in this pre-test were taught later on during lessons or students had to understand specific concepts before the application of the specific educational strategy. The KPT showed satisfactory measuring characteristics (*i.e.*, internal consistency reliability/Cronbach's alpha was 0.81; discriminate indexes for every item between 0.34 and 0.68 were all statistically significant). Kurtosis (0.67) and Skewness (0.96) coefficients show normally distributed data. KPT was designed specifically for this study and was administered by two university chemistry and chemical education professors.

Their responses provided content validation for the instrument. Students could achieve 12 points on KPT; they spent 10 minutes on average to solve the test.

KPT - sample items

Sample question No. 1

What do we call the group of elements in the periodic table in which the magnesium and calcium are classified? _____ .

Sample question No. 2

Calcium reacts with water. Name the particles that will result in the chemical reaction?

- a hydrogen molecules
- b hydrogen atoms
- c calcium ion
- d calcium atom
- e calcium hydroxide molecules

Write the correct answers _____

Sample question No. 3

Adding a few drops of phenolphthalein into the beaker after the reaction between calcium and water will turn the colour of the solution into violet. Explain why?

Achievement Tests (AT-1 and AT-2)

Both achievement tests were structured according to the concept analysis of the topic introduced in the classroom (*i.e.* alkali earth metals) not depending on the educational strategy used. The Achievement Tests 1 (AT-1) was a six-item

group paper-pencil test, composed of open-ended and multiple-choice questions. The AT-1 comprises similar chemical concepts as KPT. The AT-1 showed satisfactory measuring characteristics (*i.e.* internal consistency reliability/Cronbach's alpha was 0.73; discriminate indexes for every item between 0.29 and 0.85 were all statistically significant). Kurtosis (0.83) and Skewness (-0.32) coefficients show normally distributed data. AT-1 was designed specifically for this study, and its content validity was determined by two university chemistry and chemical education professors. As a comprehensive achievement test, the use of the AT-1 achievement test was immediately administered after students had been exposed to the specific educational strategy. Students could achieve eleven points on AT-1. Students spent 10 minutes on average on solving the test. They did not receive any feedback about their success in solving the AT-1.

Achievement Tests 1 (AT-1) - sample items

Sample question No. 1

Which particles are formed when calcium reacts with water?

- a hydrogen molecules
- b hydrogen atoms
- c calcium ions
- d calcium atoms
- e calcium hydroxide molecules

Select the correct answers: _____

Sample question No. 2

You have learned about calcium and magnesium reactivity; can you anticipate the reactivity of the second group of elements in the periodic table? With an arrow indicate the increasing reactivity of the second group elements.

beryllium magnesium calcium strontium barium

Sample question No. 3

Write the chemical equation between an element that was selected in the sample question 2 with the cold water.

The Achievement Tests 2 (AT-2) was also a six-item group paper-pencil test, composed of open-ended and multiple-choice questions. Understandably, the questions asked were similar to those in the previous tests (KPT and AT-1), since the same chemical concepts were to be assessed. The AT-2 showed satisfactory measuring characteristics. Its internal consistency reliability - Cronbach's alpha was 0.81; discriminate indexes for every item between 0.34 and 0.68 were all statistically significant. Kurtosis (-0.39) and Skewness (0.14)

coefficients show normally distributed data. AT-2 was designed specifically for this study and was administered by two university chemistry and chemical education professors. Their responses provided content validation for the instrument. As a delayed achievement test, the AT-2 test was administered two weeks after the specific educational strategy was applied in the classroom. Students could achieve twelve points on AT-2. They spent 10 minutes on average to solve the test.

Achievement Tests 2 (AT-2) - sample items

Sample question No. 1

The cleaned surfaces of calcium and magnesium have a metallic shine. If we leave them for a longer time in the air, they lose this shine. Explain why this happens.

Sample question No. 2

Which chemical equation represents the reaction of an element that reacts with cold water?

- A $\text{Ca(s)} + 2 \text{H}_2\text{O(l)} \rightarrow 2 \text{Ca(OH)}_2\text{(aq,s)}$
- B $\text{Ca(s)} + 2 \text{H}_2\text{O(l)} \rightarrow \text{Ca(OH)}_2\text{(aq,s)} + \text{H}_2\text{(g)}$
- C $\text{Mg(s)} + 2 \text{H}_2\text{O(l)} \rightarrow \text{Mg(OH)}_2\text{(aq)}$
- D $\text{Mg(s)} + 2 \text{H}_2\text{O(l)} \rightarrow \text{MgO(aq)} + \text{H}_2\text{(g)}$

Sample question No. 3

Adding a few drops of phenolphthalein into the beaker where calcium reacts with water will turn the solution from colourless to violet. What can you conclude from this observation?

- A The solution has become acidic.
- B The solution has become basic.
- C The solution has become neutral.
- D The acidity or basicity of the solution has not changed.

The concept structure of both achievement tests (AT-1 and AT-2) was similar in order to compare results and obtain data for drawing adequate conclusions. Neither test comprised any items that required specific knowledge about reading or drawing submicrorepresentations for solving the items. Statistically significant correlations between the knowledge tests ($r = 0.37$) show that the tests used in the research do measure similar chemical knowledge.

Detailed description of the teaching approaches in specific group

After the teachers applied the innovative teaching approach, they reported in detail to the researchers how they had followed the researchers' instructions. It was found that all the teachers followed the instructions appropriately, which means that the validity of the teaching strategy used was ensured.

To carry out the active learning method, special material for supporting guided active learning demonstrations (EXP1 and EXP2) was developed, in which every stage of the experimental work is quoted to enable students to follow (observe and explain) the experiment. In the material developed for a guided active learning demonstration, there are target questions, given to help teachers point out the specific phases of the experiment and help students observe and understand them. Students were given the form for a guided active learning demonstration in which all the crucial stages of the experimental work with matching questions were fulfilled. Students had to complete the columns for observations and conclusions, which were blank, during the chemical demonstration performed by the teacher.

Teachers' guide instruction form for an active learning demonstration: (students had to fill in only the white part of the table)

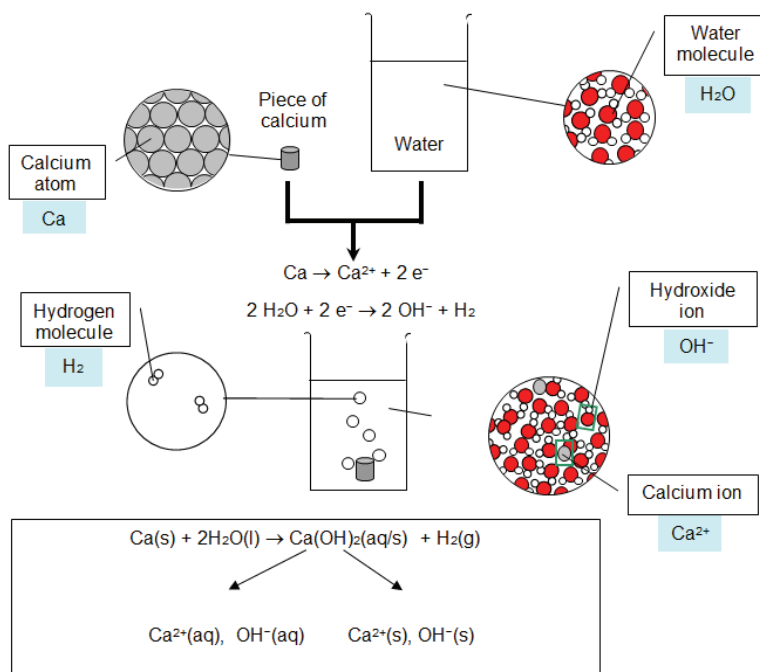
Stages of experimental work	Questions	Observations	Conclusions
1. Observe the appearance of the magnesium.	Can you notice the metallic shine? Do you think magnesium reacts with oxygen from the air?	Yes, magnesium has a metallic shine.	Magnesium reacts with oxygen from the air very slowly, so it keeps on shining.
2. Observe the appearance of calcium.	Can you notice the metallic shine? Do you think calcium reacts with oxygen from the air?	No, calcium does not have a metallic shine.	Yes, calcium reacts with oxygen from the air.
3. Drop a small piece of magnesium into the beaker with cold water.	Do you notice any changes?	No, there are no changes.	
4. Add a few drops of phenolphthalein into the beaker with magnesium and cold water.	Does the indicator change its colour? Do you think magnesium reacts with water?	No, phenolphthalein does not change its colour.	No, magnesium does not react with water during the time needed for the experiment. If we had more time, some changes might be observed.
5. Drop some granules of the calcium into the beaker with cold water.	Do you notice any changes?	Yes, we can observe bubbles of gas going out of the solution. The solution has turned muddy.	Calcium reacts with water. The reaction products are gas and some poorly soluble substance.

6. Add a few drops of phenolphthalein into the beaker with calcium and cold water.	Does the indicator change its colour? Do you think calcium reacts with water?	Yes, phenolphthalein does change its colour, since it turns from colourless into violet. White precipitate is formed.	The reaction product has basic properties. The product is poorly soluble in water; it might be calcium hydroxide.
--	--	---	---

Experimental demonstrations of the AEMP were performed by the teachers, because alkaline earth metals are very reactive, and dangerous for the 14-year-olds to handle. Slovene legislation also advises against students' individual or group experimentations with potentially dangerous substances in the classroom; therefore, the potentially more dangerous experiments are demonstrated by teachers. After the joint final discussion, students verified the correctness of their answers with the teachers. After that, this material was no longer used and could not be used while taking the achievement tests.

In addition to the form for guided active learning demonstrations, it was required that a PowerPoint presentation be developed to explain the reaction at the submicroscopic level for carrying out the EXP2. The presentation was developed in such a way that separate parts of the final picture were presented to the students. The last slide completed the whole picture.

The final PowerPoint slide of schemata of particles (*i.e.*, submicrorepresentations (SMRs) used in EXP2:



This explanation took a teacher about 10 min. The 10-min period was used only for explaining one experiment (reaction of calcium with water at three levels of chemical concepts) and also because students are used to teachers' explanations of experiments by schemata of particles (*i.e.*, submicrorepresentations (SMRs)). The time used in the EXP2 for explaining SMRs (10 minutes) was used in the CONT and EXP1 group for the activities that were not connected with the research situation (checking homework from previous lessons).

The control group was taught using the symbolic representation of the selected chemical concepts and was supported by chemical equations and teachers' explanation but was carried out without a chemical experiment and its explanation at the submicroscopic level. Teachers used photographs of the final stages of the experiments while explaining AEMP to the students in the control group. Students could observe the color of the solution (violet), and the formation of bubbles of the gas on the photo.

Students were exposed to the symbolic level (chemical symbols and equations) in the CONT and EXP1 group in such a way that teachers attempted to explain the observations from the final photo of the experiment (CONT) or from the chemical demonstrations (EXP1). Students were guided in writing chemical equations by the teacher, following the teachers' explanations of the observations. In the EXP2 treatment group, the symbolic level was introduced after the sub-microlevel of the particle interaction in the discussed reactions of alkaline earth metals had been explained. The static submicro-models of different particles interactions presented with the PowerPoint slide were translated into the chemical symbols and formulae and connected into the chemical equations. Students were familiar with SMRs for explaining experimental observations.

Students who participated in the EXP2 were exposed to such a teaching approach approximately for 1.5 years (chemistry in Grade 8 and half of Grade 9). All three groups of students participating in this study were familiar with the approach of presenting chemical concepts on three levels, because they had learned different topics by using SMRs (*e.g.*, chemical reaction, chemical bonds, acids, and bases are among the topics of Elements of the Periodic Table, which is part of the national curriculum in Slovenia for chemistry). From the topic Elements of the Periodic Table, only reactivity of the second group of elements (according to the curriculum teachers spend approx. one school hour on this sub-topic) was presented in this paper.



Erratum
(Printed version only)

1. Volume 87, Issue 1, Page 157, lines 8–11 from the top should read:

¹University of Novi Sad, Faculty of Technical Sciences, Novi Sad, Serbia and ²Jaroslav Černi
Water Institute, Belgrade, Serbia